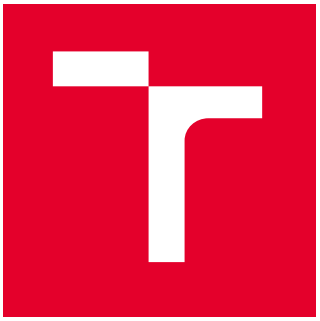

BRNO UNIVERSITY OF TECHNOLOGY

VYSOKÉ UČENÍ TECHNICKÉ V BRNĚ

FACULTY OF MECHANICAL ENGINEERING

FAKULTA STROJNÍHO INŽENÝRSTVÍ

INSTITUTE OF MACHINE AND INDUSTRIAL DESIGN

ÚSTAV KONSTRUOVÁNÍ

LIQUID LUBRICANT EVAPORATION IN SPACE APPLICATIONS

VYPAŘOVÁNÍ KAPALNÝCH MAZIV VE VESMÍRNÝCH APLIKACÍCH

DOCTORAL THESIS

DIZERTAČNÍ PRÁCE

AUTHOR — **Ing. Josef Pouzar**

AUTOR PRÁCE

SUPERVISOR — **prof. Ing. Ivan Křupka, Ph.D.**

ŠKOLITEL

BRNO 2026

STATEMENT

I hereby declare that I have written the PhD thesis *Liquid lubricant evaporation in space applications* independently, following the professional guidance of my supervisor, prof. Ing. Ivan Křupka, Ph.D., and my supervisor specialist, Ing. David Košťál, Ph.D., using the sources cited in the references.

Brno, January 2026
Josef Pouzar

BIBLIOGRAPHICAL REFERENCE

POUZAR, Josef. *Liquid lubricant evaporation in space applications*. Doctoral Thesis. Ivan KŘUPKA (supervisor). Brno: Brno University of Technology, Faculty of Mechanical Engineering, 2026.

PREFACE

This PhD thesis is a compilation work consisting of a comprehensive overview and four appended papers. It summarises my research on vacuum evaporation, molecular transport, and sealing of liquid lubricants for space applications, carried out during my doctoral studies at Brno University of Technology (BUT), Czech Republic. The research was conducted at the Faculty of Mechanical Engineering, within the Institute of Machine and Industrial Design, between September 2021 and January 2026.

My PhD was supported by a co-sponsored project with the European Space Agency (ESA) through the Open Space Innovation Platform (OSIP), which provided the main funding for both the research and my doctoral studies. Additional financial support came from Brno University of Technology, Faculty of Mechanical Engineering, Institute of Machine and Industrial Design. This thesis would not exist in its present form without the trust, encouragement, and effort of many people, to whom I am sincerely grateful.

I would like to acknowledge the European Space Agency and Brno University of Technology, and in particular my supervisor, Prof. Ing. Ivan Křupka, Ph.D., who made this co-sponsored PhD possible from the university side. From ESA, I especially thank René Seiler from the ESA Space Mechanisms team, who acted as Activity Observer within this project. His technical guidance, critical questions, constructive feedback, and continuous encouragement significantly improved the quality and relevance of this work.

My sincere thanks also go to my colleagues at Luleå University of Technology, Sweden, where I carried out one of my research internships. Prof. Lars-Göran Westerberg supervised and supported me during my stay at LTU, and Dr. Erik Nyberg provided invaluable discussions and motivation. Your help far exceeded the formal terms of a short research visit and developed into a long-term international collaboration. I am also grateful to Dr. Oleg Malyshev at Daresbury Laboratory, United Kingdom, who hosted me during another research stay and introduced me to particle accelerators and vacuum physics.

I am deeply grateful to my supervisor, Prof. Ing. Ivan Křupka, Ph.D., for his continuous guidance, patience, and trust throughout my studies, as well as for his support in securing the university contribution to the ESA project. I would also like to thank my supervisor specialist, Ing. David Košťál, Ph.D., for his technical insight and for the many hours we spent discussing experiments, simulations, and manuscripts, and for sharing both successes and setbacks along the way.

I am thankful to the Institute of Machine and Industrial Design for giving me the opportunity to experience the full spectrum of academic work, from teaching and public outreach to supervising bachelor students and taking part in other space-related projects. These activities shaped me both as a researcher and as a person.

To my colleagues, especially those in the office. Behind every piece of research and every new scientific result, there are many stories. There were moments of enthusiasm and frustration, of success and disappointment. I am glad that I could experience these stories with you, and I will remember them for the rest of my life. Thanks to our shared sense of humour, I managed to get through many difficult periods.

To my family, closest friends, and loved ones, thank you for your honesty, your unwavering support, and for believing in me even when I doubted myself. In my hardest moments, it was you who kept me going and gave me the strength to carry on.

Finally, I would like to thank myself for staying motivated when it would have been easier to give up, for not letting myself down, and for becoming the person I dreamt of being as a child. There were days of enthusiasm and pride, and there were days of doubt, fatigue, and frustration. All of them shaped me. I am grateful that during these years I not only worked, but also travelled the world, tried to live with honesty, curiosity, and courage, and cared for the people and moments that crossed my path. I lived, I cared, and I loved.

This thesis and my studies are only the visible part of a longer and sometimes difficult journey, and when I look back on this path, I am reminded of one of my favourite books, about a big panda and a tiny dragon. It says that it is not the journey or the destination that matters most, but the company along the way. I was fortunate with the company I had.

ACKNOWLEDGEMENT OF FUNDING

The author gratefully acknowledges the sources of funding that enabled this research. Financial support has been provided via the following arrangements:

- Technology Agency of the Czech Republic (TAČR), project *"Coarse Pointing Assembly for Optical Intersatellite Link"* (project no. FW01010297). This funding supported the development of the evaporation test rig and the initial experimental campaigns.
- European Space Agency (ESA) through the Open Space Innovation Platform (OSIP) under a Co-Sponsored Research Agreement (EISI), contract no. 4000139889, project *"Effect of local geometrical changes and polarization of labyrinth seal surfaces on the evaporation rate of liquid lubricants in space applications"*. This agreement provided the principal funding for the dissertation research and the author's doctoral studies.
- Programme Johannes Amos Comenius, call "Excellent Research", project *"Mechanical Engineering of Biological and Bio-inspired Systems"* (project no. CZ.02.01.01/00/22_008/0004634). This project provided additional financial support for the doctoral work and publication activities.

Any opinions, findings, and conclusions or recommendations expressed in this thesis are those of the author and do not necessarily reflect the views of the funding organizations.

ABSTRACT

This dissertation investigates evaporation and molecular transport of liquid lubricants in vacuum conditions relevant to space and translates the findings into practical guidance for labyrinth seal design. A series of custom experimental platforms was developed to generate time resolved evaporation data and to study vapor transmission through labyrinth type passages under controlled thermal and vacuum conditions. These measurements were combined with analytical modelling and high-fidelity molecular flow simulations to quantify how geometry, surface condition, and operating state influence vapor retention. Classical Langmuir predictions, using vapor pressure fits from the Clausius–Clapeyron equation, consistently overpredicted mass loss under the tested conditions. Lubricant specific correction factors were derived to match models with experiment, enabling calibrated use of simple analytical formulas in design. Experiments and simulations showed that longer and stepped labyrinth seals reduce transmission probability, that increased surface roughness lowers leakage by enhancing molecular scattering, and that rotation of seal walls further suppresses molecular flow for elongated passages. A compact, simulation-based correction model was introduced to account for surface roughness using a single amplitude metric and was validated against measurements within the studied range. The outcomes improve the predictive accuracy of evaporation estimates and provide test supported guidance on labyrinth geometry, surface roughness, and operating conditions, supporting cleaner and more reliable liquid lubricated mechanisms for space applications.

KEYWORDS

Space tribology, Vacuum evaporation, Labyrinth seals, Molecular flow, Liquid lubricants

ABSTRAKT

Tato disertační práce zkoumá vypařování a molekulární transport kapalných maziv ve vakuu odpovídajícím podmínkám vesmírného prostředí a převádí tato zjištění do praktických doporučení pro návrh labyrintových těsnění. Byla vyvinuta řada vlastních experimentálních platforem pro získání časově rozlišených dat o vypařování a pro studium přenosu par skrze labyrintové těsnění za řízených teplotních a vakuových podmínek. Naměřené hodnoty byly spojeny s analytickým modelováním a simulacemi molekulárního proudění, aby bylo kvantifikováno, jak geometrie labyrintu, struktura jeho povrchu a provozní režim ovlivňují zadržení par. Klasické predikce založené na Langmuirově přístupu, využívající aproximaci tlaku par pomocí Clausius–Clapeyronovy rovnice, systematicky nadhodnocovaly úbytek hmoty v testovaných podmínkách. Pro korelaci modelů s experimentem byly odvozeny korekční faktory specifické pro dané mazivo, což umožňuje kalibrované využití jednoduchých analytických vztahů při návrhu. Experimenty i simulace ukázaly, že delší a stupňovité labyrintové těsnění snižují pravděpodobnost průchodu vypařených molekul labyrintem, že zvýšená drsnost povrchu omezuje únik díky silnějšímu rozptylu molekul a že rotace stěn těsnění dále potlačuje průtok u protáhlých kanálů. Byl představen kompaktní, simulačně odvozený korekční model vlivu drsnosti povrchu, využívající jeden amplitudový parametr a validovaný na základě měření v rámci studovaného rozsahu. Výsledky zvyšují přesnost odhadů vypařování a poskytují testy podložená doporučení pro geometrii labyrintu, úpravu povrchu a provozní podmínky, což podporuje čistší a spolehlivější mechanismy mazané kapalinami pro kosmické aplikace.

KLÍČOVÁ SLOVA

Kosmická tribologie, Vakuové vypařování, Labyrintová těsnění, Molekulární proudění, Kapalná maziva

APPENDED PAPERS

PAPER [1]

EXPERIMENTAL STUDY OF SPACE LUBRICANT EVAPORATION IN A HIGH VACUUM ENVIRONMENT

Authors: Pouzar J., Kostal D., Sperka P., Krupka I., Hartl M.

Journal: Vacuum, Volume 219, Part A, 2024

Content: This paper presents the development and validation of a novel experimental methodology for measuring the evaporation behavior of liquid lubricants under high vacuum conditions. The results confirm significant discrepancies between experimentally measured evaporation rates and those predicted by commonly used analytical models based on vapor pressure data. These findings support the application of correction factors to improve the predictive accuracy of existing models and highlight the potential to reduce lubricant quantity, contamination risk, and overall mission cost in space mechanisms. The study also emphasizes the need for broader inter-laboratory comparisons and improved property data to enhance the reliability of evaporation predictions in practical applications.

Author contribution:

Pouzar J.: Writing – Original draft, Validation, Methodology, Investigation, Formal analysis. **Kostal D.:** Writing – Review & Editing, Supervision, Project administration, Methodology, Conceptualization. **Sperka P.:** Supervision, Methodology, Conceptualization. **Krupka I.:** Supervision, Funding acquisition. **Hartl M.:** Writing – Review & Editing, Resources.

Published by: Elsevier Ltd., *https://doi.org/10.1016/j.vacuum.2023.112758*

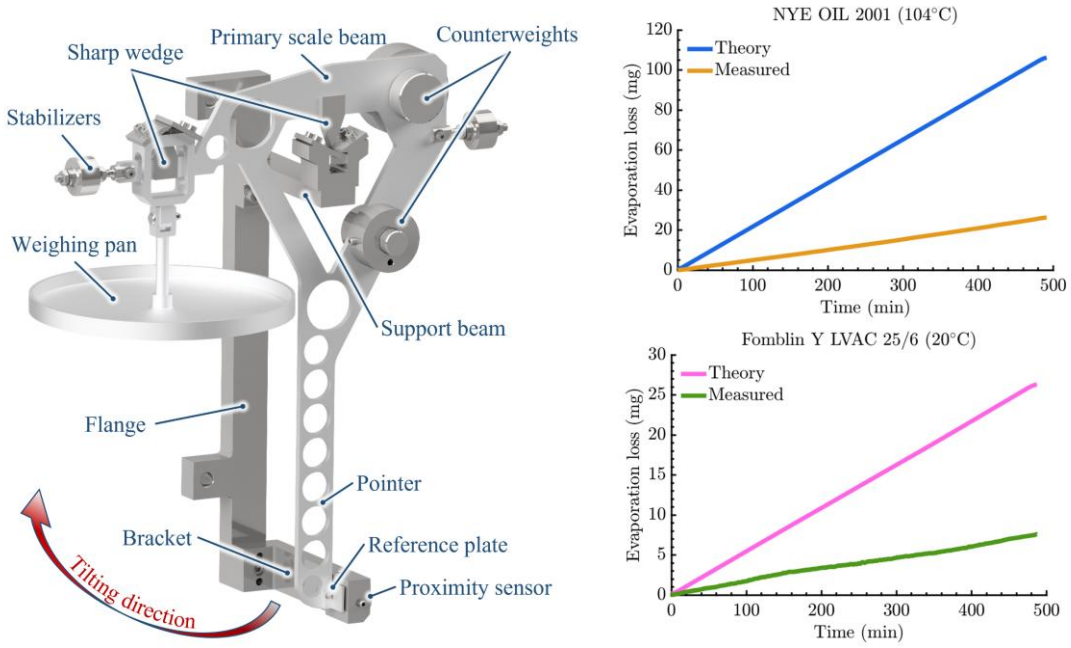

Fig. 1 Experimental setup and comparison of measured vs. theoretical evaporation rates [1]

PAPER [2]

LABYRINTH SEAL DESIGN FOR SPACE APPLICATIONS

Authors: Pouzar J., Kostal D., Westerberg L.G., Nyberg E., Krupka I.

Journal: Vacuum, Volume 232, 2025

Content: This study investigates how labyrinth seal geometry affects lubricant evaporation in ultra-high vacuum. Three seal configurations were experimentally tested and compared with analytical models and simulations using MolFlow+ and COMSOL Multiphysics. Both analytical and simulation results overestimated mass loss in short seals by more than a factor of two. For complex seals, analytical predictions underestimated mass loss by 22–27%, while simulations deviated by only 5–15%. Stepped geometries performed better by suppressing molecular beaming, which occurs when vapor molecules follow straight paths through narrow channels. A step effectively disrupted these trajectories and increased wall collisions, reducing mass loss. Best results were achieved with the step at the midpoint, where molecular flow was optimally redirected. Gap width and corridor length were key design parameters, with narrower gaps and longer paths improving sealing. Higher surface roughness enhanced molecular scattering, and local features such as relief grooves reduced flow at corners, further lowering evaporative losses.

Author contribution:

Pouzar J.: Writing – Original draft, Visualization, Validation, Software, Project administration, Methodology, Investigation, Funding acquisition, Formal analysis, Data curation, Conceptualization. **Kostal D.:** Writing – Review & Editing, Supervision, Methodology, Conceptualization. **Westerberg L.G.:** Writing – Review & Editing, Supervision, Conceptualization. **Nyberg E.:** Writing – Review & Editing, Methodology, Conceptualization. **Krupka I.:** Supervision, Resources, Funding acquisition.

Published by: Elsevier Ltd., *https://doi.org/10.1016/j.vacuum.2024.113882*

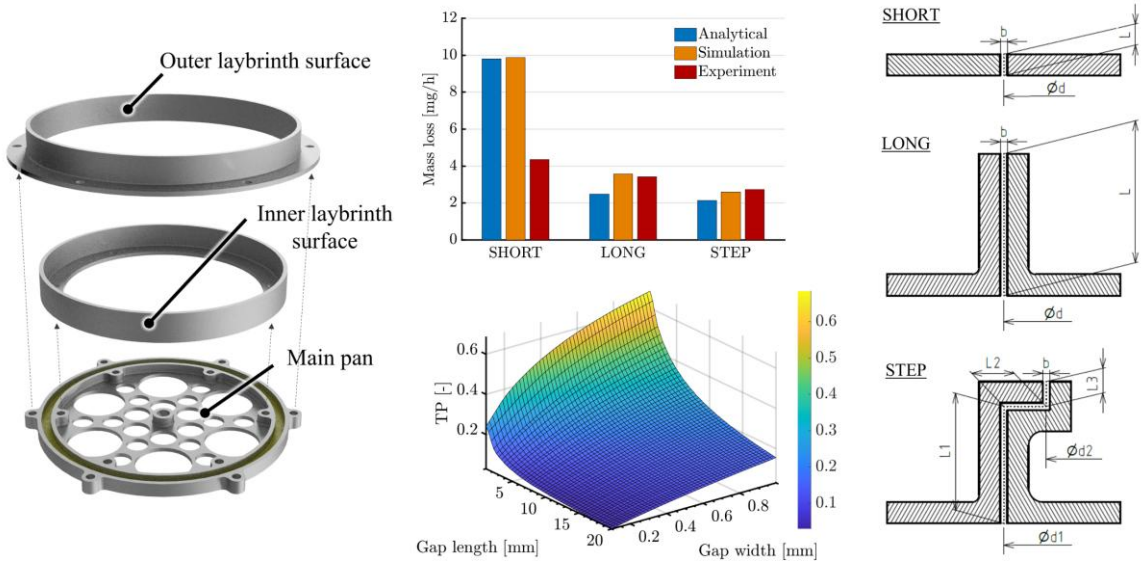

Fig. 2 Labyrinth seal configurations and comparison of analytical, simulation and experimental evaporation losses [2]

PAPER [3]

INFLUENCE OF SURFACE ROUGHNESS ON MOLECULAR FLOW THROUGH LABYRINTH SEALS FOR SPACE APPLICATIONS

Authors: Pouzar J., Kostal D., Westerberg L.G., Nyberg E., Polacek T., Jurik K., Krupka I.

Journal: Results in Engineering, Volume 28, 2025

Content: This study explores the influence of surface roughness on molecular flow through two-dimensional labyrinth seals operating under ultra-high vacuum conditions. Using synthetic roughness profiles and Monte Carlo simulations, the transmission probability of evaporated lubricant molecules is evaluated across varying surface and geometric parameters. Results reveal a strong inverse, nonlinear relationship between surface roughness and molecular transmission, particularly evident in narrow and elongated seals. A second-order correction model based on average roughness (Ra) is proposed and validated against experimental data, achieving prediction errors below 5.1%. The findings demonstrate that increasing surface roughness can enable a 35–40% reduction in channel length or increase in gap width without degrading sealing performance. This highlights the potential of controlled surface texturing as a practical design tool for optimizing seal compactness and manufacturability in space applications.

Author contribution:

Pouzar J.: Conceptualization, Data Curation, Formal Analysis, Funding acquisition, Investigation, Methodology, Project administration, Software, Validation, Visualization, Writing – Original Draft. **Kostal D.:** Conceptualization, Supervision, Writing – Review & Editing. **Westerberg L.G.:** Conceptualization, Supervision, Writing – Review & Editing. **Nyberg E.:** Conceptualization, Methodology, Writing - Review & Editing. **Polacek T.:** Validation, Methodology, Writing – Original Draft. **Jurik K.:** Software, Data curation, Writing – Review & Editing. **Krupka I.:** Funding acquisition, Resources, Supervision.

Published by: Elsevier Ltd., *https://doi.org/10.1016/j.rineng.2025.107905*

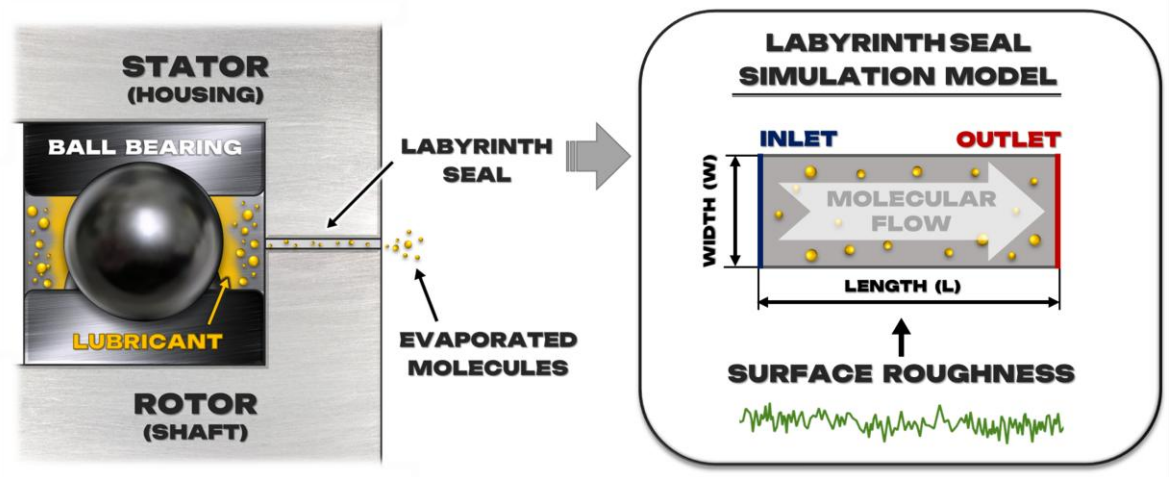

Fig. 3 Ball bearing with labyrinth seal and simulation of molecule transport over rough surfaces [3]

PAPER [4]

LABYRINTH SEAL DESIGN FOR ENHANCED SEALING OF EVAPORATED LUBRICANT MOLECULES IN SPACE MECHANISMS

Authors: Pouzar J., Kostal D., Westerberg L.G., Krupka I.

Journal: 21st European Space Mechanisms and Tribology Symposium (ESMATS), European Space Agency (ESA), Lausanne, 2025

Content: This conference paper presents an integrated summary of previous work on lubricant evaporation in vacuum and extends it with new findings on electrostatic field effects and rotational dynamics in labyrinth seals. The study combines experimental measurements, analytical modelling, and advanced simulations to evaluate how geometric features, surface roughness, and operating conditions influence molecular transport. A custom test rig with embedded electrodes was developed to assess the role of electrostatic fields, revealing modest reductions in evaporative loss for polar and ionic lubricants. Additionally, a rotating seal test system and dynamic simulations demonstrated that seal rotation decreases transmission probability in longer and stepped geometries. These results confirm that both electrostatic and dynamic influences can further improve seal effectiveness and should be considered in the design of tribological components for space applications.

Author contribution:

Pouzar J.: Conceptualization, Data Curation, Formal Analysis, Funding acquisition, Investigation, Methodology, Project administration, Software, Validation, Visualization, Writing – Original Draft. **Kostal D.:** Conceptualization, Supervision. **Westerberg L.G.:** Conceptualization, Supervision. **Krupka I.:** Funding acquisition, Resources.

Published by: European Space Agency (ESA) as part of the proceedings of the 21st European Space Mechanisms and Tribology Symposium (ESMATS), 2025

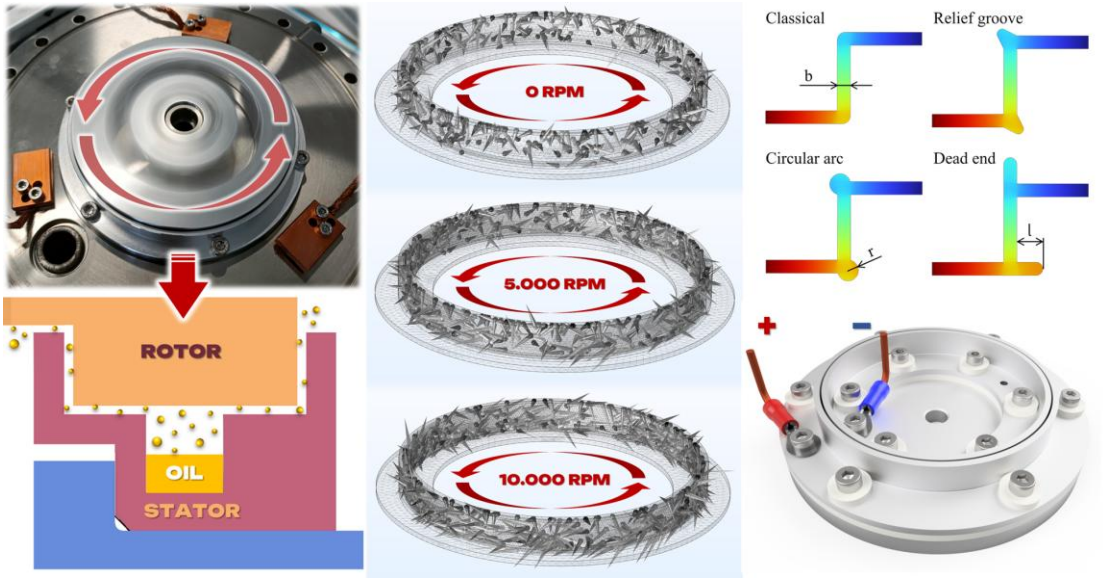

Fig. 4 Operational influences on labyrinth seal performance [4]

ABBREVIATIONS AND SYMBOLS

$A(W, L)$, $B(W, L)$, $C(W, L)$	Polynomial coefficients
$A_{i,j}$, $B_{i,j}$, $C_{i,j}$	Indexed polynomial coefficients
A, A_{or}	Area of orifice [m^2]
b	Labyrinth gap width [mm]
b_{cm}	Labyrinth gap width [cm]
b_m	Labyrinth gap width [m]
b_s	Spectral exponent [–]
C_{duct}	Conductance of duct [m^3/s]
C_{or}	Conductance of orifice [m^3/s]
CERN	The European Organization for Nuclear Research
CMG	Control moment gyroscope
d_{cm}	Diameter of annular seal [cm]
d_{eq}	Equivalent diameter [mm]
DLTR	Dynamic labyrinth test rig
dM/Adt	Evaporation rate per area [$kg/(m^2 \cdot s)$]
dm_{evap}/Adt	Evaporation rate per area [$g/(cm^2 \cdot s)$]
DOLLS	Database of liquid lubricants
dV/dt	Pumping speed [m^3/s]
ECSS	European Cooperation for Space Standardization
EHD	Elastohydrodynamic
ELTR	Electrostatic labyrinth test rig
EMC	Electromagnetic compatibility
EMIM-TFSI	1-ethyl-3-methylimidazolium bis (trifluoromethyl sulfonyl) imide
ESA	European Space Agency
ESD	Electrostatic discharge
ESMATS	European Space Mechanisms and Tribology Symposium
ESTL	European Space Tribology Laboratory
ETR	Evaporation test rig
g, $g(n)$	Gaussian random function
H	Enthalpy (heat) of vaporization [J/mol]
IL	Ionic liquid
k	Boltzmann constant [$m^2 \cdot kg/(s^2 \cdot K)$]
Kn	Knudsen number [–]

l	Recess depth [mm]
L	Corridor length [mm]
L_{cm}	Labyrinth gap length [mm]
L_m	Effective length [m]
LEO	Low Earth Orbit
LTR	Labyrinth test rig
M	Molar mass [kg/mol]
M_g	Molar mass [g/mol]
MAC	Multiply-alkylated cyklopentan
MoS_2	Molybdenum disulfide
N	Spatial frequency resolution [–]
n	Spatial frequency [–]
IMIM_TFSI	1-octyl-3-methylimidazolium bis (trifluoromethyl sulfonyl) imide
P, P_1, P_2	Pressure [Pa]
P_{mbar}	Fluid vapor pressure [mbar]
p_p	Partial pressure in the gas [Pa]
$P_s(T)$	Temperature dependent vapor pressure [mbar]
p_v	Liquid vapor pressure [Pa]
p_1, p_2	Vapor pressure [mbar]
PAO	Polyalphaolefin
PC	Parametric curve scaling factor [–]
PFPE	Perfluoropolyether
PTFE	Polytetrafluoroethylene
Q	Mass flow [kg/s]
Q_T	Throughput [m^3·Pa/s]
QCM	Quartz Crystal Microbalance
R	Universal gas constant [J/(mol·K)]
r	Circular arc radius [mm]
Ra	Arithmetic mean roughness [µm]
Rk	Core roughness depth [µm]
Rku	Kurtosis
Rpk	Reduced peak height [µm]
RPM	Rotational speed [1/min]
Rq	Root mean square roughness [µm]
Rsk	Skewness
Rvk	Reduced valley depth [µm]

RW	Reaction wheel
Sa	Arithmetic mean height [µm]
SADM	Solar array drive mechanism
Sdr	Developed interfacial area ratio [%]
SHC	Synthetic hydrocarbon
SOT	Spiral Orbit Tribometer
Sq	Squared mean height [µm]
T, T_1, T_2	Temperature [K]
TP	Transmission probability [–]
TPMC	Test-particle Monte Carlo
u, u(n)	Uniform random distribution
UHV	Ultrahigh vacuum
V, V_1, V_2	Volume [m^3]
v_{mean}	Mean molecular speed [m/s]
W	Width [mm]
x	Spatial coordinate [mm]
z, z(x)	Roughness profile height [mm]
α	Correction factor [–]
ΔP	Pressure differential [Pa]
λ	Mean free path [m]
ρ	Gas density [kg/m^3]

TABLE OF CONTENT

1 INTRODUCTION

1.1 BACKGROUND

Space technology operates under extremely demanding conditions such as intense vibrations, extreme operating temperatures, ultrahigh (UHV) to extreme vacuum, and prolonged periods of inactivity [5–7]. Most mechanisms and mechanical components in space systems are non-redundant, primarily due to strict mass and size limitations imposed by the requirements for launching objects into orbit. As a result, every mechanism represents a potential single point of failure that can compromise the entire space mission [8].

Over the past several decades, the role of tribology in space mechanisms has grown in importance as space missions have become more complex, long-lasting, and reliant on moving mechanical assemblies [9–11]. From antenna deployment systems and reaction wheels to robotic arms and planetary landers, space hardware relies on precise mechanical motion that must operate reliably without the possibility of maintenance or re-lubrication [12–16]. Unlike terrestrial applications, space mechanisms must function reliably in environments with no atmospheric pressure, which precludes convective heat transfer and allows volatile components to escape easily through evaporation [17–22]. Moreover, the effects of radiation, micrometeoroid impacts, and outgassing further complicate the long-term stability of lubricant performance [10,23,24].

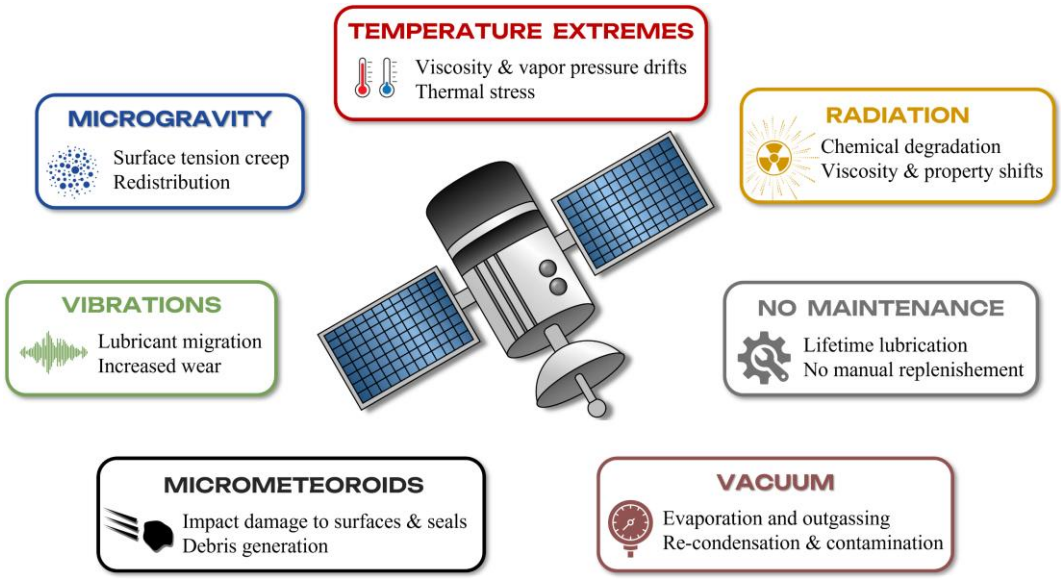

Fig. 5 Space environment factors affecting lubrication

A major contributor to premature mission failure involves tribological problems [5,9,25,26]. These typically stem from catalytic degradation of lubricants, wear of contact surfaces, and vacuum-induced evaporation of liquid lubricants [5,24–30]. Addressing these issues is critical not only for improving reliability but also for reducing economic and environmental costs and minimizing the generation of additional space debris [23,31].

To ensure the reliable operation of mechanical systems in space, friction between contact surfaces must be carefully controlled, typically using solid or liquid lubricants [13,32–35]. These lubricants may be applied individually or in hybrid configurations, where a liquid lubricant is layered over a thin film of solid lubricant to combine the advantages of both approaches [36,37]. The use of lubricants in space systems is inherently constrained by the extreme and multifaceted conditions encountered in orbit [13,38]. Solid lubricants are thermally stable and non-volatile, but their use is limited by finite lifespans and unsuitability for high cycle or continuous motion components [13,33–35,39,40]. In contrast, liquid lubricants offer replenishable films, lower friction in hydrodynamic regimes, and better thermal conductivity [34,41–47], but they are prone to degradation, especially under vacuum and temperature extremes [5,29,32].

Vacuum induced evaporation is among the most critical limitations [48–50], occurring when ambient pressure falls below the lubricant's vapor pressure. Elevated temperatures accelerate this effect through molecular decomposition [30], while low temperatures increase viscosity and impair lubricant function [25,32,38,51]. These phenomena degrade mechanical performance and elevate failure risk. Though several analytical models aim to predict evaporation rates [27,32,49], many rely on idealized assumptions. Therefore, experimental validation is crucial to refine their accuracy and applicability [48,52,53].

Evaporated molecules may also contaminate sensitive components unless restrained. To prevent this, non-contact sealing methods, particularly labyrinth seals, are widely used in space mechanisms [5,12,25,27,53–57]. These complex, narrow channels hinder molecular escape, reducing contamination risk in nearby subsystems such as optics, thermal radiators, and precision actuators [58,59]. The seal's effectiveness depends not only on geometric complexity but also on surface roughness, molecular flow regime, and operating conditions [27,32,48,57]. Both analytical and numerical tools are used to model these interactions and design more effective sealing systems [32,49,53].

1.2 MOTIVATION OF RESEARCH

Despite extensive operational experience and several theoretical studies, many aspects of lubricant evaporation in space remain insufficiently characterized. Existing analytical models provide helpful approximations but often diverge from observed behavior under vacuum, especially in realistic environmental conditions.

This dissertation addresses these limitations by developing a dedicated experimental methodology for quantifying lubricant mass loss under UHV conditions. By systematically comparing experimental results with theoretical predictions and numerical simulations, the study supports the refinement and validation of existing evaporation models. Furthermore, the research examines the influence of system design parameters and environmental factors on evaporation behavior, with particular emphasis on molecular transport through sealing structures.

A significant focus of this research is placed on labyrinth seals, which are commonly employed in space systems to restrict the migration of lubricant vapors. Despite their widespread use, a comprehensive understanding of how geometric configuration, surface roughness, and the molecular flow regime influence their performance remains limited. This work integrates experimental measurements, numerical simulations, and analytical modelling to advance insight into the governing mechanisms and to support the development of more effective sealing solutions for space missions of extended duration.

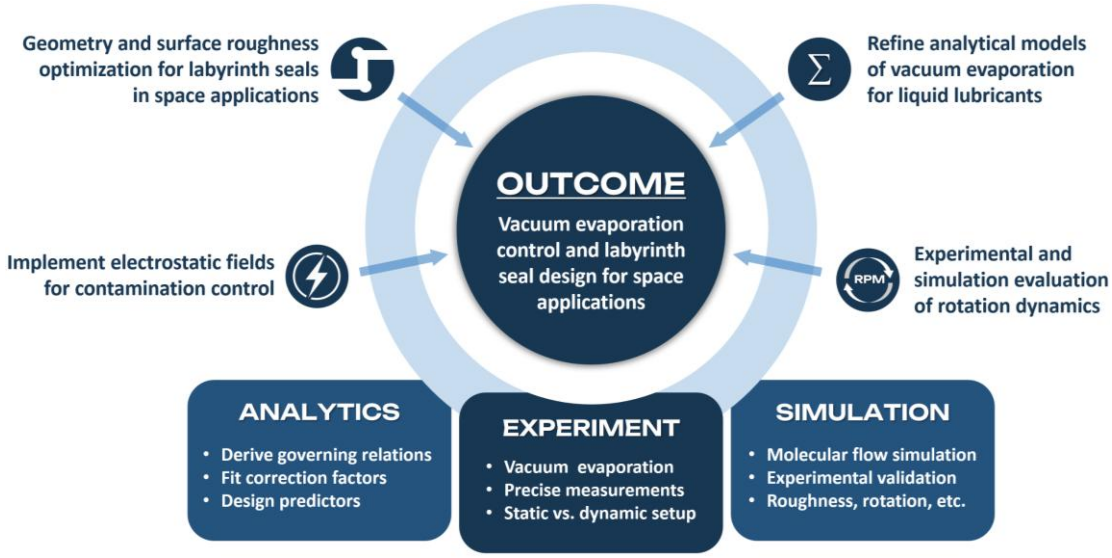

Fig. 6 Integrated approach to evaporation control and seal performance

The outcomes of this research contribute to broader objectives in space system engineering, including improved mission reliability and sustainability. These aspects are increasingly critical given the rapid expansion of satellite constellations and the growing need for long-life, maintenance-free mechanical subsystems.

1.3 SCOPE AND DELIMITATIONS

The primary focus of this dissertation is the evaporation of liquid lubricants under vacuum conditions and the methods available to reduce the resulting mass loss. Solid lubrication strategies are not explored in detail, nor is molecular transport examined under transitional or viscous flow regimes. Instead, the work centers on the development of a custom experimental setup for precise evaporation measurements in a vacuum environment, the validation and refinement of analytical evaporation models, and the simulation of molecular transport through labyrinth seal geometries. Attention is given to how surface roughness, geometric configuration, channel width and length influence the transmission probability of evaporated molecules through these seals. Although the findings aim to inform the design and optimization of vacuum-compatible tribological components, particularly non-contact sealing strategies for space applications, both the simulations and experiments were conducted at the component level rather than on complete assemblies or operational satellite configurations. As such, further extrapolation will be required to apply the results to more complex, integrated space mechanisms.

2 STATE OF THE ART

Reliable operation of space mechanisms depends heavily on effective tribological performance in vacuum, under radiation and across wide temperature ranges. Liquid lubricants are adopted in high cycle and precision space applications, but their behaviour under space relevant conditions differs from those in terrestrial systems. In particular, volatility, chemical degradation and uncontrolled migration can compromise performance and increase the risk of failure.

To mitigate mass loss and contamination, non-contact sealing methods such as labyrinth seals are often integrated into rotating subsystems. These seals restrict molecular transport through narrow and tortuous gaps, and their performance is coupled with flow regime, surface structure and operating conditions. Classical evaporation models and molecular flow relations are used together to estimate lubricant loss and its transport through confined passages.

This chapter summarizes the theoretical and methodological background. It introduces the basic tribological and physicochemical behavior of liquid lubricants in space environments, outlines the main lubricant classes, describes the mechanisms of creep and vacuum evaporation, and presents the fundamentals of testing methods and labyrinth seal modelling.

2.1 LIQUID LUBRICANTS FOR SPACE APPLICATIONS

The use of liquid lubricants in space mechanisms is a fundamental, yet highly demanding aspect of spacecraft design [7,60]. In contrast to terrestrial systems, space environments introduce extreme constraints, including high vacuum, large thermal gradients, radiation exposure, atomic oxygen interactions, and microgravity [6,61–63]. These factors have a significant impact on the physical and chemical behavior of lubricants, making space tribology a technically complex and multidisciplinary field [5,20,25,33].

Reliable lubrication requires an understanding of both tribo-physical and tribo-chemical phenomena that govern friction and wear at the molecular level [22,32,62]. Lubricants must provide sufficient film thickness and load carrying capacity while maintaining chemical stability and compatibility with materials and the external environment [41,42,62]. If lubrication is lost or degraded, mechanisms can suffer increased friction, wear and temperature, and contaminants may be transported to sensitive areas [7,60,64,65].

A key challenge is the volatility of liquid lubricants [48,50,52]. Under vacuum, molecules can leave the liquid phase once the ambient pressure drops below the vapor pressure. This process removes base oil and additives [32,49,66], alters viscosity, changes frictional behaviour, and accelerates wear. Evaporated molecules can re-condense on colder surfaces, including optical or thermal control elements, where even thin films can affect performance [58,59,66].

In addition to evaporation, lubricant migration or creep poses another important issue [23,44,67,68]. Creep refers to capillary driven redistribution of lubricant along surfaces and interfaces. It is influenced by surface tension, viscosity, film thickness, temperature gradients, and surface roughness [67,69]. It may result in lubricant starvation in the contact interface or contamination of surrounding components. To mitigate these risks, lubricants must combine low volatility with stable viscosity across temperature ranges, high surface tension, and resistance to oxidation and radiation, particularly in Low Earth Orbit (LEO) where atomic oxygen is prevalent.

Tribologically, space grade lubricants must operate across multiple lubrication regimes [5,32,38,51]. While elastohydrodynamic (EHD) lubrication is desirable for continuous motion components, such as bearings and gears, many space mechanisms operate intermittently or at low speeds [29,68]. In these conditions, mixed and boundary lubrication regimes are more common. The Stribeck curve describes the transition between these regimes based on the interplay between load, viscosity, and relative surface speed [32,45,51]. In boundary and mixed regimes, the formation of protective tribofilms is essential to reduce friction and surface wear.

2.1.1 OVERVIEW OF TYPES OF LIQUID LUBRICANTS USED

Liquid lubricants for space applications can be broadly categorized into base oils, greases, and advanced synthetic fluids such as ionic or silicic liquids [14,23,49]. Each category exhibits distinct physicochemical and tribological characteristics that influence their performance in vacuum environments, across wide temperature ranges, and under exposure to radiation or atomic oxygen. Because no single lubricant meets all requirements, selection is dictated by the mission profile, operating regime, and component design constraints [41,42,45]. Liquid lubricants used in space tribology can be grouped into [34,42,45,62,70]:

- Mineral oils – typically used in fully sealed mechanisms
- Synthetic hydrocarbons – including polyalphaolefins (PAO) and multiply alkylated cyclopentanes (MAC)
- Perfluoropolyethers (PFPE) – fully fluorinated synthetic oils with low volatility and high chemical inertness
- Silicone oils – polysiloxane-based fluids with low vapor pressure and good low temperature behavior
- Ionic liquids (ILs) – salts that are liquid at or near room temperature, with very low volatility and tunable chemistry

These fluids differ significantly in their molecular structure, volatility, viscosity-temperature behavior, surface energy, and resistance to oxidation or radiation [13,43,45,62]. Their suitability for specific applications depends on how well they perform under the lubrication regime encountered (hydrodynamic, elastohydrodynamic, mixed, or boundary), as well as their ability to maintain chemical and physical integrity under thermal, mechanical, and vacuum stress [41,42,44,45].

a. Mineral oils

Mineral oils have been widely used in terrestrial applications due to their effective boundary lubrication and good compatibility with additives [29,32,51]. In space systems, their use is limited by relatively high vapor pressure, which restricts them to fully sealed components [32,51,60]. Space grade mineral oils are typically super refined to remove volatile fractions and impurities, improving their stability and reducing outgassing [32,62]. They remain a viable option for sealed subsystems such as momentum wheels, where their well characterized behavior and wide viscosity range offer reliable performance [5,16,32,60].

b. Synthetic hydrocarbons (SHCs)

This category includes polyalphaolefins (PAO) and multiply alkylated cyclopentanes (MAC), both of which are designed to provide controlled viscosity–temperature behaviour and lower vapor pressure than typical mineral oils [13,25,32,64,71]. PAOs are synthesized through the oligomerization of alpha-olefins and provide good thermal properties, chemical stability, and lower vapor pressure, but their use in space remains limited, primarily to sealed systems or less demanding environments [5,13,32,62]. In contrast, MAC lubricants are specifically engineered for space applications, synthesized by alkylating cyclopentadiene followed by hydrogenation, allowing their molecular structure to be tailored for desired viscosity, volatility, and oxidative resistance [23,32,34,68]. Their high surface tension reduces creep risk, while low evaporation rates ensure reliable performance in vacuum. MACs also provide good wear resistance and maintain thermal and radiation stability in boundary or mixed lubrication regimes [27,32,48,49].

c. Perfluoropolyethers (PFPE)

PFPEs, marketed under names like Fomblin™, Krytox™, or Brayco™, are widely adopted due to their low vapor pressure, high viscosity index, and resistance to oxidation and radiation [13,36,62,72]. They perform well under hydrodynamic and EHD regimes, especially in continuous-motion bearings [14,32,37]. However, their low surface tension makes them susceptible to creep migration. Mitigation strategies include surface treatments or the addition of nanoparticles and fluorinated additives to suppress unwanted spreading [10,36,40,67].

d. Silicone oils

Silicone oils were commonly used in early space applications due to their low vapor pressure, excellent low temperature performance, and high viscosity index [13,32,60,62,65]. Silicone oils may show poor creep resistance and can degrade under boundary lubrication, leading to polymer like deposits on contact surfaces and contamination of nearby components [22,32,62]. Additionally, silicone vapors can condense on nearby components, contaminating sensitive elements such as optical surfaces or electrical contacts [32,58,64,73]. They are considered for non-load bearing applications, such as damping fluids.

e. Ionic liquids (ILs)

ILs are composed entirely of cations and anions and remain liquid over wide temperature ranges. Their ultra-low volatility, high thermal stability, and non-flammable nature make them promising candidates for future space lubrication [43,45,68]. However, their performance is highly sensitive to molecular structure, which can lead to unpredictable crystallization or decomposition under certain conditions [43,45,70]. Tribochemically, they can form low friction films, but their potential to induce corrosive wear must be addressed through careful formulation [15,25,45,46]. Ionic liquids may not exhibit thermally driven creep under temperature gradients, a behavior attributed to interfacial ion ordering and strong Coulombic interactions [74].

In practice, lubricant selection for space mechanisms requires balancing competing properties: low volatility, thermal and oxidative stability, surface tension, viscosity behavior, and tribofilm formation potential. Hybrid lubrication strategies that combine liquid and solid components (e.g., MAC or PFPE oils over MoS_2 or PTFE coatings) are often employed to exploit complementary strengths [32,35,36,40]. As space missions extend in duration and complexity, the development of tailored lubricants, particularly ILs and nanostructured formulations, is becoming an increasingly active area of research [25,45,62,70].

2.1.2 CREEP AND SURFACE MIGRATION

In space applications, creep refers to the gradual migration of liquid lubricants along solid surfaces, often away from the intended contact area. This phenomenon is driven by capillary forces and occurs along material interfaces or surface topographies (see Fig. 7) [42,64,75]. Key parameters influencing creep behavior include surface tension, lubricant viscosity, film thickness, temperature gradients, and surface roughness [38,67,69].

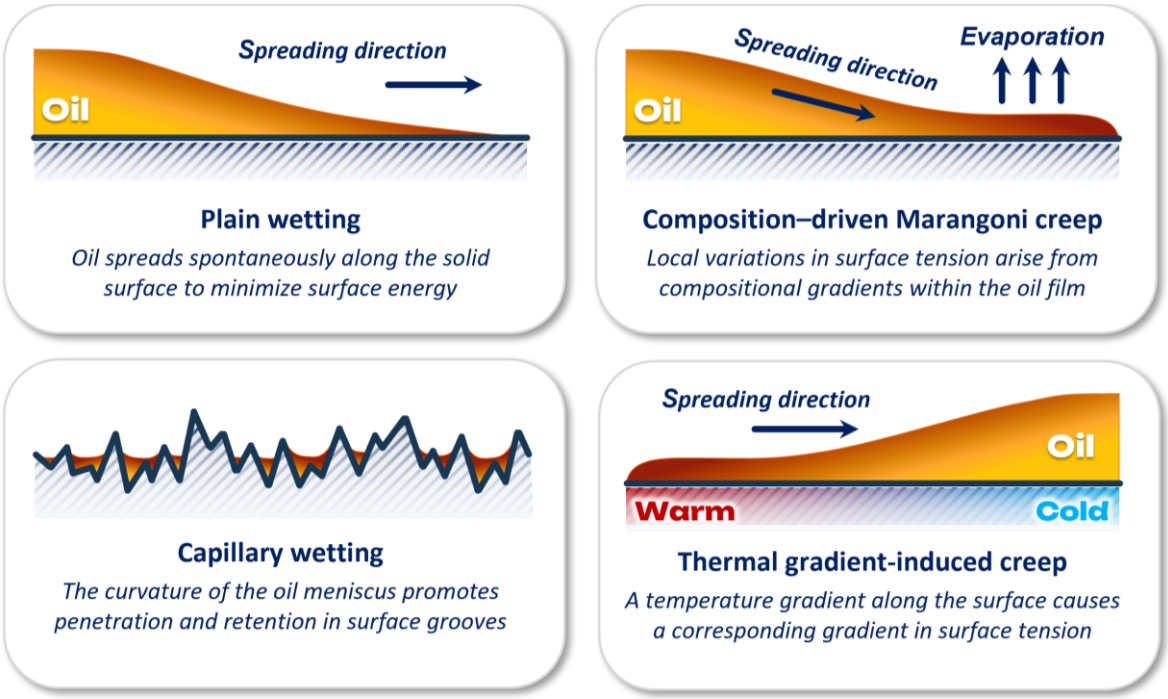

Fig. 7 Mechanisms of lubricant creep along solid interfaces

Creep can severely affect the reliability of tribological systems in space by depleting the lubricant at the contact interface, contaminating nearby components, and compromising sealing performance. In sensitive systems, this may lead to increased wear, optical degradation, or electrical failures [38,41,42,75]. Various measures are used to limit migration, including [41,69,75]:

- Surface barriers such as grooves or steps near the lubricated area
- Coatings with lower surface energy applied to adjacent regions to reduce wetting
- Tailored surface textures that guide or block liquid flow

Surface treatments designed to inhibit lubricant migration typically employ materials with low surface energy, applied near the lubricated zones to prevent capillary spreading [69]. Studies have shown that thin hydrocarbon films in vacuum can migrate under thermal gradients (see Fig. 8) at rates comparable to those observed under atmospheric conditions [19,75]. These thermal gradients may arise from frictional heating at the contact interface or from evaporation induced heat transfer, both of which can generate Marangoni stresses that promote surface flow [52,69,76].

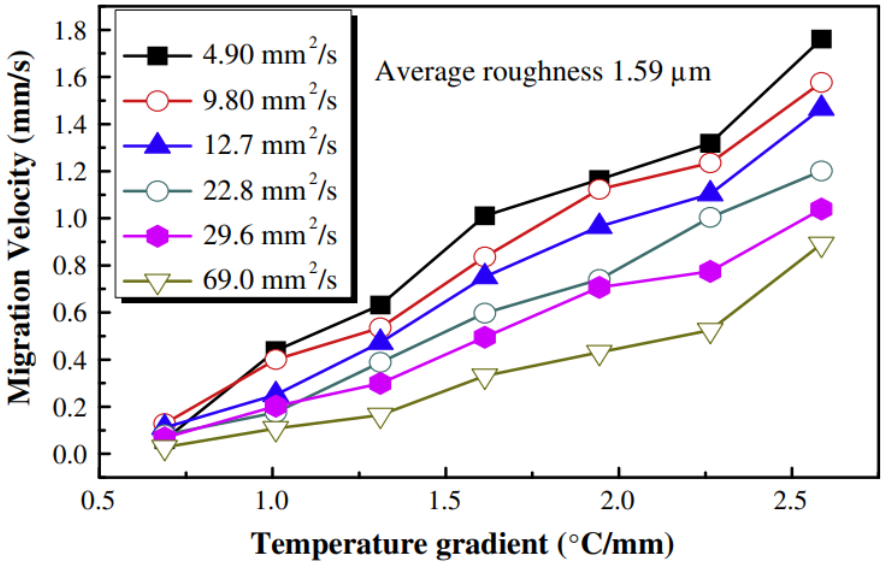

Fig. 8 Influence of oil viscosity and thermal gradient on migration rate [69]

Surface topography plays a critical role in determining the direction and intensity of lubricant creep, especially for low viscosity oils [19,52,75]. Grooves resulting from directional grinding can either hinder or facilitate lubricant migration depending on their orientation relative to the temperature gradient [69,77,78]. Experimental results demonstrate that under a certain threshold gradient, lubricants can cross grooves and continue to migrate in the direction of thermal stress [69]. These findings underscore the importance of surface engineering in controlling lubricant distribution within space mechanisms.

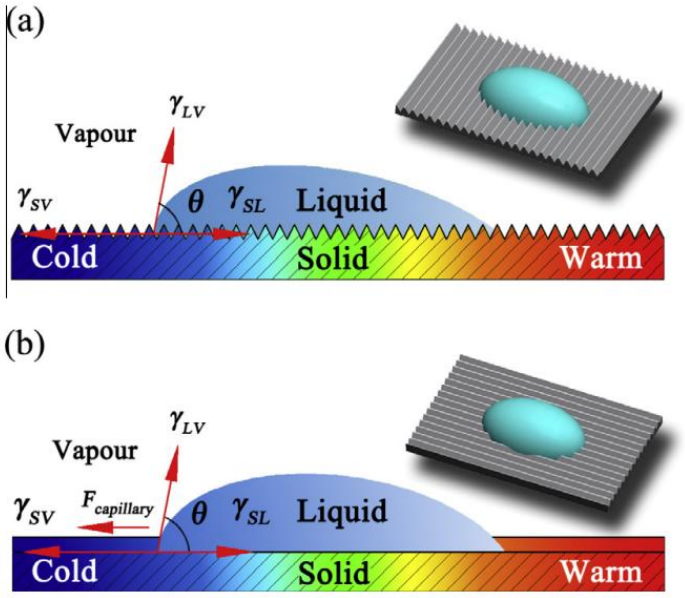

Fig. 9 Interfacial tension at the three-phase contact line of a droplet on a ground surface: (a) grinds perpendicular, (b) grinds parallel to the temperature gradient [69]

2.1.3 VACUUM EVAPORATION

Vacuum induced evaporation is one of the primary challenges limiting the long-term use of liquid lubricants in space mechanisms [5,22,32,58,79]. When ambient pressure drops below a lubricant's vapor pressure, its constituent molecules begin to escape from the liquid phase into the surrounding vacuum [27,32,49]. This process results in the gradual depletion of base oil and additives, which alters viscosity, reduces film thickness, and accelerates wear or failure at lubricated contacts [5,44,60].

The evaporation rate depends on several factors, primarily the lubricant's vapor pressure, temperature, molecular weight, and surface area exposed to vacuum [27,32,49,57]. Low molecular weight components evaporate more easily, so space qualified lubricants are typically formulated with high molecular weight components to improve retention. Evaporation is further influenced by environmental and design related factors [32,57]. For instance, thermal gradients within components can increase local evaporation by raising lubricant temperature or inducing phase separation [5,32,60]. In practice, evaporated molecules may migrate through molecular flow and re-condense on colder surfaces [32,44], leading to contamination of optics, sensors, or thermally sensitive elements [58,59,66]. Such contamination is usually irreversible and can severely degrade system performance, especially in precision applications.

To estimate lubricant mass loss under vacuum conditions, the Langmuir equation (see Eq.1) is frequently employed as an analytical model to describe the flux of vapor molecules from a liquid surface into vacuum [32,50,80]. This model, originally developed for monoatomic metallic evaporation, defines the evaporation rate per unit area as:

$$\frac{dM}{Adt} = \left(p_v - p_p\right)\sqrt{\frac{M_m}{2\pi kT}} \quad (1)$$

Once lubricant molecules evaporate into the surrounding vacuum, they are irreversibly lost from the liquid phase [44]. These molecules often re-condense on colder surfaces within the system, potentially contaminating sensitive components [32,44]. Although the Langmuir equation provides a useful first order approximation, its applicability to space lubricants is limited. The model assumes ideal behavior of non-interacting gas molecules, which neglects complexities such as polar molecular interactions, multicomponent formulations, and real surface effects [50,53,81].

In practical applications, the partial pressure p_p is typically considered negligible. This is due to the extremely long mean free path of vapor molecules in high or ultrahigh vacuum, which prevents intermolecular collisions and renders direct pressure measurements unfeasible [44,49]. However, even small uncertainties in the input parameters, particularly vapor pressure and temperature, can result in significant deviations between calculated and experimentally measured evaporation rates [32,49,82]. Additional discrepancies arise from assumptions about uniform temperature distribution, neglect of surface roughness, and limited knowledge of the lubricant's thermal history [49].

Despite its limitations, Langmuir's equation continues to be used in a modified form. Current trends focus on empirical correction factors derived from experimental data rather than replacing the model entirely [48,49,82]. For instance, the European Space Tribology Laboratory (ESTL) has introduced a modified expression to better reflect evaporation behavior of space grade lubricants:

$$\frac{dm_{evap}}{dt} = -0.044\, P_s(T)\sqrt{\frac{M}{T}} \quad (2)$$

Since vapor pressure is highly temperature dependent, it must either be measured experimentally at relevant temperatures or estimated using thermodynamic approximations. One commonly used method [66,83] is the Clausius-Clapeyron equation:

$$\ln\frac{p_2}{p_1} = \frac{H}{R}\left(\frac{1}{T_1} - \frac{1}{T_2}\right) \quad (3)$$

This equation is particularly useful for estimating vapor pressure in the absence of comprehensive manufacturer data. By using two known pressure–temperature pairs, the enthalpy of vaporization can be determined and used to extrapolate evaporation rates for operating conditions [66,83]. It is important to note, however, that the enthalpy value itself may be affected by the lubricant's thermal history, especially the presence of residual latent heat (see Fig. 10) [66].

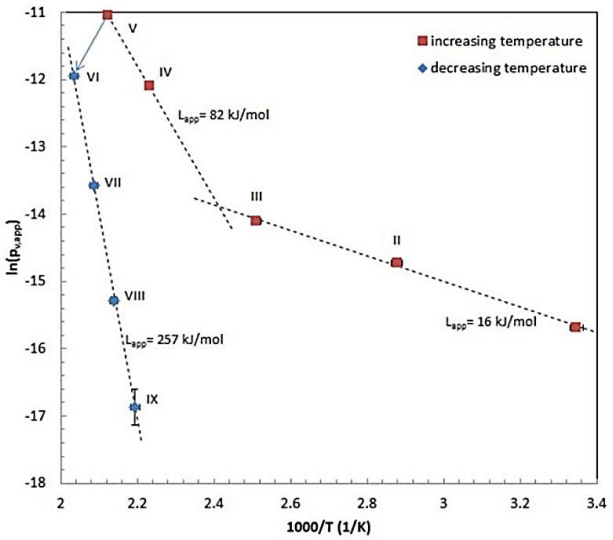

Fig. 10 Difference in the latent heat of a substance during heating (red) and cooling (blue) [66]

Testing and qualification of lubricant evaporation in space applications are governed by ECSS (European Cooperation for Space Standardization) standards [17,61,84]. These documents provide unified procedures and requirements for European space programs, including the preparation, handling, and evaluation of lubricants in evaporation experiments. Standardized methodologies are essential for generating reliable, comparable data across different mission scenarios and lubricant types.

2.1.4 EVAPORATION AND CONDENSATION CONTAMINATION

Evaporation of liquid lubricants in vacuum environments poses a serious contamination risk to nearby spacecraft subsystems, particularly optical and sensor components [59]. Migrated molecules can condense on surfaces (see Fig. 11) such as lenses, radiators, or solar cells, degrading optical transmittance, altering thermal radiative properties, and increasing stray light or temperature imbalances [17,61,84]. Past studies [30,58,59,66,85] have shown that even thin films of contaminant vapors can lead to measurable degradation in instrument performance, which is especially critical for precision optical missions like space telescopes.

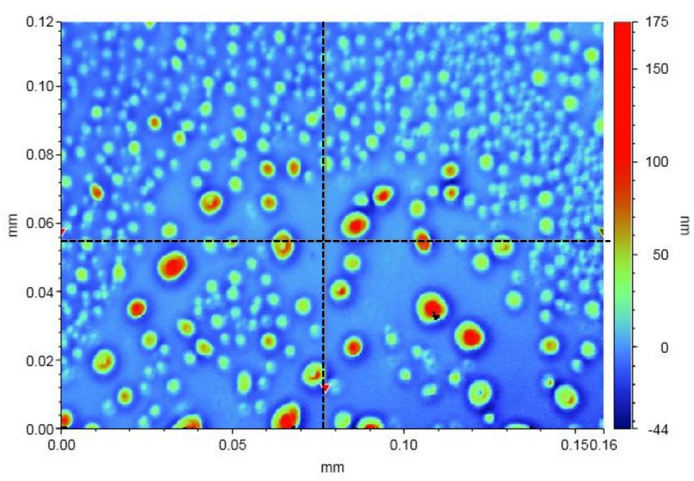

Fig. 11 Condensation of evaporated PFPE lubricant droplets on sapphire window under vacuum conditions

Accurate measurement of molecular contamination is vital. Quartz Crystal Microbalance (QCM) sensors are widely in ground testing to monitor nanoscale mass deposition due to outgassing and vapor condensation [6,66,84,86]. Thermal cycling and bake out tests are also performed to simulate both the deposition and potential removal of contaminants through controlled heating [81,84,87]. These experimental methods help validate analytical evaporation models and provide insight into re-emission behavior over time, supporting more reliable predictions of contamination buildup in operational systems.

Design level mitigation strategies play an equally important role in minimizing contaminant impact. Physical shielding techniques, such as baffles and carefully designed venting paths, help redirect evaporated vapors away from critical optical areas [6,12,54,84]. Spacecraft component layout and orientation can be optimized to avoid trapping contaminants near sensitive regions [88,89].

Emerging research directions aim to strengthen contamination control further [59,88]. Simulation tools that model molecular flow, deposition, and re-emission in realistic spacecraft geometries are being developed to support dynamic contamination risk assessment [90–92]. There is also growing interest in real time monitoring systems which could support adaptive mitigation strategies during mission [93,94].

2.2 TESTING METHODS FOR LIQUID LUBRICANTS IN SPACE APPLICATIONS

Testing methods for liquid lubricants intended for space environments can generally be classified into two main categories [44,95]. The first involves testing lubricants under full operational conditions, using vacuum chambers and thermal environments that simulate real mission profiles over extended durations [10,16,23,63]. These tests yield high fidelity data on lubricant performance but are time consuming and expensive. The second category includes accelerated testing, where extreme boundary conditions (e.g., elevated temperatures, mechanical loads, or speeds) are applied to shorten testing durations [20,30,95]. While more efficient, these tests may introduce behavior deviations, as the lubricant response under such conditions does not always reflect actual in-orbit behavior. This section reviews three key areas of testing: tribological evaluation, vapor pressure determination, and methods for quantifying evaporative losses.

2.2.1 TRIBOLOGICAL TESTING

Tribological testing under simulated space conditions is essential to evaluate friction, wear rate, lubricant consumption, and environmental influences [5,32,38,60]. These tests are generally classified as accelerated methods. Component level testing (e.g., bearings, gears) offers realistic results but at the cost of longer durations [44,73,95]. More practical alternatives include dedicated tribometers capable of simulating boundary lubrication regimes with small lubricant quantities [71,96,97].

One of the most widely used platforms is the Spiral Orbit Tribometer (SOT), which simulates angular contact bearing motion and monitors lubricant degradation and friction under vacuum [15,34,97]. The test operates in boundary lubrication with a steel ball constrained between two surfaces, rotating under axial load (see Fig. 12).

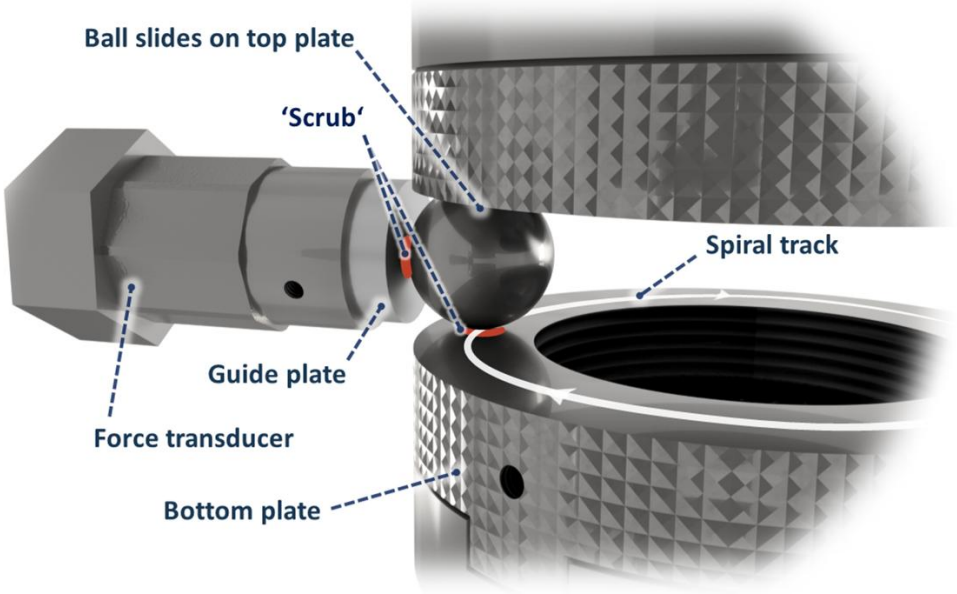

Fig. 12 Schematic of the spiral orbit tribometer (SOT)

A force sensor tracks ball movement, allowing real-time friction coefficient calculation [42,97]. Results are typically presented as friction vs. cycle count (see Fig. 13). Accelerated versions of the SOT protocol have also been developed to reduce test duration [15].

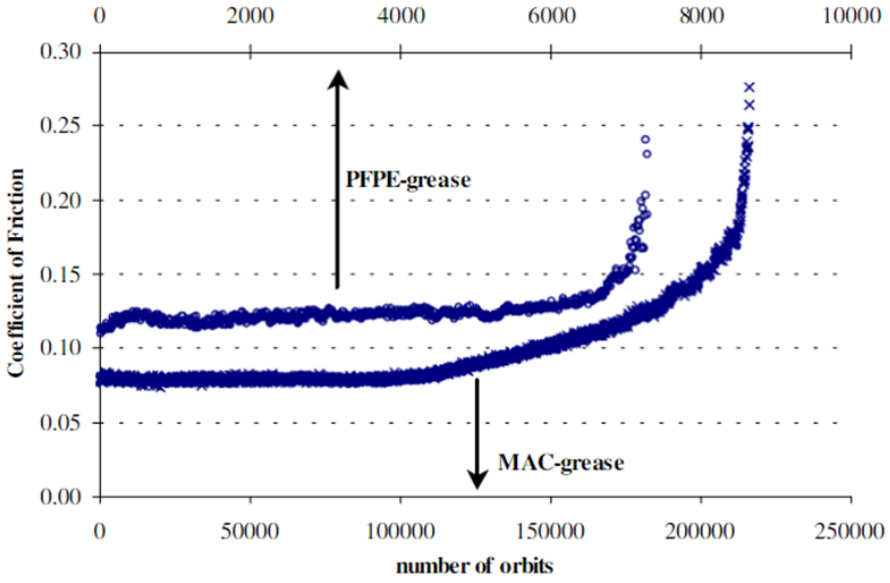

Fig. 13 Comparison of friction coefficients for two grease types measured using the SOT method [15]

Other tribometers include vacuum compatible four-ball testers and pin-on-disc or pin-on-plate configurations, which are gaining interest due to their flexibility and ability to simulate surface wear under controlled conditions [46,73,96,98]. These tests are also useful in studying lubricant evaporation indirectly, especially when operated under vacuum.

2.2.2 VAPOR PRESSURE DETERMINATION

Vapor pressure is a key parameter governing lubricant evaporation under vacuum conditions [32,49,99]. Accurate determination of this property is essential for predicting long term lubricant loss in space environments. While lubricant manufacturers commonly measure vapor pressure for quality assurance, the most widely adopted laboratory method remains the Knudsen effusion technique [48,100,101]. This approach involves quantifying the mass of material lost through a small, calibrated orifice into a vacuum chamber and calculating the vapor pressure from this rate of effusion (see Fig. 14) [47,102]. QCM sensors are typically employed to monitor mass changes, relying on shifts in the resonance frequency of a quartz crystal to detect deposition of evaporated molecules [47,86,103].

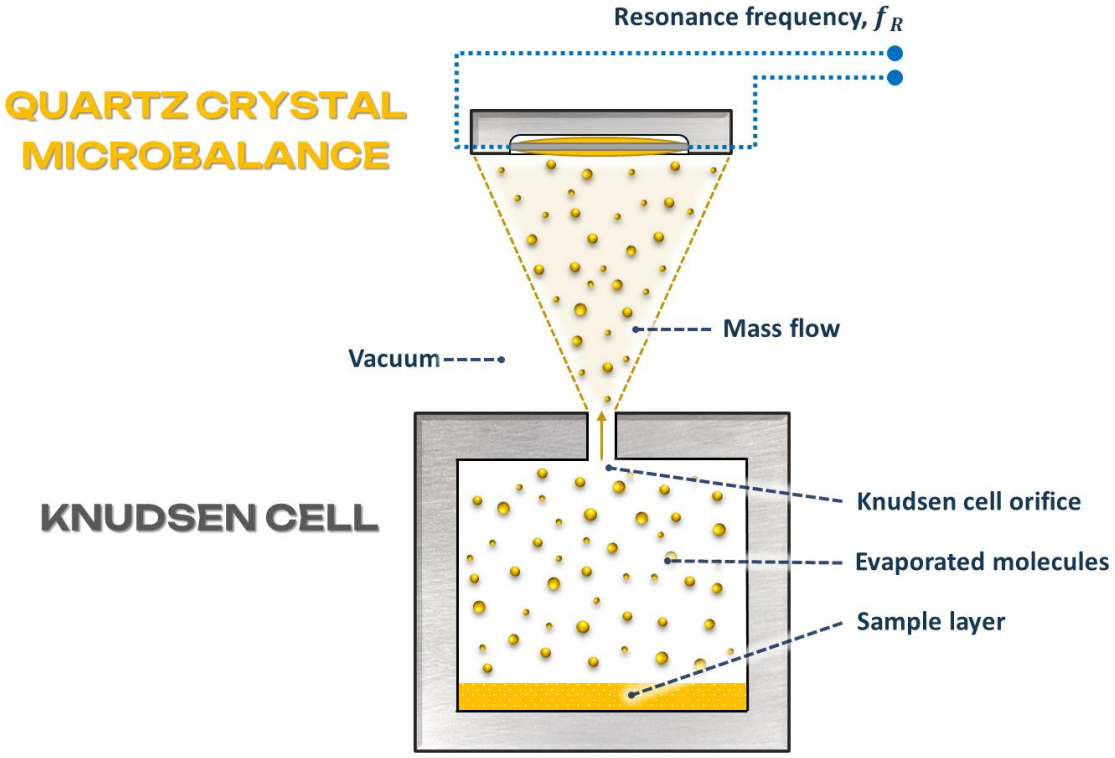

Fig. 14 Knudsen effusion method

However, a major limitation of the Knudsen method is the lack of international standardization, which leads to inconsistencies between laboratories [48,49]. As a result, vapor pressure values provided by manufacturers are best treated as indicative estimates rather than precise, application relevant constants. Studies [66,99,100,102] have shown that vapor pressure is not static over time, especially under varying thermal conditions. This temporal dependence introduces significant errors into analytical predictions, unless correction factors are implemented [53,54]. To address this, vacuum stripping is sometimes used as a pre-treatment method to remove low molecular weight volatile fractions prior to lubricant deployment in space mechanisms [53,104]. This can help stabilize lubricant composition and reduce initial evaporation spikes.

An alternative approach involves modified Langmuir based methods, which are experimentally easier to apply under boundary lubrication without inducing creep effects [48,49]. This method has similarities to Knudsen's setup and provides consistent results under controlled temperature (see Fig. 15). Studies confirm that while Langmuir models predict evaporation rates proportional to vapor pressure and temperature, they often overestimate real evaporation by several orders of magnitude, particularly in complex fluids such as lubricants [48,49,105].

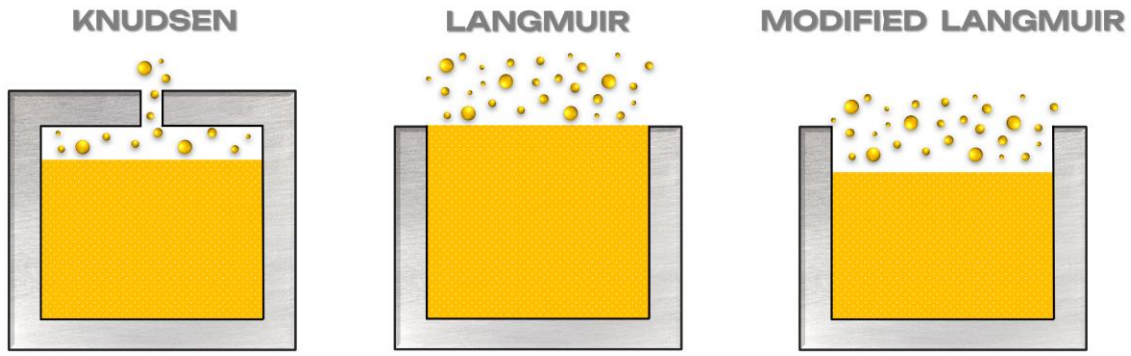

Fig. 15 Representation of experimental methods for testing the vapor pressure of liquid lubricants

Further developments in this field have been supported by ECSS standards, which define several certified procedures for accelerated vapor pressure testing using QCM based methods [17]. These experiments are typically complemented by gravimetric measurements before and after testing, ensuring cross validation of the evaporative mass loss [17,32,82]. Despite these efforts, none of the existing methods provide continuous, real-time observation of lubricant evaporation throughout the entire testing period. This remains a key limitation and highlights the need for further advancements in experimental techniques capable of monitoring dynamics of evaporation under actual space relevant conditions.

2.3 METHODS TO REDUCE LIQUID LUBRICANT LOSS

Space mechanisms are typically only partially enclosed [54,65], so the applied lubricant is not fully exposed to the space environment. In such semi-sealed designs, additional parameters enter analytical models, including the geometry of flow paths and the transmission probability of evaporated molecules [27,32,54]. The total lubricant amount is usually very small (order of milligrams) and must last for the entire mission, often longer than five years [5,16,32,55]. To prevent tribological failures over these durations, the system must either be continuously supplied with lubricant or incorporate sealing elements that limit mass loss and contamination [58,106,107]. Because seals can themselves become critical failure points, this section reviews practical strategies to reduce lubricant loss and the resulting contamination risk.

2.3.1 LUBRICATION SYSTEMS REPLENISHMENT

A reliable approach is to ensure a controlled supply of liquid lubricant to the contact throughout the mission. Depending on the mechanism, lubrication systems can be categorized as passive or active [10,16,23].

Passive systems feed the contact continuously by centrifugal action or by surface driven migration (creep). The most common solution is the centrifugal oiler, which distributes liquid or grease to the contact region using rotational acceleration [16,23]. Another passive concept uses porous materials (e.g., bearing cages) impregnated with liquid. These structures gradually supply lubricants by capillarity during the mission [14,42,62]. Such porous elements have a long heritage in space and have been widely studied in terms of evaporation, capillary transport, and lubricant circulation [42,55].

Active systems deliver a controlled amount of lubricant in response to external commands or operating conditions. Examples include an external positive-feed unit that dispenses additional lubricant when thresholds are exceeded, or a porous reservoir placed near the contact that releases liquid on demand (see Fig. 16) [23]. A common actuation method is localized heating of the porous element to trigger release [12,55]. While effective, heating introduces several side effects:

1. Differential thermal expansion between the lubricant and the porous matrix can eject liquid abruptly into contact.
2. Thermally driven Marangoni stresses alter surface tension along temperature gradients, promoting migration of liquid toward colder regions.
3. Increased liquid temperature raises vapor pressure and can initiate or accelerate evaporation.

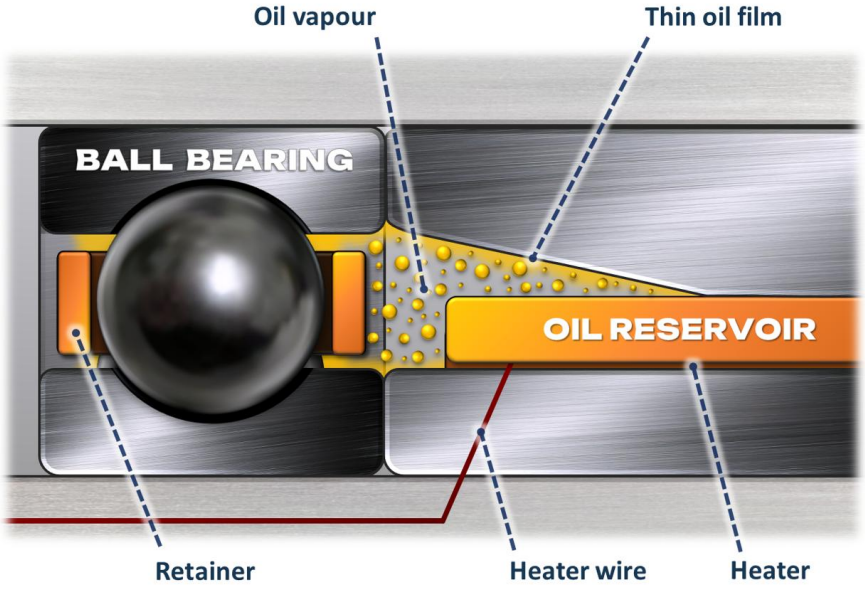

Fig. 16 Schematic of lubricant supply to a ball bearing from porous stationary reservoir

2.3.2 LABYRINTH SEALS FOR SPACE APPLICATIONS

To reduce evaporative losses and protect sensitive subsystems, non-contact labyrinth seals are widely used in space mechanisms [27,32,54]. These seals introduce narrow axial, radial, or combined gaps that separate inner and outer rotating elements and create tortuous escape paths for vapor (see Fig. 17).

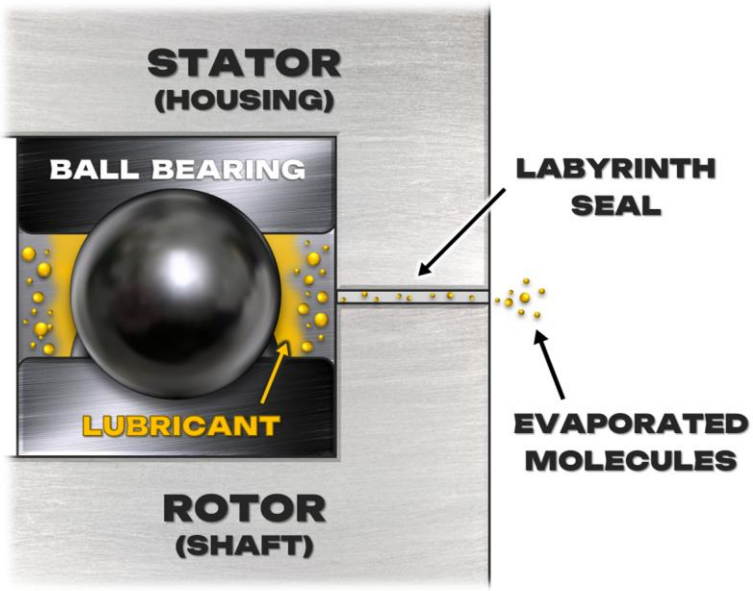

Fig. 17 Schematic of a sealed ball bearing showing labyrinth geometry and escaping vapor molecules

a. Analytical models

Under high vacuum, flow through labyrinth gaps occurs in the free molecular regime, where molecule-wall collisions dominate and intermolecular collisions are rare. The flow regime is characterized by the Knudsen number (Kn) [18,81,87], defined as

$$Kn = \frac{\lambda}{L} \tag{4}$$

where λ is the mean free path and L is a characteristic channel dimension [18,87,108]. The flow is typically continuum (viscous) for $Kn < 0.01$; transitional for $0.01 < Kn < 0.5$; and molecular for $Kn > 0.5$ (see Fig. 18) [18,81,108]. Consequently, the labyrinth gap width is a key design parameter that must balance safe running clearances with the need to restrict flow.

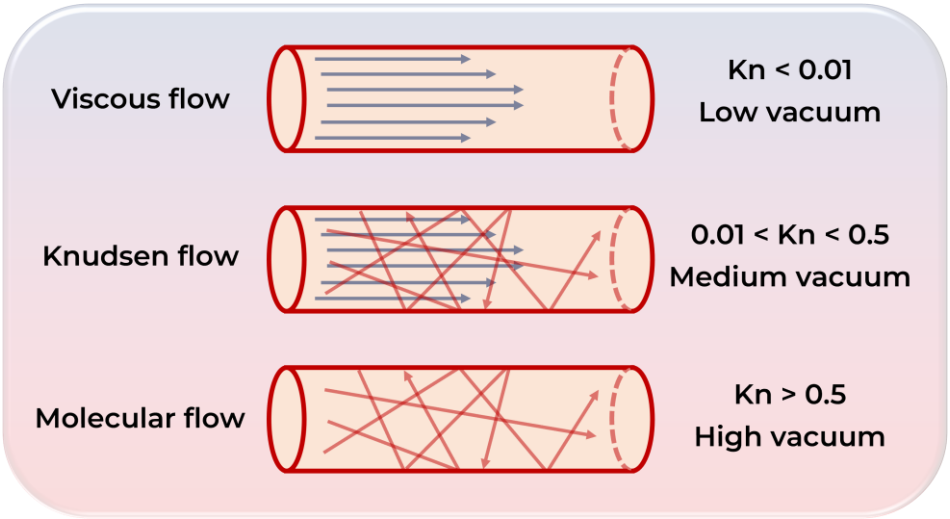

Fig. 18 Flow regime profiles as a function of Knudsen number (Kn)

In molecular flow, the net flux through a confined passage is governed by the transmission probability and the mean molecular velocity [108–111]. In vacuum technology, gas transport is commonly expressed as throughput in pressure-volume units, defined as

$$Q_T = \frac{d(PV)}{dt} = P\frac{dV}{dt} \tag{5}$$

Here, the throughput Q_T represents the power carried by a gas leaving a volume V at volumetric rate (pumping speed) dV/dt and pressure P [18,87,111]. Consider two chambers at pressures $P_1 > P_2$ connected by a duct (see Fig. 19).

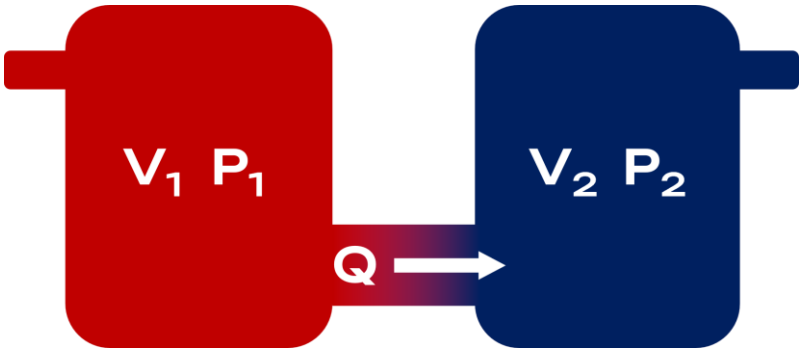

Fig. 19 Gas throughput (Q) between two chambers

The flow depends on the pressure differential $\Delta P = P_1 - P_2$ and the geometry of the connection [18,87,112]. The conductance of that duct is

$$C_{duct} = \frac{Q_T}{P_1 - P_2} = \frac{Q_T}{\Delta P} \tag{6}$$

Under high and ultrahigh vacuum, conductance is effectively independent of pressure. In the transitional and viscous regimes, it becomes dependent on pressure, so C must be evaluated for the appropriate range [18,110,112]. The molecular flow through the duct can then be expressed as a mass flow

$$Q = C_{duct} \cdot \Delta P \cdot \rho \tag{7}$$

where the vapor density ρ can be calculated as [18,81,113]

$$\rho = \frac{M}{R \cdot T} \tag{8}$$

The pressure is not considered in the Eq. (8). Conductance depends on gas species and geometry (cross-section, length, curvature) [109,112,114]. Approximating the labyrinth gap locally as an orifice of area A, the molecular flow conductance of an orifice is

$$C_{or} = \frac{v_{mean}}{4} \cdot A \tag{9}$$

with the mean molecular speed [18,81,111]

$$v_{mean} = \sqrt{\frac{8 \cdot R \cdot T}{\pi \cdot M}} \tag{10}$$

Given the geometric complexity of labyrinth seals, it is common to replace the true annular path with an equivalent rectangular duct defined by gap width b_m and effective length L_m computed from an equivalent diameter d_{eq} [18,81,112]. The effective orifice area is then

$$A_{or} = \pi \cdot b_m \cdot d_{eq} \tag{11}$$

The conductance of this element is the orifice conductance multiplied by the transmission probability (TP), which is the fraction of molecules traversing from inlet to outlet [108,109,115,116]

$$C_{duct} = C_{or} \cdot TP \tag{12}$$

can be estimated by test-particle Monte Carlo (TPMC) simulation, which tracks molecule trajectories via diffuse wall collisions, or approximated analytically. For a long rectangular duct, a widely used expression is [108,109,116]

$$TP = \frac{1}{1 + \frac{3}{8} \cdot \frac{L_m}{b_m}} \tag{13}$$

Substituting Eq. (8) – (13) into Eq. (7) yields the SI-based analytical expression for molecular mass flow through the equivalent labyrinth gap

$$Q = C_{duct} \cdot \Delta P \cdot \rho = \sqrt{\frac{8 \cdot R \cdot T}{\pi \cdot M}} \cdot \frac{\pi \cdot b_m \cdot d_{eq}}{4} \cdot \left(1 + \frac{3}{8} \cdot \frac{L_m}{b_m}\right)^{-1} \cdot \Delta P \cdot \frac{M}{R \cdot T} \tag{14}$$

After adjusting the form of the equation, we obtain the final expression

$$Q = \sqrt{\frac{1}{2 \cdot \pi \cdot R}} \cdot \pi \cdot b_m \cdot d_{eq} \cdot \Delta P \cdot \left(1 + \frac{3}{8} \cdot \frac{L_m}{b_m}\right)^{-1} \cdot \sqrt{\frac{M}{T}} \tag{15}$$

Eq. (15) is the SI model and serves as a transparent first-order estimate of mass flow through a labyrinth seal, explicitly showing the dependence on geometry (b_m, L_m, d_{eq}), species (M), and temperature (T).

A refinement of Eq. (15) was developed [27,32,57] following a comprehensive evaluation of experimental data obtained by the European Space Tribology Laboratory (ESTL). The resulting correlation provides improved agreement with experimental measurements

$$Q_m = 0{,}0436 \cdot \frac{P_{mbar}\pi d_{cm} b_{cm} \left(\frac{M_g}{T}\right)^{0,5}}{1 + 0{,}375 \cdot \frac{L_{cm}}{b_{cm}}} \tag{16}$$

It is essential to apply the correct units consistently when using Eq. (15) and Eq. (16), as discrepancies in unit conventions across different references are a common source of error [27,57]. Among available closed formulations, the ESTL model in Eq. (16) is one of the most robust for estimating the mass flow of lubricant molecules escaping through a labyrinth under vacuum. Nevertheless, it inherits limitations from geometric idealizations and boundary assumptions, and it can systematically overestimate evaporation or leakage when compared against carefully controlled experiments [27,49,57].

b. Molecular flow simulations

When labyrinth seals operate in the free molecular regime (Kn > 0.5), TPMC simulations are a natural complement to closed form models [90,117,118]. These simulations neglect intermolecular collisions and track large groups of molecules as they undergo wall collisions, adsorption/desorption, and transmission through complex passages [90,91,117]. The primary outputs are transmission probability, local molecular flux, pressure (rarely needed in pure molecular flow), residence time, and predicted deposition on cold or sensitive surfaces. Two widely used tools are MolFlow+ [119] (an open-source code developed at CERN that efficiently handles intricate 3D vacuum geometries) and the Molecular Flow module in COMSOL Multiphysics [92,120].

Accurate Monte Carlo simulation modelling hinges on a few established choices. The wall interaction law is primary diffuse (cosine) re-emission is standard in engineering vacuum analyses, while mixed diffuse/specular scattering can better represent smoother surfaces and changes the predicted transmission through bends and steps [81,90,91]. Adsorption and desorption should be included with temperature dependent behavior to capture cold surface deposition near optics [81,87,90]. Geometry fidelity matters: elbows, baffles, relief grooves, and restricted openings affect transmission and should be represented explicitly rather than collapsed into ideal ducts. In practical setups, lubricant wetted areas are modelled as outgassing patches linked to the vapor pressure and solutions are checked for statistical convergence [27,54,56,57].

2.3.3 EVAPORATION AND DISTRIBUTION CONTROL

Loss of liquid lubricant can be driven not only by volatility but also by surface-lubricant interactions [6,17,61,84]. Surface chemistry may catalyze degradation pathways or modify wetting, which in turn affects film stability and creep [29,42]. A common mitigation strategy is surface passivation or selection of less reactive finishes to suppress tribochemical reactions and stabilize the liquid film under vacuum [36,37,40,93]. These are part of standard

contamination control practice in space hardware, which focuses on finding and understanding the sources, transport paths, and susceptible surfaces before setting cleanliness and treatment requirements [6,13,29,84].

Surface topography also governs lubricant migration and the transmission probability of evaporated molecules [19,67,74]. Roughness and directional grinding marks can steer thermally driven creep, alter residence of condensate, and influence re-emission from walls [56,69]. In the molecular flow regime relevant to high and ultrahigh vacuum, wall interactions dominate transport. Increased roughness or deliberate texturing raises accommodation and scatters trajectories, which reduces forward “beaming” and lowers the net transmission probability through narrow passages [81,118,121]. TPMC and experimental studies show that surface grooves and micro features measurably reduce conductance compared with smooth ducts, providing a practical lever for labyrinth seal optimization [44,66,121,122].

Cold surfaces can be used to control vapor location. Local cold traps, baffles, or cryogenic interfaces capture outgassed species by condensation and reduce transport to sensitive areas such as optics [21,123]. This approach is embedded in contamination control standards and test methods that quantify outgassing, deposition, and re-emission using QCM under vacuum with controlled collector temperatures [6,17,84,124]. These methods provide temperature-depending deposition rates and re-emission data that support both qualification and placement of cold surfaces in flight systems.

Concepts based on electrostatic fields have also been explored: strong field gradients can, in principle, alter molecular trajectories in the free molecular regime, enabling partial focusing or interception [125]. In practical spacecraft lubrication, however, most evaporated species are neutral and only weakly polar, so field-based control remains exploratory, whereas thermal management, geometric baffling, and surface structure engineering are the primary levers for reducing migration and deposition [21,123,125].

3 LITERATURE REVIEW ANALYSIS

The state-of-the-art shows that liquid lubrication for space mechanisms is a multidimensional problem that couples vacuum physics, tribochemistry, heat transfer, and precision mechanical design. As spacecraft become more numerous and missions longer and more complex, requirements on reliability and cleanliness intensify [28,31,59,84]. Lubricant selection and implementation must therefore be made at the mechanism level with explicit consideration of evaporation resistance, creep behavior, contamination risk, and compatibility with the operational environment [13,37,45]. Although solid lubricants remain essential for some duties, the use of liquid and grease formulations is increasing because of their favorable frictional performance and cost-effectiveness [14,23,28,38]. This trend places corresponding emphasis on improving lubricant properties and, critically, on passive design measures that limit mass loss and contamination, such as optimized sealing geometries [27,58,66].

Across the reviewed sources, analytical models are routinely used to inform early choices of lubricant and seal architecture [32,49,57]. However, their predictive accuracy in realistic conditions is limited, which motivates new measurement methods and refined models that better reflect space relevant environments [49,66,88,89].

3.1 KEY FINDINGS ON LIQUID LUBRICANTS IN SPACE

Among liquid lubricants, multiply alkylated cyclopentanes (MACs) and perfluoropolyethers (PFPEs) dominate both flight usage and laboratory studies [28,29,36]. These classes offer low volatility and strong wear protection compared with many alternatives [24,29,36,44,62]. PFPEs are chemically robust but exhibit lower surface tension, which increases susceptibility to creep. MACs combine low evaporation rates with higher surface tension and strong boundary performance [14,28]. Given the extensive heritage and available data for MAC and PFPE systems, focusing experimental work on these two groups facilitates meaningful comparison with prior studies and with flight experience.

Two material properties emerge as especially consequential for space use: surface tension, which governs creep and redistribution on solid surfaces [38,64,69], and vapor pressure, which sets the driving force for evaporation into vacuum [27,32,49,57]. Both processes can trigger tribological failure and contamination of adjacent subsystems [20,22,58,88]. Of these, vacuum induced evaporation is generally the dominant life-limiting mechanism, because it acts directly with the extreme thermal environment to shrink the lubricant operating window [5,16,32,60].

3.2 EVAPORATION MODELS AND MEASUREMENTS

Evaporation intensity can be approached analytically or experimentally [27,32,82]. The Langmuir based formulations (see Eq. (1)) and the widely used ESTL variant (see Eq. (2))

remain the baseline for early prediction [27,32,53], yet they frequently overestimate measured mass loss in space relevant tests. The main sources of error identified in the literature are idealized thermal histories, uniform surface temperature assumptions, unaccounted surface roughness and geometry effects, and uncertainty in lubricant vapor pressure [30,49,53,66]. Vapor pressure itself is usually provided by manufacturers using Knudsen effusion, but procedures are not internationally standardized and reported values can deviate between laboratories [27,47,49]. Moreover, vapor pressure at a given temperature is not strictly time invariant; it can evolve with composition and thermal history [54,66,101]. Consequently, the literature increasingly recommends introducing empirically derived correction factors to align analytical predictions with experimental behavior [48,49]. Implementing such corrections requires high quality experimental data for different lubricant classes, ideally gathered with complementary instruments to cross-validate results.

Certified vacuum benches and QCM-based methods exist to determine evaporative mass loss [17,32,82], but most provide point measurements rather than continuous, time resolved evaporation histories. This limits insight into transient effects, such as initial loss of light fractions or changes due to temperature cycling. Continuous, high-resolution measurements are therefore valuable for revealing the kinetics that drive discrepancies between models and reality.

3.3 SEALING STRATEGIES AND MOLECULAR TRANSPORT

To extend the usable lifetime of liquid lubricated mechanisms and to protect sensitive payloads, non-contact labyrinth seals are widely adopted [27,32,54,57]. Multiple studies confirm that seal geometry materially influences the net loss of lubricant vapor [27,82]. Analytical throughput models, including both SI-unit expression (see Eq. (15)) and the ESTL correlation (see Eq. (16)), provide practical estimates, but similarly as to free surface evaporation models, the predictions tend to diverge from measurements [27,32,48,49,57]. This is expected in the free molecular regime, where transport is set by repeated molecule-wall interactions, the detailed transmission probability through steps and turns, and the local surface structure.

TPMC simulations have therefore become an important complement to analytics for predicting molecular transport through seals [91,117,118]. When configured with appropriate wall scattering laws, adsorption/desorption parameters, and geometry fidelity, TPMC can capture the influence of path length, baffles, steps, and roughness on transmission probability and thus on vapor retention [90,118,126]. This capability enables targeted optimization of labyrinth features for minimum throughput while respecting mechanical clearance constraints.

Despite progress, important gaps persist. We still lack a clear mapping of how each geometric feature (e.g., stepped vs. straight channels, relief grooves) and measured surface roughness affect transmission probability over practical design ranges [10,27,66,122].

Likewise, most published characterizations of seal performance are static [27,49,57]. The influence of relative rotation in operating mechanisms remains underexplored, even though rotation is intrinsic to many space subsystems.

3.4 KEY CONCLUSIONS

The literature points to four knowledge gaps that motivate the work that follows:

a. Correcting evaporation models with experiment

Classical Langmuir type formulations remain indispensable for first estimates, yet they systematically overpredict losses in space conditions [27,48,49,53]. High precision, time resolved measurements are needed to quantify corrections that account for thermal history, surface morphology, and confinement geometry, thereby narrowing the gap between prediction and observation [34,49,68,78,97].

b. Quantifying geometry and surface effects in labyrinths

Seal performance in the molecular regime is highly sensitive to internal shape and wall condition [27,54,56,57]. Systematic experiments and Monte Carlo studies are required to establish how labyrinth length, deflections, steps, and controlled roughness reduce transmission probability, enabling prescriptive design rules for vapor retention [32,90,102,122].

c. Including operational dynamics

Most available datasets are static [27,48,57], while many flight mechanisms rotate [5,6,13,25,65]. Incorporating rotation into experiments and models is expected to modify molecule–wall encounter statistics and reduce through-flow in elongated or stepped passages, with direct implications for seals in reaction wheels, CMGs, and SADMs.

d. Exploring electrostatic influence

External fields may offer an additional degree of control over molecular transport for lubricants with polar or partially charged species [45,101,125,127]. Any practical use must be consistent with spacecraft ESD and EMC constraints, yet field assisted re-adsorption could lower transmission probability and improve retention.

These conclusions motivate the experimental and numerical program presented next, including high fidelity evaporation measurements, controlled labyrinth flow studies, and the development of correction factors and design guidelines for vapor retention in space mechanisms. The subsequent chapter formalizes the research objectives and outlines the methodology used to address these gaps.

4 AIMS OF THE THESIS

The objective of this doctoral thesis is to advance the understanding of lubricant behavior in space relevant vacuum environments, particularly focusing on the processes of evaporation, molecular transport, and their mitigation through passive structural mechanisms. The evaporation of liquid lubricants in high and ultrahigh vacuum is a critical challenge in space tribology, often leading to mass loss, contamination of sensitive components, and degradation of system performance. Although existing analytical models provide a baseline for predicting evaporation rates, they tend to overestimate real world losses and fail to account for effects such as confinement geometry, dynamic operation, surface roughness, and electrostatic interactions.

This work aims to close the gap between analytical prediction and practical performance through the development and integration of validated experimental test rigs and high-fidelity simulations. It further seeks to define quantitative correction models and optimization strategies for labyrinth seals, which are commonly used in spacecraft to control lubricant migration.

The thesis is divided into several key thematic areas, each contributing to the overarching goal of improving evaporation modeling accuracy and enhancing the vapor retention efficiency of labyrinth seals (see Fig. 20). A wide array of experimental and numerical methods was used, including:

- The development of a vacuum Evaporation Test Rig (ETR) to quantify lubricant mass loss under static conditions.
- The modification of the ETR into a Labyrinth Test Rig (LTR) to investigate vapor flow through labyrinth seal geometries.
- Experimental validation of analytical evaporation models and numerical simulations.
- The formulation of a simulation-based correction model to describe the influence of surface roughness on molecular transport.
- Investigation of electrostatic fields and rotational motion as additional influencing factors on vapor retention.

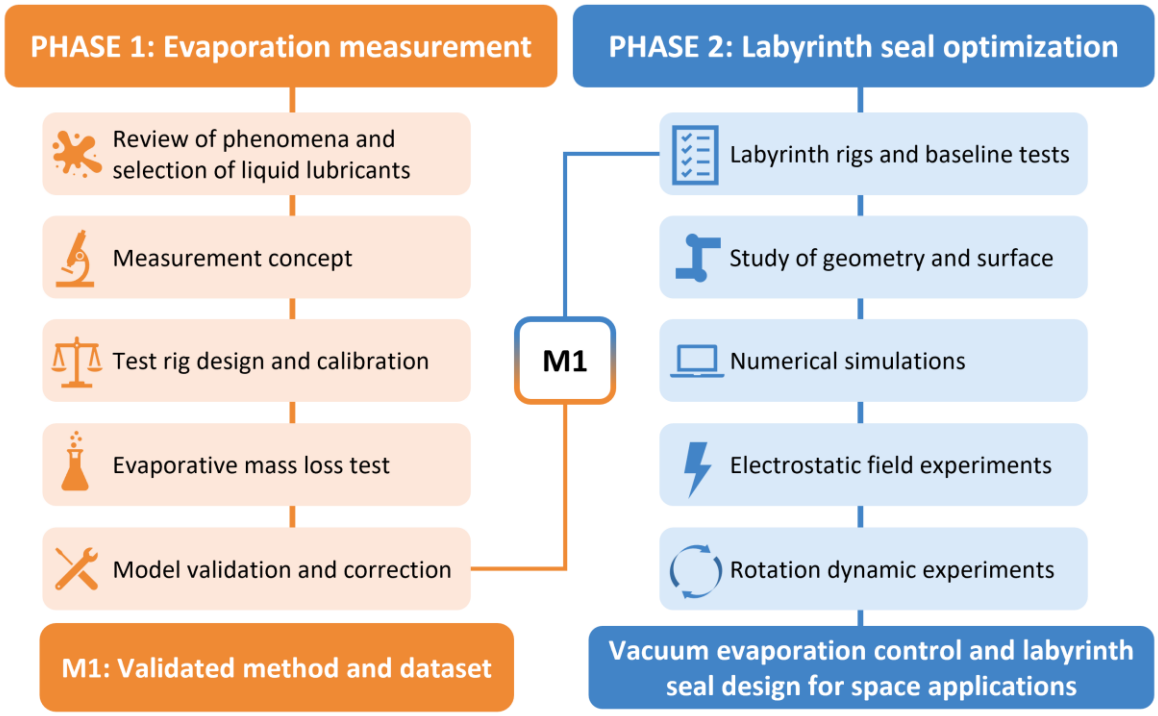

Fig. 20 Schematic view of thesis aims

This thesis focuses on the design, testing, and modeling of various physical influences affecting lubricant evaporation, leading to the formulation of correction factors and design guidelines that improve the reliability of space lubrication systems.

4.1 SCIENTIFIC QUESTIONS & HYPOTHESES

4.1.1 SCIENTIFIC QUESTION 1

How can existing analytical models for liquid lubricant evaporation in vacuum be corrected or refined using high precision experimental evaporation data?

WORKING HYPOTHESIS 1

It is possible to enhance the predictive accuracy of classical analytical evaporation models, such as the Langmuir or ESTL formulations, by introducing correction factors derived from time-resolved experimental measurements. These corrections should reflect real vacuum conditions, including effects such as surface morphology or confinement geometry. The implementation of these factors will significantly reduce the discrepancy between model predictions and experimentally observed mass loss, especially for high-viscosity and multi-component lubricants.

FUNDAMENTAL EXPLANATION

The evaporation rate of liquid lubricants in vacuum can be estimated using analytical models. The Langmuir equation (see Eq. (1)) and its ESTL modification (see Eq. (2)) are the most used models [48,50,53]. However, this classical formulation is based on several simplifying assumptions that introduce significant inaccuracies when applied to practical systems. These include the idealization of the lubricant's thermal history, uniform temperature distribution across the evaporation surface. In addition, the accurate determination of vapor pressure for specific lubricant mixtures remains challenging [66]. Due to these limitations, analytical predictions often significantly overestimate the actual evaporation rate observed in experiments. Discrepancies of several times the measured value have been reported [27,48,53]. Although these inaccuracies are well recognized in the scientific community [49], the Langmuir equation continues to be used in engineering practice, typically in a modified form that introduces empirical correction terms [17,32,82]. Current research does not focus on replacing the Langmuir equation with entirely new models. Instead, the prevailing trend is to improve its predictive accuracy by incorporating correction factors derived from controlled experimental measurements [27,49,82]. This approach retains the model’s practical simplicity while aligning it more closely with physical reality, making it a valuable tool for vacuum lubrication design and space mechanism development.

4.1.2 SCIENTIFIC QUESTION 2

What is the influence of internal geometry and surface structure of labyrinth seals on the transmission of lubricant molecules under molecular flow conditions?

WORKING HYPOTHESIS 2

The internal geometry and surface morphology of labyrinth seals have a significant impact on the molecular transmission of evaporated lubricants. By optimizing key geometrical features, such as flow path length, deflection angles, and step transitions, it is possible to substantially reduce the net flow of lubricant molecules through the seal. Additionally, modifying the surface roughness of the channel walls can increase molecular scattering, which further limits transport. The combined effect of geometric complexity and controlled surface texturing enables the design of seals with enhanced vapor retention and reduced risk of contamination in space mechanisms.

FUNDAMENTAL EXPLANATION

Well-designed labyrinth geometries in space applications can reduce lubricant mass loss [27] and lower the level of contamination affecting sensitive spacecraft components. This is primarily achieved by limiting the diffusion and re-deposition of lubricant molecules and other particulates originating from degradation and wear processes [44,66]. In the molecular flow regime, gas molecules travel without mutual collisions, and upon interacting with the channel walls, they temporarily adhere before re-emitting in a statistically randomized direction, independent of their incoming trajectory and velocity [18,38,81,87]. This behavior gives rise to the molecular beaming effect inside the labyrinth, where multiple wall interactions influence the directional distribution of the molecular flux [90,105,110]. Such effects are particularly pronounced at geometric discontinuities or directional changes in the seal path. Besides geometry, the structure of the internal surface also plays an important role. Increased surface roughness can enhance molecular scattering, effectively lengthen the path and reduce transmission probability [56,66,122,126]. As such, both macro geometry and micro scale surface characteristics are critical parameters in achieving optimal labyrinth seal performance.

4.1.3 SCIENTIFIC QUESTION 3

How does rotational motion of labyrinth seal components influence the molecular transport of evaporated lubricants under vacuum conditions?

WORKING HYPOTHESIS 3

Rotational motion of the seal's internal surfaces alters the dynamics of molecule-wall interactions, increasing the frequency and randomness of scattering events. As the rotational speed rises, the likelihood that evaporated molecules undergo momentum altering collisions with the moving walls also increases, reducing their net transmission probability through the seal. This effect should be significant for elongated or stepped geometries, where extended surface contact amplifies the interaction time. Consequently, incorporating dynamic motion into labyrinth seal design and evaluation can lead to improved vapor retention, especially in rotating subsystems of space mechanisms.

FUNDAMENTAL EXPLANATION

Labyrinth seals are widely used in spacecraft mechanisms involving relative rotational motion, such as Reaction Wheels (RWs), Control Moment Gyroscopes (CMGs), Solar Array Drive Mechanisms (SADMs), and Coarse Pointing Assemblies in optical or laser communication terminals [5,6,27,54,57,65]. These systems rely on seals to prevent lubricant loss and contamination in vacuum [22,66,88]. Despite their operational relevance, most studies on labyrinth seal behavior are conducted under static conditions, overlooking the dynamic effects introduced by rotation [27,57]. In the molecular flow regime, where intermolecular collisions are negligible, the motion of bounding surfaces significantly influences molecular trajectories [81,87]. Understanding the impact of rotation on these interactions is critical for optimizing seal performance in actively moving spacecraft subsystems.

4.1.4 SCIENTIFIC QUESTION 4

Can externally applied electrostatic fields be used to influence molecular transport through labyrinth seals and reduce lubricant evaporation in vacuum environments?

WORKING HYPOTHESIS 4

Electrostatic fields can be used as an active mechanism to influence the motion of lubricant molecules within labyrinth seals operating in the molecular flow regime. When an electric potential is applied across the seal corridor, it may interact with polar or ionic components of the lubricant, altering their trajectories and increasing their likelihood of re-adsorption to the seal walls. This effect could reduce the net transmission probability and enhance vapor retention. However, the application of electrostatic fields in vacuum must account for spacecraft specific challenges such as electrostatic charging, dielectric breakdown, and compatibility with surrounding systems. It is hypothesized that carefully controlled electric fields can improve seal performance without introducing operational risks, provided they are implemented within established spacecraft electrostatic design limits.

FUNDAMENTAL EXPLANATION

Electrostatic fields are known to influence the behavior of molecules in vacuum, particularly those with permanent dipole moments or partial charges [45,112,125]. In the context of space lubrication, this principle can be applied to reduce evaporation losses by modifying the motion of escaping molecules through the application of a directed electric field across the seal gap. Such fields may deflect the trajectories of volatile species, increase wall interactions, and thereby lower the probability of molecular escape.

While this mechanism holds promise, the integration of electrostatic fields into spacecraft hardware must be approached with caution. Electrostatic discharge (ESD) events are a known hazard in space systems, often caused by differential charging of surfaces or dielectric breakdown under vacuum [6,13,20,26]. These discharges can damage electronics, degrade materials, and pose serious risks to mission reliability. Implementing electrostatic seals requires compliance with strict design standards regarding electric field strength, gap dimensions, and insulation integrity.

5 MATERIALS AND METHODS

This chapter describes the materials and methods used to measure evaporation in vacuum, quantify molecular transport, and assess the performance of labyrinth seals. It introduces the lubricant set, the analytical formulations used for first order estimates, the custom experimental rigs, and the numerical tools used to interpret the data. It also summarizes calibration procedures, data processing steps, and uncertainty evaluation.

- Lubricants:
  - PFPE, MAC, and selected ionic liquids.
- Analytical models:
  - Langmuir-based evaporation (ESTL adaptation)
  - Clausius–Clapeyron vapor pressure interpolation
  - ESTL conductance for labyrinth flow
- Experimental rigs:
  - Evaporation test rig (ETR): measures free-surface evaporation in vacuum.
  - Labyrinth test rig (LTR): evaluates labyrinth seal geometry and surface finish.
  - Electrostatic labyrinth test rig (ELTR): A controlled electric field within the labyrinth seal channel.
  - Dynamic labyrinth test rig (DLTR): imposes controlled rotation of the seal wall.
- Simulations:
  - MolFlow+: 3D test-particle molecular flow.
  - COMSOL Multiphysics: 2D/3D studies with measured or synthetic roughness and rotating walls.
- Surface roughness: generation, profilometric measurement, and model import.

5.1 LUBRICANT TEST SAMPLES

A range of liquid lubricants was tested throughout the experimental investigations to evaluate evaporation behavior, seal retention efficiency, and the influence of electrostatic fields. The selection of lubricants reflects a deliberate effort to represent distinct chemical families commonly used in space tribology. Not all lubricants were employed in every experiment, as their use depended on the objectives and conditions of each study. Tab. 1 summarizes the key lubricants used.

Fomblin Y LVAC 25/6, a perfluoropolyether (PFPE), was the most widely used lubricant across all test campaigns due to its high vapor pressure and excellent vacuum compatibility. Its volatility at moderately elevated temperatures enabled efficient testing of both flat surface evaporation and flow through labyrinth seals.

NYE 2001, a multiply alkylated cyclopentane (MAC), was employed for high-fidelity evaporation studies where extremely low vapor pressure was essential. This lubricant is often used in spacecraft mechanisms due to its low outgassing rate and chemical stability.

For specialized experiments examining the influence of electrostatic fields on molecular transport, two ionic liquids were included: 1-ethyl-3-methylimidazolium bis (trifluoromethyl sulfonyl) imide (EMIM-TFSI) and 1-octyl-3-methylimidazolium bis (trifluoromethyl sulfonyl) imide (OMIM-TFSI). These were chosen for their negligible vapor pressure, electrochemical stability, and unique response to electric fields. The ionic liquids were not tested for static evaporation or seal performance due to their low volatility.

Tab. 1 Overview of lubricant test samples used in experimental investigations

Lubricant name	Nye 2001	Fomblin Y LVAC 25/6	EMIM-TFSI	OMIM-TFSI
Lubricant type	MAC	PFPE	IL	IL
Kinematic viscosity [cSt]	305 cSt	276 (20°C)	39.4 (20°C)	106 (20°C)
Vapor pressure [mbar]	1e-8 (20°C)	6e-8 (25°C)	–	–
	2.33e-8 (38°C)	6e-5 (100°C)	–	–
	5.70e-7 (100°C)	–	–	–
Molecular weight [g/mol]	910	3300	391.31	475.47
Density [g/cm^3]	0.84	1.90	1.52	1.32

During each test, lubricants were applied in small, controlled volumes. Film coverage and surface area uniformity were ensured through pre-tests, particularly to prevent edge drying or unwanted creep effects during heating. This lubricant set supports comparative analysis across multiple experimental platforms and provides a foundation for validating and refining both analytical and numerical models of evaporation and molecular transport.

5.2 ANALYTICAL MODELING APPROACH

Analytical models were employed in this work to estimate lubricant evaporation rates and molecular flow through labyrinth seals under high vacuum conditions. These models offer a rapid and cost-effective means of obtaining first order approximations of key parameters that influence evaporation and transmission behavior in UHV conditions. Although inherently simplified and less precise than experimental or numerical techniques, analytical approaches are invaluable during early-stage design, feasibility assessment, and comparative analysis.

5.2.1 VACUUM EVAPORATION MODELING

Lubricant mass loss due to evaporation was estimated using the ESTL adaptation of the classical Langmuir equation, as introduced in Eq. (2). This empirical model provides a practical, zero-order approximation of the evaporation rate under isothermal molecular flow conditions and is widely used for rapid estimation in space tribology applications.

In cases where vapor pressure data were unavailable for the lubricant at specific temperatures, the Clausius–Clapeyron equation (see Eq. 3) was used to interpolate values based on reference data from the ESTL Database of Liquid Lubricants (DOLLS). This enabled the construction of a continuous temperature dependent vapor pressure curve for

Fomblin Y LVAC 25/6, which was applied consistently across all analytical evaporation predictions (see Fig. 21).

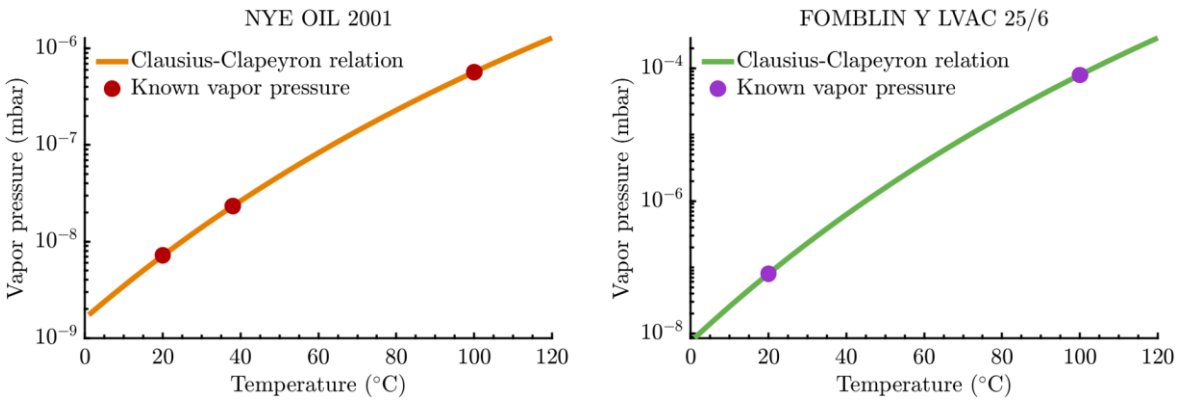

Fig. 21 Clausius-Clapeyron approximation of the oil temperature-dependent vapor pressure [1]

It is important to note that the enthalpy of vaporization can be affected by the lubricant's thermal history. As such, analytical predictions may deviate from actual behavior, particularly in cases involving multiple heating and cooling cycles.

5.2.2 MOLECULAR FLOW THROUGH LABYRINTH SEALS

To analytically estimate molecular transmission through labyrinth seals, the complex seal geometry was reduced to an equivalent linear channel defined by effective parameters: gap width, channel length, and effective annular seal gap diameter. The mass flow rate of vapor through this equivalent geometry was then calculated using the ESTL-derived formulation presented in Eq. (16), which is widely regarded as one of the most robust analytical tools for estimating molecular flow in simplified geometries under vacuum.

Despite its practicality, the ESTL model exhibits notable limitations. It assumes idealized boundary conditions and simplified geometrical representations, which frequently result in overestimation of leakage and evaporation rates when compared with experimental observations. One significant source of error lies in the vapor pressure input data, often derived from Knudsen effusion methods that lack standardized measurement protocols and may introduce uncertainty or bias.

Moreover, the model does not capture surface interactions, thermal history effects, or molecular beaming phenomena. These limitations are particularly critical when dealing with real-world labyrinth seals, where surface topography and local geometry deviations can significantly alter flow behavior. To mitigate such discrepancies, correction factors based on empirical calibration have been proposed in the literature, improving alignment with laboratory data and enhancing model reliability.

In this study, analytical predictions were used in conjunction with numerical simulations and experimental measurements to assess the validity and limitations of the analytical approach. This comparative framework enables quantitative evaluation of model performance and

supports refinement of sealing strategies for space applications. Where analytical results diverged significantly from empirical data, Monte Carlo molecular flow simulations were employed as a higher fidelity reference capable of resolving detailed gas-surface interactions.

5.3 EVAPORATION TEST RIG (ETR)

The core of the experimental setup is a custom-built Evaporation Test Rig (ETR), designed to precisely quantify lubricant evaporation in high and ultrahigh vacuum environments. The apparatus operates on a mechanical balance principle, where lubricant mass loss leads to angular displacement of a pivoted scale beam. A capacitive proximity sensor, mounted on the vacuum chamber flange, tracks the position of a reference plate attached to a pointer on the scale beam. As lubricant evaporates, the shift in mass alters the beam's equilibrium, resulting in a measurable tilt that is captured by the sensor. This displacement is then converted into evaporated mass using a pre-determined calibration factor (see Fig. 22 and Tab. 2).

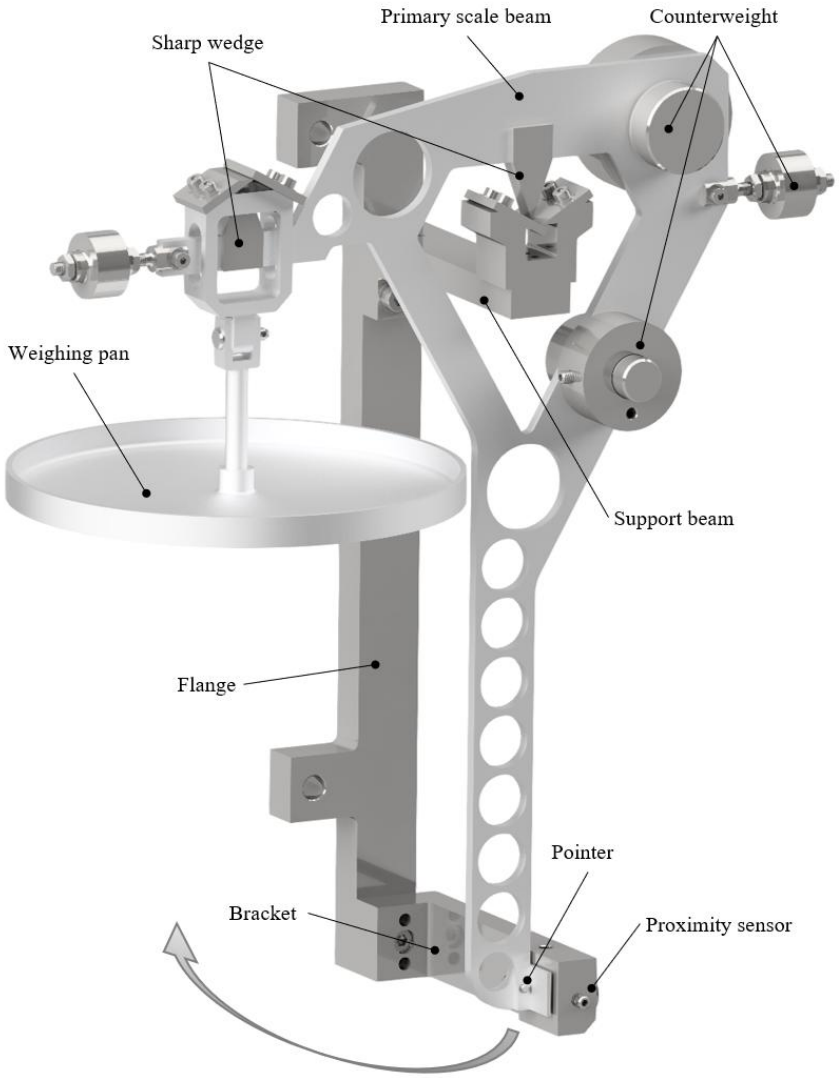

Fig. 22 Evaporation test rig (ETR) description [1]

Tab. 2 Evaporation test rig characteristics [1]

Parameter	Value
Dimensions (height, depth, width)	220 x 125 x 200 mm
Operating temperatures	–100 … +150 °C
Sample weight	10–100 g
Weighing precision	± 0.04 mg
Proximity sensor resolution (static)	0.375 nm
Proximity sensor measuring range	0.5 mm
Conversion ratio (distance/weight)	10.0 µm / 1.0 mg

The ETR's mechanical core consists of a sharp wedge pivot system supporting the beam, with a weighing pan on one side and adjustable counterweights on the other. The pointer, extending from the beam, is equipped with a reference plate that interfaces with the proximity sensor. The modularity of the setup allows for flexible configuration of its components, including interchangeable weighing pans and counterweights, enabling adaptation to a wide range of experimental scenarios such as lubricant evaporation and labyrinth seal evaluation.

The entire ETR assembly is placed inside a vacuum chamber capable of UHV operation. Thermal control is provided either externally or by localized internal resistive heating elements, enabling isothermal or accelerated testing conditions. Accurate thermal regulation is critical, given the temperature dependence of vapor pressure and lubricant behavior. Therefore, rigorous pre-calibration procedures are performed prior to measurement campaigns. These include detailed assessments of the weighing system's accuracy, displacement to mass conversion, repeatability under various conditions, and a thermal calibration that relates the measured reference temperatures to the lubricant test sample temperature.

Environmental factors such as vibration, thermal expansion, and material deformation are known to affect precision in displacement measurements. Calibration is conducted under both atmospheric and vacuum conditions to ensure consistent performance across operational regimes. Prior to each measurement cycle, a vacuum bakeout process is initiated to remove adsorbed contaminants from the chamber's interior surfaces. This is followed by thermal stabilization, where system pressure and temperature are allowed to reach equilibrium. The duration of bakeout and stabilization typically ranges from 48–72 hours, depending on the system's configuration and environmental conditions. Establishing these stable boundary conditions is essential to prevent thermal gradients and secondary condensation effects that would otherwise compromise the measurement's integrity.

In summary, the ETR provides a high resolution, modular, and thermally stable platform for investigating lubricant evaporation under conditions that closely emulate the thermal and vacuum environments encountered in space systems. Its sensitivity and reliability make it a powerful tool for generating benchmark experimental data necessary for validating analytical and simulation models.

5.4 LABYRINTH TEST RIG (LTR)

To investigate the performance of labyrinth seals under vacuum conditions, a modified version of the ETR was employed, referred to as the Labyrinth Test Rig (LTR) (see Fig. 23). The experimental configuration enables continuous measurement of lubricant evaporation through various labyrinth geometries and supports high precision in mass loss quantification.

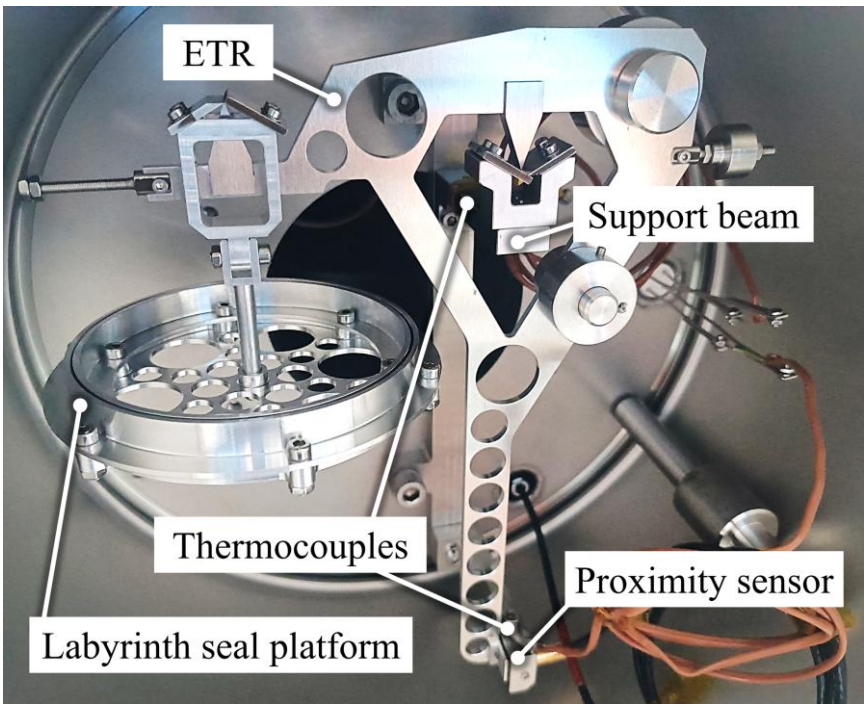

Fig. 23 Evaporation test rig (ETR) with labyrinth seal platform [2]

The LTR is based on the same mechanical principle as the original ETR, utilizing a pivoted scale beam with single-axis rotation supported by sharp edged wedges. In this configuration, a modular platform is mounted on one end of the scale beam to accommodate the labyrinth seal assembly (see Fig. 24). This assembly includes a main pan, which serves as the lubricant reservoir, and an interchangeable seal geometry. All components in contact with the lubricant or exposed to vacuum conditions are fabricated from aluminum alloy 6061 to ensure compatibility and thermal stability.

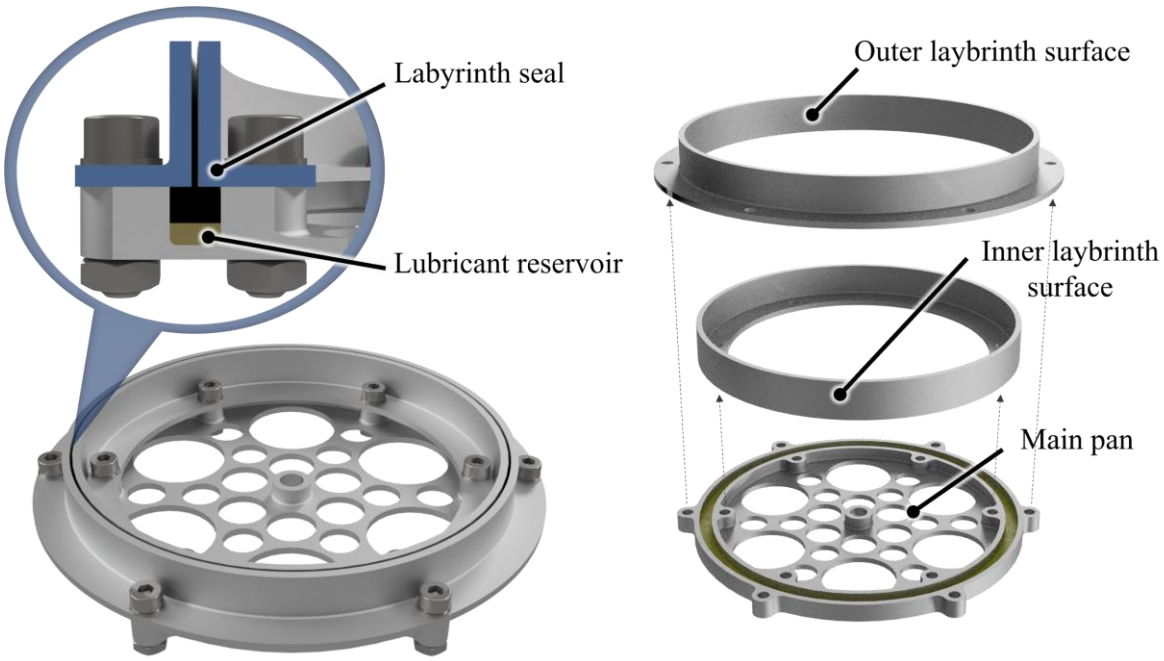

Fig. 24 Labyrinth seal platform setup and assembly breakdown [2]

Each test begins with the injection of a defined quantity of PFPE-based lubricant (Fomblin Y LVAC 25/6, see Tab. 1) into the annular reservoir of the labyrinth platform. The test assembly is completed by attaching one of three seal geometries: SHORT, LONG, or STEP (see Fig. 25), with detailed dimensions provided in Tab. 3. Prior to testing, thermal behavior and lubricant creep were evaluated through a series of pre-tests to ensure repeatability.

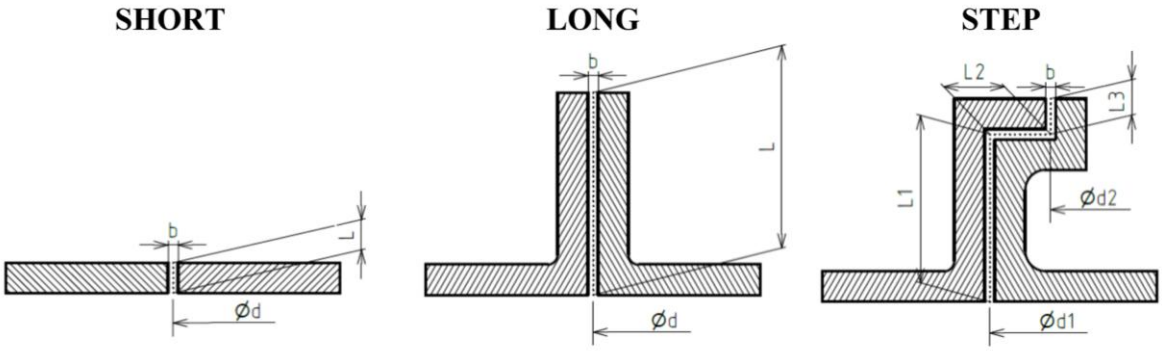

Fig. 25 Labyrinth seal geometries experimental setup (SHORT, LONG, STEP) [2]

Tab. 3 Labyrinth seal geometry dimensions [2]

Labyrinth	Width [mm]	Diameter [mm]	Length [mm]
SHORT	b = 0.5	d = 86.5	L = 1.5
LONG	b = 0.5	d = 86.5	L = 10
STEP	b = 0.5	d_1 = 86.5	L_1 = 8.25
		d_2 = 92.5	L_2 = 3.00
			L_3 = 1.75

To assess the impact of surface topography on seal performance, two variants of the LONG labyrinth seal geometry were prepared. One variant retained its original machined surface finish, while the other was mechanically polished to achieve a smoother texture. Surface roughness measurements were carried out using a Bruker Contour GTX 3D optical profilometer (see Fig. 26), providing high resolution topographical data. These surface profiles were subsequently imported into COMSOL Multiphysics simulations to enable a more accurate representation of molecular interactions within the seal.

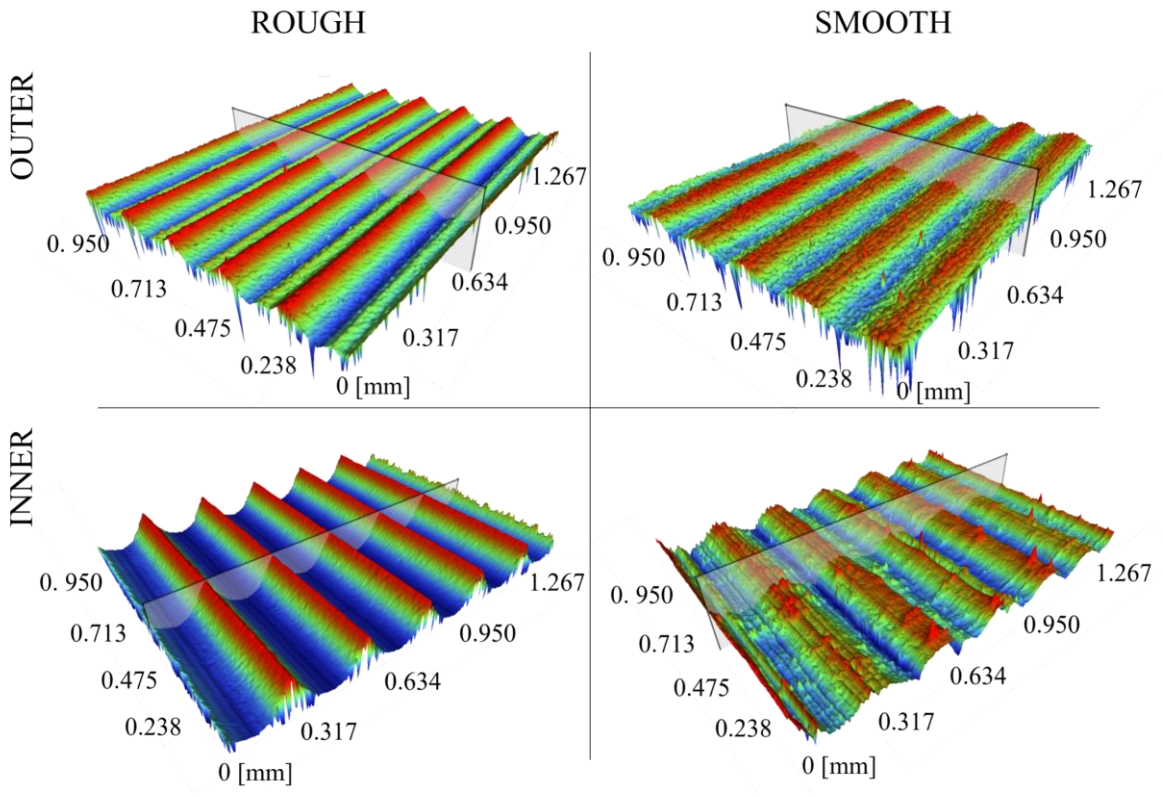

Fig. 26 Surface roughness characterization of inner and outer regions of the LONG labyrinth seal geometry using 3D optical profilometry [2]

The LTR operates under vacuum conditions representative of the free molecular flow regime, enabling realistic simulation of space-relevant environments. Its high measurement sensitivity, with the capability to detect lubricant mass losses on the order of milligrams, allows for precise evaluation of vapor retention characteristics. This level of resolution makes the system particularly well suited for investigating the influence of both seal geometry and surface roughness. By facilitating direct comparison between experimental data, analytical predictions, and numerical simulations, the LTR serves as a robust validation platform for optimizing labyrinth seal designs intended for vacuum and space applications.

5.5 ELECTROSTATIC LABYRINTH TEST RIG (ELTR)

To investigate the influence of electrostatic fields on molecular transport through labyrinth seals, a dedicated experimental platform called the Electrostatic Labyrinth Test Rig (ELTR) was developed. This system is designed for operation under UHV conditions and allows for the controlled application of electric fields across the seal structure. The setup comprises four labyrinth seals mounted on a platform inside a vacuum chamber (see Fig. 27) equipped with embedded electrodes positioned on either side of each labyrinth channel (see Fig. 28). These electrodes enable precise, spatially defined electrostatic fields to be generated by applying voltages in the range 0 to 50 V, simulating field induced polarization and electrostatic gradients representative of in-orbit conditions.

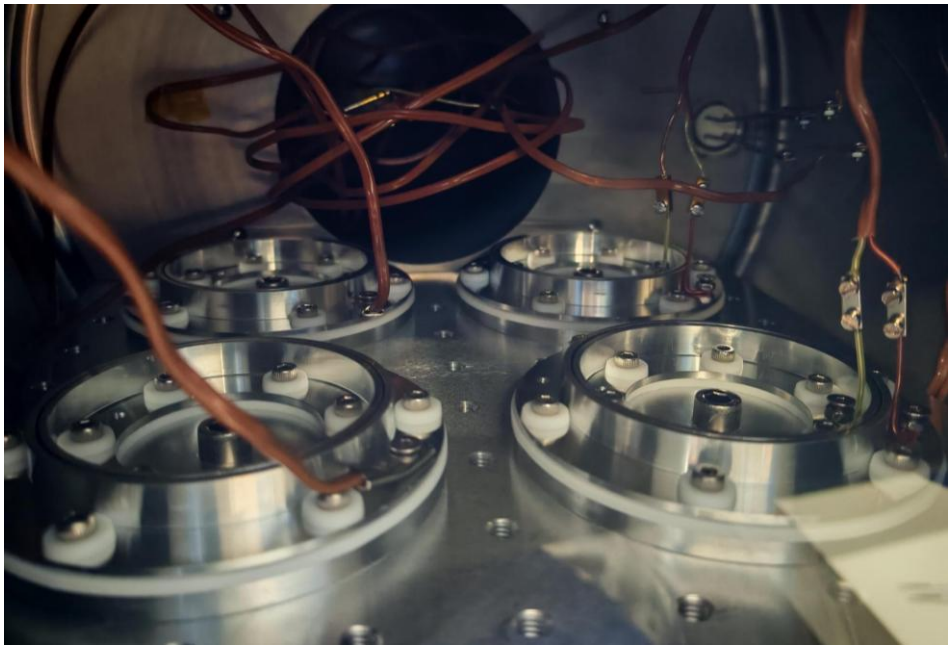

Fig. 27 Electrostatic labyrinth seal setup mounted inside the vacuum chamber

The primary objective of the ELTR is to evaluate how electric field strength, polarity, and spatial configuration influence the transmission probability of evaporated lubricant molecules under free molecular flow conditions. This extends conventional studies that primarily focus on geometric design and surface roughness.

A variety of lubricants was tested using the ELTR, with particular emphasis on comparing conventional high vacuum and space-grade lubricants with ionic liquids that exhibit distinct electrochemical behavior. The tested lubricants are summarized in Tab. 1.

Fig. 28 Electrostatic field configuration in a LONG-type straight labyrinth seal [4]

The ionic liquids were selected for their high polarizability and ionic character, which are expected to enhance their interaction with applied electric fields. Their inclusion aimed to explore whether electrostatic forces can reduce molecular transmission or modify evaporation dynamics, potentially offering a novel mechanism for enhancing sealing performance.

Overall, the ELTR provides a robust and flexible platform for evaluating the electrostatic sensitivity of various lubricant chemistries. The results contribute to a deeper understanding of the role of electric fields in molecular transport and may inform the development of next generation labyrinth sealing technologies incorporating active electrostatic control.

5.6 DYNAMIC LABYRINTH TEST RIG (DLTR)

To evaluate the influence of rotational dynamics on molecular transport through labyrinth seals, a specialized Dynamic Labyrinth Test Rig (DLTR) was developed (see Fig. 29). This experimental platform enables the investigation of how angular motion affects lubricant migration and vapor retention under space relevant vacuum conditions.

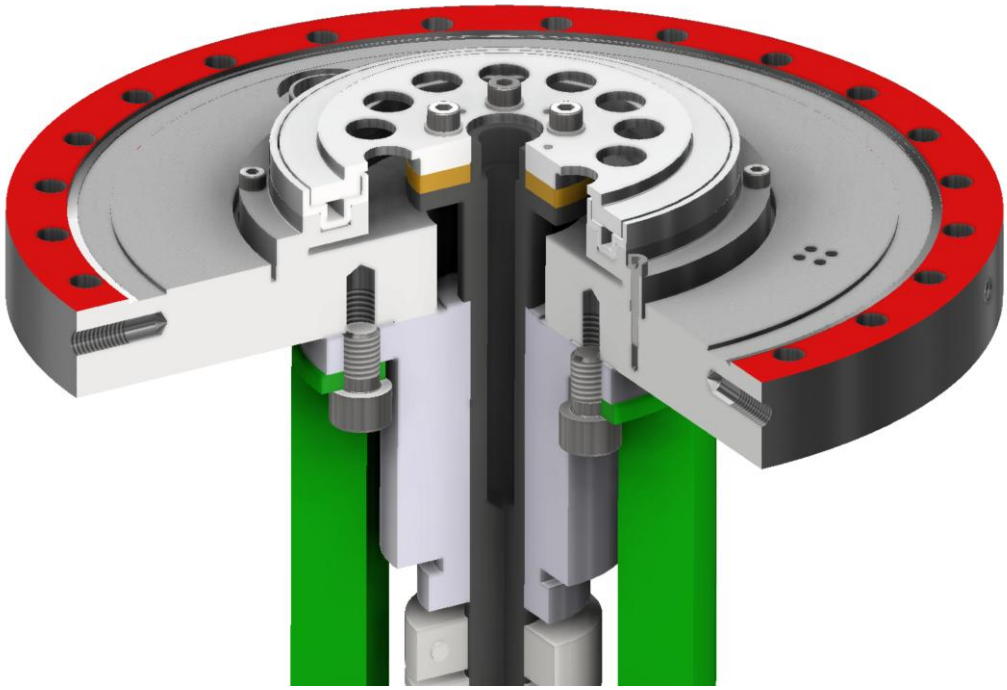

Fig. 29 Dynamic Labyrinth Test Rig (DLTR) [4]

The DLTR consists of a stationary vacuum compatible housing fitted with a rotating shaft that incorporates the labyrinth seal geometry. A precision motorized spindle is integrated into the system to control angular velocity across a broad range of operating speeds. The shaft rotation simulates real-world conditions found in spacecraft mechanisms such as reaction wheels, bearings, or drive units. Thermal control and pressure regulation are implemented to replicate UHV and temperature environments typical of orbital applications.

The labyrinth seal used in the DLTR comprises two primary components: a stator, which is mounted onto the vacuum chamber lid and houses the liquid lubricant reservoir, and a rotor, which is attached to the rotating spindle. The rotor rotates freely inside the stator without mechanical contact, maintaining a constant radial clearance of 0.5 mm. This non-contact configuration eliminates friction and wear while enabling the study of centrifugal effects on evaporated molecular transport within the seal corridor.

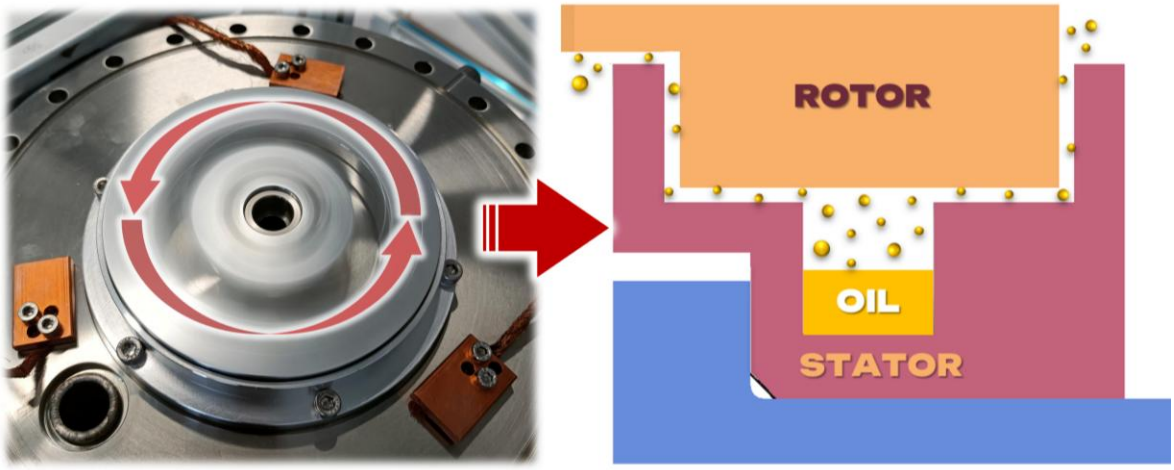

Fig. 30 Cross-sectional view of the Dynamic Labyrinth Test Rig (DLTR) showing rotor–stator seal configuration [4]

This configuration allows for the assessment of centrifugal effects and dynamic flow perturbations induced by rotation, which are not captured in static experiments or purely analytical models. By introducing a controlled rotational component, the DLTR provides valuable insights into the time dependent modulation of sealing performance and the redistribution of evaporated molecules within the seal structure.

The dynamic data obtained from the DLTR supports the refinement of numerical models that incorporate centrifugal and inertial forces and helps bridge the gap between idealized simulation conditions and operational realities of rotating space mechanisms. As such, the DLTR represents a critical component in the comprehensive evaluation of labyrinth seal behavior under dynamic vacuum conditions.

5.7 NUMERICAL SIMULATION APPROACH

To complement the experimental evaluation of labyrinth seal performance and lubricant evaporation under vacuum conditions, advanced molecular simulations were conducted using two numerical tools: MolFlow+ and COMSOL Multiphysics. These simulations were aimed at characterizing molecular transport in the free molecular flow regime, investigating the influence of geometry and surface roughness (see Fig. 31), and validating analytical predictions through high-fidelity numerical analysis.

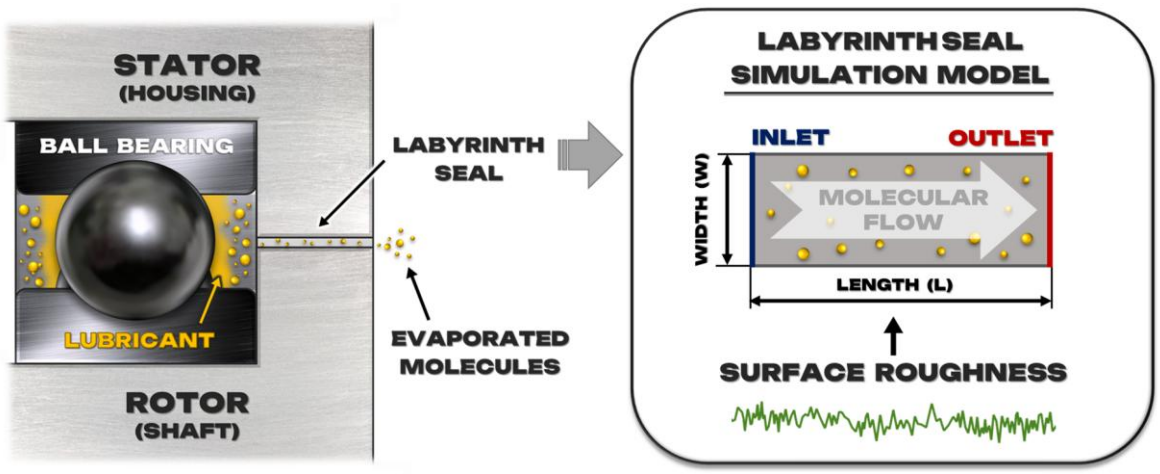

Fig. 31 Labyrinth seal with evaporating molecules and surface roughness simulation [3]

All simulation models were defined based on experimentally measured boundary conditions, including lubricant vapor pressure, chamber pressure, and thermal parameters. As the pressure at the inlet of the labyrinth seal cannot be measured directly, it was approximated in simulations by the vapor pressure of the lubricant at its corresponding operating temperature.

5.7.1 MOLFLOW+

MolFlow+ was employed to simulate molecular flow through three-dimensional labyrinth seal geometries under UHV conditions. This open-source software is specifically designed to model rarefied gas behavior in free molecular flow regimes using Monte Carlo simulations where intermolecular collisions are negligible. MolFlow+ operates by tracking the trajectories of many test particles emitted from defined surfaces, statistically evaluating their interactions with the surrounding geometry.

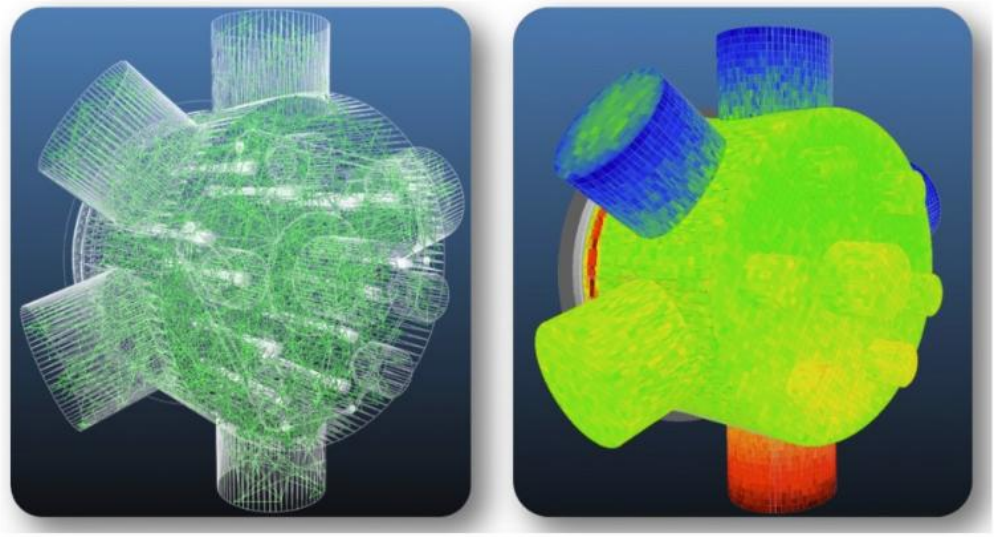

Fig. 32 MolFlow+ [119]

It was used to compute several key outputs, including spatial pressure distributions, molecular trajectories, and transmission probability across different labyrinth configurations. Its ability to simulate highly complex and non-linear geometries with sub-millimeter precision makes it particularly well suited for evaluating sealing performance in vacuum applications. The simulation results served to benchmark analytical model predictions and provided a valuable reference for assessing the relative vapor retention efficiency of various seal geometries.

5.7.2 COMSOL MULTIPHYSICS

COMSOL Multiphysics v.6.3 was employed for detailed two-dimensional and three-dimensional simulations of labyrinth seal geometries under vacuum conditions. Unlike MolFlow+, COMSOL enables the inclusion of additional physical effects that are critical to the understanding of seal performance, such as the dynamic influence of rotational motion and the incorporation of real surface roughness data acquired from profilometric measurements.

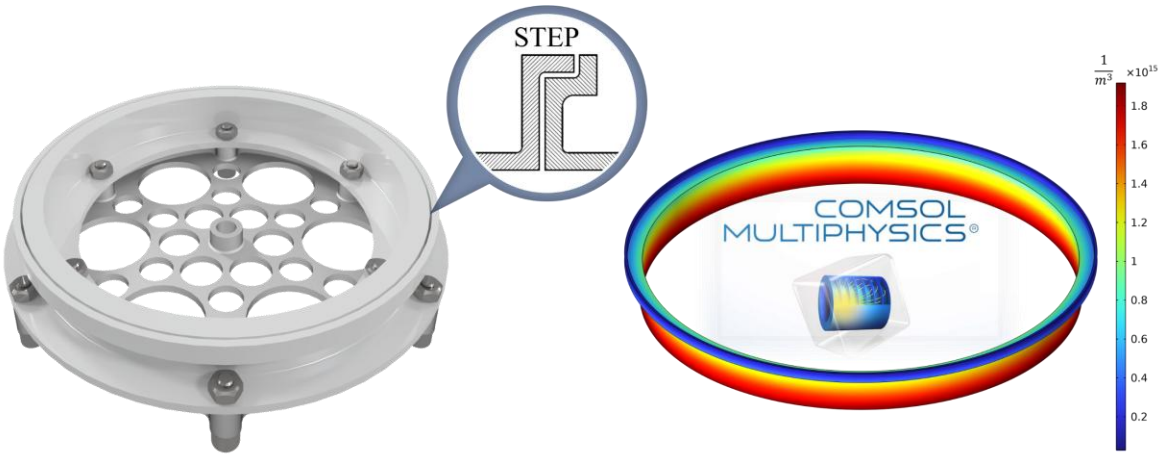

Fig. 33 COMSOL Multiphysics v6.3 model of the STEP labyrinth seal geometry

Moreover, synthetic surface roughness can be implemented directly within COMSOL through geometric perturbations applied to the seal channel walls. These perturbations are defined using statistically generated parametric curves based on spectral synthesis methods. This approach allows for controlled manipulation of roughness characteristics and enables detailed analysis of their effects on molecular transport. Two specialized physics modules within COMSOL were utilized in this work:

1) *Molecular Flow Module:* This module calculates local molecular flux and evaluates how geometric and surface features obstruct molecular flow. It can also be used to determine transmission probability based on the steady-state molecular flux balance between inlet and outlet boundaries.

2) *Particle Tracing Module:* While also capable of evaluating transmission probability, this module is particularly advantageous when simulating surface roughness effects. It allows the tracking of individual molecular trajectories in the presence of complex wall

geometries, including rough surfaces with peaks and valleys. Moreover, it supports the modeling of dynamic phenomena, such as the rotational motion of a labyrinth wall, providing deeper insight into transient molecular behavior and sealing effectiveness under real-world conditions.

5.7.3 SURFACE ROUGHNESS MODELING

To investigate the influence of surface topography, synthetic roughness profiles were generated using a spectral synthesis approach. This method is governed by three statistical parameters:

- N – Spatial frequency resolution, determining feature density,
- b_s – Spectral exponent, controlling amplitude decay,
- PC – Amplitude scaling factor, adjusting vertical roughness magnitude.

The profile height $z(x)$ was defined using the equation:

$$z = PC \cdot \sum_{n=-N}^{N} (n^2)^{-\frac{b_s}{2}} \cdot g(n) \cdot \cos\big(2\pi(nx) + u(n)\big) \tag{17}$$

where $g(n)$ is a Gaussian random variable (mean = 0, variance = 1), and $u(n)$ is a random phase uniformly distributed in the range $[-\pi/2, \pi/2]$. This approach produces non-periodic, statistically consistent profiles across multiple runs.

In COMSOL Multiphysics, each surface profile was implemented as a 1D parametric curve and assigned to the labyrinth wall boundary. To ensure symmetry and eliminate directional bias, the lower wall curve was mirrored from the upper wall. Only non-repeating segments of the generated curves were used to suppress artificial periodicity.

A total of three representative datasets (see Tab. 4) were selected, each defined by unique (N, b_s) combinations to span a broad spectrum of surface morphologies from coarse, low-frequency structures to fine, high-frequency irregularities. For each dataset, the amplitude factor PC was swept across a range of values to modulate vertical roughness levels.

Tab. 4 Overview of parameter sets used for surface generation in molecular flow simulations [3]

Dataset	Spectral resolution	Spectral exponent	Roughness amplitude scaling	
	N	b_s	PC	Number of steps
1	30	0.5	0.0005 to 0.020	12
2	50	0.05	0.0001 to 0.002	11
3	100	0.1	0.0001 to 0.001	10

Each surface profile was generated and characterized using standard roughness, including amplitude parameters (*Ra*, *Rq*, *Rk*, *Rpk*, *Rvk*) and shape descriptors (*Rsk*, *Rku*). These parameters enabled the quantitative comparison of topographic characteristics and supported the interpretation of molecular transport behavior.

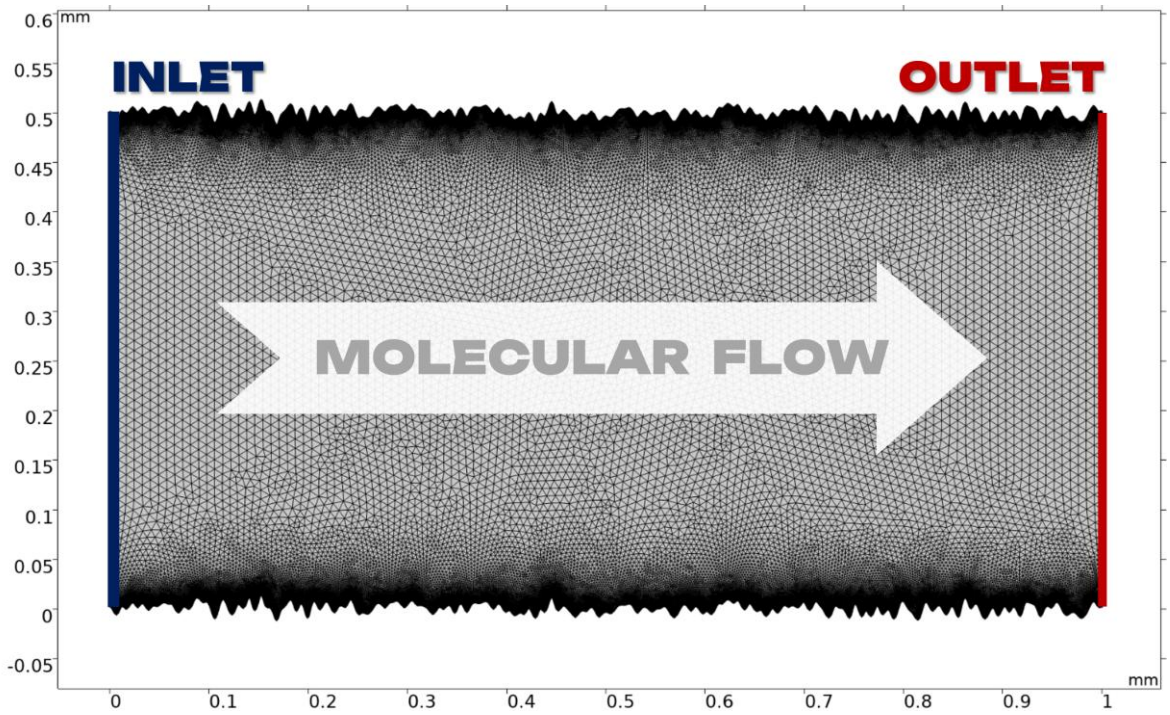

Fig. 34 Meshed 2D labyrinth geometry with synthetic surface roughness profiles [3]

The simulations were conducted under isothermal high-vacuum conditions using molecular properties representative of Fomblin Y LVAC 25/6 previously employed in experimental validation studies. An overview of the simulation setup, including geometric dimensions, meshing strategies, boundary conditions, and fluid characteristics, is provided in Tab. 5.

Tab. 5 Summary of simulation parameters and lubricant properties used for molecular flow simulations [3]

Category	Parameter	Value	Description
Geometry	Labyrinth length	1 – 10 mm	Parametrically varied to evaluate length influence
	Labyrinth width	0.2 – 1.0 mm	Parametrically varied to study confinement effects
Meshing	Grid resolution	Physics-controlled	Refined mesh near boundaries for surface details
Simulation	Temperature	373.15 K	Isothermal condition across the domain
	Inlet pressure	6E-4 Pa	Define as per boundary condition
	Outlet pressure	Total vacuum	Typically vacuum or near-zero pressure
Oil sample	Lubricant name	Fomblin Y LVAC 25/6	Perfluoropolyether (PFPE) lubricant
	Molecular weight	~3300 g/mol	Molecular mass used for simulations

5.7.4 INTEGRATED EVALUATION FRAMEWORK

By integrating MolFlow+ and COMSOL simulations with experimental and analytical studies, this work establishes a comprehensive and flexible modeling framework. MolFlow+ offers fast and accurate evaluation of molecular flow through static three-dimensional geometries, delivering valuable insights into the effects of geometric layout on pressure profiles and molecular escape probability.

COMSOL Multiphysics, on the other hand, extends the simulation capability by incorporating dynamically evolving scenarios, such as rotating seal walls, and by enabling the direct inclusion of real or synthetically generated surface roughness features. The particle tracing and molecular flow modules together provide a robust platform for analyzing transient effects, trajectory scattering, and geometric flow obstruction under UHV conditions. This integrated numerical approach enabled:

- Validation of analytical model predictions through detailed simulation outputs,
- Explanation of discrepancies observed in experimental results,
- In-depth investigation of how microstructural wall textures and macroscopic geometry affect vapor retention.

The synergy of MolFlow+ and COMSOL Multiphysics substantially strengthens the predictive capability of the overall research framework. It supports the development of optimized labyrinth seal geometries for space applications, where molecular transport efficiency under vacuum is critical.

6 RESULTS & DISCUSSION

This chapter presents the principal findings of the research, derived from a systematic combination of experimental measurements, analytical modeling, and molecular flow simulations. The objective was to investigate the mechanisms governing lubricant evaporation and molecular transport in vacuum environments, with a particular focus on the performance of labyrinth seals used in space applications.

To achieve this, a series of custom-built test rigs were employed to characterize lubricant mass loss and flow dynamics under controlled conditions. These experiments were complemented by numerical simulations and analytical assessments, providing a multi-perspective evaluation of how key physical parameters affect vapor retention. The integrated approach enabled the identification of dominant effects and the development of correction models to improve predictive accuracy.

The chapter is organized into thematic subsections, each focusing on a specific factor influencing molecular transport:

- Quantification of lubricant evaporation intensity in vacuum conditions, and comparison with analytical evaporation models.
- Influence of labyrinth geometry on seal efficiency and vapor containment.
- Effect of surface roughness on molecular transmission, including both experimental data and synthetic profile simulations.
- Analysis of molecular beaming and optimization of internal step geometry and corner features.
- Development and validation of a surface roughness correction model for transmission probability estimation.
- Evaluation of electrostatic fields as a passive method to suppress molecular escape.
- Assessment of dynamic rotational effects on molecular transmission in spinning seals.

These results collectively support the development of more efficient and reliable sealing strategies for use in space mechanisms operating in ultrahigh vacuum. Where applicable, correlations between analytical, numerical, and experimental results are provided to validate and contextualize the findings.

6.1 EVAPORATION INTENSITY

To quantify the evaporation behavior of liquid lubricants in vacuum, a dedicated ETR device was developed and employed (see Chapter 5.3). The experimental investigation focused on quantifying the evaporation behavior of two representative liquid lubricants commonly used in vacuum environments: Fomblin Y LVAC 25/6 (PFPE) and NYE 2001 (MAC). Throughout each test, key parameters such as vacuum chamber pressure, internal and

external temperatures, and the displacement of the reference plate were continuously monitored. Using a calibrated conversion method, these measurements were converted into time resolved mass loss data, allowing for a detailed evaluation of evaporation intensity under controlled vacuum conditions.

To assess the accuracy of established analytical models, the experimentally measured evaporation rates were compared against theoretical predictions based on a modified ESTL analytical framework. Due to limited availability and inconsistencies in manufacturer supplied vapor pressure data, the Clausius-Clapeyron relation was applied to estimate vapor pressure at the test temperature. This extrapolation used two reference values from the ESTL DOLLS database (see Fig. 21). The estimated vapor pressures were subsequently input into the Langmuir equation to calculate theoretical mass loss.

A comparison of experimental and analytical results (see Fig. 35 and Tab. 6) showed that theoretical models significantly overestimated evaporation rates for both lubricants. These discrepancies, consistent with earlier ESTL findings, underscore the need for model correction. Contributing factors include assumptions about vapor pressure, lubricant surface temperature, and idealized geometry. To address these limitations, empirically derived correction factors were introduced into the analytical formulation (see Tab. 7), substantially improving agreement between theoretical predictions and experimental observations.

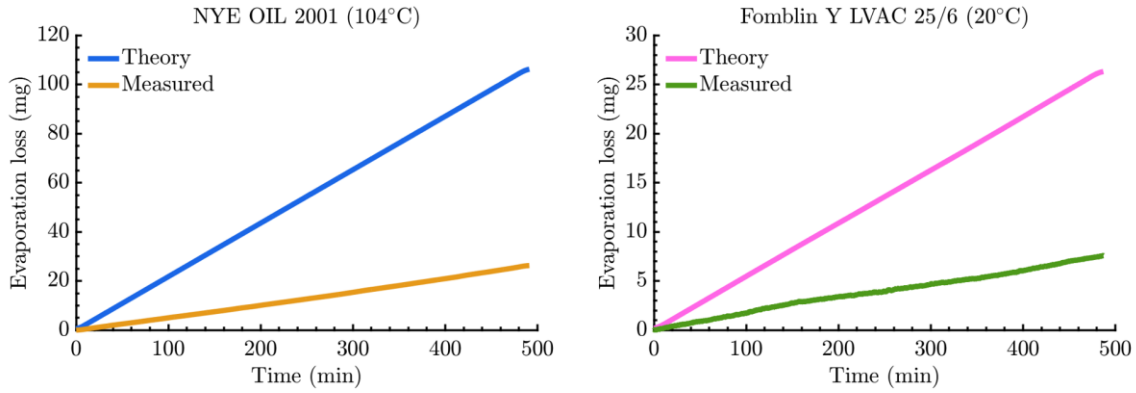

Fig. 35 Comparison of base oil evaporation losses from analytical predictions and experimental measurements [1]

Tab. 6 Comparison of analytical predictions and experimental measurements of lubricant evaporation loss [1]

Lubricant	Nye 2001	Fomblin Y LVAC 25/6
Analytical predictions	13.0 mg/h	3.0 mg/h
Experimental measurements	3.2 mg/h	0.9 mg/h
Overestimation (relative to measured)	306 %	233 %

These findings indicate that integrating experimentally derived correction factors into analytical models enables more accurate evaporation rate predictions, which can inform the reduction of lubricant quantities in vacuum systems without compromising operational reliability. This optimization has the potential to minimize contamination risks and reduce overall mission mass and associated costs.

6.1.1 CORRECTION MODEL FOR ANALYTICAL PREDICTIONS

To address the deviations observed between experimentally measured and analytically predicted evaporation rates, a correction model was developed based on the experimental data. The evaporation related mass loss was expressed using a modified form of the Langmuir equation, which incorporates an empirical correction factor to improve its accuracy for real lubricant behavior under vacuum conditions:

$$\frac{dm_{evap}}{dt} = -0.044 \frac{1}{\alpha} P_s(T) \sqrt{\frac{M}{T}} \tag{2}$$

In this formulation, the correction factor α compensates for discrepancies arising from physical effects not accounted for in the classical Langmuir model. These include molecular interactions, wetting behavior, surface heterogeneity, measurement uncertainties, and the limitations associated with the assumption of ideal gas behavior.

Using the experimental results for Fomblin Y LVAC 25/6 and NYE 2001, specific correction factors were derived for each lubricant and test condition, as summarized in Tab. 7. These values improve the predictive capability of analytical models for practical use in vacuum environments by aligning theoretical estimates more closely with observed behavior.

Tab. 7 Analytical model correction factors [1]

Lubricant	Nye 2001	Fomblin Y LVAC 25/6
Correction factor α [–]	4.1 ± 0.3	3.2 ± 0.7

This correction approach does not aim to replace the Langmuir equation but rather to enhance its applicability for complex lubricants commonly used in space systems. To ensure broader validity and robustness of the model, further research is needed. This includes extending the methodology to cover a wider range of lubricant chemistries and testing conditions and validating the model across different experimental setups. Such efforts are essential for establishing a reliable correction framework suitable for use in practice.

6.2 LABYRINTH SEAL GEOMETRY

The influence of labyrinth seal geometry on vapor retention was systematically investigated through experiments and validated using both analytical and numerical simulations. Three configurations (SHORT, LONG, and STEP; see Fig. 25) were fabricated and tested using a modified version of the ETR, referred to as the Labyrinth Test Rig (LTR) (see Chapter 5.4). This setup enabled continuous monitoring of lubricant mass loss under controlled vacuum conditions.

Time resolved experimental data demonstrated that increased geometric complexity significantly improves sealing performance. As illustrated in Fig. 36 , seals with longer flow paths and additional deflection features exhibited lower mass loss rates. Among the tested

configurations, the STEP geometry achieved the highest level of vapor retention. These findings confirm that intricate geometries are more effective in minimizing molecular leakage, consistent with previous observations in the literature [27,54,57].

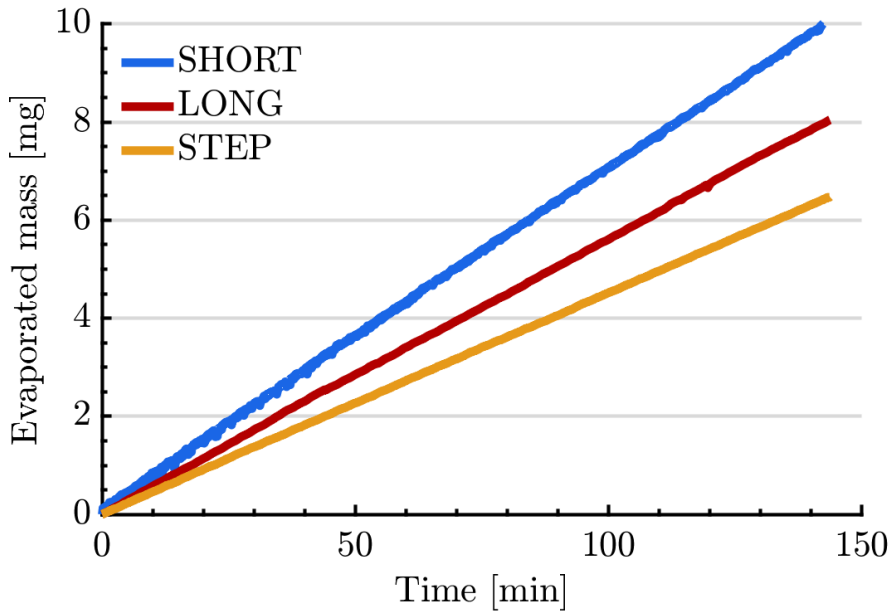

Fig. 36 Experimental measurements comparison of mass loss for various labyrinth seal geometries [2]

A comparative assessment using the ESTL analytical model (see Eq. (16)) and numerical simulations in COMSOL Multiphysics is presented in Fig. 37. The mass loss rate obtained using the three approaches is associated with specific uncertainty. For the analytical model and the simulations, this uncertainty is dominated by the input parameters, in particular the temperature determination used for the vapor pressure and evaporation rate calculations. The experimental results are limited by the measurement precision of the ETR device.

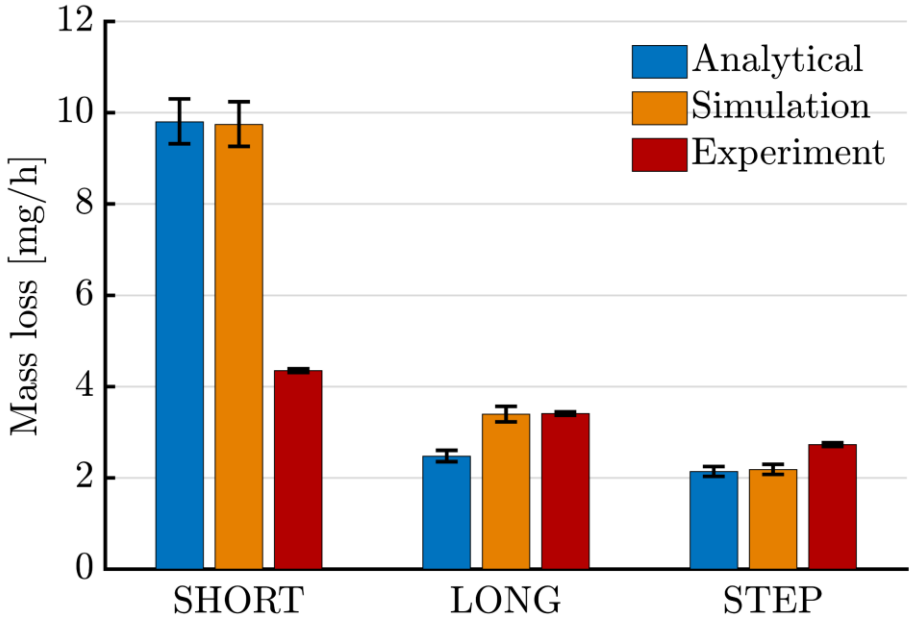

Fig. 37 Comparison of analytical, experimental, and simulation results for evaporative mass loss

For the simple SHORT configuration, both approaches overpredict the experimentally measured mass loss rate. For the more complex LONG and STEP geometries, the agreement with the experimental data improves for both approaches. In these cases, the analytical model tends to slightly underestimate mass loss, while the simulation results show the closest overall agreement, particularly for the LONG setup (see Tab. 8). Overall, increasing geometric complexity reduces the discrepancy between simplified analytical estimates and measured performance, and simulations provide the most reliable predictions for complex seal designs.

Tab. 8 Mass flow evaluation for specific labyrinths using diverse approaches

Approach	SHORT		LONG		STEP	
	[mg/h]	relative leak rate	[mg/h]	relative leak rate	[mg/h]	relative leak rate
Experiment	4.35 ± 0.04	1	3.41 ± 0.04	1	2.73 ± 0.04	1
Analytical	9.80 ± 0.5	2.25	2.48 ± 0.13	0.73	2.14 ± 0.11	0.78
Simulation	9.74 ± 0.5	2.24	3.39 ± 0.17	0.99	2.18 ± 0.11	0.80

To further investigate which geometric parameters most significantly affect transmission probability (TP), a design of experiments approach was employed. TP, defined as the ratio of molecules exiting the seal to those entering it, served as the primary metric for evaluating sealing efficiency. Simulation results shown in Fig. 38 indicate that corridor length and gap width are the most influential factors. The stepped labyrinth geometry achieved the best performance, due to its longer path and angled features that increase molecular collisions with the walls, thereby improving containment.

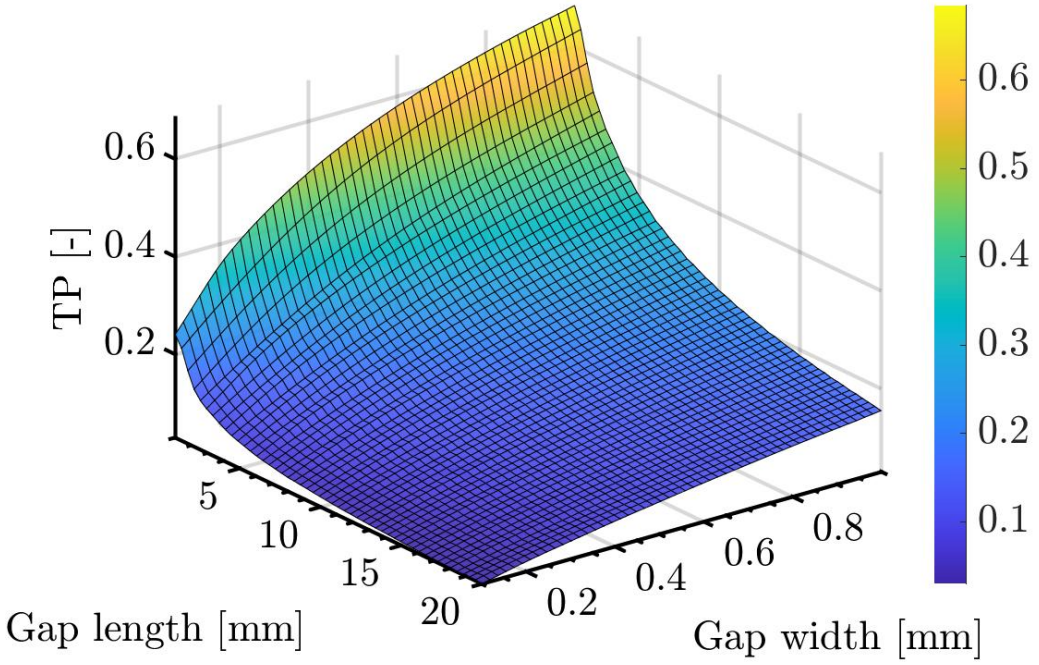

Fig. 38 Identification of key labyrinth geometry parameters impacting TP [2]

6.3 MOLECULAR BEAMING EFFECT

One of the factors often overlooked in labyrinth seal optimization is the molecular beaming effect, which arises in long and narrow channels. In such configurations, the angular distribution of molecular velocities deviates from the classical cosine profile, causing a higher number of molecules to travel directly along the seal corridor. This effect reduces the frequency of wall interactions, thereby compromising vapor retention.

To mitigate this phenomenon, complex geometries that redirect molecular paths are recommended. A particularly effective approach involves incorporating a step into the labyrinth seal that reorients the molecular flow by 90°. The placement of this step plays a critical role in reducing the beaming effect. A parametric sweep was performed in COMSOL Multiphysics by adjusting the axial step position of the STEP geometry in 0.5 mm increments along the 10 mm width of the seal. As summarized in Tab. 9 and shown in Fig. 39, the optimal step position was found to be at the midpoint of the seal, where mass loss was minimized.

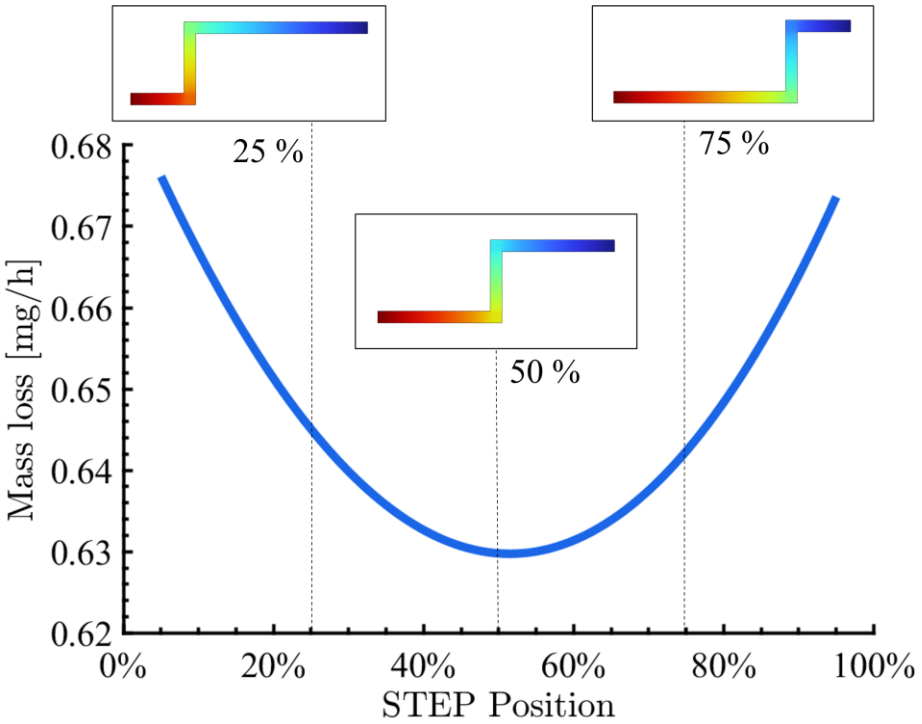

Fig. 39 Mass loss variation in labyrinth STEP geometry influenced by molecular beaming effect on step position [2]

Tab. 9 Labyrinth corner geometries and their impact on evaporated lubricant loss [2]

Step position (see Fig. 39)	Mass loss [mg/h]	Loss rate *
10 %	0.665	+ 5.19 %
25 %	0.643	+ 1.62 %
50 %	0.633	–
75 %	0.640	+ 1.24 %
90 %	0.662	+ 4.71 %

* Relative to the reference step position at the midpoint (50%) of the labyrinth seal.

Given the effectiveness of the STEP geometry in counteracting the beaming effect, additional investigation was conducted into the influence of step corner design. Conventional labyrinth seals often feature rounded corners due to manufacturing limitations, which may allow molecules to pass with reduced deflection. To address this, various corner geometries were modeled and simulated in COMSOL Multiphysics (see Fig. 40), including relief grooves and sharp transitions.

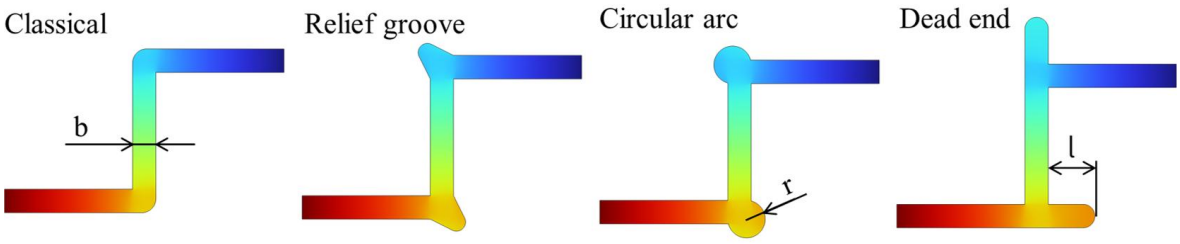

Fig. 40 Local geometries in the corner of labyrinth seals with stepped geometry [2]

Results (see Tab. 10) indicate that even minor modifications, such as implementing relief grooves, can yield meaningful improvements in sealing performance. These design changes are feasible with standard machining processes and have the potential to reduce lubricant mass loss over the operational life of a spacecraft.

Tab. 10 Labyrinth corner geometries and their impact on evaporated lubricant loss [2]

Corner geometry	Characteristic parameter	Loss reduction
Classical	–	–
Circular arc	r = b	3.8 %
Relief groove	type G *	3.9 %
Dead end	l = 2b	4.3 %

*According to ISO 18388:2016

6.4 SURFACE ROUGHNESS

Surface roughness was identified as a key factor affecting molecular transport and vapor retention in labyrinth seals operating under high vacuum conditions. Its influence was investigated through a two-stage approach that combined experimental testing with simulation-based modeling.

6.4.1 EXPERIMENTAL ANALYSIS OF ROUGHNESS EFFECTS

Initial investigations were conducted using two labyrinth seals with identical LONG geometry but differing surface finishes: one left untreated (ROUGH) and the other polished (SMOOTH). The surface topography of each seal was characterized using 3D optical profilometry (see Fig. 26), and the measured profiles were implemented into COMSOL Multiphysics simulations to enable accurate modeling of real surface geometries.

Tab. 11 Surface roughness analysis for inner and outer components of labyrinth seals [2]

Surface roughness	ROUGH		SMOOTH	
	Inner	Outer	Inner	Outer
Ra [µm]*	3.88	1.30	0.13	0.56
Sa [µm]	3.70	1.30	0.14	0.56
Sq [µm]	4.34	1.60	0.16	0.67
Sdr [µm]	1.99%	5.56%	0.01%	4.14%

* Average Ra parameter in the direction of highlighted mid-planes shown in Fig. 26

Since the analytical model (see Eq. (16)) does not account for surface texture, only experimental and simulation results were compared. Both datasets revealed a consistent difference of approximately 14% in mass loss, with the SMOOTH seal exhibiting higher leakage rates (see Fig. 41). The ROUGH seal demonstrated enhanced performance, losing 0.55 mg/h less lubricant, likely due to increased molecular scattering on its more irregular surface.

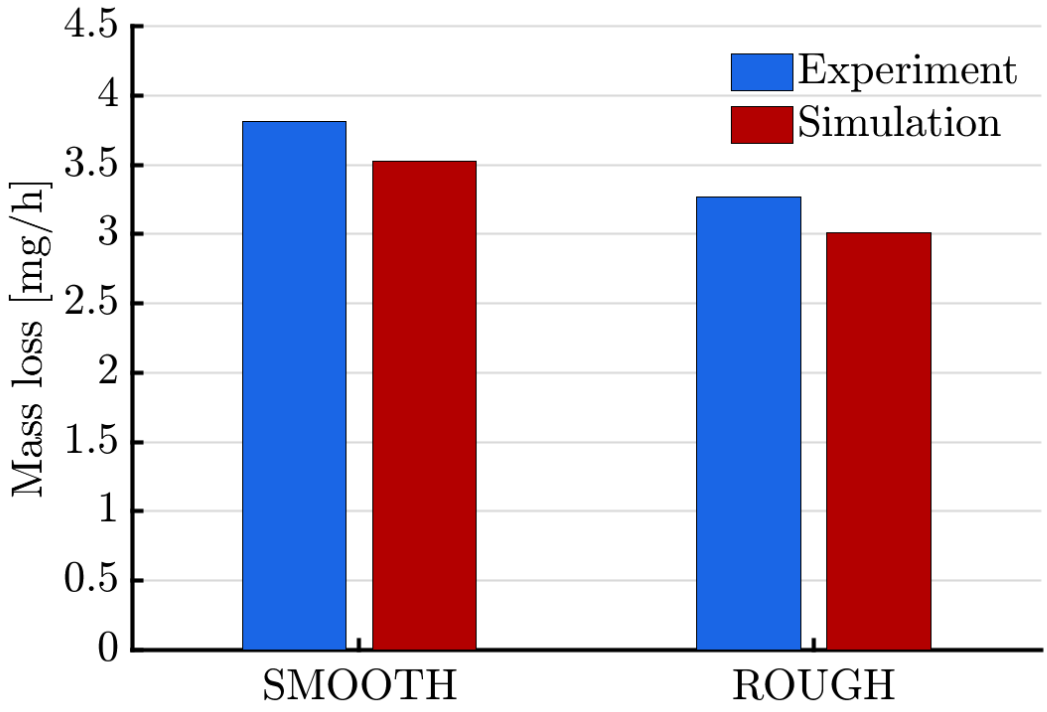

Fig. 41 Experimental and simulation investigation of surface roughness impact on labyrinth seal performance [2]

Two main effects contribute to this improvement: first, rougher surfaces present a marginally larger effective area (as indicated by the Sdr parameter in Tab. 11), and second, they create localized micro scale obstacles that interrupt direct molecular trajectories, increasing the number of wall collisions and thereby reducing net transmission probability of molecules.

6.4.2 TRANSMISSION PROBABILITY TRENDS

To generalize these findings and decouple roughness from specific manufacturing conditions, synthetic surface profiles were generated using parametric roughness modeling.

Three spectral parameters (see Tab. 4): spectral resolution (N), spectral exponent (b), and amplitude scaling coefficient (PC). These parameters governed the frequency, slope, and vertical scale of roughness features. The generated profiles were implemented into 2D labyrinth seal geometries in COMSOL Multiphysics. Simulations were conducted across a wide range of channel widths (W = 0.2–1.0 mm) and lengths (L = 1–10 mm), covering realistic seal configurations (see Tab. 5).

Contour plots of transmission probability (TP) and average surface roughness (Ra) across the spectral parameter space (N, b) revealed a strong inverse relationship: higher roughness consistently reduced molecular transmission, particularly in narrow and elongated channels where wall interactions are dominant (see Fig. 42). These findings underscore the dominant role of surface scattering in molecular transport through confined geometries.

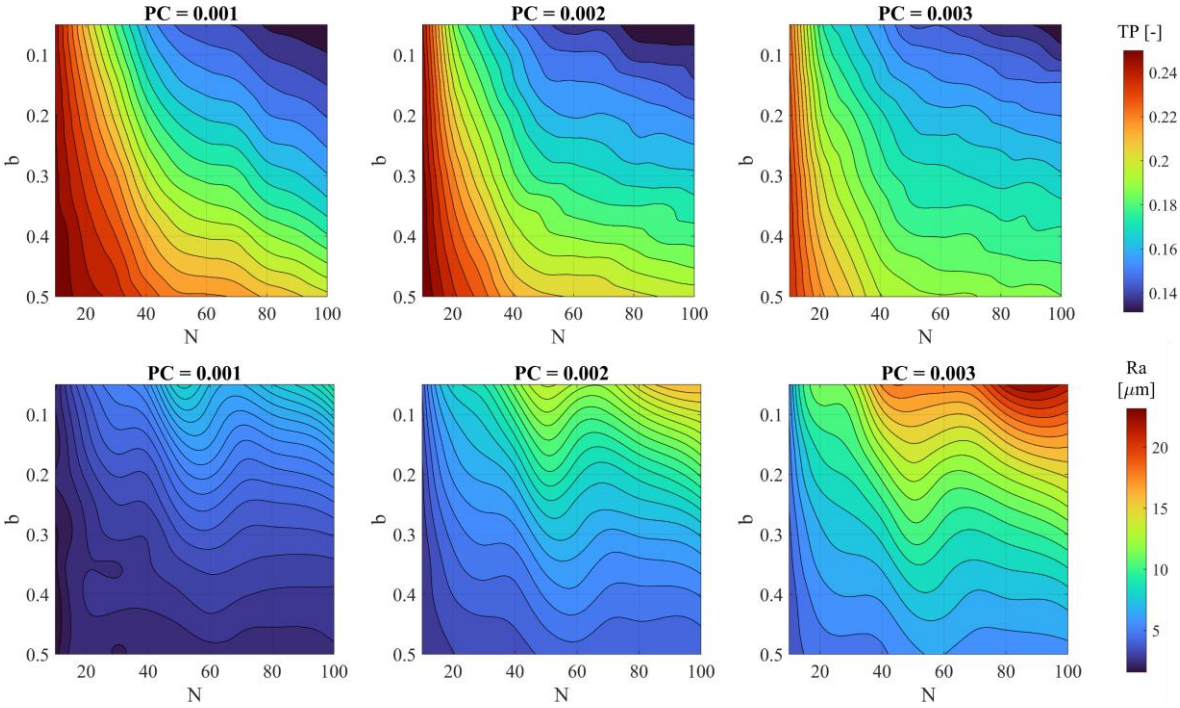

Fig. 42 Contour plots of transmission probability (TP) and average roughness (Ra) as functions of spectral parameters N and b for varying amplitude scaling (PC) [3]

Further analysis revealed a nonlinear relationship between TP and Ra across all simulated configurations. As Ra increased, TP consistently decreased, with the steepest reductions observed in narrow and elongated channels (see Fig. 43).

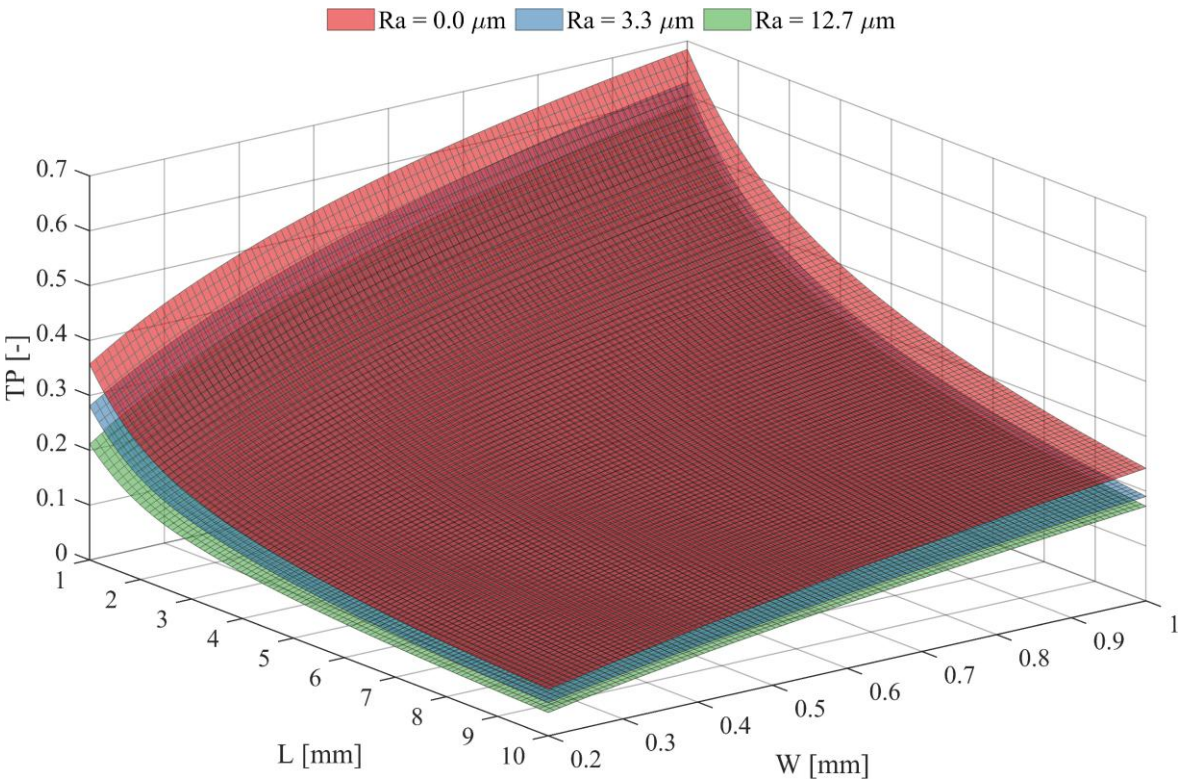

Fig. 43 Transmission probability across labyrinth length and width for varying surface roughness [3]

Quadratic fits the simulation data effectively captured this trend. TP declined sharply at low to moderate Ra levels, then gradually leveled off at higher values, indicating a saturation regime where additional roughness had diminishing impact (see Fig. 44).

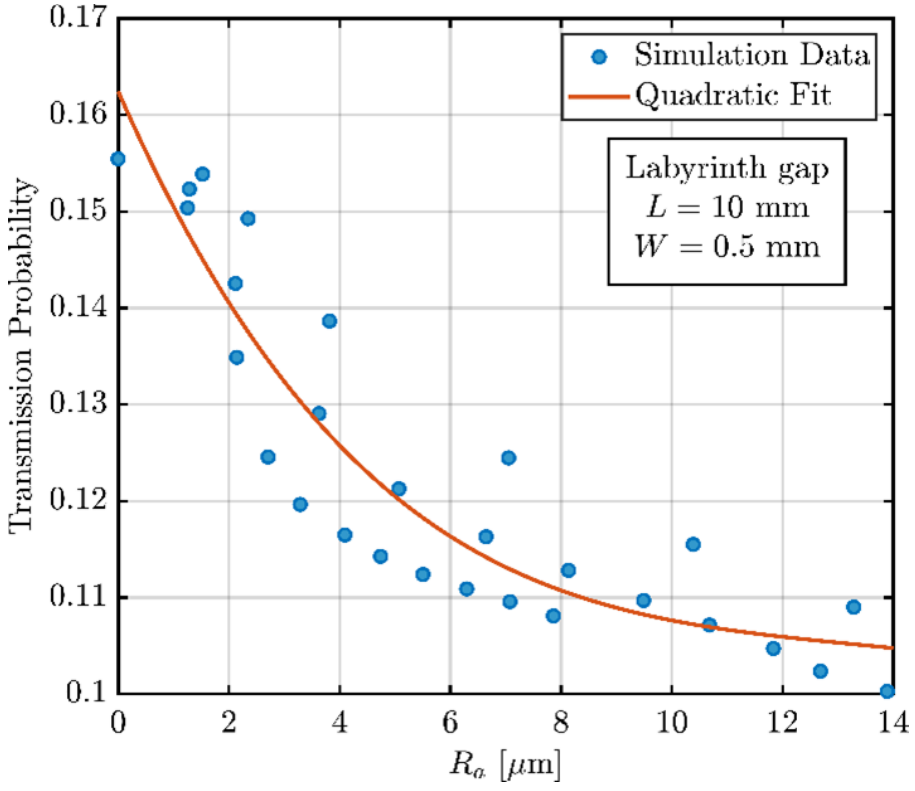

Fig. 44 Transmission probability vs. surface roughness (W = 0.5 mm, L = 10 mm) [3]

Channel geometry was also found to modulate the roughness effect in a nonlinear manner. Narrower gaps increased the likelihood of molecule-wall collisions per unit length, while longer seals intensified scattering through repeated interactions. These outcomes align with theoretical expectations in the molecular flow regime, where the mean free path exceeds channel dimensions and transport is dominated by surface interactions.

Despite variations in spectral structure among the datasets, roughness amplitude (Ra) emerged as the primary determinant of TP. This insight justified the development of a simplified correction model based solely on Ra and validated the use of amplitude-based descriptors for predicting molecular transport performance in practical labyrinth seal designs.

6.4.3 SIMULATION-BASED CORRECTION MODEL

To convert the simulation findings into a practical tool for design applications, a correction model was developed to estimate transmission probability (TP) as a function of Ra and channel geometry. The TP values exhibited a smooth, nonlinear relationship with Ra for fixed W and L values, which was effectively captured by a second-order polynomial:

$$TP\ (Ra, W, L) = A(W, L) \cdot Ra^2 + B(W, L) \cdot Ra + C(W, L) \tag{18}$$

where $A(W, L), B(W, L), C(W, L)$ are polynomial coefficients dependent on the geometric configuration and Ra is the arithmetic mean roughness (in μm). The coefficients were extracted from the simulation results by fitting curves to TP vs. Ra for each unique (W, L) combination. This generated a 3D matrix of coefficients $[A_{i,j}, B_{i,j}, C_{i,j}]$ indexed by width and length, enabling interpolation or surface fitting across arbitrary geometries within the studied range.

The complete set of polynomial coefficients is provided in the supplementary dataset [3], enabling interpolation and model application across a broad range of seal geometries. The model is especially valuable in the early stages of seal design, where quick estimations are critical for parameter screening and trade-off assessments. The correction function is valid within the range of parameters studied in the simulations:

- Surface roughness (Ra) up to approximately 13 µm
- Channel widths (W) of 0.2 – 1 mm
- Channel lengths (L) of 1 – 10 mm

Users should be cautious when applying the model beyond this validated domain. In cases involving very coarse roughness or extremely narrow channels, deviations may occur due to physical effects not fully captured by the polynomial fit, such as enhanced confinement or complex surface interactions. Additionally, while the model effectively captures the influence of roughness amplitude (Ra), it does not account for spectral attributes like spatial frequency content or slope. Future improvements could address these factors by incorporating parameters such as the spectral exponent (b_s) or compound metrics like Rq/Ra to improve predictive fidelity.

6.4.4 EXPERIMENTAL VALIDATION

To validate the model, its predictions were compared with experimental data from two labyrinth seal configurations that differed only in surface roughness. Both seals had identical dimensions (W = 0.5 mm, L = 10 mm), and evaporative mass loss measurements were used as a proxy for TP. A third configuration, with an ideally smooth surface (Ra = 0 µm), was introduced as a baseline for normalization (see Tab. 12).

Tab. 12 Comparison of model-predicted and experimental TP ratios [3]

	Ideal Labyrinth	Labyrinth 1	Labyrinth 2
Average surface roughness Ra [µm]	0.00	0.13	3.88
Labyrinth gap width W [mm]	0.5	0.5	0.5
Labyrinth gap length L [mm]	10	10	10
Model-predicted TP	0.2933	0.2924	0.2670
TP ratio (vs. Ideal Labyrinth)	1.0000	0.9968	0.9104
Measured evaporative loss	–	3.8 mg/h	3.3 mg/h
Evaporative loss ratio (vs. Labyrinth 1)	–	1.0000	0.8684
Predicted TP ratio (vs. Labyrinth 1)	–	1.0000	0.9131
Relative error (prediction vs. measurement)	–	0.0 %	5.1 %

Surface roughness was characterized by using a Bruker Contour GTX 3D optical profilometer. Model-predicted TP values were normalized relative to the ideal seal and compared against normalized experimental mass loss ratios. The comparison confirmed excellent agreement, with a maximum relative error of just 5.1%, validating the model's predictive utility.

These results confirm the correction model's validity and reliability for predicting TP reductions due to surface roughness. The model's simplicity and accuracy make it a valuable design tool. However, caution is warranted when applying it beyond the validated range, particularly in geometries with extremely high Ra, non-uniform topography, or 3D effects. Further experimental data covering more surface types and including spectral metrics would strengthen future model refinements.

6.4.5 DESIGN TRADE-OFFS AND MODEL LIMITATIONS

Beyond its predictive capability, the correction model developed in this study reveals an important design implication: surface roughness can serve as a compensatory parameter for geometric limitations in labyrinth seal design. Simulation results showed that increasing the average roughness amplitude (Ra) enables a reduction in channel length or a widening of the channel gap by approximately 35–40%, while maintaining a constant transmission probability (see Fig. 45). This opens new possibilities for improving design flexibility, reducing seal volume, and simplifying manufacturing processes, particularly in space systems where compactness and reliability are essential.

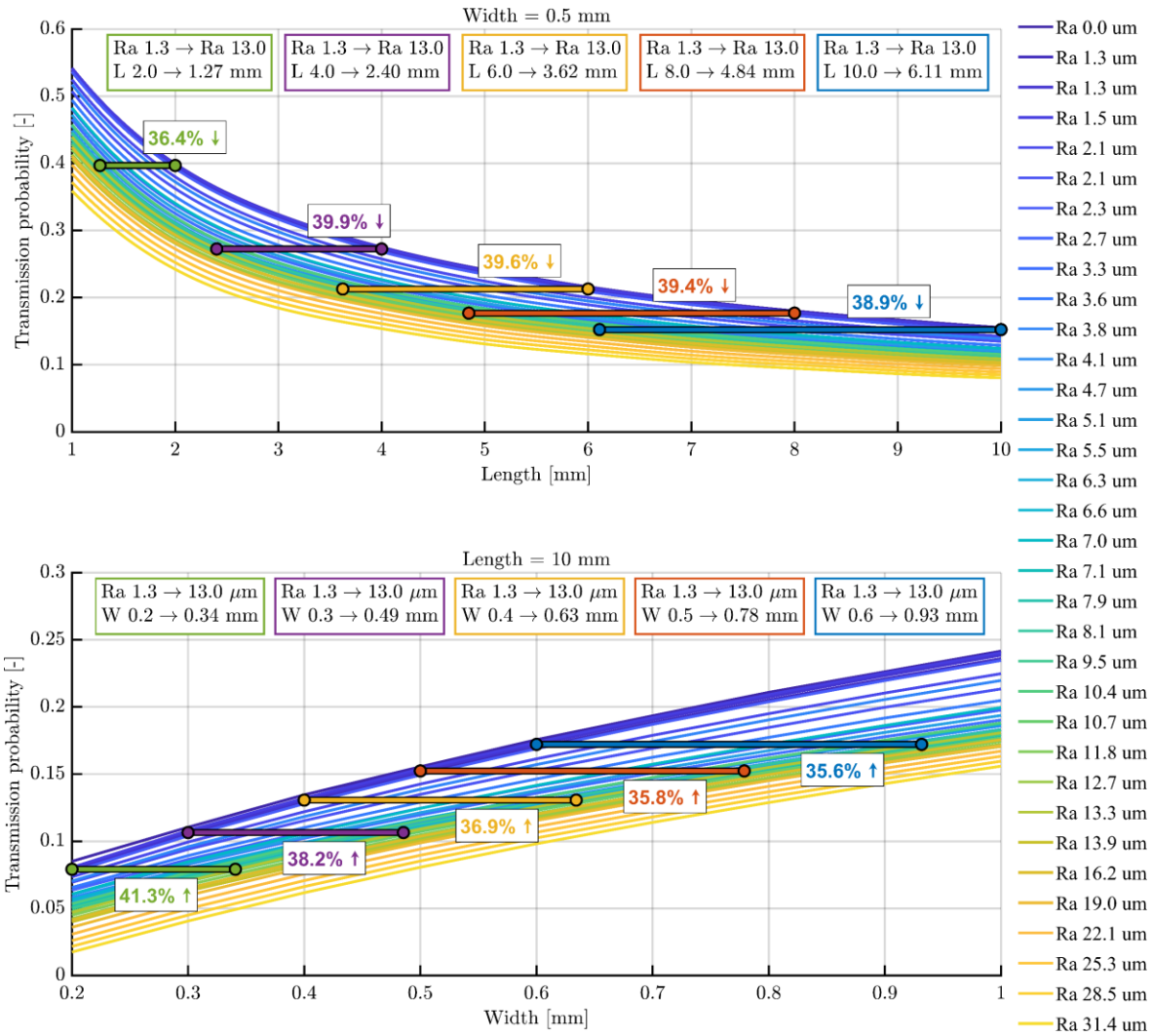

Fig. 45 Design trade-offs enabling seal length reduction or gap widening via increased surface roughness at constant transmission probability [3]

Despite its demonstrated utility, several limitations must be considered when applying the model. First, the use of synthetically generated roughness profiles, although systematic and reproducible, may not fully reflect the complexity of real surfaces. Machined or worn components often exhibit statistical irregularities, anisotropy, or localized defects that are not captured in idealized simulations. As such, model predictions may deviate when applied to actual surface finishes.

Second, the model is based on two-dimensional (2D) simulations. While this simplifies the computational process and captures dominant transport trends, it inherently omits three-dimensional (3D) effects that can influence molecular dynamics. Features such as cross-sectional curvature, surface variation, and complex corner geometries are not represented, and their influence on flow behavior warrants further investigation.

Third, the model relies exclusively on Ra as a scalar descriptor of surface morphology. While Ra effectively captures the amplitude driven component of molecular scattering, it does not account for higher order statistical properties such as skewness, kurtosis, peak sharpness, or surface anisotropy. These characteristics may influence flow in more irregular or asymmetric

configurations. In addition, gas-surface interaction effects, such as adsorption, desorption, and energy accommodation, are not considered, although they could become significant under specific environmental conditions, especially in reactive or high-temperature vacuum applications.

Lastly, the model's applicability is constrained by the spectral and geometric range used during its development. Predictions outside the validated Ra, W, and L domains, or under substantially different spectral profiles, should be interpreted with caution. Future developments should focus on:

- Incorporating real surface data from experimental profilometry.
- Extending simulations to 3D geometries.
- Including spectral descriptors (e.g., b exponent, Rq/Ra ratio).
- Accounting for thermophysical properties and surface chemistry.

These enhancements would improve robustness and extend the model's relevance for broader engineering applications.

6.5 ELECTROSTATIC FIELD

The influence of electrostatic fields on molecular transport through labyrinth seals was experimentally evaluated using the ELTR. This setup enabled the application of a constant 50 V electric field across the seal corridor under controlled high vacuum conditions. Four lubricants were tested, including MAC and PFPE oils and two ionic liquids (see Tab. 1), each evaluated under both neutral (0 V) and charged (50 V) conditions.

The results are summarized in Tab. 13 , which presents the measured evaporative mass loss and the relative change under electrostatic excitation. A slight reduction in mass loss was observed for Fomblin Y LVAC 25/6 (PFPE) and 1-Methyl-3-octylimidazolium TFSI (IL1), indicating a mild suppressive effect of the electric field on molecular escape. The ionic liquid 1-Ethyl-3-methylimidazolium TFSI (IL2) showed the largest reduction of 7.4%. In contrast, Nye 2001 (MAC) exhibited negligible change, suggesting minimal field sensitivity.

Tab. 13 Lubricant evaporative mass loss with and without electrostatic field [4]

	Mass loss [mg/h]		Electrostatic influence
	0 V	50 V	
PFPE	0.361	0.343	– 5.0 %
MAC	0.085	0.087	+ 2.0%
IL1	0.055	0.053	– 2.7 %
IL2	0.040	0.037	– 7.4 %

These results suggest that electrostatic fields may marginally enhance vapor retention, particularly for ionic or high molecular weight lubricants. However, the observed effects were relatively small, and further investigation is needed to draw definitive conclusions.

Future studies should incorporate higher field strengths, improved measurement accuracy, and tighter control of environmental parameters.

It is also important to consider the potential risks associated with electrostatic field application, such as micro-arcing, dielectric breakdown, and interference with sensitive electronics. Any practical use of this technique must carefully balance performance benefits with operational safety and reliability in spaceflight conditions.

6.6 ROTATIONAL DYNAMICS

The impact of rotational motion on molecular transport was assessed through COMSOL Multiphysics simulations for three labyrinth seal configurations: SHORT, LONG, and STEP. Each geometry was modeled with rotational motion applied to the inner wall, representing conditions encountered in high-speed space mechanisms. The resulting transmission probability (TP) was evaluated as a function of rotational speed in revolutions per minute (RPM).

Simulation results, shown in Fig. 46, revealed a clear decrease in TP with increasing RPM for the LONG and STEP configurations. This trend reflects enhanced molecule-wall interactions introduced by rotational dynamics, which increase the likelihood of momentum-altering collisions and reduce molecular transmission through the seal. In contrast, the SHORT geometry exhibited negligible change across the tested speed range, due to its limited wall length and lower probability of wall encounters.

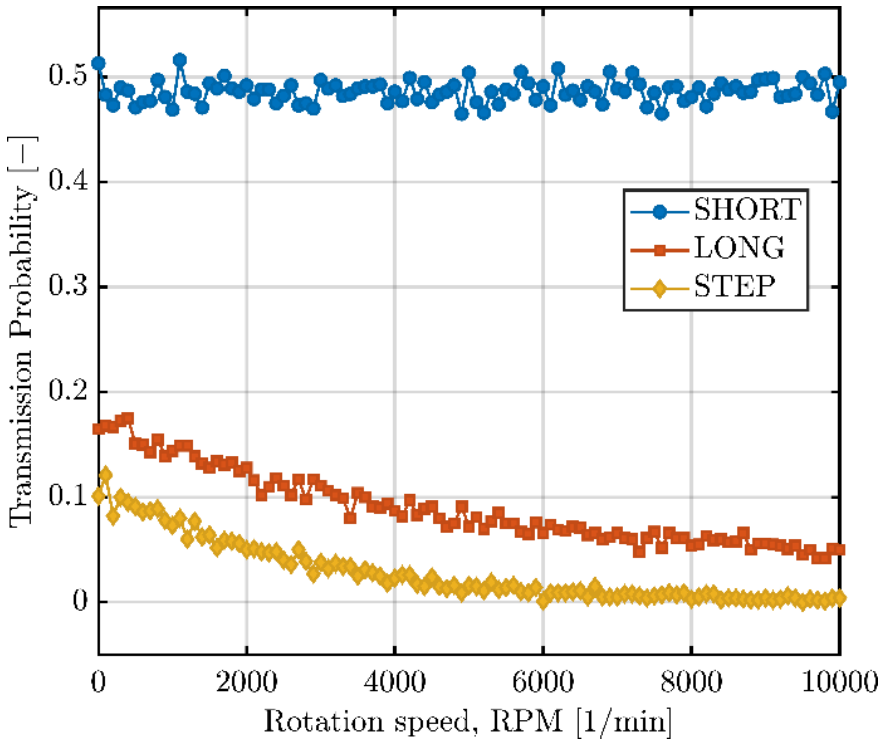

Fig. 46 Transmission probability vs. rotor speed for labyrinth seal geometries [4]

Due to physical limitations of the experimental apparatus, the exact geometries used in the simulation study could not be replicated in physical tests. Instead, experimental measurements were conducted using a dedicated Dynamic Labyrinth Test Rig (DLTR), which employed a different but representative seal geometry. This setup enabled real-time monitoring of lubricant mass loss under both static (0 RPM) and rotating (2000 RPM) conditions using Fomblin Y LVAC 25/7 as the test sample.

The results, summarized in Tab. 14 confirm the influence of rotational dynamics on molecular retention. Both simulation and experimental data showed a consistent reduction in mass loss of approximately 9–11 % when the labyrinth wall was spinning. The close agreement between experimental and numerical results validates the ability of the simulation model to capture essential physical mechanisms governing dynamic seal behavior.

Tab. 14 Simulation and experimental results for static and rotating labyrinth seal (0 and 2000 rev. per minute) [4]

	0 RPM	2000 RPM	Spin influence
Simulation	0.178 mg/h	0.161 mg/h	– 9.05 %
Experiment	0.188 mg/h	0.168 mg/h	– 10.6 %

These findings underscore the importance of including dynamic effects in labyrinth seal evaluations. The strong correlation between simulated and experimental results supports the applicability of numerical models for predicting performance under rotation. Given that many space mechanisms involve spinning components, accounting for the influence of rotational dynamics is essential for reliable vapor containment and overall seal effectiveness in operational environments.

7 CONCLUSIONS

This dissertation aims to improve the understanding of liquid lubricant behavior in space-relevant vacuum conditions and to translate that understanding into practical design guidance for space mechanisms. The work combines new, time resolved evaporation measurements, a dedicated test rig for labyrinth seals, development and calibration of analytical models, and high-fidelity molecular flow simulations. The experimental program covers both static and rotating conditions with controlled thermal environments, and results are cross-checked against independent gravimetric assessments. The modeling effort introduces empirical correction factors for classical evaporation formulas and validates transmission probability estimates with TPMC simulations. The study focuses on two lubricant families central to space applications, MAC and PFPE base oils, and on labyrinth seals as passive structures for vapor retention in rotating subsystems.

The main outcomes are presented in two parts. The first summarizes the scientific contributions, including quantitative discrepancies between analytical predictions and measurements, calibrated corrections for evaporation models, and verified relationships between seal geometry, surface roughness, and molecular transmission. The second provides engineering guidance that is directly applicable to the design and verification of labyrinth seal implementations, covering geometry selection, surface finish targets, beaming mitigation features, and the observed influence of rotation, along with clear statements of measurement uncertainty and applicability limits.

7.1 SCIENTIFIC OUTCOMES

1) Time resolved evaporation data and corrected analytics

A vacuum compatible ETR device was designed and used to generate time resolved evaporation data for two space relevant base oils (PFPE; Fomblin Y LVAC 25/6, and MAC; Nye 2001). Classical analytical predictions, obtained by combining Clausius–Clapeyron vapor pressure estimates with Langmuir expressions, consistently overpredicted mass loss by 230–310% under the tested conditions. An empirical correction factor was introduced to reconcile model outputs with measurements, yielding lubricant specific values with quantified uncertainty. This establishes a transparent procedure to calibrate analytical models against experiment rather than proposing a universal constant.

2) Geometry-performance relationships for labyrinth seals

An LTR device enabled controlled comparison of three seals (SHORT, LONG, STEP). Increased geometric complexity reduced evaporative loss, with the stepped layout performing best. Analytical correlations provided correct trends but appreciable error for simple passages, while molecular flow simulations matched experiments within about 5–15% for complex geometries. A sensitivity study identified corridor length and gap width as the dominant contributors to transmission probability.

3) Molecular beaming effect identified

Long, narrow passages exhibited molecular beaming that reduced wall collisions and increased through flow. Introducing a 90° step suppressed molecular beaming effect. A parametric study showed optimal placement near the corridor midpoint minimized loss. Local features at corners influenced performance measurably: relief grooves or sharp transitions provided small but consistent improvements.

4) Quantified influence of surface roughness and a compact correlation model

Paired experiments on nominally identical seals with different finishes, supported by simulations using measured profiles, showed that rougher walls lowered mass loss by roughly 14% for the tested case. A simulation-based correction model was formulated that predicts transmission probability as a function of Ra and channel geometry (width and length). The model reproduces measured trends with about 5% error within its validated domain (Ra up to ~13 μm, widths 0.2–1.0 mm, lengths 1–10 mm).

5) Dynamic effects confirmed for rotating labyrinth seals

Molecular flow simulations and a dedicated rotating test rig showed that wall rotation reduces transmission probability in elongated or stepped passages. For the tested conditions, rotation of the inner member produced a reduction in evaporative mass loss of about 9–11%. Short passages showed negligible sensitivity, consistent with fewer wall interactions.

6) Electrostatic influence observed to be small at low field strength

Applying a constant 50 V potential across the seal corridor produced only minor reductions in mass loss for PFPE and ionic liquids and no meaningful change for MAC oil. Within the range explored the effect was small, so no general performance claim is made. These results define baseline expectations and inform the design of future, stronger field studies.

7.2 ENGINEERING REMARKS

1) Evaporation prediction and budgeting

Use classical Langmuir analytics for initial assessment, then calibrate with lubricant and condition specific correction factors derived from time resolved tests. This reduces overestimation and allows tighter lubricant mass budgets without compromising reliability. The thesis provides the calibration workflow and representative factors for Fomblin Y LVAC 25/6 and Nye 2001 under the reported conditions.

2) Seal geometry selection and prioritization

Prefer stepped labyrinths over simple straight gaps when space permits. Increase effective path length and control gap width as the primary levers for lowering transmission probability. Place the principal 90° step near the corridor midpoint to counter beaming. Where feasible, incorporate small corner features such as relief grooves or sharp step transitions to gain additional, incremental reductions.

3) Using surface roughness as a design variable

Within the validated range, increasing Ra can trade against channel length or gap width while keeping transmission probability roughly constant. For preliminary design, the provided correction model allows about 35–40% reduction in length or comparable gap widening for suitably increased roughness, subject to mission-specific limits on wear, debris, and cleanliness. Specify roughness targets together with geometry and verify with profilometry.

4) Simulation-informed verification

Adopt a staged assessment: start with the SI analytical expression for quick screening, use the ESTL correlation for cross-check, then refine with molecular flow simulation for shortlisted geometries. Simulations reproduced complex seal performance within about 5–15% in this work and are recommended to finalize designs before hardware tests.

5) Account for operational rotation

For mechanisms that rotate, include the observed reduction in transmission for long or stepped geometries in performance estimates. Use static predictions as an upper bound and apply rotation aware simulations or tests during verification. Do not expect meaningful benefit in very short passages.

6) Electrostatic concepts remain exploratory

At 50 V the observed effect on mass loss was small. Electrostatic methods should not be relied upon for vapor retention without further evidence at higher fields and with careful attention to spacecraft charging, breakdown limits, and electromagnetic compatibility.

7) Testing and data practices

For evaporation characterization, use continuous, time-resolved measurements under controlled vacuum and temperature, and cross-check with gravimetric totals. Estimate vapor pressure at test temperatures consistently, document uncertainty, and report correction factors with bounds. For seals, test representative geometries in vacuum and, where applicable, under rotation to confirm model predictions before flight qualification.

7.3 LIMITATIONS

This work was performed at the component level rather than on flight qualified assemblies. The study considered two representative base oils, one MAC and one PFPE. The thermal and pressure ranges covered typical space conditions but did not include deep cryogenic or high temperature extremes, and thermal cycling was limited. Vapor pressure inputs were estimated with Clausius–Clapeyron fits based on manufacturers reference data, which introduces uncertainty. Labyrinth studies focused on three geometry configurations. Simulations of surface roughness influence were primarily two-dimensional, and the roughness model used Ra as the sole descriptor within a defined parameter range. The rotation study used surrogate geometry and modest speeds, so the results are indicative rather than comprehensive. Electrostatic effects were explored at a single, low field level in controlled bench tests; spacecraft level risks such as ESD and EMC were not assessed. Contamination was inferred from mass loss and transmission probability metrics. Direct optical performance impacts or spatial deposition maps were not measured.

7.4 FUTURE WORK

Several extensions would strengthen and broaden the results:

- Expand time-resolved evaporation measurements to a wider set of liquids (additional MAC and PFPE grades, ionic liquids, and selected greases), include controlled thermal histories and broader thermal cycling, and measure vapor pressure directly under identical conditions to reduce uncertainty input.
- Add combined environments, including radiation and atomic-oxygen exposure, to quantify coupled influences on evaporation and seal performance.
- Extend the rotation campaign to higher speeds, varied duty cycles, and matched geometries, and derive dynamic correction factors suitable for design use.
- Incorporate in-situ sensing (QCM arrays, optical thickness probes, or microbalances) to map local flux and deposition over long durations.
- Evolve the roughness study to 3D, include anisotropy and spectral descriptors, and validate across more manufactured surfaces. Convert the results into design charts and simple correction functions with stated validity ranges.
- Explore electrostatic actuation more broadly, including higher but safe fields, pulsed excitation, and compatibility with spacecraft ESD and EMC constraints.

- Broaden the role of labyrinths beyond vapor retention to mitigation of particulate ingress. Dedicated studies that couple molecular transport with particle filtration will be valuable for dusty environments, for example mechanisms operating on Mars where seals must suppress both evaporated lubricant and fine regolith intrusion.

7.5 CLOSING REMARKS

This dissertation advances both understanding and practice of liquid lubrication in vacuum. Scientifically, it shows that classical evaporation formulas overpredict mass loss under space-relevant conditions and demonstrates how time-resolved measurements can calibrate them to match reality. It also clarifies how labyrinth geometry and surface condition govern molecular transmission and confirms that calibrated TPMC simulations can reproduce measured trends. Practically, the work translates these findings into design-oriented guide: how to select and design labyrinth geometries, where to place deflection features to counter beaming, how much surface roughness reduces transmission within a defined range, and what performance changes to expect under rotation. Together, these results support cleaner, long-duration, and more reliable space mechanisms that rely on liquid lubricants in vacuum, while outlining a clear path for extending the methods to broader lubricant families, more complex geometries, and mission level contamination control.

8 LIST OF PUBLICATIONS

POUZAR, J., KOSTAL, D., SPERKA, P., KRUPKA, I., HARTL, M. Experimental study of space lubricant evaporation in a high vacuum environment. Vacuum, 2024, 219(A), 112758. ISSN 0042-207X. https://doi.org/10.1016/j.vacuum.2023.112758

POUZAR, J., KOSTAL, D., WESTERBERG, L. G., NYBERG, E., KRUPKA, I. Labyrinth seal design for space applications. Vacuum, 2025, 232, 113882. ISSN 0042-207X. https://doi.org/10.1016/j.vacuum.2024.113882

POUZAR, J., KOSTAL, D., WESTERBERG, L. G., NYBERG, E., POLACEK, T., JURIK, K., KRUPKA, I. Influence of surface roughness on molecular flow through labyrinth seals for space applications. Results in Engineering, 2025, 28, 107905. ISSN 2590-1230. https://doi.org/10.1016/j.rineng.2025.107905

POUZAR J., KOSTAL D., WESTERBERG L.G., KRUPKA I. *Labyrinth seal design for enhanced sealing of evaporated lubricant molecules in space mechanisms*. 21st European Space Mechanisms and Tribology Symposium (ESMATS), 2025. https://www.esmats.eu/esmatspapers/pastpapers/pdfs/2025/pouzar.pdf

9 LITERATURE

[1] Pouzar J, Kostal D, Sperka P, Krupka I, Hartl M. Experimental study of space lubricant evaporation in a high vacuum environment. Vacuum 2024; Volume 219, 112758. https://doi.org/10.1016/j.vacuum.2023.112758.

[2] Pouzar J, Kostal D, Westerberg L-G, Nyberg E, Krupka I. Labyrinth seal design for space applications. Vacuum 2025; Volume 232, 113882. https://doi.org/10.1016/j.vacuum.2024.113882.

[3] Pouzar J, Kostal D, Westerberg L-G, Nyberg E, Polacek T, Jurik K, et al. Influence of Surface Roughness on Molecular Flow Through Labyrinth Seals for Space Applications. Results in Engineering 2025; Volume 28, 107905. https://doi.org/10.1016/j.rineng.2025.107905.

[4] Pouzar J, Kostal D, Westerberg LG, Krupka I. Labyrinth seal design for enhanced sealing of evaporated lubricant molecules in space mechanisms, 21st European Space Mechanisms and Tribology Symposium (ESMATS); 2025.

[5] Roberts EW. Space tribology: its role in spacecraft mechanisms. J Phys D Appl Phys 2012; 45:503001. https://doi.org/10.1088/0022-3727/45/50/503001.

[6] ESA-ESTEC R& SD. ECSS-E-ST-33-01C Rev.2 – Mechanisms (1 March 2019) 2019:97.

[7] Roberts EW, Todd MJ. Space and vacuum tribology. Wear 1990; 136:157–67. https://doi.org/10.1016/0043-1648(90)90078-O.

[8] Butler RW. A Primer on Architectural Level Fault Tolerance (NASA/TM-2008-215108). 2008.

[9] Bhat BN. Aerospace Materials and Applications. vol. 255. 1st ed. Reston,VA: American Institute of Aeronautics and Astronautics, Inc.; 2018. https://doi.org/10.2514/4.104893.

[10] Schüler F, Holynska M, Henry T, Buttery M, Meier-Kirchner K, Göhringer C. Development of a Space Grease Lubricant with Long-Term-Storage Properties. Lubricants 2024; 12:72. https://doi.org/10.3390/lubricants12030072.

[11] Zhou M, Tong R, Zhang T, Liu G. Application of MoS2 in the space environment: a review. Frontiers of Mechanical Engineering 2023; 18:39. https://doi.org/10.1007/s11465-023-0755-1.

[12] Durand MM, Meurisse M-H, Vergne P, Sicre J, M. Lubricant Supply by Porous Reservoirs in Space Mechanisms. In: Flamand L, J.-M. Georges DD, Priest M, Taylor CM, Ehret P, Childs THC, et al., editors. Thinning Films and Tribological Interfaces, vol. 38, Elsevier; 2000, p. 777–85. https://doi.org/10.1016/S0167-8922(00)80180-7.

[13] Sun X. Solid Lubricants for Space Mechanisms. In: Wang QJ, Chung Y-W, editors. Encyclopedia of Tribology, Boston, MA: Springer US; 2013, p. 3165–72. https://doi.org/10.1007/978-0-387-92897-5_1230.

[14] Prozhega M V, Albagachiev AYu, Smirnov NI, Smirnov NN. Lubricating Materials for Mechanisms Operating in Space. Journal of Friction and Wear 2018; 39:335–40. https://doi.org/10.3103/S106836661804013X.

[15] Marchetti M, William RJ, Street KW, Pepper S V, Jansen MJ. Preliminary Evaluation of Greases for Space Mechanisms Using a Vacuum Spiral Orbit Tribometer. NASA 2001:10. https://ntrs.nasa.gov/api/citations/20020012806/downloads/20020012806.pdf.

[16] Sathyan K, Hsu HY, Lee SH, Gopinath K. Long-term lubrication of momentum wheels used in spacecrafts—An overview. Tribol Int 2010; 43:259–67. https://doi.org/10.1016/j.triboint.2009.05.033.

[17] ESA-ESTEC R& SD. ECSS-Q-TM-70-52A – Kinetic outgassing of materials for space (25 November 2011). Noordwijk, Netherlands: 2011. https://ecss.nl/hbstms/ecss-q-tm-70-52a-kinetic-outgassing-.

[18] The Vacuum Technology Book | Volume II. vol. 2. Pfeiffer Vacuum; 2013.

[19] Fote AA, Slade RA, Feuerstein S. Thermally Induced Migration of Hydrocarbon Oil. Journal of Lubrication Technology 1977; 99:158–62. https://doi.org/10.1115/1.3453002.

[20] Wang J, Mo Z, Zhang H, Liu H, Zeng X, Miao Q. Failure Mechanism and Accelerated Life Test Design of Space Bearing. 2018 Prognostics and System Health Management Conference (PHM-Chongqing), IEEE; 2018, p. 882–7. https://doi.org/10.1109/PHM-Chongqing.2018.00158.

[21] Hengeveld D, Mathison M, Braun J, Groll E, Williams A. Review of Modern Spacecraft Thermal Control Technologies. HVAC&R Res 2010; 16:189–220. https://doi.org/10.1080/10789669.2010.10390900.

[22] Krishnan S, Lee S-H, Hsu H-Y, Konchady G. Lubrication of Attitude Control Systems. Advances in Spacecraft Technologies, vol. 4, InTech; 2011. https://doi.org/10.5772/13354.

[23] Buttery M, Lewis S, Kent A, Bingley R, Cropper M. Long-Term Storage Considerations for Spacecraft Lubricants. Lubricants 2020; 8:32. https://doi.org/10.3390/lubricants8030032.

[24] Wolfberger A, Hausberger A, Schlögl S, Hołyńska M. Assessment of the chemical degradation of PFPE lubricants and greases for space applications: implications for long-term on-ground storage. CEAS Space Journal 2021; 13:377–88. https://doi.org/10.1007/s12567-021-00348-6.

[25] Eiden M, Seiler R. Space mechanisms and tribology challenges of future space missions. Acta Astronaut 2004; 55:935–43. https://doi.org/10.1016/j.actaastro.2004.04.011.

[26] Merstallinger A, Holzbauer R, Bamsey N. Cold Welding in Hold Down Points of Space Mechanisms Due to Fretting When Omitting Grease. Lubricants 2021; 9:72. https://doi.org/10.3390/lubricants9080072.

[27] Anderson MJ, Freeman S, Roberts EW. Evaporative losses of vacuum-compatible oils through labyrinth seals. In: Harris R ~A., editor. ESMATS, vol. 524, 2003, p. 255–70.

[28] Prozhega M V, Reschikov EO, Smirnov NN. Research of the Lifetime and Lubricant Properties of Greases for Rolling Bearings Operating in Space Conditions. Journal of Friction and Wear 2021; 42:431–7. https://doi.org/10.3103/S1068366621060088.

[29] Jones WR, Jansen MJ. Tribology for space applications. Proceedings of the Institution of Mechanical Engineers, Part J 2008;222. https://doi.org/10.1243/13506501JET305.

[30] Gleirscher M, Wolfberger A, Schlögl S, Hołyńska M, Hausberger A. Accelerated Thermo-Catalytic Degradation of Perfluoropolyether (PFPE) Lubricants for Space Applications. Lubricants 2023; 11:81. https://doi.org/10.3390/lubricants11020081.

[31] ESA Space Debris Office. ESA'S ANNUAL SPACE ENVIRONMENT REPORT. 2025.

[32] Roberts EW, Eiden M. Space Tribology Handbook. vol. 2. 5th ed. ESR Technology Ltd.; 2013.

[33] Lince JR. Effective Application of Solid Lubricants in Spacecraft Mechanisms. Lubricants 2020; 8:74. https://doi.org/10.3390/lubricants8070074.

[34] Buttery M. An Evaluation of Liquid, Solid, and Grease Lubricants for Space Mechanisms Using a Spiral Orbit Tribometer 2010. https://esmats.eu/amspapers/pastpapers/pdfs/2010/buttery.pdf.

[35] Vanhulsel A, Velasco F, Jacobs R, Eersels L, Havermans D, Roberts EW, et al. DLC solid lubricant coatings on ball bearings for space applications. Tribol Int 2007; 40:1186–94. https://doi.org/10.1016/j.triboint.2006.12.005.

[36] Buttery M, Kent A, Forster D, Vortsellas A. Hybrid lubrication of PFPE Fluids and Sputtered MoS2 2018.

[37] Bingley R, Buttery M, Kelly G, Kent AVA. Hybrid Lubrication as a Practical Candidate for Space Mechanism Applications. ESMATS 2021.

[38] Roberts EW, Todd MJ. Space and vacuum tribology. Wear 1990; 136:157–67. https://doi.org/10.1016/0043-1648(90)90078-O.

[39] Vazirisereshk MR, Martini A, Strubbe DA, Baykara MZ. Solid Lubrication with MoS2: A Review. Lubricants 2019; 7:57. https://doi.org/10.3390/lubricants7070057.

[40] Mukhtar SH, Gulzar A, Saleem S, Wani MF, Sehgal R, Yakovenko AA, et al. Advances in development of solid lubricating MoS2 coatings for space applications: A review of modeling and experimental approaches. Tribol Int 2024; 192:109194. https://doi.org/10.1016/j.triboint.2023.109194.

[41] Zaretsky E V. Liquid lubrication in space. Tribol Int 1990; 23:75–93. https://doi.org/10.1016/0301-679X(90)90041-M.

[42] Fusaro R. Liquid lubrication for space applications. NASA 2001:42. https://ntrs.nasa.gov/api/citations/20010049424/downloads/20010049424.pdf.

[43] Nyberg E, Schneidhofer C, Pisarova L, Dörr N, Minami I. Ionic Liquids as Performance Ingredients in Space Lubricants. Molecules 2021;26. https://doi.org/10.3390/molecules26041013.

[44] Kadoski Tadeusz; Wojdyna P. Liquid lubricants for space engineering and methods for their testing. J KONES Powertrain and Transport 2011;18.

[45] Cai M, Yu Q, Liu W, Zhou F. Ionic liquid lubricants: when chemistry meets tribology. Chem Soc Rev 2020; 49:7753–818. https://doi.org/10.1039/D0CS00126K.

[46] Masuko M, Jones WR, Jansen R, Ebihara B. A Vacuum four-ball tribometer to evaluate liquid lubricants for space applications. Lubrication Engineering 1994:13. https://www.researchgate.net/publication/236567326_A_Vacuum_four-ball_tribometer_to_evaluate_liquid_lubricants_for_space_applications.

[47] Santos LMNBF, Ferreira AIMCL, Štejfa V, Rodrigues ASMC, Rocha MAA, Torres MC, et al. Development of the Knudsen effusion methodology for vapour pressure measurements of low volatile liquids and solids based on a quartz crystal microbalance. J Chem Thermodyn 2018; 126:171–86. https://doi.org/10.1016/j.jct.2018.07.004.

[48] ESTL. Evaporation Lives of Space Oils. ESA-ESTL-TM-0162 01- 2019.

[49] Stanley S. HM. ESA-ESTL-TM-0162 01- An Experimental Assessment of the Evaporation Lives of Space Oils. 2018.

[50] Langmuir I. VAPOR PRESSURES, EVAPORATION, CONDENSATION AND ADSORPTION. J Am Chem Soc 1932; 54:2798–832. https://doi.org/10.1021/ja01346a022.

[51] Wang QJ, Chung Y-W, editors. Encyclopedia of Tribology. Boston, MA: Springer US; 2013. https://doi.org/10.1007/978-0-387-92897-5.

[52] Hu H, Larson RG. Analysis of the Effects of Marangoni Stresses on the Microflow in an Evaporating Sessile Droplet. Langmuir 2005; 21:3972–80. https://doi.org/10.1021/la0475270.

[53] Carré DJ, Bertrand PA. A Model to Calculate Evaporative Oil Loss in Spacecraft Mechanisms. Tribology Transactions 1999; 42:282–8. https://doi.org/10.1080/10402009908982218.

[54] Gardos MN. Labyrinth Sealing of Aerospace Mechanisms—Theory and Practice. A S L E Transactions 1974; 17:237–50. https://doi.org/10.1080/05698197408981462.

[55] Marchetti M, Jones WR, Pepper S V, Jansen MJ, Predmore RE. In-Situ, On-Demand Lubrication System for Space Mechanisms. Tribology Transactions 2003; 46:452–9. https://doi.org/10.1080/10402000308982650.

[56] Piska M, Metelkova J. On the Influence of Surface Roughness on Molecular Flow and Geometric Compensation in Vacuum Labyrinth Seals. MM Science Journal 2014; 2014:476–80. https://doi.org/10.17973/MMSJ.2014_06_201408.

[57] Rowntree A. ESTL-TM-238 - A Review of Oil Loss Models for Labyrinth Seals and Filters for Space Applications 2000.

[58] Tondu T, Vanhove E, Roussel JF, Faye D. Mixture Effects in Contaminant Reemission. J Spacecr Rockets 2016; 53:1172–7. https://doi.org/10.2514/1.A33507.

[59] Suliga A, Ergincan O, Rampini R. Modeling of Spacecraft Outgassed Contamination Levels by Thermogravimetric Analysis. J Spacecr Rockets 2021; 58:1010–6. https://doi.org/10.2514/1.A35020.

[60] Briscoe HM. Why space tribology? Tribol Int 1990; 23:67–74. https://doi.org/10.1016/0301-679X(90)90040-V.

[61] ESA-ESTEC R& SD. ECSS-E-ST-10-04C Rev.1 – Space Engineering, Space Environment. Noordwijk, Netherlands: 2020.

[62] Nautiyal H, Singh S, Gautam RKS, Goswami RN, Khatri OP, Verma P, et al. The state of art on lubrication methods in space environment. Phys Scr 2024;99. https://doi.org/10.1088/1402-4896/ad1d3e.

[63] Lu Y, Shao Q, Yue H, Yang F. A Review of the Space Environment Effects on Spacecraft in Different Orbits. IEEE Access 2019; 7:93473–88. https://doi.org/10.1109/ACCESS.2019.2927811.

[64] Fleischauer PD, Hilton MR. Applications of space tribology in the USA. Tribol Int 1990; 23:135–9. https://doi.org/10.1016/0301-679X(90)90046-R.

[65] Miyoshi K. Aerospace mechanisms and tribology technology. Tribol Int 1999; 32:673–85. https://doi.org/10.1016/S0301-679X(99)00092-4.

[66] Hołyńska M, Sarah R-C, Orcun E, Bruno B, Claudia A, Riccardo R. Lessons Learnt from Lubricants' Testing at Estec Materials' Laboratories 2021:5.

[67] Hampson MR, Wardzinski B. The Evaluation and Validation of New Creep Barrier Films for Prevention of Oil Loss by Migration. In: Ouwehand L, editor. ESA Special Publication, vol. 737, 2015, p. 30.

[68] Fan X, Fu H, Li W, Zhu M. Exploring Lubrication Function of MACs Greases for TC4 Alloy Under Sliding and Fretting Conditions. Tribol Lett 2018; 66:135. https://doi.org/10.1007/s11249-018-1091-1.

[69] Dai Q, Huang W, Wang X. Surface roughness and orientation effects on the thermo-capillary migration of a droplet of paraffin oil. Exp Therm Fluid Sci 2014; 57:200–6. https://doi.org/10.1016/j.expthermflusci.2014.04.023.

[70] Nancarrow P, Mohammed H. Ionic Liquids in Space Technology - Current and Future Trends. ChemBioEng Reviews 2017; 4:106–19. https://doi.org/10.1002/cben.201600021.

[71] Jones WR, Poslowski AK, Shogrin BA, Herrera-Fierro P, Jansen MJ. Evaluation of Several Space Lubricants Using a Vacuum Four-Ball Tribometer. Tribology Transactions 1999; 42:317–23. https://doi.org/10.1080/10402009908982223.

[72] Solvay Specialty Polymers. Fomblin® PFPE Lubes for Vacuum Applications 2017.

[73] Nevshupa RA, Conte M, Igartua A, Roman E, de Segovia JL. Ultrahigh vacuum system for advanced tribology studies: Design principles and applications. Tribol Int 2015; 86:28–35. https://doi.org/10.1016/j.triboint.2015.01.020.

[74] Huang W, Wang X. No migration of ionic liquid under temperature gradient. Colloids Surf A Physicochem Eng Asp 2016; 497:167–70. https://doi.org/10.1016/j.colsurfa.2016.03.002.

[75] Zhang J. MoS 2 Lubricating Film Meets Supramolecular Gel: A Novel Composite Lubricating System for Space Applications. ACS Appl Mater Interfaces 2021;13. https://doi.org/10.1021/acsami.1c20182.

[76] Tadmor R. Marangoni flow revisited. J Colloid Interface Sci 2009; 332:451–4. https://doi.org/10.1016/j.jcis.2008.12.047.

[77] Cheng T, Zhao B, Chao J, Meeks SW, Velidandea V. The lubricant migration rate on the hard disk surface. Tribol Lett 2001; 9:181–5. https://doi.org/10.1023/A:1018813022532.

[78] Grützmacher PG, Jalikop S V, Gachot C, Rosenkranz A. Thermocapillary lubricant migration on textured surfaces - a review of theoretical and experimental insights. Surf Topogr 2021;9:013001. https://doi.org/10.1088/2051-672X/abd07c.

[79] Keller A, Karlson K-O, Grebe M, Schüler F, Goehringer C, Epp A. Practical Evaluation of Ionic Liquids for Application as Lubricants in Cleanrooms and under Vacuum Conditions. Lubricants 2024; 12:194. https://doi.org/10.3390/lubricants12060194.

[80] Langmuir I. The Vapor Pressure of Metallic Tungsten. Physical Review 1913; 2:329–42. https://doi.org/10.1103/PhysRev.2.329.

[81] Malyshev OB. Vacuum in Particle Accelerators. Wiley; 2019. https://doi.org/10.1002/9783527809134.

[82] Buttery M, Gaillard L, Rajala S, Roberts E, Rohr T. Fomblin Z25: A New Method for its Degradation Assessment & Proposal for Safe Operation in Space 2013.

[83] Koutsoyiannis D. Clausius–Clapeyron equation and saturation vapour pressure: simple theory reconciled with practice. Eur J Phys 2012; 33:295–305. https://doi.org/10.1088/0143-0807/33/2/295.

[84] ESA-ESTEC R& SD. ECSS-Q-ST-70-01C – Cleanliness and contamination control (15 November 2008). 2008.

[85] Seasly E, Wrigglesworth W. Blind to Chemistry: Molecular Contaminant Films We Could Be Missing During Visual Inspections and the Potential Impact to System Performance. Journal of the IEST 2020; 63:13–20. https://doi.org/10.17764/1557-2196-63.1.13.

[86] Dirri F, Palomba E, Longobardo A, Zampetti E, Saggin B, Scaccabarozzi D. A review of quartz crystal microbalances for space applications. Sens Actuators A Phys 2019; 287:48–75. https://doi.org/10.1016/j.sna.2018.12.035.

[87] Nagamitsu Yoshimura. Vacuum Technology. Berlin, Heidelberg: Springer Berlin Heidelberg; 2008. https://doi.org/10.1007/978-3-540-74433-7.

[88] Dworkin JP, Adelman LA, Ajluni T, Andronikov A V., Aponte JC, Bartels AE, et al. OSIRIS-REx Contamination Control Strategy and Implementation. Space Sci Rev 2018; 214:19. https://doi.org/10.1007/s11214-017-0439-4.

[89] Hansen P, Townsend J, Hedgeland R. Lessons Learned from the Hubble Space Telescope (HST) Contamination Control Program. Journal of the IEST 2007; 50:44–60. https://doi.org/10.17764/jiet.50.1.c7835r3280617256.

[90] Kersevan R, Ady M. Recent developments of Monte-Carlo codes Molflow+ and Synrad+. 10th International Particle Accelerator Conference 2019:1327–30. https://doi.org/10.18429/JACoW-IPAC2019-TUPMP037.

[91] Kersevan R, Pons J-L. Introduction to MOLFLOW+: New graphical processing unit-based Monte Carlo code for simulating molecular flows and for calculating angular coefficients in the compute unified device architecture environment. Journal of Vacuum Science & Technology A: Vacuum, Surfaces, and Films 2009;27:1017–23. https://doi.org/10.1116/1.3153280.

[92] COMSOL. COMSOL Multiphysics | Molecular Flow Module 2023.

[93] Abraham NS, Hasegawa MM, Wooldridge EM, Henderson-Nelson KA. The use of the Molecular Adsorber Coating technology to mitigate vacuum chamber contamination during Pathfinder testing for the James Webb Space Telescope. In: Egges J, Soares CE, Wooldridge EM, editors., 2016, p. 99520C. https://doi.org/10.1117/12.2236704.

[94] Brockwell TG, Meech KJ, Pickens K, Waite JH, Miller G, Roberts J, et al. The mass spectrometer for planetary exploration (MASPEX). 2016 IEEE Aerospace Conference, IEEE; 2016, p. 1–17. https://doi.org/10.1109/AERO.2016.7500777.

[95] Lewis SD, Buttery M, Poyntz-Wright O, Kent A, Vortsellas A. Accelerated testing of tribological components - Uncertainties and solutions 2018.

[96] Li Z, Zhang Z, Yong Q, Ma G, Wei A, Wang H. Novel Tribometer for Coated Self-Lubricating Spherical Plain Bearings in a Vacuum. Lubricants 2022; 10:291. https://doi.org/10.3390/lubricants10110291.

[97] Jones WR, Pepper S V, Jansen MJ, Nguyen QN, Kingsbury EP, Loewenthal S, et al. A New Apparatus to Evaluate Lubricants for Space Applications - The Spiral Orbit Tribometer (SOT). SAE Transactions 2000; 109:1048–53. https://doi.org/10.4271/2000-01-1828.

[98] Parthasarathi NL, Jose B, Davinci MA, Arivazhagan N, Vasudevan M. Effect of nitrogen on high temperature dry sliding wear of 316L (N) stainless steel. Journal of Mechanical Science and Technology 2024; 38:5449–58. https://doi.org/10.1007/s12206-024-0918-y.

[99] Mondal B, Mukherjee T, Finch NW, Saha A, Gao MZ, Palmer TA, et al. Vapor Pressure versus Temperature Relations of Common Elements. Materials 2022; 16:50. https://doi.org/10.3390/ma16010050.

[100] García J, Abou Naccoul R, Fernández J, Razzouk A, Mokbel I. Vapor-Pressure Measurements and Modeling of Dipentaerythritol Ester Lubricants. Ind Eng Chem Res 2011; 50:4231–7. https://doi.org/10.1021/ie102166r.

[101] Morales W, Street KW, Richard RM, Valco DJ. Tribological Testing and Thermal Analysis of an Alkyl Sulfate Series of Ionic Liquids for Use as Aerospace Lubricants. Tribology Transactions 2012; 55:815–21. https://doi.org/10.1080/10402004.2012.715322.

[102] Iizuka A, Shibata E, Sato M, Nakamura T. Vapor pressure measurements of PbBr2 by the Knudsen effusion method and identification of its vapor species. Thermochim Acta 2015; 622:103–6. https://doi.org/10.1016/j.tca.2015.10.014.

[103] Jones WR, Jansen MJ, Gschwender LJ, Snyder CE, Sharma SK, Predmore RE, et al. The tribological properties of several silahydrocarbons for use in space mechanisms. Journal of Synthetic Lubrication 2004; 20:303–15. https://doi.org/10.1002/jsl.3000200404.

[104] Dijkstra AJ. Vacuum Stripping. Edible Oil Processing from a Patent Perspective, Boston, MA: Springer US; 2013, p. 205–18. https://doi.org/10.1007/978-1-4614-3351-4_9.

[105] Livesey G. Flow of gases through tubes and orifices. In: Lafferty JM, editor., Foundations of Vacuum Science and Technology; 1998, p. 25.

[106] Tong R, Liu G. Friction Property of Impact Sliding Contact under Vacuum and Microgravity. Microgravity Sci Technol 2019; 31:85–94. https://doi.org/10.1007/s12217-018-9667-9.

[107] Tribble AC, Boyadjian B, Davis J, Haffner J, McCullough E. Contamination control engineering design guidelines for the aerospace community. In: Glassford APM, Breault RP, Pompea SM, editors., 1996, p. 4–15. https://doi.org/10.1117/12.258298.

[108] Buhl R. Calculating the speed of pumping systems. Vacuum 1966; 16:187–91. https://doi.org/10.1016/0042-207X(66)91164-X.

[109] Santeler DJ, Boeckmann MD. Molecular flow transmission probabilities of rectangular tubes. Journal of Vacuum Science & Technology A: Vacuum, Surfaces, and Films 1991;9:2378–83. https://doi.org/10.1116/1.577280.

[110] Kersevan R. Analytical and numerical tools for vacuum systems. Vacuum in Accelerators 2007:28. https://doi.org/10.5170/CERN-2007-003.285.

[111] O'Hanlon JF. A User's Guide to Vacuum Technology. Wiley; 2003. https://doi.org/10.1002/0471467162.

[112] Dushman S, Lafferty JM, Peacock RN. Scientific Foundations of Vaccum Technique. J Electrochem Soc 1963; 110:77C. https://doi.org/10.1149/1.2425722.

[113] Lafferty JM, editor. Foundations of Vacuum Science and Technology. New York: John Wiley & Sons; 1998.

[114] Shafaat Gharamaleki Y, Shams M. Numerical investigation of conductance of porous media in high vacuum systems. Vacuum 2011; 86:311–7. https://doi.org/10.1016/j.vacuum.2011.07.045.

[115] Füstöss L. Calculation of transmission probability in molecular flow through straight tubes. Vacuum 1970; 20:279–83. https://doi.org/10.1016/S0042-207X(70)80360-8.

[116] Li Y, Chen X, Wang L, Guo L, Li Y. Molecular flow transmission probabilities of any regular polygon tubes. Vacuum 2013; 92:81–4. https://doi.org/10.1016/j.vacuum.2012.11.013.

[117] Papadopoulos CE, Yeung H. Uncertainty estimation and Monte Carlo simulation method. Flow Measurement and Instrumentation 2001; 12:291–8. https://doi.org/10.1016/S0955-5986(01)00015-2.

[118] Sun H, Faghri M. Effect of Surface Roughness on Nitrogen Flow in a Microchannel Using the Direct Simulation Monte Carlo method. Numeri Heat Transf A Appl 2003; 43:1–8. https://doi.org/10.1080/10407780307302.

[119] CERN. MolFlow+ A Monte-Carlo Simulator package developed at CERN 2023.

[120] COMSOL Multiphysics® v. 6.2. www.comsol.com. COMSOL AB, Stockholm, Sweden. n.d.

[121] Shams M, Khadem MH, Hossainpour S. Direct simulation of roughness effects on rarefied and compressible flow at slip flow regime. International Communications in Heat and Mass Transfer 2009; 36:88–95. https://doi.org/10.1016/j.icheatmasstransfer.2008.08.018.

[122] Sazhin O. The effect of surface roughness on internal free molecular gas flow. Vacuum 2019; 159:287–92. https://doi.org/10.1016/j.vacuum.2018.09.031.

[123] Marengo M, Zhdanov S, Chignoli L, Cossali GE. Micro-Heat-Sinks for Space Applications. ASME 2nd International Conference on Microchannels and Minichannels, ASMEDC; 2004, p. 87–95. https://doi.org/10.1115/ICMM2004-2323.

[124] ASTM. E1559-09 Test Method for Contamination Outgassing Characteristics of Spacecraft Materials 2022. https://doi.org/10.1520/E1559-09R22.

[125] Vogel M. Molecules in electromagnetic fields: from ultracold physics to controlled chemistry. Contemp Phys 2020; 61:307–8. https://doi.org/10.1080/00107514.2021.1890826.

[126] Ji Y, Yuan K, Chung JN. Numerical simulation of wall roughness on gaseous flow and heat transfer in a microchannel. Int J Heat Mass Transf 2006; 49:1329–39. https://doi.org/10.1016/j.ijheatmasstransfer.2005.10.011.

[127] Ticconi F, Pulvirenti L, Pierdicc N. Models for Scattering from Rough Surfaces. Electromagnetic Waves, InTech; 2011. https://doi.org/10.5772/19318.

10 APPENDED PAPERS

PAPER [1]

EXPERIMENTAL STUDY OF SPACE LUBRICANT EVAPORATION IN A HIGH VACUUM ENVIRONMENT

Pouzar et al.

Vacuum, Volume 219, Part A, 2024

doi: 10.1016/j.vacuum.2023.112758

Vacuum 219 (2024) 112758

Contents lists available at ScienceDirect

Vacuum

journal homepage: www.elsevier.com/locate/vacuum

Experimental study of space lubricant evaporation in a high vacuum environment

Josef Pouzar *, David Kostal, Petr Sperka, Ivan Krupka, Martin Hartl

Faculty of Mechanical Engineering, Brno University of Technology, Brno, 61669, Czech Republic

ARTICLE INFO

Handling Editor: Oleg Malyshev

Keywords:
Space tribology
Vacuum evaporation
Multiply-alkylated cyclopentane
Perfluoropolyether

ABSTRACT

The liquid lubricant evaporation in space applications poses significant challenges, raising the risk of inaccurate estimation of lubricant implementation and the potential contamination of satellite subsystems. The study of vacuum evaporation becomes highly relevant with the increasing use of liquid lubricants in satellite constellations. This research presents a novel methodology for assessing the lubricant evaporation rate, focusing on establishing a correlation between existing analytical models and experimental measurements. The obtained experimental results clearly demonstrate a disparity between the existing analytical models and the measured evaporated mass of vacuum base oils. Importantly, these results indicate higher evaporation rates predicted by the analytical approach. This emphasises the importance of refining the analytical models to accurately predict the amount of liquid lubricant evaporated.

1. Introduction

Space mechanisms operate under harsh conditions, including extreme vibrations, deep vacuum, significant temperature variations, and long periods of inactivity [1]. Redundancy is often limited in space mechanisms due to mass and size constraints, meaning that any malfunction or failure of these mechanisms can compromise the mission. Tribological failures, resulting from catalytic degradation processes, fretting, or vacuum evaporation, are among the primary causes of premature termination of space missions [2–6].

To prevent tribological failures, solid lubricants such as MoS_2 and PTFE, as well as liquid lubricants like PFPE and MAC, are commonly employed [7–9]. These lubricants can be used separately or in a hybrid combination, where the liquid lubricant acts as a protective layer over a thin-film coating of solid lubricant [10,11]. Their choice depends on the operating conditions, particularly the ambient temperature and vacuum pressure [8,12].

Liquid lubricants encompass a group of lubricants that include base lubricating oils and greases, which consist of base oil, additives, and thickeners [13,14]. Thickeners can serve as reservoirs for retaining the base lubricating oil [15]. Commonly used lubricants in space mechanisms and laboratory testing include mineral oils, silicones, esters, perfluoropolyether (PFPE), synthetic hydrocarbons (SHC), multiply alkylated cyclopentanes (MACs), and ionic compounds [14–17]. MAC and PFPE are particularly popular lubricants due to their properties [18]. PFPE lubricants have high density and extremely low vapor pressure [15,16,18] but are more prone to creep and autocatalytic degradation [16,19]. MAC lubricants offer a combination of excellent wear protection, low evaporation rates, and reduced tendency to creep, making them highly suitable for laboratory testing [13,16,18].

The extensive use of liquid lubricants in space applications is driven by the increasing number of satellite constellations in recent years and the need to extend their service life [20,21]. These lubricants are chosen for their satisfactory properties and cost-effectiveness [18]. However, their application is limited by the extreme operating temperatures and vacuum evaporation encountered in space environments.

Extreme temperatures present challenges for liquid lubricants, as high temperatures can cause molecular decomposition and low temperatures result in undesirable increases in viscosity [3]. Vacuum evaporation amplifies these challenges by causing contact drying and potential contamination of sensitive components, leading to performance degradation or malfunctions [22–24]. Vacuum evaporation of base oils and greases occurs when the ambient vacuum pressure reaches the substance vapor pressure [6,7,25]. The loss of molecules from the substance can be estimated using the Langmuir equation [7,26,27], which defines the rate at which the liquid's vapor strikes an area of interface between the mono-molecular fluid and the surrounding environment:

* Corresponding author.
E-mail address: Josef.Pouzar@vut.cz (J. Pouzar).

https://doi.org/10.1016/j.vacuum.2023.112758
Received 31 July 2023; Received in revised form 23 October 2023; Accepted 1 November 2023
Available online 2 November 2023
0042-207X/© 2023 Elsevier Ltd. All rights reserved.

Nomenclature

dM/Adt	Evaporation rate per area [kg/m^{2}s]
p_v	Liquid vapor pressure [Pa]
p_p	Partial pressure in the gas [Pa]
M	Molar mass [g/mol]
k	Boltzmann constant [m^{2}kg/s^{2}K]
T	Substance temperature [K]
dm_{evap}/dt	Evaporation rate per area [g/cm^{2}s]
$P_s(T)$	Temperature dependent vapor pressure [mbar]
p_1, p_2	Vapor pressure [mbar]
R	Gas constant [J/molK]
L	Enthalpy (heat) of vaporization [J/mol]
α	Correction factor [−]

$$\frac{dM}{Adt} = (p_v - p_p)\sqrt{M/2\pi kT} \tag{1}$$

Once a molecule evaporates, it does not return to the substance but condenses on colder surfaces and might contaminate sensitive devices [7,16]. The input parameters in Eq. (1) must be accurately determined, as any inaccuracies can result in a significant disparity between analytical and experimental evaluations [25,28,29]. The fundamental model for the vacuum evaporation of pure chemical compounds is the ESTL (European Space Tribology Laboratory) zero-order Langmuir equation [7,29–31], which is a modification of the original Langmuir equation Eq. (1) and is defined as follows:

$$\frac{dm_{evap}}{dt} = -0.044 P_s(T)\sqrt{M/T} \tag{2}$$

The vapor pressure is temperature-dependent, and this dependency can be interpreted by the Clausius-Clapeyron law [28,32], which enables the estimation of vapor pressure at a specific temperature:

$$\ln\frac{p_2}{p_1} = \frac{L}{R}\left(\frac{1}{T_1} - \frac{1}{T_2}\right) \tag{3}$$

The intensity of lubricant vacuum evaporation can be assessed either under real operating conditions (highly accurate but expensive and time-consuming) or through accelerated testing procedures [16,33,34]. Accelerated tests condense the testing period and impose intensified boundary conditions (e.g., temperature, load, speed) [16,33]. This offers a cost-effective and time-efficient alternative to real-condition testing but may introduce potential measurement deviations [33,34]. Several certified accelerated testing facilities employ in-situ quartz crystal microbalance (QCM) for evaluating the lubricant evaporation intensity [30]. The experimental results are compared with external laboratory balance measurements taken before and after the experiment to ensure reliable data acquisition [7,29,30]. However, none of these measurement methods can directly observe the evaporation process, which could be valuable for further research.

This study focuses on the vacuum evaporation process, as it is the most influential process in liquid lubricant application and contamination. While the evaporation intensity can be easily determined through analytical calculations, practical experience and previous research indicate that the results may not be accurate. To validate this assumption, a new in-situ measurement methodology has been developed to study the process of vacuum evaporation and compared the experimental results with analytical calculations.

2. Materials and methods

2.1. Evaporation test rig

The Evaporation test rig (ETR) is a novel test apparatus designed for quantifying liquid lubricant evaporation in high and ultra-high vacuum environments. The experiment methodology employed is similar to that of a balance scale. The ETR consists of a primary pivoted scale beam with a weighing pan for sample testing, as well as counterweights on the opposite side (see Fig. 1). The scale beam and weighing pan holder are connected to sharp wedges that allow for single-axis rotation. The tips of the wedges make linear contact with a pressed razor at an obtuse angle. To ensure isolation, the ETR is placed on a support beam connected to a flange of the vacuum chamber. The flange incorporates a bracket that holds a capacitive proximity sensor. This sensor measures the distance from the elongated compensative part of the scales, known as the pointer. The pointer tip is fitted with a reference plate, which serves as a reference surface for the proximity sensor.

During the process of lubricant evaporation, the ETR undergoes tilting to maintain balance as a result of the changing weight. The displacement of the pointer caused by this tilting is measured by the proximity sensor. The measured displacement is then used to calculate the total mass evaporated over time, considering variables such as pressure and temperature. The ETR is operated within a vacuum chamber that is equipped with an external heating source, which can be either a thermal chamber or localized heating with appropriate insulation. This setup allows for accelerated testing and precise control of temperature conditions. The modular characteristics of the ETR (see Table 1) offer flexibility in interchanging components, such as the weighing pan and counterweights, facilitating the investigation of various experiments, including testing labyrinth seals and studying outgassing behavior.

2.2. Test sample

MAC base oil NYE OIL 2001 and PFPE base oil FOMBLIN Y LVAC 25/6 were selected for experiments conducted in this study (see Table 2). NYE OIL 2001 is a frequently used oil in space applications [35] with low vapor pressure, making it suitable for the experimental accelerated

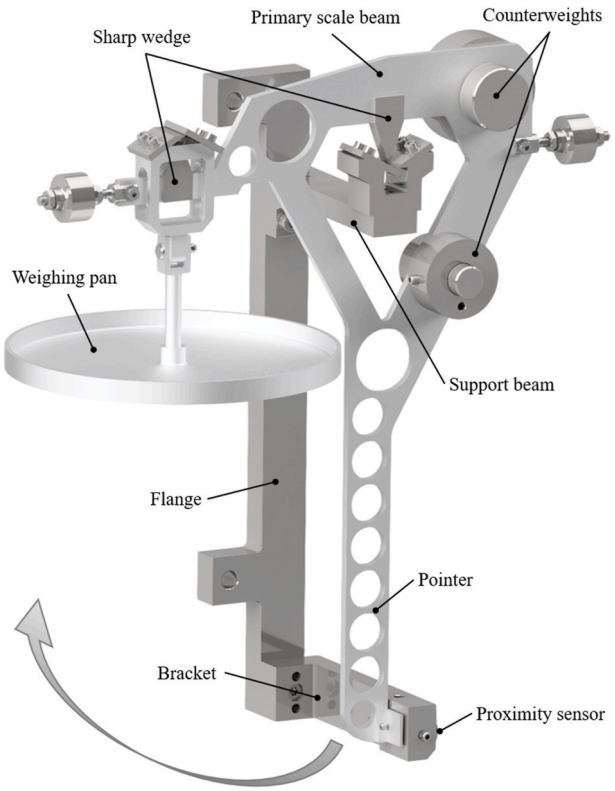

Fig. 1. Evaporation test rig description.

Table 1
Evaporation test rig characteristics.

Parameter	Value
Dimensions (W, H, D)	220 × 125 × 200 mm
Operating temperatures	−100 … 150 °C
Sample weight	10–100 g
Weighing precision	±0.04 mg

Table 2
Tested base oils properties.

Lubricant name	NYE OIL 2001	FOMBLIN Y LVAC 25/6
Lubricant type	MAC	PFPE
Kinematic viscosity (20 °C)	305 cSt	276 cSt
Vapor pressure (mbar)	1.00×10^{-8} (20 °C)	7.98×10^{-8} (25 °C)
	2.33×10^{-8} (38 °C)	7.98×10^{-5} (100 °C)
	5.70×10^{-7} (100 °C)	
Molecular weight (g/mol)	910	3300
Density (g/cm^3)	0.84	1.90

Table 3
Evaporation rate results.

Lubricant	NYE OIL 2001	FOMBLIN Y LVAC 25/6
Operating temp.	104 °C	20 °C
Theory (mg/h)	13.0	3.0
Measured (mg/h)	3.2	0.9

conditions. FOMBLIN Y LVAC 25/6 is a vacuum-compatible oil selected in its higher vapor pressure, allowing vacuum evaporation experiments at room temperatures. The lubricant test sample is applied onto the annulus surface of the weighing pan, where it spreads uniformly owing to its low viscosity. The lubricant surface area is considered equivalent to the annulus surface, which can be easily determined. The amount of oil used in the test may vary, primarily depending on the molar mass of the lubricant. It is crucial to ensure complete coverage of the entire pan surface to accurately determine the lubricant surface area and achieve an optimal film height, thus minimizing the drying potential.

2.3. Calibration

Before conducting experimental testing, it is essential to calibrate the measuring device to establish accurate conversion ratios and input parameters. The calibration procedure, detailed in the discussion chapter, encompasses multiple phases, including the assessment of weighing accuracy, repeatability, and temperature analysis. The calibration results for NYE OIL 2001 are presented in Table 4 to Table 6.

2.4. Thermal stabilization

To ensure consistent boundary conditions during experimental measurements, it is essential, to begin with a vacuum system bakeout process. Bakeout involves heating the vacuum system to a temperature range of 150–200 °C under vacuum conditions for a sufficient duration [36]. This process effectively removes absorbed impurities present within the vacuum system. The bakeout is followed by a thermal stabilization procedure to establish steady-state operating temperatures and maintain constant conditions. During the stabilization phase, the system's internal temperature becomes evenly distributed, the pressure decreases to the desired vacuum level to initiate evaporation, and most contaminants and volatile compounds in the lubricant evaporate. The bakeout and thermal stabilization duration typically lasts 2–3 days, depending on the ambient conditions within the vacuum chamber and the specific heating mechanism employed. Ensuring a uniform temperature distribution is crucial to prevent the formation of temperature gradients and subsequent condensation of evaporated molecules.

Table 4
ETR calibration – atmosphere.

Number of measurements		7
Proximity sensor	resolution (static)	0.375 nm
	measuring range	0.5 mm
Calibration weight	calibrated weight (E1)	5.0 mg
Distance change	average distance change	89.9 µm
	tolerance (scatter)	±0.7 µm
	accuracy	1.5 %
Ratio (atmosphere)	distance/weight	17.9 µm/1.0 mg
Inverse determination	distance change	36.1 µm
	calibrated weight (F2)	2.0 mg
	weight determination	2.006 (±0.015) mg

Table 5
Thermal detection analysis results.

Temperature (°C)	NYE OIL 2001	FOMBLIN Y LVAC 25/6
Heating	140.0	21.5
Weighing pan	104.0	20.0
Support beam	104.6	21.6
Bracket	103.5	19.8
Thermocouples type		K (PFA)
Thermocouples accuracy		±0.75 %

Table 6
ETR Calibration – Vacuum results for NYE OIL 2001.

Analytical balance	readout	0.1 mg
	linearity	0.3 mg
Operating temperature		104.20 °C
Distance change		41.1 µm
Evaporated lubricant weight		4.1 mg
Ratio (vacuum)		10.0 µm/1.0 mg

3. Results

The experiment employs NYE OIL 2001 and FOMBLIN Y LVAC 25/6 base oils as suitable liquid lubricants for this specific application. Throughout the measurement process, several parameters are recorded, including the vacuum pressure, the distance of the reference plate, and the external and internal temperatures of the reference points. The initial position of the reference plate is set at the closest distance to the proximity sensor. As the lubricant evaporates and undergoes a mass loss, the reference plate progressively moves away from the proximity sensor within the measurement range. The change in weight on the weighing pan is determined by analyzing the corresponding distance change and utilizing the acquired conversion ratio.

3.1. Evaporation model

The evaporated amount of lubricant obtained through experimental measurement is compared with analytical calculations of vacuum evaporation. For the analytical approach, it is used the modified ESTL model (see Eq. 2). The Clausius-Clapeyron law (see Eq. 3) is applied to determine the temperature-dependent oil vapor pressure at a specific operating temperature due to the lack of information provided by the manufacturer. By utilizing two known vapor pressures from the ESTL Database of Liquid Lubricants (DOLLS), it becomes possible to determine the enthalpy and estimate the vapor pressure at the desired temperature (see Fig. 2). It is important to note that the enthalpy of vaporization is influenced by the substance's properties, particularly its thermal history with temperature changes, whether increasing or decreasing [28].

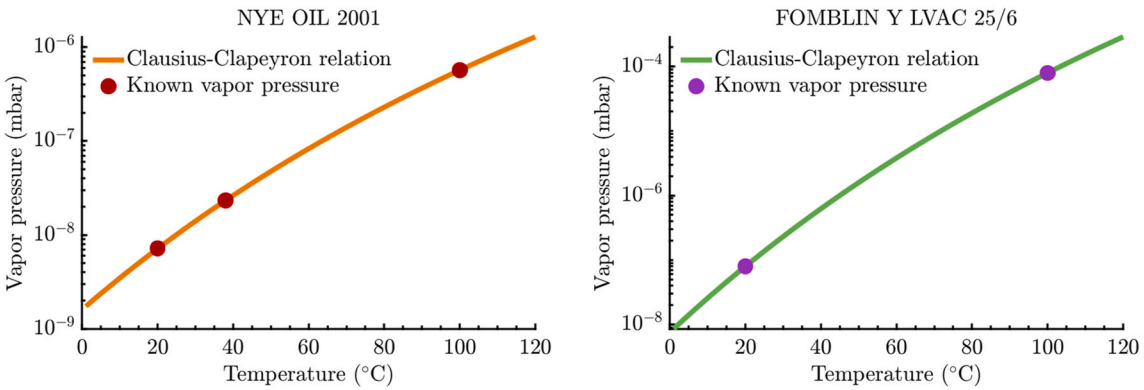

Fig. 2. Clausius-Clapeyron approximation of the oil temperature-dependent vapor pressure.

3.2. Temperature

The system monitors and records the temperature of specific reference points (see Fig. 3) throughout the experiment. By utilizing the recorded temperatures and employing thermal detection analysis during the calibration procedure, it is possible to estimate the surface temperature of the lubricant. The lubricant temperature is approximated by referencing the temperature of the bracket, which demonstrates stable and reliable thermal characteristics. The evaluation of the temperature gradient between the weighing pan and the bracket shows Table 5.

3.3. Pressure

The vacuum pressure during the experiment is measured using full range Pirani/Cold cathode vacuum gauge with measuring range between 1×10^{-9} to 1000 mbar. The pressure inside the vacuum chamber does not directly affect the calculation of the evaporation rate. However, it serves as a verification that the ambient vacuum pressure is lower than the vapor pressure of the substance, confirming the occurrence of evaporation (see Fig. 4). The pressure inside the vacuum chamber is continuously reduced by the turbo-molecular pump, leading to a progressive decrease in pressure.

3.4. Evaporation intensity

The primary objective of this study is to accurately determine the quantity of evaporated lubricant and evaluate the evaporation intensity. An inverse weight determination method is utilized for this experiment, which relies on the changes in reference plate distance, along with the appropriate conversion ratio (see Table 6). The experimental results obtained from this method are then compared to the analytical

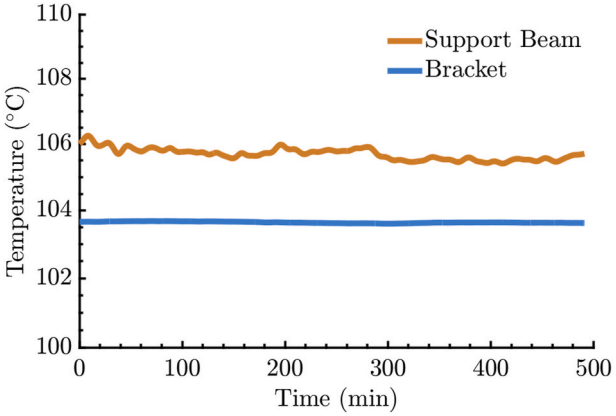

Fig. 3. Temperature distribution during the experiment.

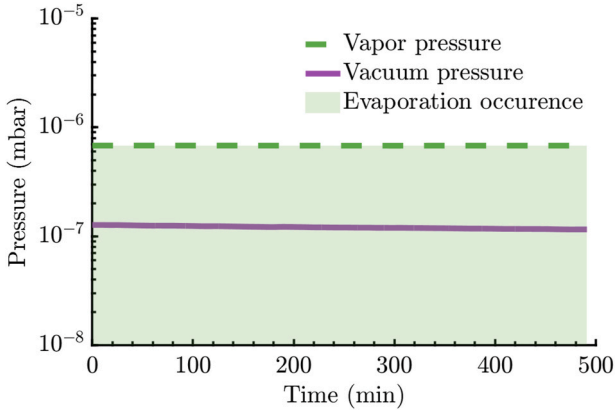

Fig. 4. Evaporation indication of NYE OIL 2001 based on vapor and vacuum pressure during the experiment.

calculation of the evaporation rate based on the ESTL model (see Eq. 2). By comparing the results obtained from both approaches (see Fig. 5), the time-dependent amount of evaporated lubricant can be established.

Both approaches demonstrate a comparable dependency with variations, in line with previous research conducted by ESTL [25,34]. The results clearly demonstrate that evaporation occurs at a consistent rate, primarily influenced by the ambient temperature. The evaporation rate comparison results presented in Table 3 provide clear evidence that the theoretical calculations based on the Langmuir equation predict higher evaporative losses compared to the experimental measurements.

4. Discussion

The study introduces a novel methodology for evaluating the evaporation intensity of space lubricants under vacuum conditions and provides clear evidence of the inaccuracies inherent in the analytical models used to estimate lubricant evaporation losses. The analytical calculations and the measurement methodology are susceptible to inaccuracies and errors, resulting in deviations in the obtained results.

Inaccuracies stemming from experiments directly impact the outcomes [34]. Therefore, before each experimental measurement, it is essential to perform a calibration procedure to determine conversion parameters, establish boundary conditions, and assess measuring accuracy. For calibration in atmospheric conditions, milligram-calibrated weights of classes E1 and F2 are utilized, following the OIML standard [37]. This calibration procedure establishes the relationship between the weight difference on the weighing platform and the corresponding change in the distance of the reference plate from the proximity sensor. An inverse weight determination procedure is conducted based on the measured displacement to validate the previously acquired results (see

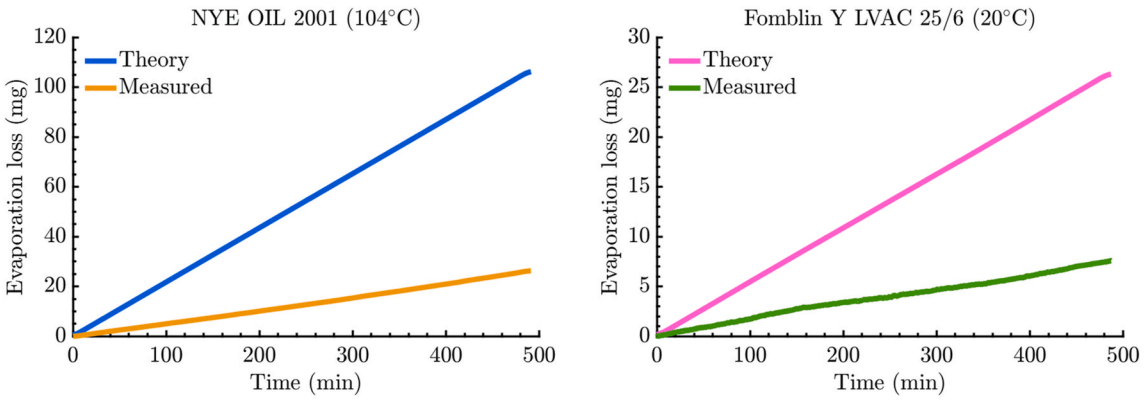

Fig. 5. Comparison of base oil evaporation loss by analytical (theory) and experimental (measured) approach.

Table 4). The accuracy of the measurement is influenced by various environmental factors, including vibrations transmitted to the experimental device, ambient temperature, and air circulation.

The accelerated experiment of NYE OIL 2001 is conducted under elevated temperatures, resulting in vacuum evaporation at higher pressures. The FOMBLIN Y LVAC 25/6, due to its relatively higher vapor pressure, is tested under room temperature conditions. Temperature is a critical parameter that affects the substance vapor pressure, requiring a temperature detection analysis. During the experiments, two thermocouples are used to monitor the temperature of the support beam and the bracket (see Fig. 1). It is crucial to accurately determine the temperature of the lubricant surface, as it significantly influences the results of analytical calculations. However, the ETR system does not incorporate a temperature sensor for the lubricant sample to avoid compromising precision. Consequently, a temperature detection analysis is carried out before the actual experiments (see Fig. 6). It is assumed that the temperature of the lubricant surface is the same as that of the weighing pan due to convection effects. The outcomes of the temperature detection analysis are presented in Table 5.

The final calibration procedure involves determining the conversion ratio under vacuum conditions at the specified operating temperature corresponding with the experimental testing conditions. The weighing pan holding the oil sample is weighed using an analytical laboratory balance before and after the vacuum test. This allows for the precise determination of the weight of the evaporated lubricant. Subsequently, the observed change in distance of the reference plate is compared to the corresponding change in weight, enabling the calculation of the conversion ratio for the vacuum experiment (see Table 6).

While it is challenging to completely eliminate certain disruptive

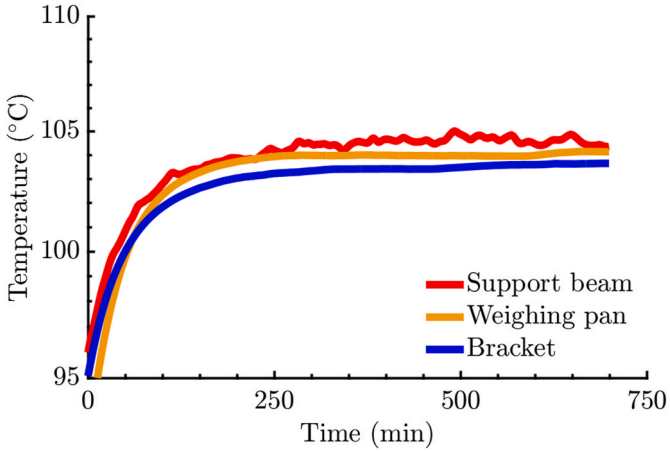

Fig. 6. Thermal detection analysis for NYE OIL 2001 experiment.

factors that can introduce measurement inaccuracies, efforts can be made to partially suppress or filter these factors. One of the primary disruptive factors is temperature, which represents a critical parameter directly influencing the experiment. Temperature fluctuations can impact the obtained results and potentially lead to misinterpretation. Moreover, temperature variations can affect the design of the ETR due to material thermal expansion. Consequently, changes in component dimensions can lead to shifts in the center of gravity and alter the proximity sensor's measurements. The performance of the proximity sensor is also influenced by the operating temperature. Therefore, it is essential to consistently monitor and control the temperature throughout the experimental and calibration procedures.

Vibration is a significant disturbance that can compromise the accuracy of measurements, given the extraordinary sensitivity of the ETR. Vibrations may originate from the vacuum pump or external sources and can be transmitted to the ETR through the balance contact, resulting in persistent signal noise or sudden fluctuations. Intense vibrations can displace the balance wedge, resulting in a discontinuity in the measured distance or, experiment termination. Therefore, the implementation of a suitable passive damping mechanism is highly recommended. Other significant disruptive factors that cannot be controlled or preceded include the condensation and reemission of evaporated molecules [24, 38] on the surfaces of the ETR and the misalignment of the contact between the proximity sensor and the reference plate.

The inaccuracies in analytical calculations can be attributed to several approximations of the evaporation intensity and other simplifications [25]. This includes the thermal history of the testing lubricant sample, approximation of lubricant temperature and vapor pressure, or the surface area determination (affected by weighing pan tilt, lubricant wetting ability, or surface unevenness). The original Langmuir equation (see Eq. 1) assumes the liquid is a gas in which the vapor diffuses according to the liquid's vapor pressure. In real applications and experimental testing, the partial vapor pressure is assumed to be zero, as the mean free path of the evaporated molecules is sufficiently large to avoid mutual collisions [29], and a direct measurement during experiments is not possible [25].

The Langmuir equation was initially developed to describe the evaporation of monoatomic metal molecules, and its analytical approach is not highly accurate for determining the evaporation intensity of larger molecules or molecules with polar bonds [23]. Although the equation is known to be inaccurate, it has been historically used to determine the evaporation intensity of space lubricants. Current efforts aim to adapt the equation using correction factors based on experimental research rather than replacing it [25,29]. Utilizing the experimental results, correction factors can be established for the analytical model to calculate the evaporation rate for the tested lubricants (see Table 7). These correction factors incorporate uncertainties stemming from the lubricant surface temperature, ETR accuracy and laboratory microbalance. Reducing the test temperature leads to a proportional

Table 7
Analytical model correction factors.

Lubricant	NYE OIL 2001	FOMBLIN Y LVAC 25/6
Correction factor α (−)	4.1 ± 0.3	3.2 ± 0.7

increase in measurement error as changes in mass become more challenging to resolve [25].

In evaluating the sources of differences between the model and measured values, it is evident that the inaccuracies in both experimental measurements and analytical calculations play significant roles. The calibration procedures under atmospheric and vacuum conditions ensure measurement accuracy, with temperature fluctuations, vibrations, and material thermal expansion consideration. Even minor fluctuations in temperature can impact results and sensor performance. Vibrations pose a challenge due to the measuring device sensitivity, demanding a passive damping mechanism implementation to suppress signal noise. Additionally, disruptive factors like condensation and reemission of evaporated molecules and misalignment of the proximity sensor contribute to measurement inaccuracies. Besides the inaccuracies arising from experimental measurement, the analytical model approximations and simplifications inherent in the Langmuir equation are notable sources of deviation when applied to larger polar-bond molecules. Efforts to adapt the equation using correction factors derived from experimental data represent a step toward enhancing the accuracy of analytical models.

Vacuum evaporation of liquid lubricant can be influenced by other physical processes such as diffusion within the substance, where molecules migrate from areas of high concentration toward the substance surface. Diffusion might dominate in the early stages of evaporation when a significant lubricant film thickness is present, enabling molecules from deeper layers to reach the surface. As the film thickness decreases, desorption becomes more significant, leading to increased evaporation intensity as molecules gain energy to escape. Both processes may occur simultaneously, making the overall process intricate and challenging to accurately model. Recognizing the complexities of related evaporation processes is imperative and limiting for the physical modelling. Continuous refinement of experimental methods and analytical approaches is essential to address these challenges and attain more precise results in space lubricant evaporation studies.

5. Conclusion

The experimental results obtained in this study validate the ETR measurement methodology as a novel approach for quantifying evaporative losses of liquid lubricants under vacuum conditions. Furthermore, the study confirms the difference in the measured evaporation intensity and the analytical models commonly employed to optimize the implemented amount of lubricant in space mechanisms such as rolling bearings and assess contamination rates, especially important in optical systems and mirrors. Specifically, this research focuses on evaluating the evaporation behavior of MAC base oil NYE OIL 2001 and PFPE base oil FOMBLIN Y LVAC 25/6, which have not been extensively investigated. Consequently, this study provides valuable insights into lubricant behavior and contributes essential experimental data for future investigations.

As the use of liquid lubricants in satellite constellations continues to increase, the presented results become even more significant. The results reveal that the tested oil samples exhibit a lower evaporation rate than predicted by analytical models utilizing reported vapor pressure values. These observed disparities between the analytical and experimental approaches align with previous assumptions and findings presented by ESTL, thereby providing an additional understanding of the testing methodology for studying the evaporation process. These findings suggest the potential for reducing the lubricant quantity used in space applications by up to correction factors presented in Table 7, which could result in decreased contamination levels and mission costs. The modification of the Langmuir equation (see Eq. 2) with the implementation of the correction factor (α) can be expresses as follows:

$$\frac{dm_{evap}}{dt} = -0.044 \frac{1}{\alpha} P_s(T) \sqrt{\frac{M}{T}} \tag{4}$$

The fundamental challenge lies in the limited availability of information regarding lubricant properties, coupled with potential inaccuracies in their evaluation by manufacturers. It is imperative to compare various liquid lubricant evaporation measurements from different facilities to enhance analytical models with correction factors for more accurate predictions of evaporation rate in practical applications.

CRediT authorship contribution statement

Josef Pouzar: Writing – original draft, Validation, Methodology, Investigation, Formal analysis. **David Kostal:** Writing – review & editing, Supervision, Project administration, Methodology, Conceptualization. **Petr Sperka:** Supervision, Methodology, Conceptualization. **Ivan Krupka:** Supervision, Funding acquisition. **Martin Hartl:** Writing – review & editing, Resources.

Declaration of competing interest

The authors declare the following financial interests/personal relationships which may be considered as potential competing interests: Ivan Krupka reports financial support was provided by Ministry of Education Youth and Sports of the Czech Republic.

Data availability

Data will be made available on request.

Acknowledgment

This research was carried out under the project FSI–S-23-8245 with financial support from the Ministry of Education, Youth and Sports of the Czech Republic.

References

[1] ESA-ESTEC R& SD, ECSS-E-ST-33-01C Rev.2 – Mechanisms, 2019, 2019:97, https://ecss.nl/standard/ecss-e-st-33-01c-rev-2-1-march-2019-space-engineering-mechanisms/.
[2] M. Eiden, R. Seiler, Space mechanisms and tribology challenges of future space missions, Acta Astronaut. 55 (2004) 935–943, https://doi.org/10.1016/j.actaastro.2004.04.011.
[3] E.W. Roberts, Space tribology: its role in spacecraft mechanisms, J. Phys. D Appl. Phys. 45 (2012), 503001, https://doi.org/10.1088/0022-3727/45/50/503001.
[4] A. Merstallinger, R. Holzbauer, N. Bamsey, Cold welding in hold down points of space mechanisms due to fretting when omitting grease, Lubricants 9 (2021) 72, https://doi.org/10.3390/lubricants9080072.
[5] A. Wolfberger, A. Hausberger, S. Schlögl, M. Hołyńska, Assessment of the chemical degradation of PFPE lubricants and greases for space applications: implications for long-term on-ground storage, CEAS Sp J 13 (2021) 377–388, https://doi.org/10.1007/s12567-021-00348-6.
[6] M. Anderson, S. Freeman, E.W. Roberts, Evaporative losses of vacuum-compatible oils through labyrinth seals, in: Proc 10th Eur Sp Mech Tribol Symp, vol. 524, 2003, pp. 255–270. https://ui.adsabs.harvard.edu/abs/2003ESASP.524..265A.
[7] E.W. Roberts, M. Eiden, Space Tribology Handbook, fifth ed., (v2). ESR Technology Ltd., 2013. https://www.esa.int/esapub/bulletin/bullet94/ROB.pdf.
[8] X. Sun, Solid lubricants for space mechanisms, in: Q.J. Wang, Y.-W. Chung (Eds.), Encycl. Tribol., Springer US, Boston, MA, 2013, pp. 3165–3172, https://doi.org/10.1007/978-0-387-92897-5_1230.
[9] J.R. Lince, Effective application of solid lubricants in spacecraft mechanisms, Lubricants 8 (2020) 74, https://doi.org/10.3390/lubricants8070074.
[10] R. Bingley, M. Buttery, G. Kelly, A.V.A. Kent, Hybrid Lubrication as a Practical Candidate for Space Mechanism Applications, ESMATS, 2021. https://www.esmats.eu/esmatspapers/pastpapers/pdfs/2021/bingley.pdf.
[11] M. Buttery, A. Kent, D. Forster, A. Vortsellas, Hybrid lubrication of PFPE fluids and sputtered MoS2, ESMATS 14 (2018). https://esmats.eu/amspapers/pastpapers/pdfs/2018/buttery.pdf.

[12] E.W. Roberts, M.J. Todd, Space and vacuum tribology, Wear 136 (1990) 157–167, https://doi.org/10.1016/0043-1648(90)90078-O.
[13] X. Fan, H. Fu, W. Li, M. Zhu, Exploring lubrication function of MACs greases for TC4 alloy under sliding and fretting conditions, Tribol. Lett. 66 (2018) 135, https://doi.org/10.1007/s11249-018-1091-1.
[14] M. Cai, Q. Yu, W. Liu, F. Zhou, Ionic liquid lubricants: when chemistry meets tribology, Chem. Soc. Rev. 49 (2020) 7753–7818, https://doi.org/10.1039/D0CS00126K.
[15] W.R. Jones, M.J. Jansen, Tribology for space applications, Proc. Inst. Mech. Eng. Part J J Eng Tribol 222 (2008) 997–1004, https://doi.org/10.1243/13506501JET305.
[16] Tadeusz Kadoski, P. Wojdyna, Liquid lubricants for space engineering and methods for their testing, J KONES Powertrain Transp 18 (2011). https://www.researchgate.net/publication/267767121_Liquid_lubricants_for_space_enginee.
[17] E. Nyberg, C. Schneidhofer, L. Pisarova, N. Dörr, I. Minami, Ionic liquids as performance ingredients in space lubricants, Molecules 26 (2021), https://doi.org/10.3390/molecules26041013.
[18] M.V. Prozhega, A.Y. Albagachiev, N.I. Smirnov, N.N. Smirnov, Lubricating materials for mechanisms operating in space, J. Frict. Wear 39 (2018) 335–340, https://doi.org/10.3103/S106836661804013X.
[19] M. Buttery, S. Lewis, A. Kent, R. Bingley, M. Cropper, Long-Term storage considerations for spacecraft lubricants, Lubricants 8 (2020) 32, https://doi.org/10.3390/lubricants8030032.
[20] M.V. Prozhega, E.O. Reschikov, N.N. Smirnov, Research of the lifetime and lubricant properties of greases for rolling bearings operating in space conditions, J. Frict. Wear 42 (2021) 431–437, https://doi.org/10.3103/S1068366621060088.
[21] ESA Space Debris Office, ESA'S ANNUAL SPACE ENVIRONMENT REPORT, 2022. Darmstadt, Germany, https://www.sdo.esoc.esa.int/environment_report/Space_Enviro.
[22] S. Krishnan, S.-H. Lee, H.-Y. Hsu, G. Konchady, Lubrication of attitude control systems, Adv. Spacecr. Technol. 4 (2011), https://doi.org/10.5772/13354. InTech.
[23] P. Rahimi, C. Ward, Kinetics of evaporation: statistical rate theory approach, Int. J. Therm. 8 (2005), https://doi.org/10.5541/ijot.142.
[24] T. Tondu, E. Vanhove, J.F. Roussel, D. Faye, Mixture effects in contaminant reemission, J. Spacecraft Rockets 53 (2016) 1172–1177, https://doi.org/10.2514/1.A33507.
[25] S. Stanley, M. Hampson, ESA-ESTL-TM-0162 01- an Experimental Assessment of the Evaporation Lives of Space Oils, 2018. https://www.esrtechnology.com/index.php/jdownloads/send/2-estl-members-library/2259-tm-0162-01-esa-evaporation-lives-of-space-oils.
[26] I. Langmuir, The vapor pressure of metallic tungsten, Phys. Rev. 2 (1913) 329–342, https://doi.org/10.1103/PhysRev.2.329.
[27] I. Langmuir, Vapor pressures, evaporation, condensation and adsorption, J. Am. Chem. Soc. 54 (1932) 2798–2832, https://doi.org/10.1021/ja01346a022.
[28] M. Hołyńska, R.-C. Sarah, E. Orcun, B. Bruno, A. Claudia, R. Riccardo, Lessons Learnt from Lubricants' Testing at Estec Materials' Laboratories, 2021, p. 5. https://www.esmats.eu/esmatspapers/pastpapers/pdfs/2021/holynska.pdf.
[29] M. Buttery, L. Gaillard, S. Rajala, E. Roberts, T. Rohr, A. Merstallinger, Fomblin Z25: A New Method for its Degradation Assessment & Proposal for Safe Operation in Space, vol. 9, 2013. https://esmats.eu/esmatspapers/pastpapers/pdfs/2013/buttery.pdf.
[30] ESA-ESTEC R& SD, ECSS-Q-TM-70-52A: Kinetic Outgassing of Materials for Space, 2011 (25 November 2011). Noordwijk, Netherlands, https://ecss.nl/hbstms/ecss-q-tm-70-52a-kinetic-outgassing-.
[31] A. Rowntree, ESTL-TM-238 - A Review of Oil Loss Models for Labyrinth Seals and Filters for Space Applications, 2000.
[32] D. Koutsoyiannis, Clausius–Clapeyron equation and saturation vapour pressure: simple theory reconciled with practice, Eur. J. Phys. 33 (2012) 295–305, https://doi.org/10.1088/0143-0807/33/2/295.
[33] J. Wang, Z. Mo, H. Zhang, H. Liu, X. Zeng, Q. Miao, Failure mechanism and accelerated life test design of space bearing, in: 2018 Progn. Syst. Heal. Manag. Conf., IEEE, 2018, pp. 882–887, https://doi.org/10.1109/PHM-Chongqing.2018.00158.
[34] S.D. Lewis, M. Buttery, O. Poyntz-Wright, A. Kent, A. Vortsellas, Accelerated testing of tribological components - Uncertainties and solutions, https://esmats.eu/amspapers/pastpapers/pdfs/2018/lewis2.pdf, 2018.
[35] M. Buttery, An Evaluation of Liquid, Solid, and Grease Lubricants for Space Mechanisms Using a Spiral Orbit Tribometer, 2010. https://esmats.eu/amspapers/pastpapers/pdfs/2010/buttery.pdf.
[36] J.T. Yates, Experimental Innovations in Surface Science, Springer International Publishing, Cham, 2015, https://doi.org/10.1007/978-3-319-17668-0.
[37] OIML. OIML R111:2004, Weights of Classes E1, E2, F1, F2, M1, M1–2, M2, M2–3 and M3, 2004. https://www.oiml.org/en/files/pdf_r/r111-1-e04.pdf.
[38] A. Suliga, O. Ergincan, R. Rampini, Modeling of spacecraft outgassed contamination levels by thermogravimetric analysis, J. Spacecraft Rockets 58 (2021) 1010–1016, https://doi.org/10.2514/1.A35020.

PAPER [2]

LABYRINTH SEAL DESIGN FOR SPACE APPLICATIONS

Pouzar et al.

Vacuum, Volume 232, 2025
doi: 10.1016/j.vacuum.2024.113882

An update to this article is included at the end

Vacuum 232 (2025) 113882

Contents lists available at ScienceDirect

Vacuum

journal homepage: www.elsevier.com/locate/vacuum

Labyrinth seal design for space applications

Josef Pouzar [a,*], David Kostal [a], Lars-Göran Westerberg [b], Erik Nyberg [c], Ivan Krupka [a]

[a] Faculty of Mechanical Engineering, Brno University of Technology, Brno, 61669, Czech Republic
[b] Division of Fluid and Experimental Mechanics, Luleå University of Technology, SE-971 87, Luleå, Sweden
[c] Division of Machine Elements, Luleå University of Technology, SE-971 87, Luleå, Sweden

ARTICLE INFO

Handling Editor: Prof. L.G. Hultman

Keywords:
Vacuum evaporation
Molecular flow
Labyrinth seals
Contamination
Liquid lubricants
Space tribology

ABSTRACT

Labyrinth seals, extensively used in space applications, serve to prevent the loss of liquid lubricants and shield satellite subsystems from contamination. These seals are essential for the reliable functioning of bearings and for protecting satellite subsystems from contamination. This study compares analytical predictions of lubricant loss against experimental measurements and computer simulations to optimize labyrinth seal configurations. Analytical models tend to overestimate mass loss by 5–8 times compared to experimental data, indicating limited reliability for complex seal geometries. Simulations using MolFlow+ and COMSOL Multiphysics align closely with experimental results, providing accurate mass loss predictions. Key findings highlight that labyrinth length, width, and surface roughness are critical factors in minimizing evaporative mass loss. Notably, stepped labyrinth seals with relief grooves and optimized step positioning effectively reduce molecular beaming effects and improve sealing performance compared to straight geometries. Effective sealing not only reduces mission failures but also helps to minimize space debris, thereby promoting safer satellite missions.

Abbreviations and Symbols

b	Labyrinth gap width [mm]	P_i	Inlet pressure [Pa]
d, $d_{1,2}$	Diameter of annular seal [mm]	P_o	Outlet pressure [Pa]
ESTL	European Space Tribology Laboratory	Q	Flow rate [mbar·mm^3/s]
ETR	Evaporation Test Rig	Q_m	Mass loss [g/s]
Kn	Knudsen number [−]	r	Circular arc radius [mm]
L, $L_{1,2,3}$	Labyrinth path length [mm]	*Ra*	Average roughness [μm]
l	Recess depth [mm]	*Sa*	Arithmetic mean height [μm]
λ	Mean free path [mm]	*Sdr*	Developed interfacial area ratio [%]
M	Lubricant molar mass [g/mol]	*Sq*	Squared mean height [μm]
N_0, N	Number of molecules (inlet, outlet) [−]	T	Absolute temperature [K]
PFPE	Perfluoropolyether	*TP*	Transmission probability [−]
P	Fluid vapor pressure [torr]	v	Average molecular velocity [m/s]

1. Introduction

Space technology operates under demanding conditions, where mechanical components often lack redundancy due to weight and size limitations, thus posing a risk of satellite failure if malfunctions occur during a mission. Tribological failures, resulting from inadequate liquid lubrication, such as lubricant creep [1,2], thermo-catalytic degradation [3], and vacuum evaporation [4–6], are primary contributors to mission failures.

There is a growing potential for utilizing greases and base oils in space applications, coupled with a need to extend their service life [7]. However, their utility is limited by extreme temperatures and vacuum evaporation, which pose risks of breakdown and contamination [5,8,9]. High temperatures can induce molecular decomposition, while low temperatures lead to undesirable viscosity increases [5]. Vacuum evaporation occurs when the ambient vacuum pressure reaches the substance vapor pressure [10–12], exacerbating challenges by causing contact drying and potential contamination [8,9], ultimately jeopardizing subsystem performance or leading to complete failure. This concern is compounded by the inclusion of delicate optical elements in scientific missions [13].

In space applications, mechanisms containing liquid lubricants are partially enclosed [14], with lubricants shielded from the open environment using non-contact labyrinth seals. These seals incorporate narrow pathways strategically positioned between inner and outer

* Corresponding author.
E-mail address: Josef.Pouzar@vut.cz (J. Pouzar).

https://doi.org/10.1016/j.vacuum.2024.113882
Received 12 August 2024; Received in revised form 30 October 2024; Accepted 24 November 2024
Available online 26 November 2024
0042-207X/© 2024 The Authors. Published by Elsevier Ltd. This is an open access article under the CC BY license (http://creativecommons.org/licenses/by/4.0/).

rotating parts of mechanisms [12,14,15]. The thickness of the labyrinth gap is a critical parameter, balancing safe mechanism operation against flow restriction. Current research overlooks the individual effects of labyrinth geometry and surface topography optimization on reducing liquid lubricant loss [12,16,17]. Further investigation is needed to fully understand and optimize these crucial components.

This study examines the performance of labyrinth seals in vacuum environments, aiming to understand and enhance their effectiveness. By integrating analytical models, simulation, and experimental validation, the research offers comprehensive insights into labyrinth seal behavior under varying conditions. Additionally, the study explores the impact of surface topography on lubricant loss and addresses the molecular beaming effect in narrow passages [18,19]. These findings are crucial for optimizing labyrinth seal design to minimize lubricant loss and contamination. By preventing tribological failures and contamination associated with liquid lubricant evaporation, the likelihood of mission failures is significantly reduced, thus decreasing economic and environmental production impacts and mitigating orbital pollution—a threat to current and future space ventures [20].

2. Material and methods

2.1. Experimental measurements

Experimental measurements are conducted to obtain real-world data regarding the performance of the labyrinth seals. These empirical results serve as a crucial benchmark for validating the accuracy of the analytical and simulation outcomes and assessing the practical applicability of the modelled parameters.

2.1.1. Evaporation test rig

For the experimental measurement of lubricant loss due to vacuum evaporation, the modified Evaporation Test Rig (ETR) equipment [6] is employed; see Fig. 1, developed specifically for continuous measurement of mass loss resulting from evaporation under vacuum conditions. The setup is based on a balance-scale mechanism, comprising a pivoted scale beam with a labyrinth seal platform on one side and counterweights on the opposite side. The system is equipped with sharp wedges, allowing single-axis rotation, and is balanced on a support beam within a vacuum chamber. A capacitive proximity sensor, fixed to the chamber flange, measures the displacement of the scale pointer during lubricant evaporation. This displacement is used to calculate mass loss over time, accounting for variations in pressure and temperature. The ETR operates under controlled vacuum conditions with externally applied heating. The experimental testing begins after temperature stabilization, which is achieved by maintaining constant thermo-vacuum conditions for 24 h. The conversion ratio between the proximity sensor's displacement signal and mass loss is 10.0 μm per 1.0 mg, with a weighing precision of ±0.04 mg under thermo-vacuum conditions.

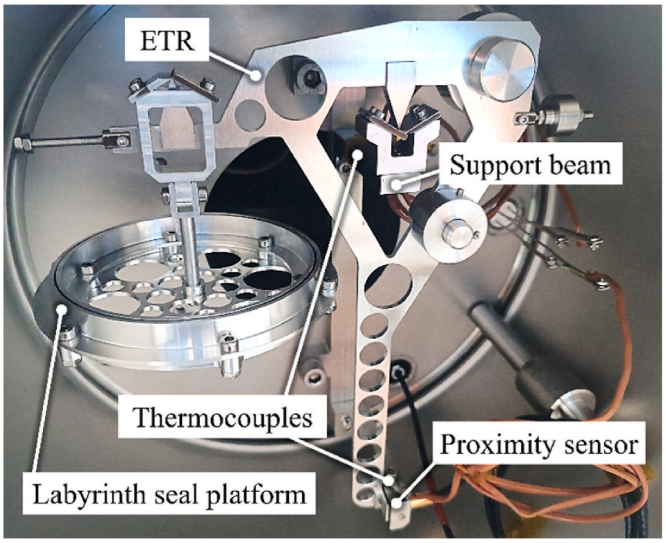

Fig. 1. Evaporation test rig (ETR) with labyrinth seal platform.

The labyrinth seal platform is modular, facilitating the testing of various labyrinth seal geometries. It consists of a main pan attached to the ETR, housing the liquid lubricant reservoir, and accommodating various labyrinth configurations (Fig. 2) for testing under high vacuum and elevated temperatures. All components of the labyrinth seal platform (main pan, labyrinth seals) are made of aluminum alloy 6061.

2.1.2. Test sample

The Evaporation test rig setup ensures precise evaluation of labyrinth seal performance. The chosen geometries for experimental testing are selected to be comparable with the simulation and analytical models. Three specific geometries in Fig. 3 are implemented during the experimental testing, with dimensions specified in Table 1.

In addition to the overall geometries, the "LONG" labyrinth seal was prepared in two variations, each with different surface roughness, to allow further evaluation (refer to Chapter 3.2). All labyrinth seal samples were tested with the same oil to ensure consistency in assessing their effectiveness.

In this study, a low-outgassing oil, FOMBLIN Y LVAC 25/6 [35], was selected for experimental testing due to its vacuum compatibility; see Table 2. The lubricant test sample is applied to the annulus reservoir of the labyrinth seal test rig pan (Fig. 2). The amount of lubricant applied must be sufficient to achieve an optimal film height covering the entire reservoir area to prevent local drying. However, excessive lubricant may lead to undesired creep through the seal, potentially compromising the experimental evaluation. Prior to experimentation, a series of pre-tests were conducted to assess the thermal conditions of the setup and evaluate creep intensity.

2.1.3. Experimental procedure

During the experimental measurements, only one specific labyrinth seal geometry can be evaluated at a time. First, the sample oil is injected into the labyrinth seal reservoir in an amount specified in Table 2. The chosen labyrinth seal geometry (SHORT, LONG, or STEP) is then mounted onto the reservoir using screws, ensuring a secure fit to maintain the labyrinth gap conditions throughout the test. This labyrinth assembly is subsequently attached to the Evaporation Test Rig (ETR), and experimental testing under vacuum conditions is initiated.

To facilitate the vacuum evaporation of the oil, experiments are conducted at elevated temperatures. Increased temperatures raise the oil's vapor pressure, promoting its evaporation. As the oil evaporates, the ETR balance system compensates for the mass loss by tilting. This tilt is measured by a proximity sensor, which translates the tilt data into mass loss using calibrated parameters.

All subsequent experiments are conducted under consistent conditions, including a heating temperature of 170 °C, a setpoint temperature for the labyrinth seals of 90 °C (±5 °C), a setpoint vacuum pressure of 2E-5 mbar, and a duration inside the vacuum chamber of 24 h. These controlled parameters ensure the reproducibility of the results.

2.2. Analytical model

In our experiments, evaporated lubricant molecules travel in the molecular flow regime, characterized by extremely low gas densities and long mean free paths between molecules, as described by the Knudsen number [21,22].

$$Kn = \frac{\lambda}{L}, \tag{1}$$

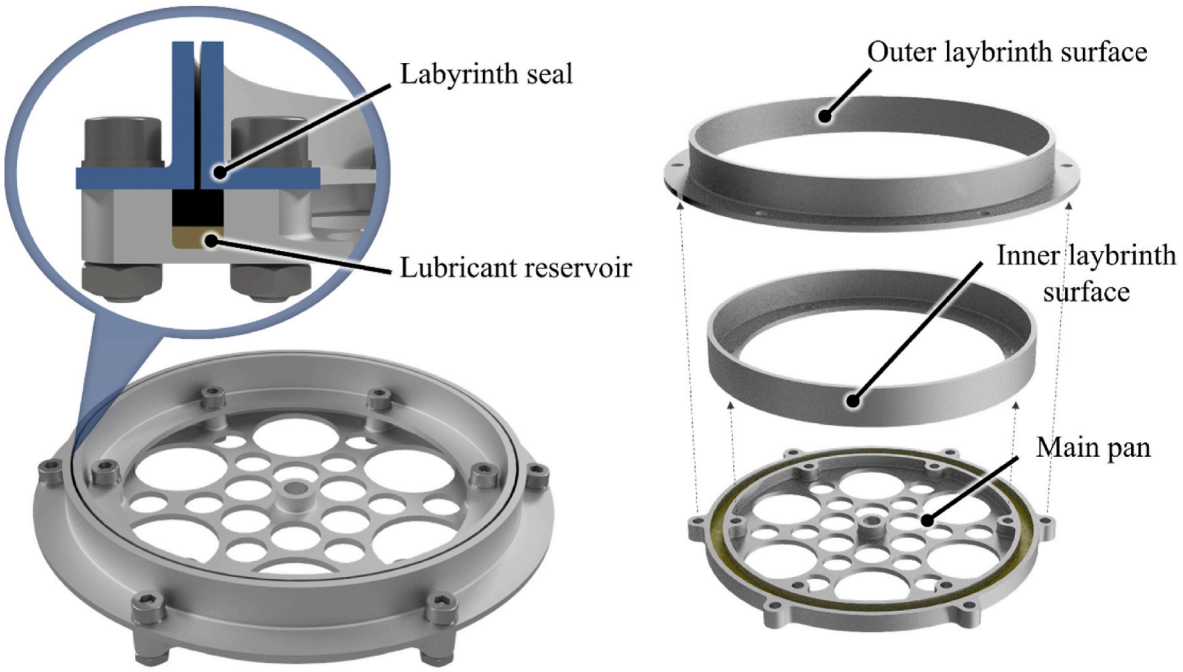

Fig. 2. Labyrinth seal platform setup and assembly breakdown.

where λ is the mean free path of the gas molecules, and L is a characteristic length of the system, such as the chamber diameter or length [16,23]. Lower Knudsen numbers ($Kn < 0.01$) indicate viscous or continuum flow, where intermolecular collisions dominate. As the Knudsen number increases above 0.5, intermolecular collisions become rare, and surface interactions prevail [16,23,24]. Under the vacuum conditions used during these experiments, with pressures around 2E−5 mbar, and temperatures around 81 °C the Knudsen number (Kn) ranges from approximately 11 to 13. This range places the system firmly in the free molecular flow regime ($Kn > 0.5$), where molecular movement is largely influenced by interactions with the chamber surfaces rather than collisions between molecules [16,23,24]. Within the labyrinth, the molecules temporarily adhere to surfaces before dispersing, losing their previous direction and velocity with each interaction [23].

Evaluating evaporation rates of liquid lubricants in space requires analytical and experimental methods [12,15,25], with analytical models serving as vital tools for predicting lubricant loss due to vacuum evaporation [15,26–28]. To calculate the flow rate or leakage through labyrinth seals analytically, the labyrinth original geometry configuration must undergo a conversion to a linearized state, wherein its diameter, gap width and length dimensions are equivalently represented [15]. This linearized labyrinth representation facilitates the calculation of the flow rate using a combination of pressure gradient, molecule transmission probability through the labyrinth, and average molecular velocity according to

$$Q = \frac{(P_i - P_o)\pi dbv}{\left(4 + \frac{1,5}{b}\right)}. \tag{2}$$

Based on a detailed analysis of experimental data from ESTL, a refinement to Eq. (2) has been proposed [12] to offer the most accurate correlation with real-world tests currently available, serving as an expression for the flow of molecules. Importantly, this refinement maintains consistency with the previous approach regarding the process of simplifying analytical computations [15], such that the overall methodology remains coherent and practical for implementation in relevant applications

$$Q_m = 0,0436 \bullet \frac{P\pi db\left(\frac{M}{T}\right)^{0,5}}{1 + 0,375 \bullet \frac{L}{b}}. \tag{3}$$

The ESTL model presented in Eq. (3) serves as the most reliable analytical instruments for predicting the quantity of lubricant molecules leaking through the labyrinth seal. However, these analytical models exhibit inherent limitations [12,15,27] mainly due to their simplified geometrical representations and possibly due to lubricant thermal history and inaccurate vapor pressure determination [17,29,30]. Comparison with experimentally measured results indicates overestimation of the analytical evaporation rates prediction by an order of magnitude [11,12]. Manufacturers typically determine vapor pressure using the Knudsen effusion method, which lacks standardization and potentially yields inaccuracies [11,31]. Proposed correction factors aim to align analytical predictions with real-world scenarios, relying on experimental data [11,29].

Despite widespread adoption, analytical models frequently fall short in accurately predicting evaporated molecule flow rates [6,12]. Addressing these disparities may involve employing numerical simulation tools, such as Monte Carlo random sampling functions [30,32,33]. Monte Carlo simulation stands as a robust computational technique crucial for acquiring numerical approximations of molecular flow behavior within complex systems or processes [19,34].

For predicting the mass of lubricant evaporation through specific labyrinth seal geometries, the ESTL model presented in Eq. (3) is typically utilized, despite its demonstrated lack of accuracy. This analytical model will be employed to compare the predicted evaporation rates with simulation and experimental measurements. This comparative approach aims to highlight the discrepancies between the analytical predictions and the more precise data obtained from simulations and experimental tests, thereby facilitating improvements in the predictive accuracy of lubricant evaporation rates for space applications.

2.3. Modeling and simulation

This phase focuses on developing mathematical models to accurately simulate molecular flow within labyrinth seal geometries. The input

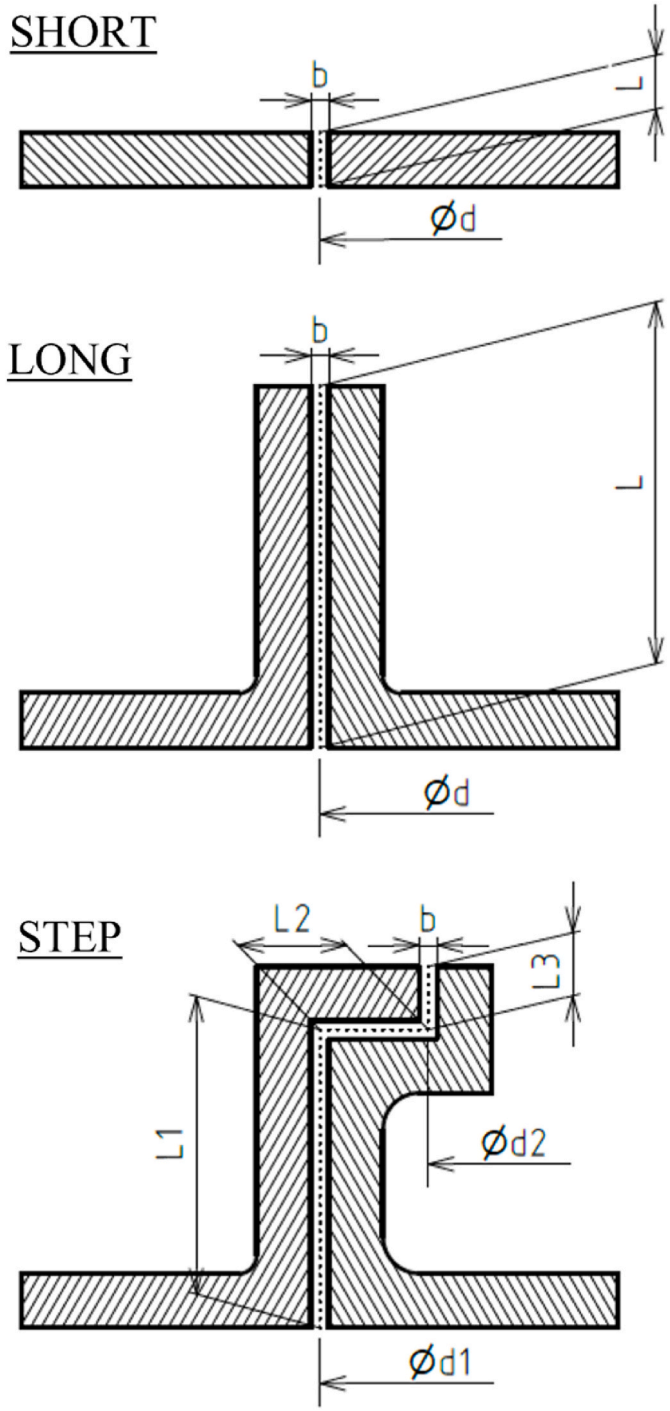

Fig. 3. Labyrinth seal geometries and their experimental setup (SHORT, LONG, STEP).

Table 1
Labyrinth seal geometry dimensions.

Labyrinth	Width	Diameter	Length
	[mm]		
SHORT	b = 0.5	d = 86.5	L = 1.5
LONG	b = 0.5	d = 86.5	L = 10
STEP	b = 0.5	d_1 = 86.5 d_2 = 92.5	L_1 = 8.25 L_2 = 3.00 L_3 = 1.75

Table 2
Oil test sample properties [35].

Lubricant name	FOMBLIN Y LVAC 25/6
Lubricant type	PFPE
Vapor pressure (mbar)	6e-8 (25 °C) 6e-5 (100 °C)
Kinematic viscosity (cSt)	276 (20 °C)
Viscosity index	113
Molecular weight (g/mol)	3300
Density (g/cm^3)	1.90
Applied oil sample:	
mass (g)	1.8–2
volume (ml)	0.95–1.05

data for the simulations and analytical models are derived from boundary conditions measured during the experimental phase. These include the temperature of the labyrinth seal, the vacuum chamber pressure, and the parameters of the evaporated oil; see Table 2. Since the pressure inside the labyrinth seal reservoir (at the labyrinth seal inlet) cannot be measured directly, it is assumed to be equal to the oil vapor pressure in the simulation models.

Through these simulations, critical parameters influencing seal performance are identified and comprehensively described. This serves as the foundation for understanding the dependence between various labyrinth geometry factors and their impact on seal effectiveness in preventing molecular flow. To simulate space conditions and molecular flow regimes within labyrinth seal geometries, two representative software tools are utilized.

2.3.1. *MolFlow+*

MolFlow + [36] is employed for molecular flow simulation and evaluation of labyrinth seal geometry parameters. It is primarily used for pressure distribution calculations within complex geometries under ultra-high vacuum conditions [36,37]. The software employs Monte Carlo simulation techniques to accurately model particle behavior in rarefied gas environments, making it particularly suitable for analyzing molecular flow.

2.3.2. *COMSOL multiphysics*

For the purpose of comparing simulation results, COMSOL Multiphysics v.6.2 software [38] was integrated into the research methodology. The software accommodates various study types, encompassing stationary and time-dependent (transient) studies, as well as linear and nonlinear studies. In this research, two distinct modules are employed:

a) **Molecular Flow Module:** Simulating kinetic gas flows, this module offers specialized physics interfaces ideal for vacuum systems simulation. It is designed to address kinetic gas flows with Knudsen numbers greater than 0.1, encompassing both the transitional and free molecular flow interfaces. In our experiments, the Knudsen numbers exceeded 11, making this module highly appropriate for our application. This method computes flow by integrating fluxes from all visible surfaces, with dependencies confined to surface variables.
b) **Particle tracing module:** This module provides a versatile tool for tracking particles through various geometries under different forces. The mathematical particle tracing interface allows for flexible formulation of particle motion using Lagrangian or Hamiltonian approaches, ideal for free molecular flow simulations. Special variables offer insights into particle populations and statistical data, aiding in analysis. This module computes quantities like particle count and transmission probability, facilitating the visualization and analysis of particle trajectories.

3. Results

The results encompass analytical, experimental, and simulation approaches, which are compared and collectively evaluated. The main evaluation subject is a set of three labyrinth seals (Table 1), featuring precisely manufactured and measured geometries utilized in both analytical and simulation models. For experimental testing, the modified ETR measuring device [6] is employed, along with the labyrinth seal assembly, to continuously measure lubricant mass loss resulting from vacuum evaporation. Subsequent research extends to evaluating the overall geometry's impact on the labyrinth seal's effectiveness, as well as exploring the influence of surface roughness and molecular beaming effects occurring in narrow corridors within the molecular flow regime.

3.1. Labyrinth comparison

The experimental section initially compares three labyrinth geometries (Fig. 3) through multiple independent measurements. The measured results obtained from the ETR are depicted as displacement signals, which are then converted into lubricant mass loss using calibration ratios. As a result, the measurement outcomes portray a continuous signal of lubricant mass loss over a specified time period for all three types of labyrinth seal geometries; Fig. 4. To further validate the measured mass loss, the experimental setup is weighed both before and after the experiment. The results clearly indicate that more complex geometries exhibit superior sealing capabilities, aligning closely with the expected behavior according to the research [12,14,27].

The temperature and pressure of experimental measurements were recorded and subsequently incorporated into the analytical and simulation models to achieve close correlation. The analytical approach utilized the ESTL model (Eq. (3)), while both the MolFlow+ and COMSOL Multiphysics software were employed for simulation. A comparison of the results obtained from all three approaches is shown in Fig. 5 and reveals that the analytical approach yields significantly greater mass loss, potentially due to simplifications inherent in the analytical model. Conversely, the simulation approach closely aligns with experimentally acquired results. When comparing mass loss and relative leak rate, using the experimental results as a reference (see Table 3), the analytical model overestimates the leak rate 5–8 times, while simulations deviate by only 29 % at most. These findings indicate that simulation models offer a better fit for complex geometries, though they may be less accurate for shorter labyrinth gaps.

Expanding upon the previous findings, a design of experiment analysis was undertaken to comprehensively explore the principal influencing parameters of labyrinth seals. To facilitate a meaningful

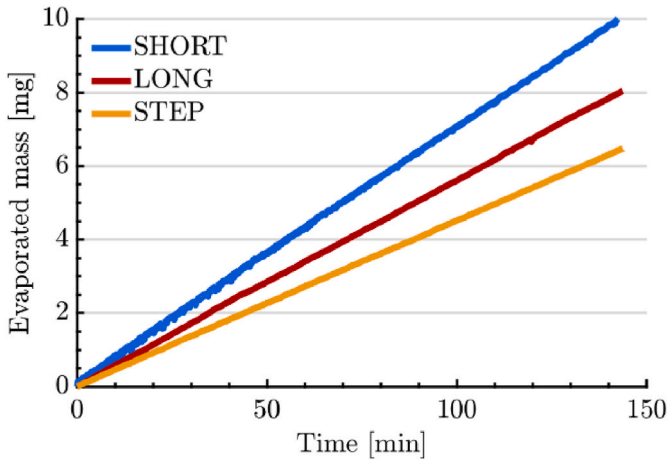

Fig. 4. Experimental measurements comparison of mass loss for various labyrinth seal geometries.

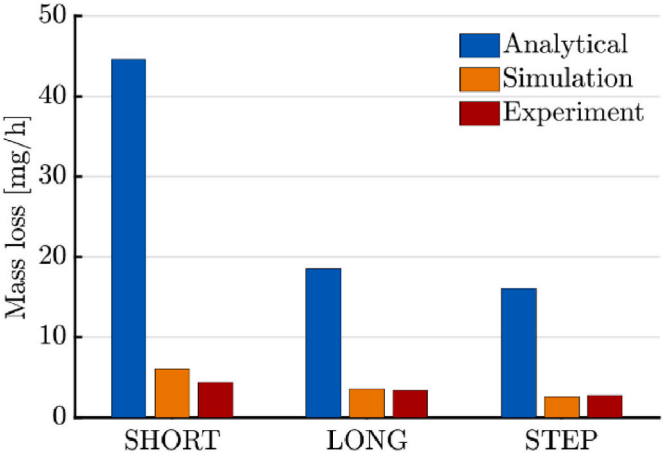

Fig. 5. Comparison of analytical, experimental and simulation approaches of evaporation mass loss.

comparison of labyrinth parameters, the evaluation of transmission probability (TP) is employed, indicating the ratio of molecules traversing from the inlet to the outlet [23,39].

$$TP = \frac{N}{N_0}, \tag{4}$$

where N is the number of molecules at the outlet, and N_0 is the number of molecules at the inlet. This probability, essential for conductance calculations, offers a convenient metric for comparing labyrinth geometry parameters. Notably, the primary influencing parameters encompass the width of the labyrinth gap and the length of the corridor, as depicted in Fig. 6. These results align with the assumptions derived from previous research.

According to the results shown in Fig. 4, the labyrinth seal with a stepped geometry is the most effective sealing solution, largely due to its extended corridor length, identified as the primary influencing parameter in Fig. 6. The longer corridor increases the probability of molecular interactions with the seal surfaces before molecules reach the outlet. Additionally, the stepped structure introduces multiple surfaces at various angles, which increases the likelihood of molecules reflecting off these surfaces rather than passing directly through the seal. This reflective behavior disrupts the direct flow of molecules, significantly reducing transmission probability and enhancing overall sealing performance. The combination of an elongated path and multiple reflection points within the stepped geometry creates a more efficient barrier to molecular flow compared to simpler seal designs.

3.2. Surface roughness

In addition to considering the overall geometry of the labyrinth seal, surface topography must also be taken into account, as it can significantly impact conductance results. Current knowledge lacks evidence of surface roughness evaluation in labyrinth seals for space applications. Therefore, a series of experimental tests were conducted to underscore the importance of the surface roughness parameter. Two LONG geometry labyrinth seals produced using a turning machining process and with different surface finishes - one untreated (ROUGH) and the other polished (SMOOTH) - were compared (Table 4). The inner and outer surface roughness of the labyrinth seal was assessed using a Contour GT-X 3D optical profilometer (Fig. 7), and the data was subsequently incorporated into the COMSOL Multiphysics simulation environment for molecular flow analysis, considering real surface topography.

The analytical model does not include a surface texture parameter; therefore, it will not be compared further with other approaches. The comparison between experimental measurements and simulations

Table 3
Mass flow evaluation for specific labyrinths using diverse approaches.

Approach		SHORT		LONG		STEP	
		[mg/h]	relative leak rate	[mg/h]	relative leak rate	[mg/h]	relative leak rate
Experiment		4.350	1	3.41	1	2.73	1
Analytical		32.81	7,54	19.27	5,65	16.69	6,11
Simulation	MolFlow+	5.39	1,24	3.24	0,95	2.33	0,85
	COMSOL	5.63	1,29	3.58	1,05	2.72	1,00

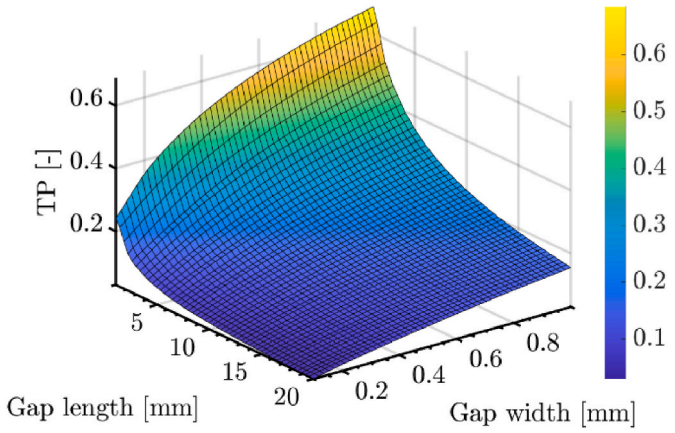

Fig. 6. Identification of key labyrinth geometry parameters impacting transmission probability (TP).

Table 4
Surface roughness analysis for inner and outer components of labyrinth seals.

Surface roughness	ROUGH		SMOOTH	
	Inner	Outer	Inner	Outer
Ra [μm][a]	3.88	1.30	0.13	0.56
Sa [μm]	3.70	1.30	0.14	0.56
Sq [μm]	4.34	1.60	0.16	0.67
Sdr [μm]	1.99 %	5.56 %	0.01 %	4.14 %

[a] Average Ra parameter in the direction of highlighted mid-planes shown in Fig. 7.

reveals a significant influence of surface roughness on the mass loss of evaporated lubricant molecules; see Fig. 8. The intensity of mass loss varies by 14.4 % in experimental measurements and 14.6 % in simulations for the different surface roughness. The results presented have been unified to ensure comparability across the same seal geometries, with one being subjected to a polishing process.

Based on the experimental measurements, the sealing efficiency of the SMOOTH labyrinth seal decreased by 14.4 % due to its lower surface roughness, resulting in an overall lubricant loss that was 0.55 mg/h higher compared to the ROUGH labyrinth seal, which featured a higher surface roughness. The increased roughness in the ROUGH seal likely enhanced the interaction between the seal surfaces and the evaporating lubricant molecules, contributing to better sealing performance. Surfaces with higher area roughness exhibit improved sealing effectiveness which can be interpreted in two ways:

1) Increased surface roughness results in approximately a 1.7 % larger area for molecular adhesion (refer to the Sdr parameter in Table 4).
2) Higher surface roughness introduces geometrically complex passages, impeding molecule propagation.

3.3. Molecular beaming effect

One of the factors that has not been considered in the optimization of labyrinth seal geometry design is the phenomenon of molecular beaming effect, which occurs in long and narrow tubes. When the impingement rate for the tube facets in the normal direction is higher than for the parallel facets, the angular distribution of molecular velocities is no longer cosine-like, resulting in more molecules traveling along the labyrinth corridor path [19,40]. This beaming effect is always present and should be taken into account in the optimization of labyrinth geometry as it may influence the overall mass loss of lubricant molecules.

To mitigate the molecular beaming effect, it is recommended to employ more intricate geometries that redirect the flow of molecules, preventing them from traveling in a straight line. An effective geometry involves a stepped configuration, altering the direction of molecular flow by 90°. Careful consideration should be given to the placement of the step within the labyrinth to minimize the impact of the molecular beaming effect. To achieve this, a simulation of the original stepped labyrinth seal, used in the experimental measurements, was performed using COMSOL Multiphysics software. Adjustments were made to the step position along the entire length of the labyrinth by performing a parametric sweep across the 10 mm width of the labyrinth in 0.5 mm increments. The results in Table 5 indicate the favorable placement of the step in the middle of the labyrinth seal (Fig. 9), effectively reducing the growing influence of the molecular beaming effect.

Given the existence of the molecular beaming effect and the necessity for a stepped geometry in labyrinth seals to effectively diminish its impact, further research into the geometry of the step corner has been conducted. In the corner where the molecular beam strikes the surface and disperses the molecules, the corner geometry is essential for disrupting the spread of molecules through the labyrinth seal.

Conventionally, the classical geometry of a manufactured labyrinth seal lacks corner optimization, and the corner is rounded due to the manufacturing process. Consequently, this geometrical shape increases the likelihood of molecules propagating further, necessitating its elimination. To address this issue, a series of local geometrical shapes for the corner were simulated using COMSOL Multiphysics (Fig. 10), and their impact in terms of mass loss reduction was assessed; see Table 6. Based on these findings, it is recommended to incorporate corner shaping into the manufacturing process, such as implementing corner relief grooves. These geometric modifications, designed to be produced using conventional machining processes, contribute to a slight reduction in mass loss while potentially yielding significant lubricant savings over the satellite's lifetime.

4. Discussion

The study aims to explore the fundamental aspects of labyrinth seals used in space mechanisms, focusing on understanding the behavior of liquid lubricant molecules that evaporate in vacuum conditions. To understand how lubricant molecules leak through these seals, we use three methods: experimental testing, analytical analysis, and computer simulation.

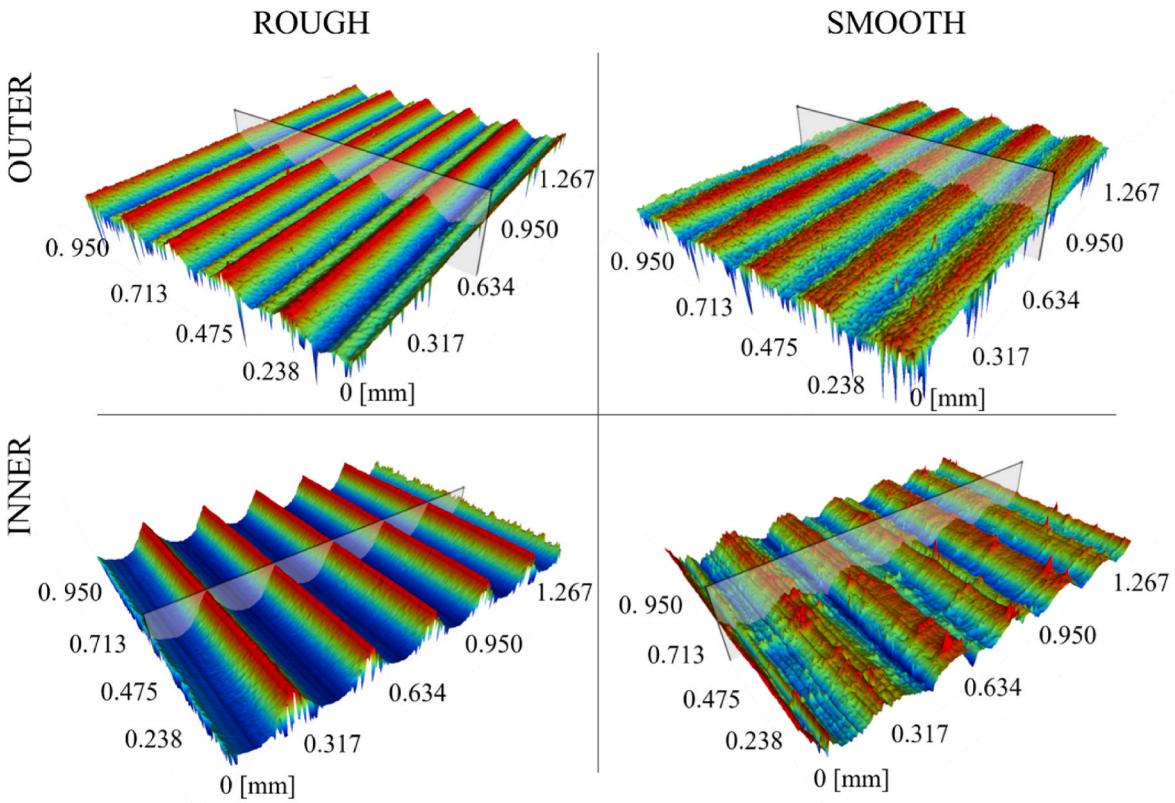

Fig. 7. Surface roughness analysis for inner and outer components of labyrinth seal LONG geometries using a 3D optical profilometer.

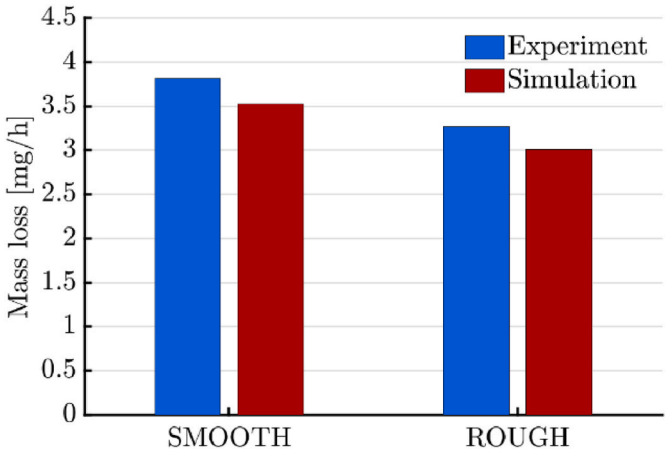

Fig. 8. Experimental and simulation investigation of surface roughness impact on labyrinth seal performance.

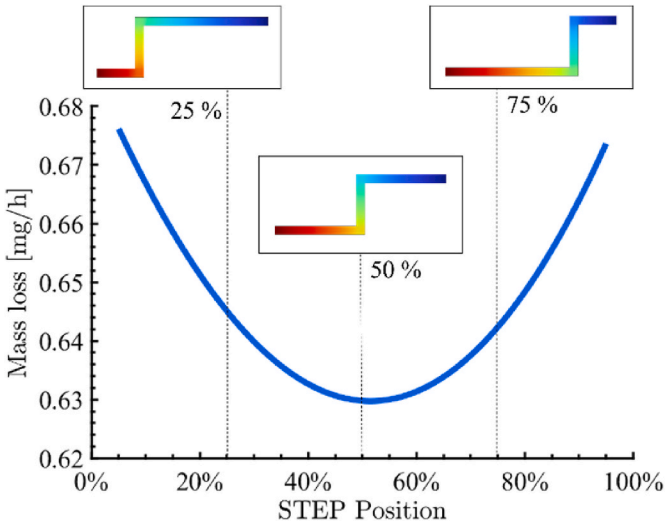

Fig. 9. Mass loss variation in labyrinth STEP geometry influenced by molecular beaming effect on step position.

Table 5
Labyrinth corner geometries and their impact on evaporated lubricant loss.

Step position (see Fig. 9)	Mass loss [mg/h]	Loss rate[a]
10 %	0.665	+5.19 %
25 %	0.643	+1.62 %
50 %	0.633	–
75 %	0.640	+1.24 %
90 %	0.662	+4.71 %

[a] Relative to the reference step position at the midpoint (50 %) of the labyrinth seal.

Experimental testing is crucial for comparing the outcomes of the analytical and simulation approaches. The main inaccuracies arise from the experimental measurements, so each measurement must undergo a calibration procedure before the actual test. Calibration focuses primarily on temperature distribution measurement, the conversion ratio between proximity sensor distance change and actual weight loss, and achievable vacuum conditions. The conversion ratio calibration for the evaporation test rig is performed before each labyrinth seal modification. The detailed process for this calibration is described in previous research [6].

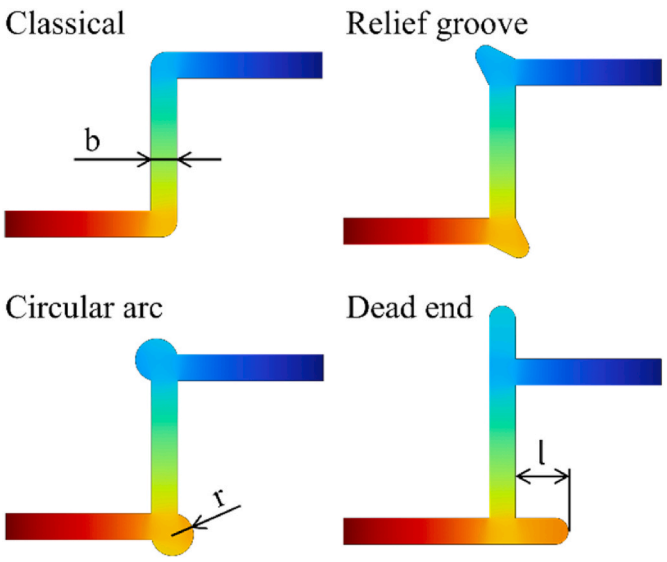

Fig. 10. Local geometries in the corner of labyrinth seals with stepped geometry.

Table 6
Labyrinth corner geometries and their impact on evaporated lubricant loss.

Corner geometry	Characteristic parameter	Loss reduction
Classical	–	–
Circular arc	r = b	3.8 %
Relief groove	type G[a]	3.9 %
Dead end	l = 2b	4.3 %

[a] ISO 18388:2016.

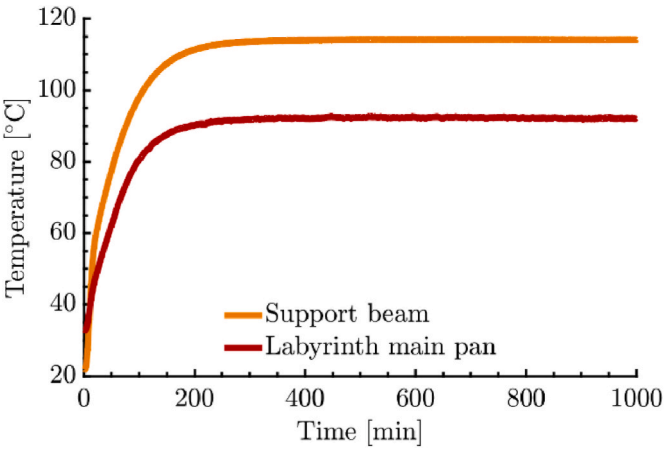

Fig. 11. Thermal calibration analysis for labyrinth seal test rig experiments.

Temperature is the most critical parameter influencing the evaporation process, as it directly affects the substance's vapor pressure [12,41]. During the experiments, it is not possible to measure the exact temperature of the oil sample inside the labyrinth seal test rig. To address this, we perform a thermal calibration procedure before experimental testing, where reference temperatures are measured at specific locations (see. Fig. 1) and at the main pan of the labyrinth seal platform (see Fig. 11). The measured temperature difference of approximately 20 °C between the labyrinth seal and the support beam holding the evaporation test rig is primarily due to the differing mechanisms of heat transfer affecting each component. The support beam is directly connected to the heated vacuum chamber, which allows for efficient heat conduction. In contrast, the labyrinth seal experiences heating predominantly through radiation. The presence of very limited conductive paths makes radiative heat transfer the dominant mechanism, which is less efficient compared to conduction. It was experimentally verified in a dedicated test with additional thermocouples that the lubricant surface temperature is equal to the reservoir temperature and the labyrinth seal gap surface, due to convection effects.

Despite initial thermal calibration, the oil surface temperature remains estimated, as thermocouples cannot be placed in the pan during evaporation tests without compromising weighing precision. The test rig for the labyrinth seals and the oil are maintained at a temperature of 92.0 (±0.3) °C, which is dependent on the geometry. Once the substance starts to evaporate at specific temperatures and pressures, it cools down as a result of the evaporation process. The temperature subsequently stabilizes at a new value depending on the evaporation rate of the cooling liquid and the external heating. This derived temperature introduces the primary inaccuracy in both the analytical and simulation approaches. Nonetheless, during the experiments with various labyrinth seals, the thermal conditions remained consistent, with a maximum deviation of only 1 °C; see Fig. 12.

The vapor pressure of the liquid lubricant is estimated using the Clausius-Clapeyron approximation [17,42], making it entirely dependent on the known vapor pressures provided by the manufacturer. However, the Knudsen effusion method used by manufacturers for vapor pressure determination lacks standardization. Consequently, the vapor pressure values in the oil datasheet might be inaccurately determined, leading to discrepancies in experimental and other results [11,31]. To address this issue, it is advisable to test the oil's vapor pressure using the Knudsen effusion method prior to the experimental measurements. However, in our experiments, vapor pressures were sourced from the datasheet, which could potentially influence the results obtained through analytical and simulation approaches. Although the exact deviation in vapor pressure measurement is unknown, the simulation results align well with the experimental data.

The pressure of the vacuum chamber is measured outside the labyrinth seal test rig as it can't be directly measured inside the labyrinth seal. Therefore, the exact pressure in the lubricant reservoir at the inlet to the labyrinth seal is assumed to be equal to the vapor pressure of the liquid lubricant. The pressure inside the vacuum chamber was monitored during the experiments and remained constant at 2E-5 (±1E-6) mbar. At the set oil temperatures, the oil's vapor pressure is estimated to be 3.3E-5 (±7E-7) mbar, slightly higher than the chamber's vacuum pressure. While this difference is small, the primary indicator of the evaporation process is the measured change in distance, which follows a mostly linear trend and only occurs once oil evaporation begins.

Other significant disruptive factors in the experimental

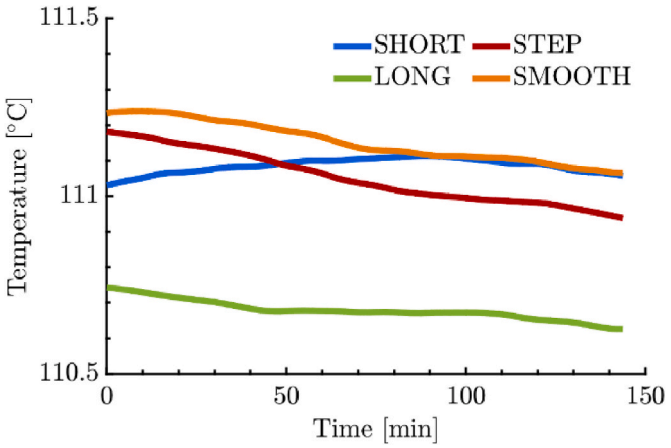

Fig. 12. Temperatures of support beam during the experiments for various labyrinth seals.

measurements stem from the design of the labyrinth seal test rig. Unwanted movement of the lubricant in the test rig may occur during sample handling due to the absence of a porous reservoir. Additionally, temperature and pressure variations over time during the experiment can lead to lubricant creep. The oil may creep along the surface, through the labyrinth seal gap, and even through the tightening contact surfaces. This could lead to increased weight loss due to the greater oil surface area, thus increasing evaporation intensity. During the calibration and experimental testing, lubricant creep was addressed through visual inspections before and after the experiments; however, it was not observed at all. In actual space applications, labyrinth seals incorporate anti-creep barrier surface coatings with low surface tension [43] to prevent lubricant creep through the seal. However, these films were not used during the experiments because visual inspections did not detect any creep. Additionally, using barrier films could have distorted the results, especially when measuring the effect of labyrinth seal surface roughness.

The inaccuracies of the analytical evaporation model for labyrinth seals stem from several simplifications. The model simplifies the complex geometry of the labyrinth seal, thereby overlooking the behavior of molecules in the molecular flow regime and the emergence of the molecular beaming effect. Another simplification involves approximating the labyrinth transmission probability, which should ideally be calculated differently for each type of geometry. These simplifications cause the analytical model to be less accurate in predicting lubricant loss during the vacuum evaporation process, with accuracy varying based on the seal's geometry; see Fig. 5.

Discrepancies between simulation models and experimental measurements may arise mainly from the real oil temperature and assumption of a uniform temperature distribution across the seal. Other limitations of the simulation model stem from surface roughness generation, mesh finesse, pressure distribution, and the numerical model used. Despite these challenges, the solid simulation model remains the closest to experimental measurements. Therefore, it is recommended to simulate each labyrinth seal assembly with an optimized simulation model and calibrated initial conditions to accurately predict lubricant mass loss over time.

5. Conclusion

The vacuum evaporation intensity of space oils through labyrinth seals was investigated using experimental, analytical, and simulation approaches. The study underscores the need to refine analytical models, as they tend to overestimate mass loss by 5–8 times compared to experimental results. It also demonstrates a strong correlation between simulation results and experimental data. The simulation tools MolFlow+ and COMSOL Multiphysics are recommended for accurately predicting oil evaporative mass loss.

Key findings regarding the influence of labyrinth seal geometry on molecular flow include:

- Stepped labyrinth seal configurations provide enhanced sealing performance. A comparison of two labyrinth seals—one featuring a straight, long corridor and the other a stepped configuration—reveals that the stepped seal, which is 30 % longer, should theoretically provide a 16 % improvement in sealing effectiveness due to its increased length. However, the stepped design actually achieved a 20 % improvement, indicating additional benefits from the stepped geometry itself.
- Molecular beaming effects within labyrinth seals contribute to oil mass loss. This effect can be significantly reduced by using a stepped configuration with the step positioned at the midpoint of the seal, which best distributes the molecular beaming effect. Conversely, placing the step near the inlet or outlet can negatively impact sealing performance by increasing the mass loss rate by up to 5 %.
- Surface roughness impacts molecular transmission probability. A comparison between two seals, with average surface roughness values of Ra 2.6 and Ra 0.3, shows that the seal with greater roughness achieves a 14.4 % improvement in sealing performance over the smoother seal.
- Local geometrical adjustments, such as adding relief grooves, can enhance sealing efficiency. Depending on the specific modification, sealing effectiveness can improve by up to 4 %.

CRediT authorship contribution statement

Josef Pouzar: Writing – original draft, Visualization, Validation, Software, Project administration, Methodology, Investigation, Funding acquisition, Formal analysis, Data curation, Conceptualization. **David Kostal:** Writing – review & editing, Supervision, Methodology, Conceptualization. **Lars-Göran Westerberg:** Writing – review & editing, Supervision, Conceptualization. **Erik Nyberg:** Writing – review & editing, Methodology, Conceptualization. **Ivan Krupka:** Supervision, Resources, Funding acquisition.

Declaration of competing interest

The authors declare the following financial interests/personal relationships which may be considered as potential competing interests: Josef Pouzar reports financial support was provided by European Space Agency. Ivan Krupka reports financial support was provided by European Union. If there are other authors, they declare that they have no known competing financial interests or personal relationships that could have appeared to influence the work reported in this paper.

Acknowledgment

This research was supported by the activity "Effect of local geometrical changes and polarization of labyrinth seal surfaces on the evaporation rate of liquid lubricants in space applications", funded as a Discovery element contract 4000139889 by the European Space Agency; and by the project "Mechanical Engineering of Biological and Bio-inspired Systems", funded as project No. CZ.02.01.01/00/22_008/0004634 by Programme Johannes Amos Comenius, call Excellent Research.

Data availability

The data supporting the findings of this study are openly available on [Zenodo.org] at [https://doi.org/10.5281/zenodo.12190559], reference number [12190559].

References

[1] M. V Prozhega, E.O. Reschikov, N.N. Smirnov, Research of the lifetime and lubricant properties of greases for rolling bearings operating in space conditions, J. Frict. Wear 42 (2021) 431–437, https://doi.org/10.3103/S1068366621060088.
[2] W.R. Jones, M.J. Jansen, Tribology for space applications, Proc. Inst. Mech. Eng., Part J 222 (2008), https://doi.org/10.1243/13506501JET305.
[3] M. Gleirscher, A. Wolfberger, S. Schlögl, M. Hołyńska, A. Hausberger, Accelerated thermo-catalytic degradation of perfluoropolyether (PFPE) lubricants for space applications, Lubricants 11 (2023) 81, https://doi.org/10.3390/lubricants11020081.
[4] M. Eiden, R. Seiler, Space mechanisms and tribology challenges of future space missions, Acta Astronaut. 55 (2004) 935–943, https://doi.org/10.1016/j.actaastro.2004.04.011.
[5] E.W. Roberts, Space tribology: its role in spacecraft mechanisms, J. Phys. D Appl. Phys. 45 (2012) 503001, https://doi.org/10.1088/0022-3727/45/50/503001.
[6] J. Pouzar, D. Kostal, P. Sperka, I. Krupka, M. Hartl, Experimental study of space lubricant evaporation in a high vacuum environment, Vacuum 219 (2024) 112758, https://doi.org/10.1016/j.vacuum.2023.112758.
[7] M. V Prozhega, A.Yu Albagachiev, N.I. Smirnov, N.N. Smirnov, Lubricating materials for mechanisms operating in space, J. Frict. Wear 39 (2018) 335–340, https://doi.org/10.3103/S106836661804013X.
[8] S. Krishnan, S.-H. Lee, H.-Y. Hsu, G. Konchady, Lubrication of attitude control systems, in: Advances in Spacecraft Technologies, InTech, 2011, https://doi.org/10.5772/13354.

[9] T. Tondu, E. Vanhove, J.F. Roussel, D. Faye, Mixture effects in contaminant reemission, J. Spacecraft Rockets 53 (2016) 1172–1177, https://doi.org/10.2514/1.A33507.
[10] A. Merstallinger, R. Holzbauer, N. Bamsey, Cold welding in hold down points of space mechanisms due to fretting when omitting grease, Lubricants 9 (2021) 72, https://doi.org/10.3390/lubricants9080072.
[11] ESTL, Evaporation lives of space oils, ESA-ESTL-TM-0162 01-, https://llviewersg3a.com/webviewer.php?doc=316948, 2019. (Accessed 14 June 2024).
[12] M.J. Anderson, S. Freeman, E.W. Roberts, Evaporative losses of vacuum-compatible oils through labyrinth seals, in: R.~A. Harris (Ed.), ESMATS, 2003, pp. 255–270. https://www.esmats.eu/esmatspapers/pastpapers/pdfs/2003/anderson.pdf. (Accessed 14 June 2024).
[13] A. Suliga, O. Ergincan, R. Rampini, Modeling of spacecraft outgassed contamination levels by thermogravimetric analysis, J. Spacecraft Rockets 58 (2021) 1010–1016, https://doi.org/10.2514/1.A35020.
[14] M.N. Gardos, Labyrinth sealing of aerospace mechanisms—theory and practice, A S L E Transactions 17 (1974) 237–250, https://doi.org/10.1080/05698197408981462.
[15] E.W. Roberts, M. Eiden, Space Tribology Handbook, fifth ed., ESR Technology Ltd., 2013. https://llviewersg3a.com/webviewer.php?doc=308770. (Accessed 14 June 2024).
[16] O. Sazhin, The effect of surface roughness on internal free molecular gas flow, Vacuum 159 (2019) 287–292, https://doi.org/10.1016/j.vacuum.2018.09.031.
[17] M. Hołyńska, R.-C. Sarah, E. Orcun, B. Bruno, A. Claudia, R. Riccardo, Lessons Learnt from Lubricants' Testing at Estec Materials' Laboratories, 2021, p. 5. https://www.esmats.eu/esmatspapers/pastpapers/pdfs/2021/holynska.pdf.
[18] R. Kersevan, Analytical and numerical tools for vacuum systems, Vacuum in Accelerators (2007) 28, https://doi.org/10.5170/CERN-2007-003.285.
[19] O.B. Malyshev, Vacuum in Particle Accelerators, Wiley, 2019, https://doi.org/10.1002/9783527809134.
[20] M. Buttery, S. Lewis, A. Kent, R. Bingley, M. Cropper, Long-term storage considerations for spacecraft lubricants, Lubricants 8 (2020) 32, https://doi.org/10.3390/lubricants8030032.
[21] G. Livesey, Flow of gases through tubes and orifices, in: J.M. Lafferty (Ed.), Foundations of Vacuum Science and Technology, 1998, p. 25. https://atomoptics-nas.uoregon.edu/~tbrown/files/strontium_vacuum_system/Research.
[22] A. Berman, Vacuum engineering calculations, formulas, and solved exercises, in: Vacuum Engineering Calculations, Formulas, and Solved Exercises, Elsevier, 1992, pp. xi–xii, https://doi.org/10.1016/B978-0-12-092455-4.50003-9.
[23] The vacuum technology book | volume II, Pfeiffer Vacuum, 2013, pp. 9–20. https://know-how-book.pfeiffer-vacuum.com/en/container!download.action@referer=1456&download=%252Ffilepool%252Ffile%252Fliterature%252Fvacuum-technology-book-ii-part-2.pdf.
[24] W. Steckelmacher, A review of the molecular flow conductance for systems of tubes and components and the measurement of pumping speed, Vacuum 16 (1966) 561–584, https://doi.org/10.1016/0042-207X(66)91416-3.
[25] M. Buttery, L. Gaillard, S. Rajala, E. Roberts, T. Rohr, Fomblin Z25: a new method for its degradation assessment & proposal for safe operation in space. https://esmats.eu/esmatspapers/pastpapers/pdfs/2013/buttery.pdf, 2013. (Accessed 2 April 2024).
[26] P. Kadoski Tadeusz, Wojdyna, Liquid lubricants for space engineering and methods for their testing, J. KONES Powertrain Trans. 18 (2011). https://www.researchgate.net/publication/267767121_Liquid_lubricants_for_space_engineering_and_methods_for_their_testing.
[27] A. Rowntree, ESTL-TM-238 - A Review of Oil Loss Models for Labyrinth Seals and Filters for Space Applications, 2000.
[28] R.& S.D. ESA-ESTEC, ECSS-Q-TM-70-52A: kinetic outgassing of materials for space (25 November 2011), Noordwijk, Netherlands, https://ecss.nl/hbstms/ecss-q-tm-70-52a-kinetic-outgassing, 2011.
[29] H.M. Stanley S, ESA-ESTL-TM-0162 01- an experimental assessment of the evaporation lives of space oils. https://www.esrtechnology.com/index.php/jdownloads/send/2-estl-members-library/2259-tm-0162-01-esa-evaporation-lives-of-space-oils, 2018.
[30] D.J. Carré, P.A. Bertrand, A model to calculate evaporative oil loss in spacecraft mechanisms, Tribol. Trans. 42 (1999) 282–288, https://doi.org/10.1080/10402009908982218.
[31] L.M.N.B.F. Santos, A.I.M.C.L. Ferreira, V. Štejfa, A.S.M.C. Rodrigues, M.A. A. Rocha, M.C. Torres, F.M.S. Tavares, F.S. Carpinteiro, Development of the Knudsen effusion methodology for vapour pressure measurements of low volatile liquids and solids based on a quartz crystal microbalance, J. Chem. Thermodyn. 126 (2018) 171–186, https://doi.org/10.1016/j.jct.2018.07.004.
[32] CERN, MolFlow+ A monte-carlo simulator package developed at CERN. https://molflow.web.cern.ch/, 2023.
[33] COMSOL, COMSOL Multiphysics | molecular flow module. https://www.comsol.com/molecular-flow-module, 2023.
[34] C.E. Papadopoulos, H. Yeung, Uncertainty estimation and Monte Carlo simulation method, Flow Meas. Instrum. 12 (2001) 291–298, https://doi.org/10.1016/S0955-5986(01)00015-2.
[35] Solvay Specialty Polymers, Fomblin® PFPE lubes for vacuum applications. https://www.solvay.com/sites/g/files/srpend221/files/2018-07/fomblin-pfpe-lubes-for-vaccum-applications-en.pdf, 2017.
[36] R. Kersevan, M. Ady, Recent developments of monte-carlo codes Molflow+ and Synrad+. 10th International Particle Accelerator Conference, 2019, pp. 1327–1330, https://doi.org/10.18429/JACoW-IPAC2019-TUPMP037.
[37] R. Kersevan, J.-L. Pons, Introduction to MOLFLOW+: new graphical processing unit-based Monte Carlo code for simulating molecular flows and for calculating angular coefficients in the compute unified device architecture environment, J. Vac. Sci. Technol. A: Vacuum, Surfaces, and Films 27 (2009) 1017–1023, https://doi.org/10.1116/1.3153280.
[38] COMSOL Multiphysics® v. 6.2. www.comsol.com. COMSOL AB, Stockholm, Sweden., (n.d.). www.comsol.com (accessed February 27, 2024).
[39] K. Jousten, Wutz Handbuch Vakuumtechnik, Vieweg+Teubner Verlag, Wiesbaden, 2004, https://doi.org/10.1007/978-3-322-96971-2.
[40] J.M. Lafferty (Ed.), Foundations of Vacuum Science and Technology, John Wiley & Sons, New York, 1998.
[41] S.D. Lewis, M. Buttery, O. Poyntz-Wright, A. Kent, A. Vortsellas, Accelerated testing of tribological components - uncertainties and solutions. https://esmats.eu/amspapers/pastpapers/pdfs/2018/lewis2.pdf, 2018.
[42] D. Koutsoyiannis, Clausius–Clapeyron equation and saturation vapour pressure: simple theory reconciled with practice, Eur. J. Phys. 33 (2012) 295–305, https://doi.org/10.1088/0143-0807/33/2/295.
[43] M.R. Hampson, B. Wardzinski, in: L. Ouwehand (Ed.), The Evaluation and Validation of New Creep Barrier Films for Prevention of Oil Loss by Migration, ESA Special Publication, 2015, p. 30. https://www.esmats.eu/esmatspapers/pastpapers/pdfs/2015/hampson.pdf.

Update

Vacuum

Volume 238, Issue , August 2025, Page

DOI: https://doi.org/10.1016/j.vacuum.2025.114434

Vacuum 238 (2025) 114434

Contents lists available at ScienceDirect

Vacuum

journal homepage: www.elsevier.com/locate/vacuum

Corrigendum to labyrinth seal design for space applications [Vacuum 232 (2025) 113882]

Josef Pouzar [a,*], David Kostal [a], Lars-Göran Westerberg [b], Erik Nyberg [c], Ivan Krupka [a]

[a] Faculty of Mechanical Engineering, Brno University of Technology, Brno, 61669, Czech Republic
[b] Division of Fluid and Experimental Mechanics, Luleå University of Technology, SE-971 87, Luleå, Sweden
[c] Division of Machine Elements, Luleå University of Technology, SE-971 87, Luleå, Sweden

The authors regret to inform readers about two significant issues identified in the published article regarding the use of an analytical equation, known as the ESTL model, for predicting the evaporative leakage of lubricant molecules through labyrinth seals.

First, the ESTL model was used in the article for predictive calculations. However, the cited reference contained incorrect units for the equation, leading to discrepancies between the reported analytical predictions and those that would have been obtained using the correct units. Upon recalculating the results with the corrected units, notable differences were observed compared to the original analytical predictions. To clarify this issue, we present the corrected ESTL equation with appropriate indexing to ensure clarity and transparency regarding the correct unit usage. Additionally, the abbreviations and symbols have been updated accordingly.

Abbreviations and Symbols

B	Labyrinth gap width [mm]	P_i	Inlet pressure [Pa]
b_{cm}	Labyrinth gap width [cm]	P_o	Outlet pressure [Pa]
d, $d_{1,2}$	Diameter of annular seal [mm]	Q	Flow rate [mbar·mm^3/s]
d_{cm}	Diameter of annular seal [cm]	Q_m	Mass loss [g/s]
ESTL	European Space Tribology Laboratory	r	Circular arc radius [mm]
ETR	Evaporation Test Rig	Ra	Average roughness [μm]
L, $L_{1,2,3}$	Labyrinth path length [mm]	Sa	Arithmetic mean height [μm]
L_{cm}	Labyrinth path length [cm]	Sq	Squared mean height [μm]
L	Recess depth [mm]	T	Absolute temperature [K]
M	Lubricant molar mass [g/mol]	TP	Transmission probability [−]
PFPE	Perfluoropolyether	v	Average molecular velocity [m/s]
P_{mbar}	Fluid vapor pressure [mbar]		

$$Q_m = 0,0436 \cdot \frac{P_{mbar}\pi d_{cm} b_{cm}\left(\frac{M}{T}\right)^{0.5}}{1 + 0,375 \cdot \frac{L_{cm}}{b_{cm}}} \quad (3)$$

Second, a mathematical error was identified in the implementation of the analytical equation within the computational code, which affected the evaluation of the ESTL model. After correcting this error, the updated analytical results were validated by comparison with data from other institutions, demonstrating improved correlation and accuracy.

A revised comparison of the results obtained from all three approaches—analytical, simulation, and experimental—is shown in Fig. 5. The updated findings confirm that both the analytical and simulation models significantly overestimate mass loss for short labyrinth geometries. However, for complex seals, the analytical approach slightly underestimates mass loss, while the simulation results closely align with the experimentally acquired data. When comparing mass loss and relative leak rates using the experimental results as a reference (see Table 3), both the analytical model and simulations overestimate the leak rate of short labyrinth gaps by more than a factor of two. In contrast, for complex labyrinths, the relative leak rate deviations range between 22 and 27 % for the analytical model and 5–15 % for the simulations.

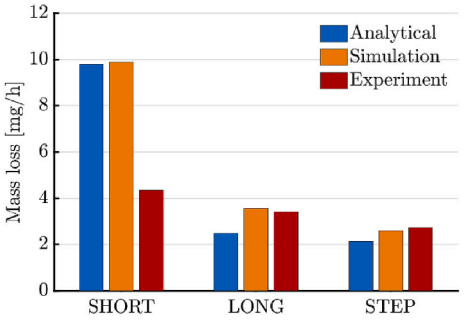

Fig. 5. Comparison of analytical, experimental and simulation approaches of evaporation mass loss.

DOI of original article: https://doi.org/10.1016/j.vacuum.2024.113882.
* Corresponding author.
E-mail address: Josef.Pouzar@vut.cz (J. Pouzar).

https://doi.org/10.1016/j.vacuum.2025.114434

Available online 28 May 2025
0042-207X/© 2025 The Author(s). Published by Elsevier Ltd. This is an open access article under the CC BY license (http://creativecommons.org/licenses/by/4.0/).

Tab. 3
Mass flow evaluation for specific labyrinths using diverse approaches

Approach		SHORT		LONG		STEP	
		[mg/h]	relative leak rate	[mg/h]	relative leak rate	[mg/h]	relative leak rate
Experiment		5.47	1	3.41	1	2.73	1
Analytical		9.80	1.79	2.48	0,73	2.14	0,78
Simulation	MolFlow+	9.46	1.73	3.24	0,95	2.33	0,85
	COMSOL	9.89	1.81	3.58	1,05	2.72	1,00

These findings underscore the limitations of mass loss predictions for short labyrinth seals, where both the analytical model and simulations overestimate the loss by more than a factor of two compared to experimental measurements. However, for complex labyrinths, simulation results demonstrate strong agreement with experimental data.

As a result of these corrections, the analytical equations were recalculated, and the updated values have been provided. Importantly, the key conclusions of the article remain unchanged. These corrections do not affect the main findings or the overall validity of the paper.

The authors believe that these corrections emphasize the critical importance of using correct units in analytical models—an essential consideration in the field. This corrigendum aims to contribute to future research by highlighting the necessity of precision in unit usage and model implementation.

The authors sincerely apologize for any inconvenience this may have caused.

PAPER [3]

INFLUENCE OF SURFACE ROUGHNESS ON MOLECULAR FLOW THROUGH LABYRINTH SEALS FOR SPACE APPLICATIONS

Pouzar et al.

Results in Engineering, Volume 28, 2025
doi: 10.1016/j.rineng.2025.107905

Results in Engineering 28 (2025) 107905

Contents lists available at ScienceDirect

Results in Engineering

journal homepage: www.sciencedirect.com/journal/results-in-engineering

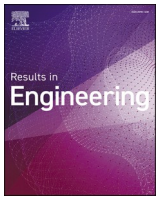

Influence of surface roughness on molecular flow through labyrinth seals for space applications

Josef Pouzar [a,*], David Kostal [a], Lars-Göran Westerberg [b], Erik Nyberg [c], Tomas Polacek [a], Karel Jurik [d], Ivan Krupka [a]

[a] Faculty of Mechanical Engineering, Brno University of Technology, Brno 61669, Czech Republic
[b] Division of Fluid and Experimental Mechanics, Luleå University of Technology, SE-971 87 Luleå, Sweden
[c] Division of Machine Elements, Luleå University of Technology, SE-971 87 Luleå, Sweden
[d] Faculty of Electrical Engineering and Communication, Brno University of Technology, Brno 61600, Czech Republic

ARTICLE INFO

Dataset link: https://doi.org/10.5281/zenodo.15649645

Keywords:
Labyrinth seal
Surface roughness
Transmission probability
Molecular flow
Space mechanisms

ABSTRACT

Labyrinth seals are commonly used in space mechanisms to reduce evaporative losses of lubricant molecules and limit the transport of contaminants. Analytical models and numerical simulations for predicting mass flow through these seals typically assume smooth, idealized surfaces, neglecting the effects of realistic surface roughness. This study systematically investigates the impact of surface roughness on the transmission probability (TP) of oil molecules using Monte Carlo simulations under free molecular flow conditions. Key geometric and surface parameters including average roughness (Ra), corridor length, and seal width are varied to evaluate their influence on molecular transport. The results demonstrate that surface roughness significantly reduces TP and molecular flux, especially in narrow and elongated geometries. Furthermore, increasing surface roughness by an order of magnitude enables a reduction in channel length or an increase in gap width by approximately 35–40 % while maintaining equivalent transmission probability. Based on these findings, a correction model is proposed to improve prediction accuracy and is validated against experimentally measured oil evaporative losses. This work highlights the potential of controlled surface texturing as a design strategy to both enhance sealing effectiveness and enable geometric reductions for improved compactness and manufacturability.

Abbreviations and Symbols

$a(n)$	Wave amplitude [mm]
$A(W, L)$, $B(W, L)$, $C(W, L)$	Polynomial coefficients
$A_{i,j}$, $B_{i,j}$, $C_{i,j}$	Indexed polynomial coefficients
b	Spectral exponent
$f(x)$	Synthetic roughness profile [mm]
g, $g(n)$	Gaussian random function
$h(n)$	Synthetized profile amplitude [mm]
L	Corridor length [mm]
m	Number of data points
n	Spatial frequency
N	Spatial frequency resolution
N_0	Number of molecules entering
N_1	Number of molecules exiting
PC	Parametric curve scaling factor
$PFPE$	Perfluoropolyether
Ra	Arithmetic mean roughness [μm]
Rk	Core roughness depth [μm]
Rku	Kurtosis
Rpk	Reduced peak height [μm]
Rq	Root mean square roughness [μm]
Rsk	Skewness
Rvk	Reduced valley depth [μm]
TP	Transmission probability [-]
u	Uniform random distribution
$u(n)$	Uniform random phase
W	Corridor width [mm]
x	Spatial coordinate [mm]
z	Roughness profile height [mm]
$\bar{z}$	Mean profile height [mm]
z_i	Discrete height value [mm]

* Corresponding author.
E-mail address: Josef.Pouzar@vut.cz (J. Pouzar).

https://doi.org/10.1016/j.rineng.2025.107905
Received 17 October 2025; Accepted 23 October 2025
Available online 24 October 2025
2590-1230/© 2025 The Authors. Published by Elsevier B.V. This is an open access article under the CC BY license (http://creativecommons.org/licenses/by/4.0/).

1. Introduction

In space applications, mechanical systems containing liquid lubricants must be sealed to prevent lubricant loss and preserve long-term functionality [1–4]. Non-contact labyrinth seals are widely employed for this purpose, offering a passive means of restricting the migration of lubricant molecules in ultra-high or extreme vacuum environments [5–8]. These seals incorporate a narrow corridor between stationary and rotating components (see Fig. 1), effectively limiting molecular flow without introducing friction or wear [4,7,9]. Preserving lubricant within these systems is critical to ensuring the longevity and reliability of space mechanisms [1,10,11]. The escape and subsequent condensation of evaporated molecules on sensitive surfaces such as optical elements can degrade performance and jeopardize mission success [4,12,13]. These risks underscore the importance of reliable sealing to limit molecular leakage and extend the service life of lubricated systems in space.

Labyrinth seals for space applications may consist of straight channels or more complex geometries [5,6,8]. However, the primary parameters governing molecular flow restriction are the corridor length and width [5,8]. A careful balance between these two parameters is required to ensure mechanical safety while effectively reducing molecular transmission [4,5]. Predicting lubricant evaporative losses can be approached through analytical models or numerical simulations [4,5,7,8]. Both methodologies usually assume smooth internal surfaces with no surface roughness [4,8]. The influence of realistic surface roughness arising from machining [14,15], material processing [16,17], or operational wear [18,19], is neglected despite its potential to alter molecular scattering behaviour and significantly impact transmission probability [20–25]. This effect is particularly important in narrow and elongated seal geometries, where interactions between molecules and surface features are more frequent and cumulative [22,26].

This study investigates the influence of surface roughness on the molecular flow of lubricant through two-dimensional labyrinth seals operating under vacuum conditions. By employing synthetically generated rough surface profiles combined with Monte Carlo simulations, the analysis explores the interaction between roughness parameters and seal geometry, including corridor length and width. The primary outcome is a simulation-based correction model that refines conventional smooth-surface predictions by incorporating realistic surface roughness effects representative of actual labyrinth seals. This model provides a practical and physically grounded tool for predicting lubricant evaporation and highlights the potential to compensate for geometric constraints through surface texturing, enabling possible reductions in seal dimensions without compromising sealing performance.

2. Material and methods

To evaluate the impact of surface roughness on molecular transmission, a numerical model of a straight, two-dimensional labyrinth seal was developed. This geometry, representative of those used in ball bearing systems [4,5], consists of a narrow corridor through which lubricant molecules evaporate and diffuse under vacuum conditions [8,27]. Fig. 1 illustrates the modelled configuration, showing the migration of evaporated molecules along the seal path.

The simulation includes surface roughness on the seal walls to investigate its possible effect on molecular scattering and transmission probability. Synthetic rough profiles were generated using statistical parameters characteristic of real labyrinth seals and integrated into a molecular flow simulation tool. This method enables the tracking of individual molecular trajectories and allows for assessing how surface topography may influence 38 molecular transport through the seal.

2.1. Surface roughness modeling

Simulations were performed using COMSOL Multiphysics 6.3 [28], utilizing the Free Molecular Flow module [29]. Since this module do not natively support surface roughness parameters, surface roughness was instead introduced as a geometric modification of the canal walls in a 2D simulation domain.

A common approach to modelling surface roughness is based on its spatial frequency content, analogous to the Fourier representation of temporal signals [20,30–33]. This approach allows for the synthesis of roughness profiles by summing a finite number of cosine waves with randomized amplitudes and phases. In one spatial dimension, an elementary cosine wave is given by

$$\cos(2\pi(\boldsymbol{nx})) \tag{1}$$

where n is the spatial frequency and x is the spatial coordinate. The synthetic surface roughness profile height z as a function $f(x)$ is synthesized as a discrete superposition of such wave

$$z = f(\boldsymbol{x}) = \sum_{n=-N}^{N} \boldsymbol{a}(\boldsymbol{n})\cos\left(2\pi(\boldsymbol{nx}) + u(n)\right) \tag{2}$$

Here $a(n)$ is wave amplitude, and $u(n)$ is random phase angle drawn from a uniform distribution over the interval $[-\pi/2, \pi/2]$, that cosine term span the full range from –1 to 1. Isotropy is achieved by including both positive and negative frequency components symmetrically ($-N$, N). To reflect realistic surface statistics, the amplitude is computed as

$$a(\boldsymbol{n}) = g(n)\cdot h(\boldsymbol{n}) \tag{3}$$

where

$$h(\boldsymbol{n}) = \frac{1}{(\boldsymbol{n}^2)^{b/2}} \tag{4}$$

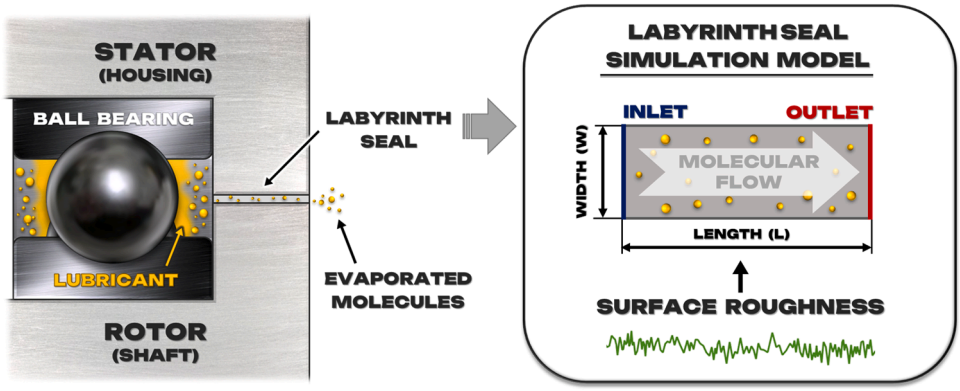

Fig. 1. Visualization of a ball bearing system with an integrated labyrinth seal and evaporating molecules, coupled with a simulation model incorporating surface roughness geometry.

The spectral envelope *h(n)* attenuates high-frequency components. The spectral exponent *b* controls the rate of amplitude decay with frequency, while *g(n)* is a Gaussian random function with zero mean and unit variance. Since the resulting function *f(x)* is inherently periodic, only a subdomain (i.e., [0, 1]) was extracted to mitigate visible periodicity in the final geometry.

In practice, roughness profiles were implemented in COMSOL as parametric curves, representing height perturbations. These curves were then extruded to form the sidewalls of the labyrinth seal corridor. Each curve was generated using a spectral synthesis function combining Gaussian (*g*) and Uniform (*u*) random distributions, expressed as

$$z = PC \bullet \sum_{n=-N}^{N} \left(n^2\right)^{-\frac{b}{2}} \cdot g(n) \bullet \cos(2\pi(nx) + u(n)) \tag{5}$$

Here, *N* is the spatial frequency resolution, and *b* is the spectral exponent controlling amplitude decay with frequency. The scaling factor, referred to as the parametric curve (*PC*) coefficient, was varied to generate different roughness amplitudes. Multiple values of *PC* were applied across simulations for each (*N, b*) pair to produce a comprehensive range of surface roughness levels. These curves were interpolated and applied to the geometry boundaries in COMSOL, enabling precise control of wall roughness during meshing and simulation.

2.2. Surface generation and evaluation of surface roughness profiles

To investigate how mathematical parameters influence the physical characteristics of surface topography, a parametric study was conducted by systematically varying the *N, b* and *PC*. These parameters define the surface structure in the spatial frequency domain:

- *N* controls the spatial resolution, determining the number and density of peaks,
- *b* governs the rate of amplitude attenuation across frequencies,
- *PC* scales the overall amplitude of the roughness profile.

A comprehensive set of synthetic surface profiles was generated for a range of *N, b* and *PC* combinations (see Fig. 2) summarized in Table 1. This results in a comprehensive grid of synthetic surfaces designed to probe both low-frequency (coarse) and high-frequency (fine) features under different amplitude scaling regimes. Several widely used surface roughness parameters were extracted from each profile, as one parameter cannot adequately describe the surface properties [34]. These parameters are further described together with their mathematical definitions, and responses to the varying spectral inputs. The resulting data provided a foundation for selecting representative surfaces used in subsequent molecular flow simulations.

2.2.1. Arithmetic mean roughness (Ra)

The arithmetic mean roughness is one of the most used surface roughness parameters in engineering [15,35]. It represents the average of the absolute deviations from the mean line of the surface profile and

Table 1
Overview of adjustable parameters used to simulate surface topography.

Parameter	Range	Step
N	10 – 100	10
b	0.05 – 0.5	0.05
PC	0.001 – 0.003	0.001

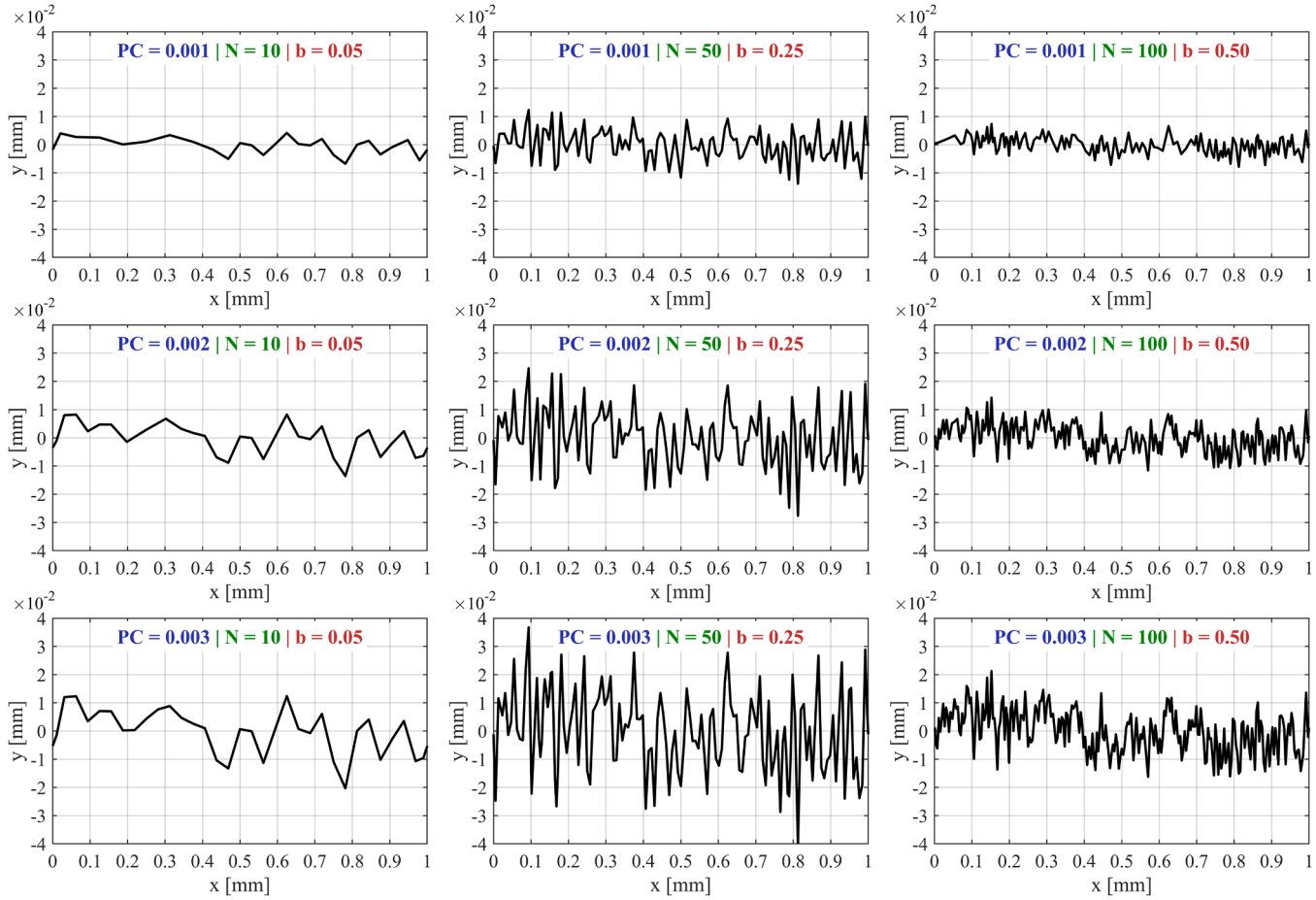

Fig. 2. Synthetic surface roughness profiles generated for varying spectral resolution (*N*), spectral exponent (*b*) and parametric curve coefficients (*PC*).

gives a general indication of surface height variation [36–38].

$$Ra = \frac{1}{L}\int_0^L |z(x)|\, dx \;\approx\; \frac{1}{m}\sum_{i=1}^{m} |z_i| \tag{6}$$

where z_i are the discrete height values of the profile and m is the number of data points. The Fig. 3(i) shows the variation of the *Ra* as a function of *N* and *b* for different values of the *PC*. As expected, increasing *N* introduces finer spatial details, while decreasing *b* results in rougher, more irregular surfaces with higher *Ra* values. Across all simulations, *Ra* increases nearly linearly with *PC*, confirming its primary role in scaling the vertical amplitude of the roughness profiles. Surfaces generated with lower *N* and higher *b* generally exhibit lower *Ra* values. However, as *PC* increases, its influence becomes more dominant, leading to a pronounced amplification of surface roughness regardless of the underlying spectral characteristics.

2.2.2. Root mean square roughness (Rq)

The root mean square roughness quantifies the standard deviation of the surface height. Calculated values are similar to *Ra* but emphasizes larger deviations due to squaring the profile values [36–38].

$$Rq = \sqrt{\frac{1}{L}\int_0^L z^2(x)\, dx} \;\approx\; \sqrt{\frac{1}{m}\sum_{i=1}^{m} z_i^2} \tag{7}$$

The root mean square roughness is particularly valuable in applications where sensitivity to outlier features or overall roughness energy is critical. Compared to *Ra, Rq* typically yields slightly higher values for the same surface due to its squared deviation weighting. Fig. 3(ii) shows the influence of the spectral parameters *N* and *b* on *Rq* for various *PC* values. The observed trends closely mirror those of *Ra*, with *Rq* generally increasing as *N* increases and *b* decreases, reflecting the heightened surface complexity. As expected, *Rq* values consistently exceed *Ra* due to the squaring of height deviations in its calculation.

2.2.3. Skewness (Rsk)

Skewness quantifies the asymmetry of a surface profile about its mean line. A negative *Rsk* indicates a prevalence of valleys, while a positive *Rsk* suggests a prevalence of peaks [38].

$$Rsk = \frac{1}{Rq^3} \bullet \frac{1}{L}\int_0^L z^3(x)dx \;\approx\; \frac{1}{Rq^3} \bullet \frac{1}{m}\sum_{i=1}^{m} (z_i - \bar{z})^3 \tag{8}$$

Skewness (see Fig. 3 (iii)) is primarily influenced by the spectral resolution N: low *N* tends to produce surfaces with deep valleys and sharp peaks, resulting in more pronounced asymmetry. In contrast, high *N* yields smoother, more balanced surfaces, causing skewness to approach zero regardless of the *PC* value. The effect of the spectral exponent *b* on skewness is relatively minor compared to *N* and PC. Surfaces generated with the lowest *PC* (i.e., 0.001) exhibit the most irregular and unpredictable skewness values. As *PC* increases, these irregularities are reduced, and skewness becomes more stable across different spectral configurations.

2.2.4. Kurtosis (Rku)

Kurtosis characterizes the profile's deviation from a Gaussian distribution in terms of the concentration of surface features [38]. A value of $Rku = 3$ corresponds to a normal (Gaussian) distribution. Values greater than 3 (leptokurtic) suggest the presence of pronounced peaks or deep valleys, while values <3 (platykurtic) indicate a flatter surface topology.

$$Rku = \frac{1}{Rq^4} \bullet \frac{1}{L}\int_0^L z^4(x)dx = \frac{1}{Rq^4} \bullet \frac{1}{m}\sum_{i=1}^{m} (z_i - \bar{z})^4 \tag{9}$$

The results in Fig. 3(iv) suggests that kurtosis does not consistently increase with spectral resolution (N). Instead, the spectral exponent (*b*), which controls the damping of high-frequency components, appears to have a greater influence: as *b* decreases, isolated protrusions and depressions become more pronounced, theoretically leading to higher kurtosis values. Additionally, kurtosis decreases with increasing *PC*, gradually approaching the Gaussian reference value of 3. This trend indicates that surfaces with low *PC* retain sharper features and more isolated peaks or valleys, while higher *PC* values smooth these extremes by scaling the amplitude, resulting in profiles with fewer distinct high or low points.

2.2.5. Bearing curve parameters (Rk, Rpk, Rvk)

The bearing (Abbott-Firestone) curve parameters provide insight into the functional performance of a surface [38–41]. These include the core roughness depth (*Rk*), reduced peak height (*Rpk*) above the core material, and reduced valley depth (*Rvk*), which are extracted by fitting the linear portion of the material ratio curve and extrapolating to estimate the peak and valley contributions [14,19,37,18].

These roughness parameters are closely influenced by machining processes, especially turning, where characteristics such as *Rk, Ra* and *Rq* often display a near-linear relationship with the feed rate [37,40,18]. This correlation enables reliable prediction and modelling of surface topography based on known cutting speeds and feed conditions [42,43].

Bearing curve parameters *Rk, Rpk*, and *Rvk* (see Fig. 4) follow trends similar to those observed for *Ra* and *Rq*, exhibiting consistent dependence on the spectral parameters *N, b*, and *PC*. The core roughness depth (*Rk*) generally decreases with increasing *b*, indicating smoother surfaces as high-frequency components reduce the vertical extent of the load-bearing region. All three parameters scale approximately linearly with *PC*, reaffirming its role as a vertical amplification factor. These findings highlight the sensitivity of functional surface parameters to both spectral shape and amplitude scaling. Their combined evaluation offers deeper insight into the evolution of surface topography and its potential impact on contact mechanics and tribological performance.

2.3. Molecular flow simulation setup

To evaluate the influence of surface roughness on molecular flow behaviour, a series of simulations were conducted using COMSOL Multiphysics 6.3, under free molecular flow conditions. The geometry of the model consisted of a 2D labyrinth seal corridor defined by inlet and outlet boundaries and two parallel walls formed by the synthetic surface roughness profiles.

To ensure geometric symmetry and isolate the effect of surface topography, the same parametric curve was used for both labyrinth walls. Specifically, the roughness profile was first generated for one wall (lower boundary), and the second wall (upper boundary) was created by duplicating this curve and shifting it vertically along the y-axis by a distance equal to the labyrinth width. This setup ensured that both walls had matching roughness features, avoiding discrepancies caused by independent wall geometries.

The simulations were run under isothermal high-vacuum conditions, with molecular properties based on Fomblin Y LVAC 25/6 a perfluoropolyether (PFPE) lubricant used in prior experimental validation studies [3,5]. The geometrical dimensions, meshing settings, simulation parameters, and fluid properties used in the simulations are summarized in Table 2.

Geometrical parameters including channel length and width were varied systematically to assess how confinement and seal dimensions interact with surface roughness. The analysis of the simulation results focused on two key evaluation metrics: the transmission probability and the molecular flux at the outlet. The transmission probability (*TP*) provides a dimensionless measure of flow efficiency [5,44,45]

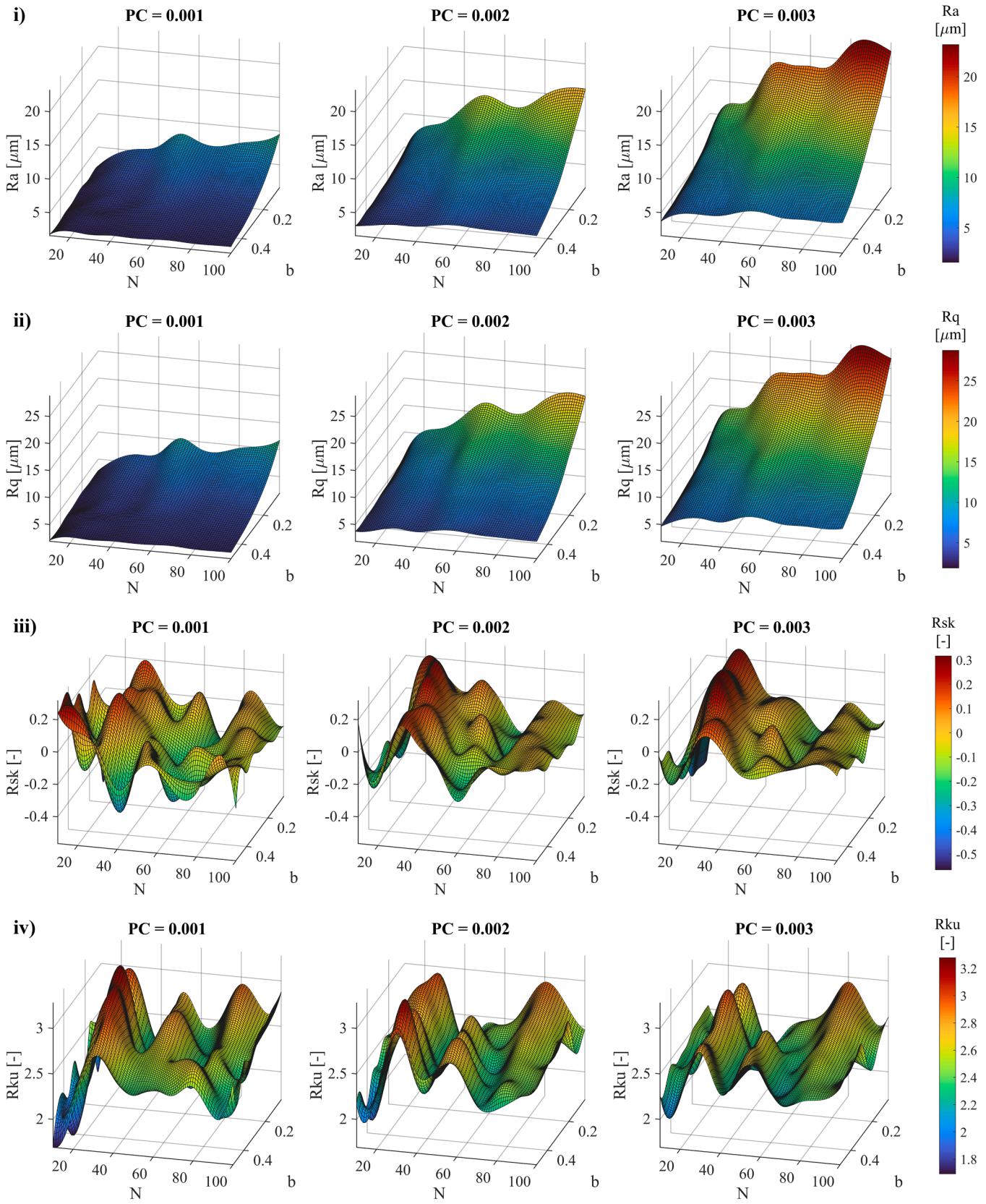

Fig. 3. Surface roughness parameters vs spectral parameters *N* and *b* for varying *PC*: Ra (i), Rq (ii), Rsk (iii), Rku (iv).

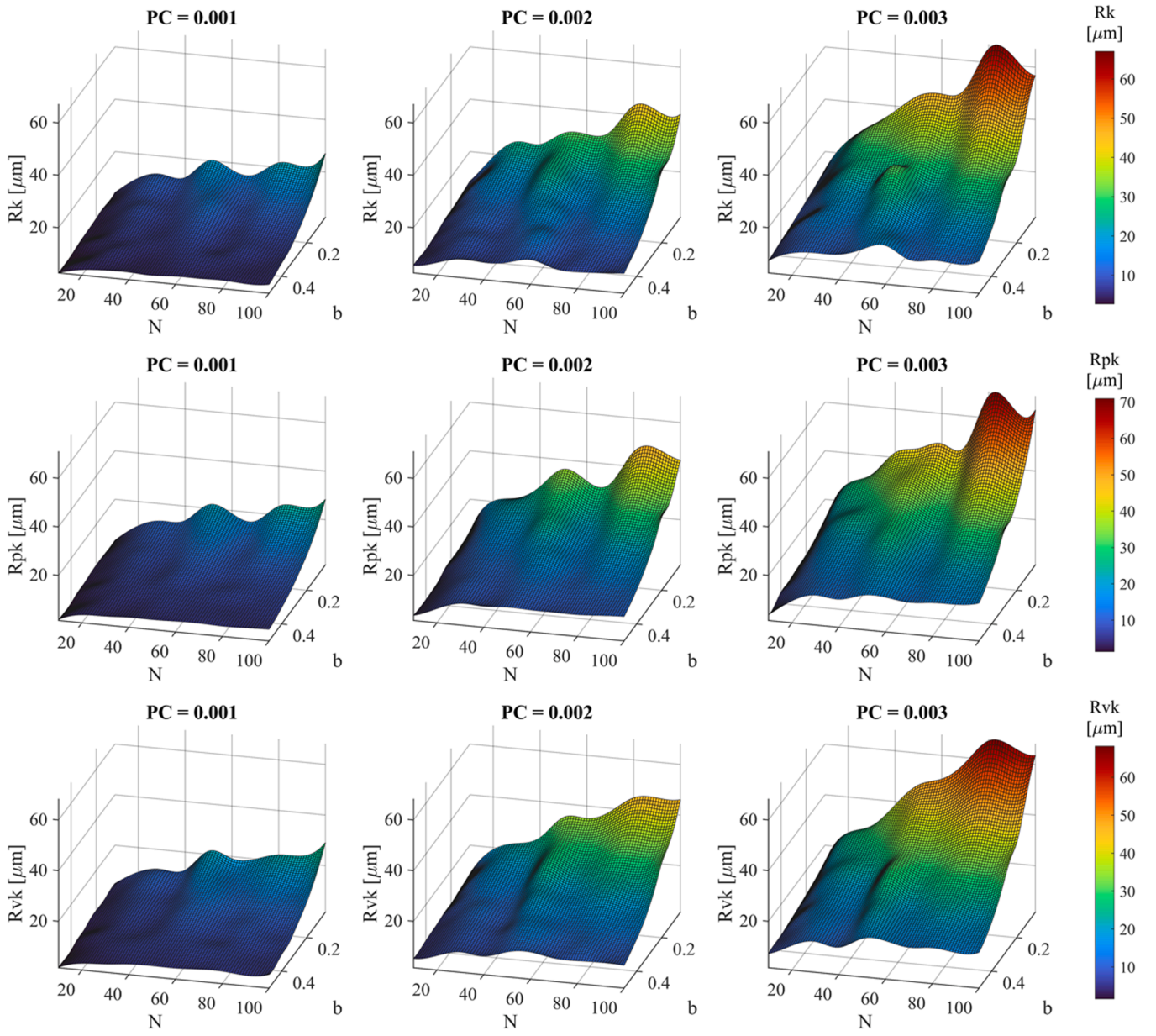

Fig. 4. Bearing curve parameters *Rk, Rpk*, and *Rvk* across *N, b*, and *PC*.

Table 2
Summary of simulation parameters and lubricant properties used for molecular flow simulations.

Category	Parameter	Value	Description
Geometry	Labyrinth length (L)	1 – 10 mm	Parametrically varied to evaluate length influence
	Labyrinth width (W)	0.2 – 1.0 mm	Parametrically varied to study confinement effects
Meshing	Grid resolution	Physics-controlled	Refined mesh near boundaries for surface details
Simulation conditions	Temperature (T)	373.15 K	Isothermal condition across the domain
	Inlet pressure	6E-4 Pa	Define as per boundary condition
	Outlet pressure	Total vacuum	Typically vacuum or near-zero pressure
Oil sample	Lubricant name	Fomblin Y LVAC 25/6	Perfluoropolyether (PFPE) lubricant
	Molecular weight	~3300 g/mol	Molecular mass used for molecular flow simulations

$$TP = \frac{\boldsymbol{N}_1}{\boldsymbol{N}_0} \tag{10}$$

where N_0 represents the total number of molecules entering the channel, and N_1 corresponds to the number of molecules successfully exiting through the outlet. This metric offers a clear and intuitive indication of the sealing performance of the labyrinth geometry and is particularly valuable in molecular flow regimes [5,44]. Its normalized form allows for greater generalization of results across varying boundary conditions, which is critical for the development of simulation-based correction functions introduced in later sections of this work.

In contrast, the mass flow at the outlet, which represents the absolute number of molecules per unit area and time reaching the exit, is more directly tied to the specific pressure and temperature conditions imposed in the simulation. While it provides additional physical insight and supports validation with experimental measurements, it is less transferable across scenarios without recalibration. Therefore, transmission probability was prioritized as the central comparative metric in this study, serving as the foundation for assessing how variations in

surface roughness affect molecular flow through the seal.

To systematically assess the influence of each parameter on transmission behaviour, three representative datasets were selected for detailed simulation (see Table 3), covering a wide spectrum of roughness structures from coarse, low-frequency features to finely resolved microstructures. The selected datasets span a broad range of spectral configurations, from coarse, low-frequency structures to finely resolved, high-frequency surfaces.

Among the evaluated parameters, the *PC* factor plays a primary role in scaling the amplitude of surface profiles and thus has a direct influence on amplitude-related roughness metrics such as *Ra, Rq, Rk, Rpk*, and *Rvk*. These parameters exhibited nearly linear increases with *PC*. The skewness (*Rsk*) and kurtosis (*Rku*) demonstrated more nuanced, nonlinear responses, particularly at lower *PC* values. These findings highlight the complex interplay between spectral structure and vertical scaling in determining the overall surface character. The datasets cover a range of surface morphologies, from dominant low-frequency fluctuations to compactly arranged fine features.

3. Results

To evaluate the influence of surface roughness on molecular transport, synthetic roughness profiles were generated through a parametric sweep of three key variables: spectral resolution (N), spectral exponent (b), and vertical scaling factor (PC). These parameters respectively govern the spatial frequency content, spectral decay, and amplitude of the surface profiles. The transmission probability results, evaluated across the three amplitude scaling values are summarized in Fig. 5.

The results show that increasing N significantly reduces transmission probability (*TP*), following a second-order trend. In contrast, decreasing *b* leads to an approximately linear drop in *TP*, indicating that low-frequency roughness features play a key role in impeding molecular passage. Variations in *PC* influence the curvature of the *N–TP* relationship. Higher PC values cause transmission probability to decline more steeply at low N, amplifying the impact of roughness height on molecular transmission.

A 2D contour analysis of *TP* and *Ra* across *N* and *b* for different *PC* values (see Fig. 5) confirms a consistent inverse relationship where *TP* decreases consistently with increasing *Ra*. This underscores how spectral parameters shape surface morphology and influence molecular flow.

3.1. Characterization of synthetic surface roughness datasets

The synthetic roughness datasets (see Table 3) were integrated into COMSOL Multiphysics simulations of molecular flow through 2D labyrinth seal geometries. For each surface profile, the labyrinth corridor was constructed with matching wall curves, and simulations were run across multiple channel widths and lengths as summarized in Table 2. This approach enabled an in-depth examination of how surface roughness, when interacting with geometry, influences transmission probability and molecular flux.

For each dataset, surface profiles were generated and evaluated using standard roughness metrics, including amplitude parameters (*Ra, Rq, Rk, Rpk, Rvk*) and shape descriptors (*Rsk, Rku*). The trends observed across the *PC* sweep reveal how different spectral configurations influence the geometry and statistical properties of the rough surfaces.

Table 3
Overview of parameter sets used for surface generation in molecular flow simulations.

Dataset	Spectral resolution N	Spectral exponent B	Roughness amplitude scaling	
			PC	Number of steps
1	30	0.5	0.0005 to 0.020	12
2	50	0.05	0.0001 to 0.002	11
3	100	0.1	0.0001 to 0.001	10

3.1.1. Dataset 1 – moderate resolution, coarse structures

Dataset 1 represents rough surfaces dominated by low-frequency fluctuations with clearly defined peaks and valleys. The spectral resolution is moderate ($N = 30$) and the relatively high spectral exponent ($b = 0.5$) emphasizes large-scale features. This dataset is particularly suited to evaluate how prominent topographical features scatter molecular trajectories.

The amplitude-related surface roughness parameters (*Ra, Rq, Rk, Rpk, Rvk*) increased approximately linearly with *PC* (see Fig. 6). In contrast, the shape descriptors *Rsk* and *Rku* demonstrated nonlinear behaviour, especially at low *PC* values, indicating enhanced asymmetry and peak sharpness at small amplitudes.

3.1.2. Dataset 2 – high resolution, broad variability

In Dataset 2, the spectral resolution is increased to $N = 50$ and the spectral exponent is reduced to $b = 0.05$. This configuration results in surface profiles with weaker spectral decay and more uniformly distributed spatial frequencies resembling a white noise texture. The result is a high-frequency surface rich in fine structure and randomness.

Despite the increase in resolution, the amplitude parameters continue to scale predictably with *PC* (see Fig. 7). However, *Rsk* and *Rku* show greater sensitivity and fluctuation due to the fine-scale randomness becoming more pronounced at higher spatial resolution.

3.1.3. Dataset 3 – very high resolution, fine-scale features

Dataset 3 explores the limits of spectral resolution with $N = 100$ and a moderate spectral exponent ($b = 0.1$), generating highly detailed profiles with dense, fine-scale features. To isolate the influence of small amplitude variations, *PC* values are constrained to a narrow range ($0.0001 – 0.001$).

The increased resolution led to a denser distribution of surface irregularities, which strongly affects molecular scattering even at minimal vertical scaling. The effect of *PC* on all roughness parameters was less pronounced in absolute terms (see Fig. 8).

3.2. Combined analysis across datasets

The synthetic surface roughness profiles described in Section 3.1 were incorporated into COMSOL Multiphysics simulations to assess their influence on molecular transport through 2D labyrinth seal geometries. For each profile, a matching channel geometry was constructed by embedding the corresponding surface curve into both walls of the labyrinth (see Fig. 1). Simulations were performed for a range of corridor widths ($W = 0.2 – 1$ mm) and lengths ($L = 1 – 10$ mm), as summarized in Table 2.

Each rough surface configuration was benchmarked against a smooth-wall reference ($Ra = 0$), enabling quantitative evaluation of how surface roughness impedes molecular flow. Across all datasets, an increase in surface roughness (i.e., higher *PC* values) consistently resulted in lower transmission probabilities (see Fig. 9). The smooth reference surface exhibited the highest transmission probability across all geometries.

The effects of roughness were modulated by both corridor length and width (see Fig. 10):

- Corridor Length (*L*): Longer channels provided more opportunities for molecule-wall interactions. This resulted in cumulative scattering effects, especially for profiles with high spectral resolution. For these cases, the transmission probability often exhibited exponential decay with length.

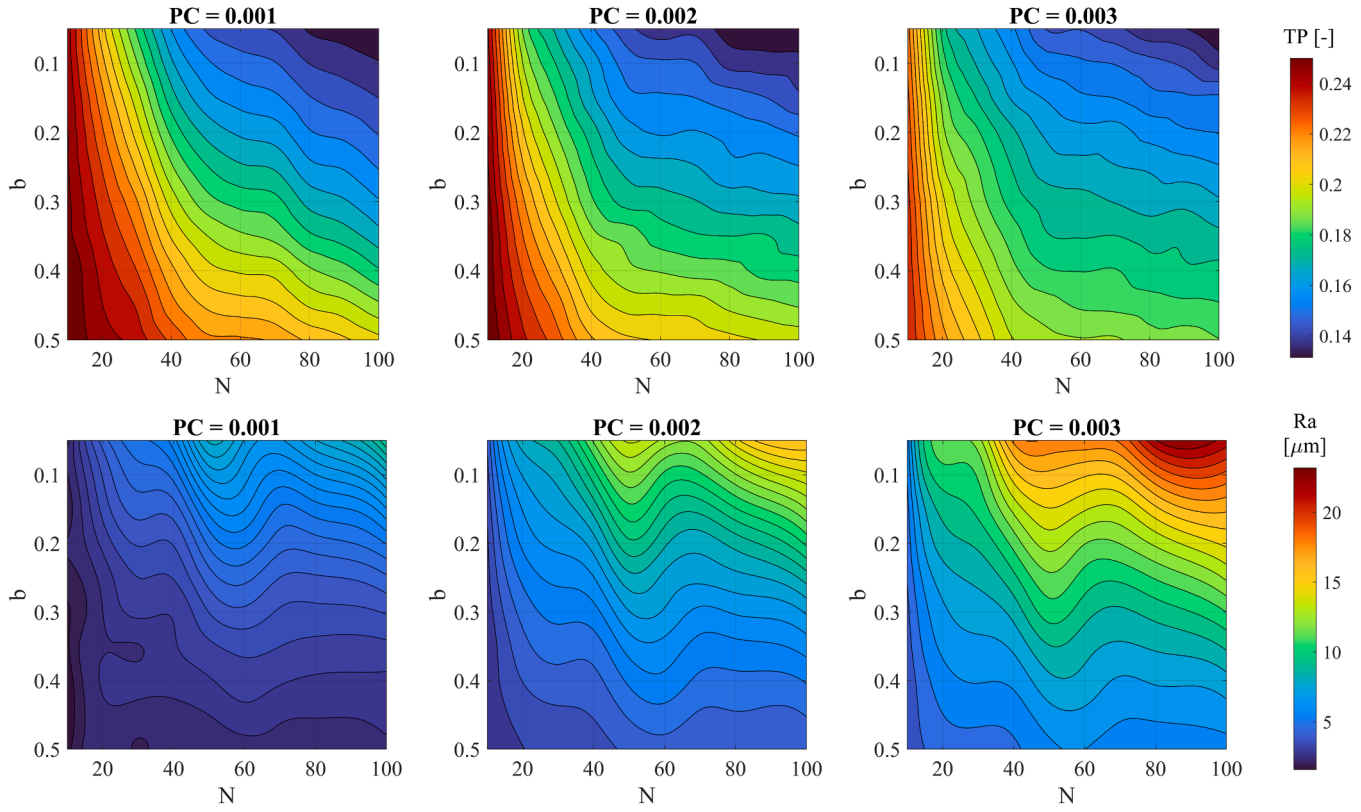

Fig. 5. Contour plots of transmission probability (*TP*) and average roughness (*Ra*) as functions of spectral parameters *N* and *b* for varying amplitude scaling (*PC*).

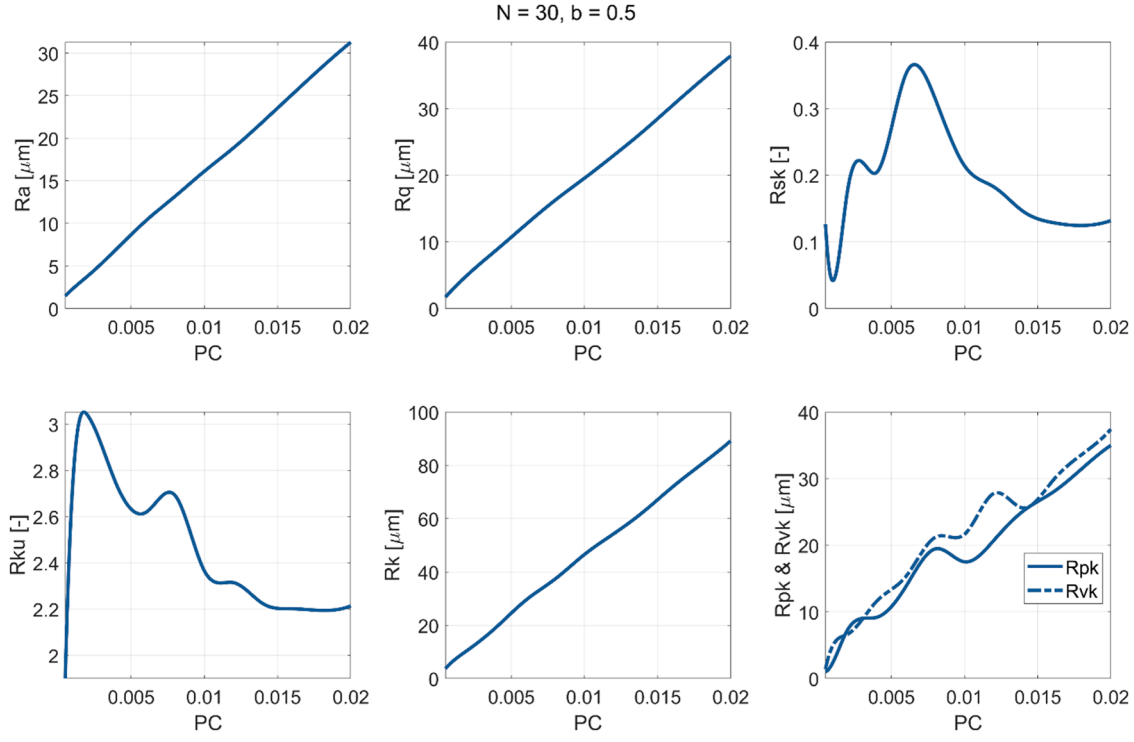

Fig. 6. Surface roughness parameters as a function of *PC* (Dataset 1, $N = 30$, $b = 0.5$).

- Corridor Width (*W*): In narrow geometries, molecular trajectories are more frequently intercepted by rough walls, amplifying the effect of surface irregularities. This led to steep, often nonlinear declines in transmission probability even at moderate *Ra* values. Wider channels demonstrated a reduced sensitivity, though the damping effect of roughness remained evident.

To systematically describe these dependencies, second-order

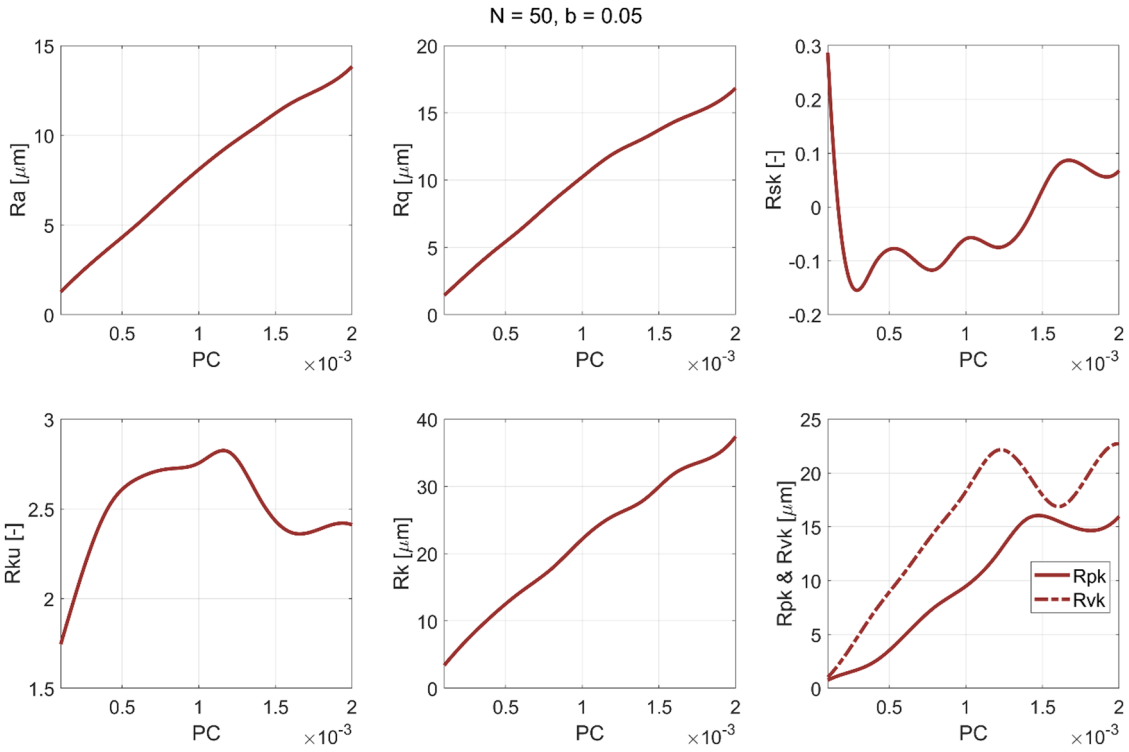

Fig. 7. Surface roughness parameters as a function of *PC* (Dataset 2, $N = 50$, $b = 0.05$).

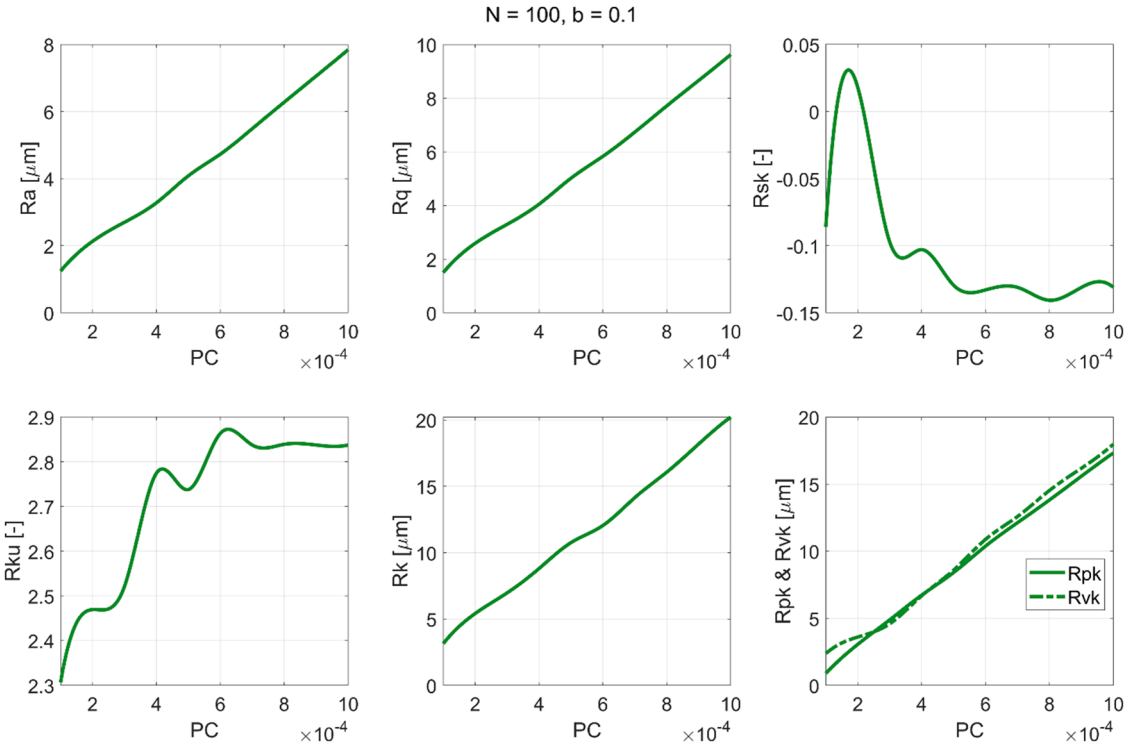

Fig. 8. Surface roughness parameters as a function of *PC* (Dataset 3, $N = 100$, $b = 0.1$).

polynomial fits of transmission probability versus *Ra* were computed for each (*W, L*) combination. The coefficients of these fits revealed clear trends, highlighting how both the amplitude and spectral characteristics of surface roughness affect flow resistance. These trends offer a foundation for developing correction models or relationships to estimate *TP* in rough microchannels.

3.3. Simulation-based correction model

Based on the extensive simulation results presented in Sections 3.1 and 3.2, a clear relationship was established between transmission probability (*TP*), surface roughness characteristics, and labyrinth geometry. These insights formed the basis for developing a simulation-

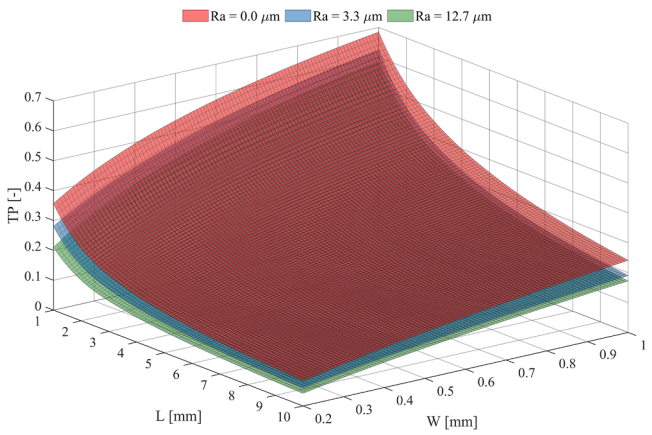

Fig. 9. Transmission probability across labyrinth length and width for varying surface roughness.

based correction model that estimates *TP* in 2D labyrinth seals as a function of surface roughness (quantified by *Ra*), and corridor geometry (length *L* and width *W*).

3.3.1. Model structure

From the simulation data, transmission probability was found to follow a smooth, nonlinear trend when plotted against *Ra* for fixed *W* and *L*. This trend was best captured by following second-order polynomial fit for calculating the corrected transmission probability (*TP*):

$$TP\ (\boldsymbol{Ra},\ \boldsymbol{W},\ \boldsymbol{L}) = A(\boldsymbol{W},\boldsymbol{L}) \bullet \boldsymbol{Ra}^2 + B(\boldsymbol{W},\boldsymbol{L}) \cdot Ra + C(W,L) \tag{11}$$

where *A(W, L), B(W, L), C(W, L)* are polynomial coefficients dependent on the geometric configuration and *Ra* is the arithmetic mean roughness (in μm). The coefficients were extracted from the simulation results by fitting curves to *TP* vs. *Ra* for each unique (*W, L*) combination. This generated a 3D matrix of coefficients [$A_{i,j}$, $B_{i,j}$, $C_{i,j}$] indexed by width and length, enabling interpolation or surface fitting across arbitrary geometries within the studied range. The complete set of fitted coefficients for all simulated W and L combinations is provided in the supporting data (see Data Availability Statement), allowing it to directly apply the correction model.

3.3.2. Model application

The developed correction model estimates the transmission probability (TP) of molecules through a labyrinth seal based on the surface roughness parameters of the seal walls, eliminating the need for extensive simulations. To apply the model:

1. Determine the surface roughness *Ra* (e.g., from measurement or simulation).
2. Identify the target channel dimensions (*W, L*).
3. Obtain the corresponding polynomial coefficients *A(W, L), B(W, L)* and *C(W, L)* from the supporting dataset provided with this study (see Data Availability Statement).
4. Calculate the transmission probability using the correction function Eq. (11).

This approach enables fast and flexible prediction of *TP* for design evaluations, roughness tolerance analyses, or process sensitivity studies. The model is especially valuable in the early stages of seal design, where quick estimations are critical for parameter screening and trade-off assessments. The correction function is valid within the range of parameters studied in the simulations:

- Surface roughness (*Ra*) up to approximately 13 μm
- Channel widths (*W*) of 0.2 – 1 mm
- Channel lengths (*L*) of 1 – 10 mm

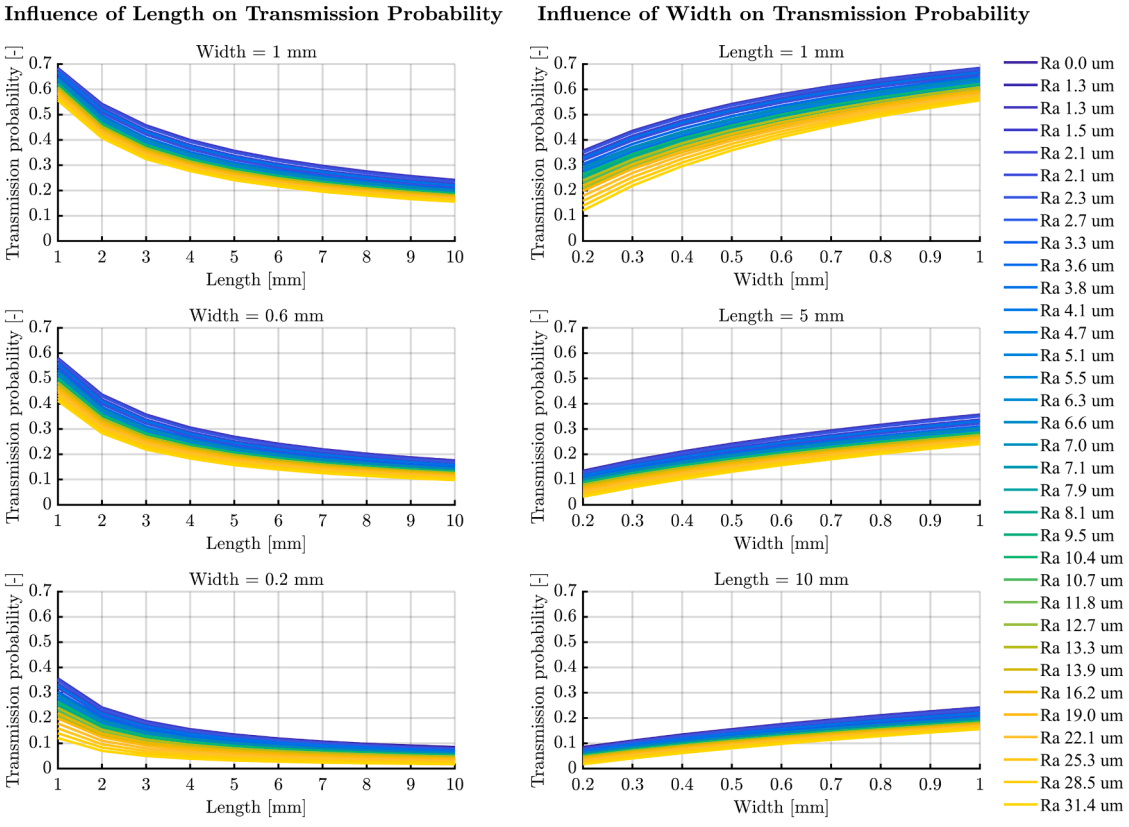

Fig. 10. Length and width effects on transmission probability across all surface roughness datasets.

Limitations should be noted when applying the model outside this parameter space. At extreme values (very high roughness or ultra-narrow channels) extrapolated predictions may diverge from actual physical behaviour due to geometric confinement or surface interactions not fully captured in the polynomial fit. Moreover, while the model captures the influence of roughness amplitude, it does not explicitly account for spectral characteristics (e.g., slope, spatial frequency), which may further influence molecular scattering. Future improvements could incorporate such features, for instance by introducing a spectral weighting term based on the roughness exponent b, or by including secondary metrics like the Rq/Ra ratio.

In summary, the model serves as a reliable and efficient tool for estimating molecular flow performance in rough microchannels, with potential for further extension to account for additional roughness descriptors and more complex geometries.

3.3.3. Model validation with experimental data

To evaluate the predictive capability of the proposed correction model, a comparison was made against experimentally measured evaporative mass losses through two labyrinth seal configurations exhibiting different surface roughness levels. These experiments, conducted in prior work [5], assessed the sealing performance of various labyrinth configurations during vacuum evaporation of a liquid lubricant.

All labyrinth seals shared identical channel dimensions: length $L = 10$ mm and width $W = 0.5$ mm, ensuring that the only varying factor was the surface roughness (see Table 4). For validation, an Ideal labyrinth with zero surface roughness ($Ra = 0$ μm) was introduced as a baseline reference to which the transmission probability (TP) predictions from the correction model were normalized (see Table 5). The experimental configurations (Labyrinth 1 and Labyrinth 2) were characterized using a Bruker Contour GTX 3D optical profilometer.

The model-predicted transmission probabilities (TP) for all three seals were calculated using the correction function Eq. (11). These values were then normalized relative to the Ideal labyrinth ($Ra = 0$ μm) to highlight the effect of roughness on molecular transport. To validate the model's predictive accuracy, the predicted TP ratios were then compared against the experimental ratios of evaporative mass loss, which serve as a physical proxy for relative transmission probability. This comparison approach provides insight into both the model's theoretical consistency and its empirical relevance. The results are summarized in Table 5.

These results confirm that the proposed correction model provides reliable prediction of molecular transport through rough labyrinth geometries, with a relative error of 5.1 % in the tested range. The close agreement demonstrates the robustness of the Ra-driven model structure and supports its practical applicability in early design and tolerance studies of microstructured channels under molecular flow.

Nonetheless, it should be noted that the correction model remains simulation-based and may deviate when applied beyond the calibration range (e.g., ultra-high Ra, channel widths below 0.2 mm, or non-uniform 3D roughness distributions). Additional experimental validation, including more diverse surface profiles and spectral characterizations, would further improve confidence in the model and enable potential extensions.

Table 4
Ideal and experimental conditions for labyrinth seal validation.

Category	Parameter	Value
Ideal labyrinth	Length (L)	10 mm
	Width (W)	0.5 mm
	Evaporative mass loss	–
	Surface roughness	Ra 0.00
Labyrinth 1	Length (L)	10 mm
	Width (W)	0.5 mm
	Evaporative mass loss	3.8 mg/h
	Surface roughness	Ra 0.13
Labyrinth 2	Length (L)	10 mm
	Width (W)	0.5 mm
	Evaporative mass loss	3.3 mg/h
	Surface roughness	Ra 3.88

Table 5
Comparison of model-predicted and experimentally measured transmission probability (TP) ratios for two labyrinth seals with different surface roughness levels.

	Ideal Labyrinth	Labyrinth 1	Labyrinth 2
Model-predicted TP	0.2933	0.2924	0.2670
TP ratio (vs. Ideal Labyrinth)	1.0000	0.9968	0.9104
Measured evaporative loss	–	3.8 mg/h	3.3 mg/h
Evaporative loss ratio (vs. Labyrinth 1)	–	1.0000	0.8684
Predicted TP ratio (vs. Labyrinth 1)	–	1.0000	0.9131
Relative error (prediction vs. measurement)	–	0.0 %	5.1 %

4. Discussion

The simulation results demonstrated a consistent inverse relationship between surface roughness and transmission probability (TP). As the average roughness Ra increased, TP decreased across all straight labyrinth configurations. This trend was especially pronounced in narrower and longer channels, where increased confinement and extended interaction paths led to a higher likelihood of molecule-wall collisions. These findings highlight that even moderate increases in surface irregularity can result in measurable reductions in molecular flow.

All simulations were run under isothermal conditions with a constant wall temperature without considering the thermal expansion of material. Chemical interactions and surface reactions were excluded, and material-dependent accommodation was not modeled. These assumptions isolate the effect of geometric roughness on transmission probability.

The data exhibit a clear decreasing trend of TP as surface roughness increases. A quadratic curve was fitted to the data to visualize the general trend (see Fig. 11) for one set of labyrinth seal dimensions ($W = 0.5$ mm, $L = 10$ mm). The parabolic shape of the fitted curve confirms that even moderate increases in roughness lead to non-linear reductions in TP. Interestingly, the curve begins to flatten at higher roughness

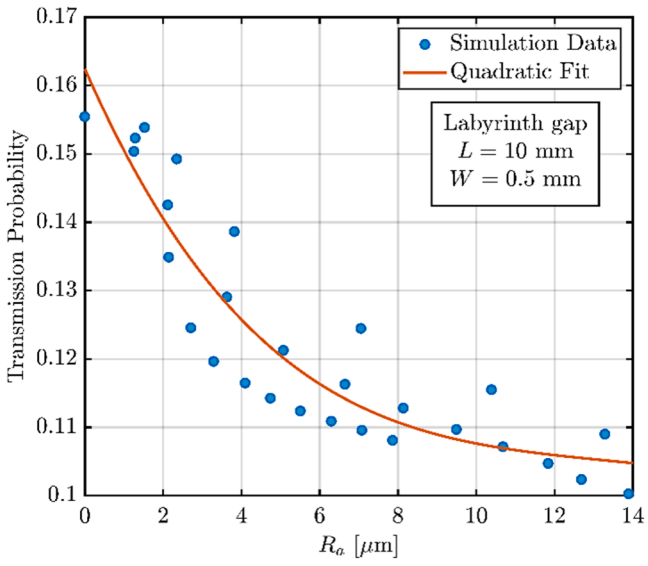

Fig. 11. Transmission probability vs. surface roughness ($W = 0.5$ mm, $L = 10$ mm).

levels, suggesting a saturation regime where further increases in roughness cause diminishing effects on *TP*.

Labyrinth seal corridor width (*W*) and length (*L*) were shown to modulate the effect of surface roughness non-linearly. Narrower channels amplified the influence of surface asperities by increasing the probability of collisions per unit path length, while longer channels introduced a cumulative scattering effect. This aligns with theoretical expectations in the molecular flow regime [5,26,46], where the mean free path exceeds the characteristic geometry, and the interactions of molecules with the wall dominate the transport behaviour. The strength of this geometric dependence justified the development of a simulation-based correction model.

This second-order polynomial correction model successfully generalized transmission probability across all datasets. Despite the variation in spectral properties (e.g., different *N* and *b* values), the dominant influence on *TP* was clearly attributed to the amplitude of surface roughness (*Ra*), rather than its spectral distribution. This allowed the model to be simplified without compromising predictive power for most practical configurations.

The model's predictive performance was validated by comparison with two experimental measurements of evaporative mass loss in previously tested labyrinth seals [5]. The correction model predicted *TP* ratios with a relative error of 5.1 %, demonstrating high agreement with physical observations. This confirms the model's utility for estimating molecular flow losses in seals with known surface roughness characteristics.

In addition to its predictive capabilities, the simulation data revealed a valuable design implication: surface roughness can serve as a compensatory parameter for geometric constraints in labyrinth seal design. Specifically, increasing the average roughness amplitude (*Ra*) allows for either a reduction in channel length or an increase in gap width of approximately 35–40 %, while maintaining a constant transmission probability (see Fig. 12). This finding underscores the potential of controlled surface texturing as a strategic approach to reduce molecular flow losses, enhance design flexibility, and improve the compactness and manufacturability of vacuum labyrinth seal systems.

Despite the model's strengths, several limitations must be acknowledged. The use of synthetically generated surface profiles may not fully capture the statistical complexity, anisotropy, or localized defects present in real-world machined or worn surfaces [17,37], potentially limiting the model's applicability to actual engineering conditions. Additionally, the simulations are restricted to a two-dimensional (2D) domain, which simplifies the inherently three-dimensional (3D) nature of practical labyrinth geometries. Effects such as edge curvature, cross-sectional variation, and out-of-plane confinement may alter molecular flow in ways not represented here.

The model also relies on the average roughness parameter (*Ra*) as a scalar descriptor of surface morphology. While effective for capturing broad trends in transmission probability, *Ra* omits higher-order surface characteristics such as skewness, kurtosis, or peak-valley asymmetry, which could influence flow behavior, particularly in more irregular or asymmetric profiles. Furthermore, the model does not account for temperature effects [1,4,47] or material specific gas-surface interactions, such as adsorption, desorption, or energy accommodation,

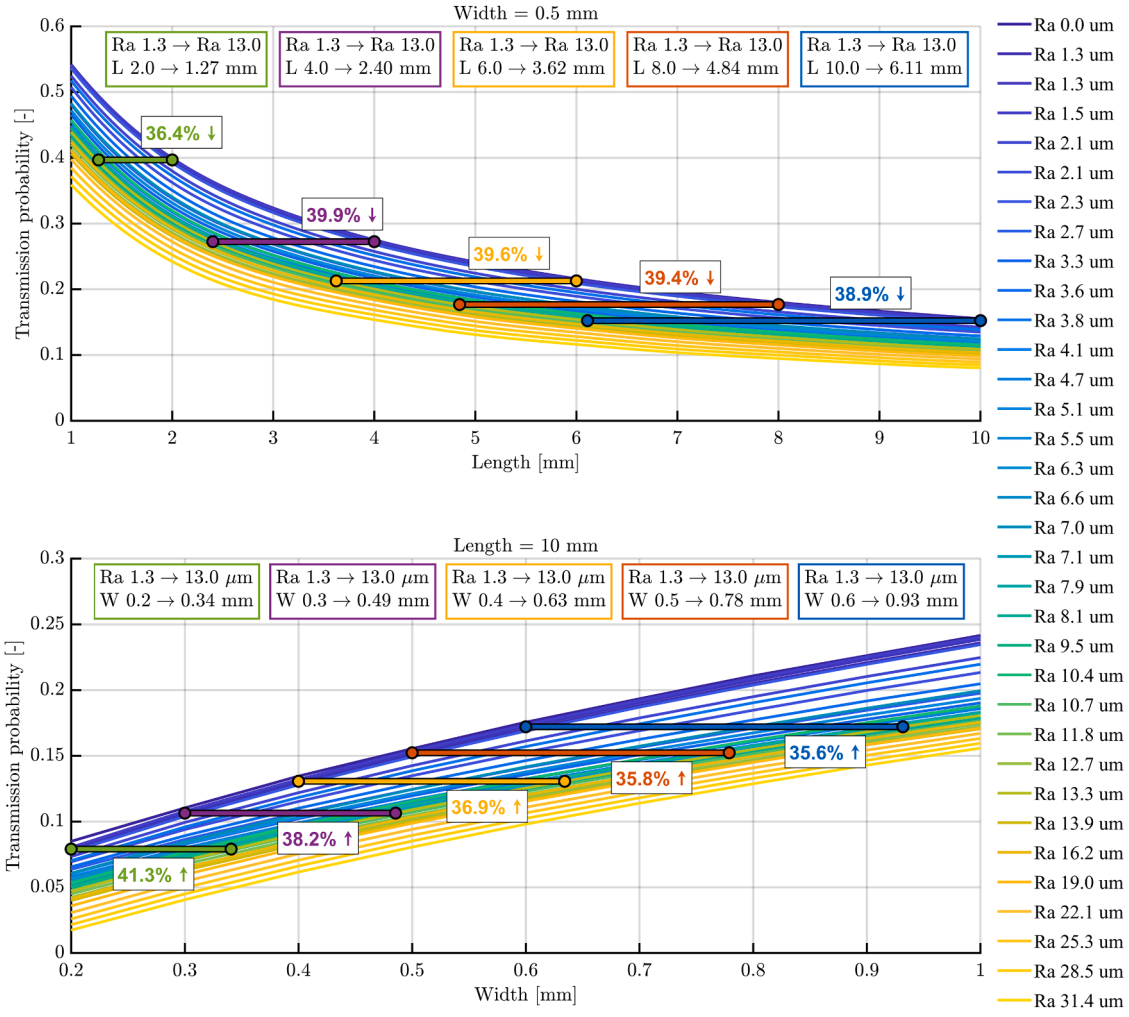

Fig. 12. Design trade-offs enabling seal length reduction or gap widening via increased surface roughness at constant transmission probability.

which may become significant in high-vacuum or reactive environments and could affect the scattering dynamics of molecules [26,47,48].

Finally, as a simulation-based fitted model, its predictive accuracy is constrained by the parameter space explored during its development. Application beyond the validated spectral and geometric ranges may introduce error, and caution is warranted when generalizing to untested conditions. These limitations suggest directions for future refinement, including incorporation of experimental surface data, extension to 3D geometries, and consideration of advanced surface descriptors and thermophysical effects.

5. Conclusion

This study systematically investigates the influence of surface roughness on molecular flow through two-dimensional (2D) labyrinth seals under ultra-high vacuum conditions. By integrating synthetic rough surface profile generation with molecular flow simulations and correction model development, it reveals a clear and consistent relationship between arithmetic mean roughness (*Ra*) and the transmission probability (*TP*) of evaporated lubricant molecules. These findings provide valuable insights for predicting evaporative mass loss and optimizing seal performance.

The results demonstrate a strong inverse correlation between surface roughness and transmission probability, characterized by a nonlinear, saturating decline – most pronounced at lower roughness levels (up to approximately $Ra = 6.0$ μm). Geometric parameters such as channel length and width significantly modulate this effect, with narrower and longer seals intensifying flow resistance due to increased molecule-wall interactions. To generalize these observations, a second-order polynomial correction model based on *Ra* was developed (see Eq.(11)), offering reliable *TP* predictions across a range of seal configurations. providing reliable TP predictions across diverse seal configurations. The model exhibited strong agreement with experimental data, maintaining prediction errors within 5.1 % (see Table 5).

Importantly, the study reveals that increasing surface roughness by an order of magnitude enables either a reduction in labyrinth seal channel length or an increase in gap width by approximately 35–40 %, while maintaining the same transmission probability (see Fig. 12). This insight highlights the potential of controlled surface texturing to improve design flexibility by allowing more compact or manufacturable seal geometries without compromising molecular flow performance.

Key outcomes of this study are:

- Surface roughness impedes molecular flow, with increasing *Ra* leading to decreased transmission probability.
- The effect of roughness is nonlinear, showing greatest sensitivity up to $Ra \approx 6.0$ μm and saturating at higher levels.
- Seal geometry (length and width) strongly influences the impact of roughness, particularly in narrow and elongated configurations.
- A second-order correction model based on *Ra* enables accurate, simplified *TP* predictions across various geometries.
- The model's predictions show strong agreement with experimental results, confirming its practical utility in optimizing labyrinth seals for vacuum applications.
- Controlled surface roughness can be leveraged as a design parameter to reduce seal length or increase gap width by up to 40 %, enhancing compactness and manufacturability without loss of performance.

Declaration of generative AI and AI-assisted technologies in the manuscript preparation process

During the preparation of this work, the author used ChatGPT (OpenAI) for grammar correction and stylistic improvements. After using this tool, the author carefully reviewed and edited the content to ensure accuracy and takes full responsibility for the final version of the manuscript.

Data availability statement

The data supporting the findings of this study are openly available on [Zenodo.org] at [https://doi.org/10.5281/zenodo.15649645], reference number [15,649,645].

CRediT authorship contribution statement

Josef Pouzar: Conceptualization, Data curation, Formal analysis, Funding acquisition, Investigation, Methodology, Project administration, Software, Validation, Visualization, Writing – original draft. **David Kostal:** Conceptualization, Supervision, Writing – review & editing. **Lars-Göran Westerberg:** Conceptualization, Supervision, Writing – review & editing. **Erik Nyberg:** Conceptualization, Methodology, Writing – review & editing. **Tomas Polacek:** Methodology, Validation, Writing – original draft. **Karel Jurik:** Data curation, Software, Writing – review & editing. **Ivan Krupka:** Funding acquisition, Resources, Supervision.

Declaration of competing interest

The authors declare the following financial interests/personal relationships which may be considered as potential competing interests:

Josef Pouzar reports financial support was provided by European Space Agency. Ivan Krupka reports financial support was provided by European Union. If there are other authors, they declare that they have no known competing financial interests or personal relationships that could have appeared to influence the work reported in this paper.

Acknowledgment

This work was supported by the activity "Effect of local geometrical changes and polarization of labyrinth seal surfaces on the evaporation rate of liquid lubricants in space applications", funded as contract Nr. 4000139889 by the European Space Agency; and by the project "Mechanical Engineering of Biological and Bio-inspired Systems", funded as project No CZ.02.01.01/00/22_008/0004634 by Programme Johannes Amos Comenius, call Excellent Research.

Data availability

https://doi.org/10.5281/zenodo.15649645 (The data supporting the findings of this study are openly available on [Zenodo.org] at [], reference number [15,649,645].)

References

[1] S. Krishnan, S.-H. Lee, H.-Y. Hsu, G. Konchady, Lubrication of attitude control systems, in: Advances in Spacecraft Technologies, InTech, 2011. https://doi.org/10.5772/13354.
[2] ESTL, Evaporation Lives of Space Oils, ESA-ESTL-TM-0162 01, 2019. https://llviewersg3a.com/webviewer.php?doc=316948. accessed June 14, 2024.
[3] J. Pouzar, D. Kostal, P. Sperka, I. Krupka, M. Hartl, Experimental study of space lubricant evaporation in a high vacuum environment, Vacuum. 219 (2024) 112758, https://doi.org/10.1016/j.vacuum.2023.112758.
[4] E.W. Roberts, M. Eiden, Space Tribology Handbook, 5th ed., ESR Technology Ltd, 2013. https://llviewersg3a.com/webviewer.php?doc=308770. accessed June 14, 2024.
[5] J. Pouzar, D. Kostal, L.-G. Westerberg, E. Nyberg, I. Krupka, Labyrinth seal design for space applications, Vacuum. 232 (2025) 113882, https://doi.org/10.1016/j.vacuum.2024.113882.
[6] M.N. Gardos, Labyrinth sealing of aerospace mechanisms—theory and practice, A S L E Trans. 17 (1974) 237–250, https://doi.org/10.1080/05698197408981462.
[7] M.J. Anderson, S. Freeman, E.W. Roberts, in: R.~A. Harris (Ed.), Evaporative Losses of Vacuum-Compatible Oils Through Labyrinth Seals, ESMATS, 2003, pp. 255–270. https://www.esmats.eu/esmatspapers/pastpapers/pdfs/2003/anderson.pdf. accessed June 14, 2024.
[8] A. Rowntree, ESTL-TM-238 - a review of oil loss models for labyrinth seals and filters for space applications. https://llviewersg3a.com/webviewer.php?doc=316948, 2000 accessed September 6, 2025.

[9] E.W. Roberts, Space tribology: its role in spacecraft mechanisms, J. Phys. D. Appl. Phys. 45 (2012) 503001, https://doi.org/10.1088/0022-3727/45/50/503001.
[10] M. Buttery, S. Lewis, A. Kent, R. Bingley, M. Cropper, Long-term storage considerations for spacecraft lubricants, Lubricants. 8 (2020) 32, https://doi.org/10.3390/lubricants8030032.
[11] T. Tondu, E. Vanhove, J.F. Roussel, D. Faye, Mixture effects in contaminant reemission, J. Spacecr. Rockets. 53 (2016) 1172–1177, https://doi.org/10.2514/1.A33507.
[12] P. Kadoski Tadeusz, Wojdyna, liquid lubricants for space engineering and methods for their testing, J. KONES Powertrain Transp. 18 (2011). https://www.researchgate.net/publication/267767121_Liquid_lubricants_for_space_engineering_and_methods_for_their_testing.
[13] A. Suliga, O. Ergincan, R. Rampini, Modeling of spacecraft outgassed contamination levels by thermogravimetric analysis, J. Spacecr. Rockets. 58 (2021) 1010–1016, https://doi.org/10.2514/1.A35020.
[14] M. Hasegawa, A. Seireg, R.A. Lindberg, Surface roughness model for turning, Tribol. Int. 9 (1976) 285–289, https://doi.org/10.1016/0301-679X(76)90019-0.
[15] K. Palová, T. Kelemenová, M. Kelemen, Measuring procedures for evaluating the surface roughness of machined parts, Appl. Sci. 13 (2023) 9385, https://doi.org/10.3390/app13169385.
[16] H. Puga, J. Grilo, V.H. Carneiro, Ultrasonic assisted turning of Al alloys: influence of material processing to improve surface roughness, Surfaces 2 (2019) 326–335, https://doi.org/10.3390/surfaces2020024.
[17] S.J. Zhang, S. To, S.J. Wang, Z.W. Zhu, A review of surface roughness generation in ultra-precision machining, Int. J. Mach. Tools. Manuf. 91 (2015) 76–95, https://doi.org/10.1016/j.ijmachtools.2015.02.001.
[18] C. Felho, G. Varga, Theoretical roughness modeling of hard turned surfaces considering tool wear, Machines 10 (2022) 188, https://doi.org/10.3390/machines10030188.
[19] K.J. Stout, T.G. King, D.J. Whitehouse, Analytical techniques in surface topography and their application to a running-in experiment, Wear. 43 (1977) 99–115, https://doi.org/10.1016/0043-1648(77)90046-1.
[20] F. Ticconi, L. Pulvirenti, N. Pierdicc, Models for Scattering from Rough Surfaces, Electromagnetic Waves, InTech, 2011, https://doi.org/10.5772/19318.
[21] Q. Dai, W. Huang, X. Wang, Surface roughness and orientation effects on the thermo-capillary migration of a droplet of paraffin oil, Exp. Therm. Fluid. Sci. 57 (2014) 200–206, https://doi.org/10.1016/j.expthermflusci.2014.04.023.
[22] R. Kersevan, Analytical and numerical tools for vacuum systems, Vac. Accel. (2007) 28, https://doi.org/10.5170/CERN-2007-003.285.
[23] M. Shams, M.H. Khadem, S. Hossainpour, Direct simulation of roughness effects on rarefied and compressible flow at slip flow regime, Int. Commun. Heat Mass Transf. 36 (2009) 88–95, https://doi.org/10.1016/j.icheatmasstransfer.2008.08.018.
[24] Y. Ji, K. Yuan, J.N. Chung, Numerical simulation of wall roughness on gaseous flow and heat transfer in a microchannel, Int. J. Heat. Mass Transf. 49 (2006) 1329–1339, https://doi.org/10.1016/j.ijheatmasstransfer.2005.10.011.
[25] H. Sun, M. Faghri, Effect of surface roughness on nitrogen flow in a microchannel using the direct simulation Monte Carlo method, Numeri. Heat. Transf. a Appl. 43 (2003) 1–8, https://doi.org/10.1080/10407780307302.
[26] O.B. Malyshev, Vacuum in Particle Accelerators, Wiley, 2019, https://doi.org/10.1002/9783527809134.
[27] B.T. Porodnov, P.E. Suetin, S.F. Borisov, V.D. Akinshin, Experimental investigation of rarefied gas flow in different channels, J. Fluid. Mech. 64 (1974) 417–438, https://doi.org/10.1017/S0022112074002485.
[28] COMSOL Multiphysics® v. 6.2. COMSOL AB, Stockholm, Sweden., (n.d.). www.comsol.com (accessed February 27, 2024).
[29] COMSOL, COMSOL Multiphysics | Molecular Flow Module. https://www.comsol.com/molecular-flow-module, 2023.
[30] N. Morrison, Introduction to Fourier Analysis, John Wiley & Sons, 1994.
[31] E.M. Stein, R. Shakarchi, Fourier analysis: An Introduction, Princeton University Press, 2003.
[32] B. Sjodin, How to Generate Random Surfaces in COMSOL Multiphysics®, COMSOL, 2017. https://www.comsol.com/blogs/how-to-generate-random-surfaces-in-comsol-multiphysics. accessed May 26, 2025.
[33] M.F. Barnsley, R.L. Devaney, B.B. Mandelbrot, H.-O. Peitgen, D. Saupe, R.F. Voss, The Science of Fractal Images, Springer New York, New York, NY, 1988, https://doi.org/10.1007/978-1-4612-3784-6.
[34] M.N. Goodhand, K. Walton, L. Blunt, H.W. Lung, R.J. Miller, R. Marsden, The limitations of "Ra" to describe surface roughness. Volume 5C: Heat Transfer, American Society of Mechanical Engineers, 2015, https://doi.org/10.1115/GT2015-43329.
[35] Q.J. Wang, Y.-W. Chung (Eds.), Encyclopedia of Tribology, Springer US, Boston, MA, 2013, https://doi.org/10.1007/978-0-387-92897-5.
[36] B.N.J. Persson, On the use of surface roughness parameters, Tribol. Lett. 71 (2023) 29, https://doi.org/10.1007/s11249-023-01700-z.
[37] M. Piska, J. Metelkova, On the influence of surface roughness on molecular flow and geometric compensation in vacuum labyrinth seals, MM Sci. J. 2014 (2014) 476–480, https://doi.org/10.17973/MMSJ.2014_06_201408.
[38] ISO 21920-2:2021 Geometrical product specifications (GPS) — Surface texture: profile part 2: terms, definitions and surface texture parameters, 2021.
[39] ISO 25178-2:2021 Geometrical product specifications (GPS) — Surface texture: areal part 2: terms, definitions and surface texture parameters, 2021.
[40] G.P. Petropoulos, A.A. Torrance, C.N. Pandazaras, Abbott curves characteristics of turned surfaces, Int. J. Mach. Tools. Manuf. 43 (2003) 237–243, https://doi.org/10.1016/S0890-6955(02)00240-7.
[41] P. He, S. Lu, Y. Wang, R. Li, F. Li, Analysis of the best roughness surface based on the bearing area curve theory, Proc. Inst. Mech. Eng. J: J. Eng. Tribol. 236 (2022) 527–540, https://doi.org/10.1177/13506501211018937.
[42] A. Doniavi, Empirical modeling of surface roughness in turning process of 1060 steel using factorial design methodology, J. Appl. Sci. 7 (2007) 2509–2513, https://doi.org/10.3923/jas.2007.2509.2513.
[43] D. Vukelic, K. Simunovic, Z. Kanovic, T. Saric, K. Doroslovacki, M. Prica, G. Simunovic, Modelling surface roughness in finish turning as a function of cutting tool geometry using the response surface method, gaussian process regression and decision tree regression, Adv. Prod. Eng. Manag. 17 (2022) 367–380, https://doi.org/10.14743/apem2022.3.442.
[44] O. Sazhin, The effect of surface roughness on internal free molecular gas flow, Vacuum. 159 (2019) 287–292, https://doi.org/10.1016/j.vacuum.2018.09.031.
[45] K. Jousten, W.H. Vakuumtechnik, Vieweg+Teubner Verlag, Wiesbaden, 2004, https://doi.org/10.1007/978-3-322-96971-2.
[46] The Vacuum Technology Book, II, Pfeiffer Vacuum, 2013. | Volume.
[47] M. Gleirscher, A. Wolfberger, S. Schlögl, M. Hołyńska, A. Hausberger, Accelerated thermo-catalytic degradation of perfluoropolyether (PFPE) lubricants for space applications, Lubricants. 11 (2023) 81, https://doi.org/10.3390/lubricants11020081.
[48] M. Hołyńska, R.-C. Sarah, E. Orcun, B. Bruno, A. Claudia, R. Riccardo, Lessons learnt from lubricants' Testing at Estec Materials' laboratories. https://www.esmats.eu/esmatspapers/pastpapers/pdfs/2021/holynska.pdf, 2021.

PAPER [4]

LABYRINTH SEAL DESIGN FOR ENHANCED SEALING OF EVAPORATED LUBRICANT MOLECULES IN SPACE MECHANISMS

Pouzar et al.

Proceedings of the 21st European Space Mechanisms and Tribology Symposium (ESMATS), Lausanne, 2025

LABYRINTH SEAL DESIGN FOR ENHANCED SEALING OF EVAPORATED LUBRICANT MOLECULES IN SPACE MECHANISMS

Josef Pouzar [(1)], David Kostal [(1)], Lars-Göran Westerberg [(2)], Ivan Krupka [(1)]

[(1)] Faculty of Mechanical Engineering, Brno University of Technology, Brno, Czech Republic
[(2)] Division of Fluid and Experimental Mechanics, Luleå University of Technology, Luleå, Sweden

ABSTRACT

This study evaluates labyrinth seals for space mechanisms to enhance lubricant retention and reduce contamination under vacuum conditions. It examines the influence of seal geometry including length, width, surface roughness, and stepped features through analytical models, numerical simulations, and experimental validation. Surface roughness and geometric complexity strongly affect molecular transmission, while electrostatic fields and rotational dynamics further improve sealing performance. Experimental evaporation measurements align closely with simulations and validate correction models that incorporate surface roughness effects. These results guide the design of labyrinth seals for space applications.

1 INTRODUCTION

Space mechanisms face extreme conditions such as ultra-high vacuum, temperature extremes, vibrations, and long inactivity, challenging the reliability of lubricated components. Liquid lubricants like perfluoropolyether (PFPE) and multiply alkylated cyclopentane (MAC) are commonly used, but lubricant loss through vacuum evaporation can cause contamination and wear.

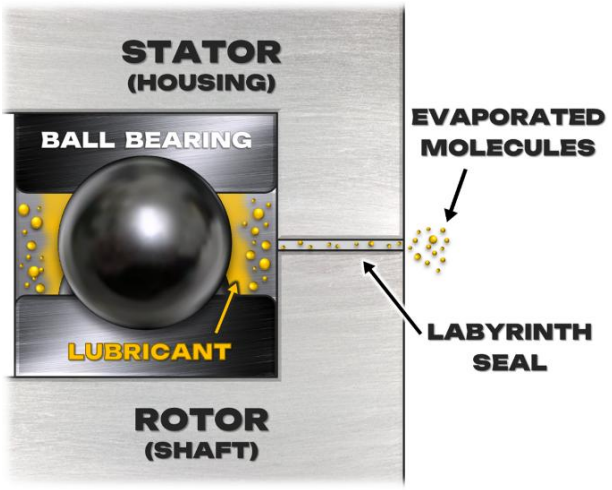

Figure 1. Ball bearing system with integrated straight labyrinth seal between stator and rotor [1]

Non-contact labyrinth seals restrict evaporated lubricant migration without frictional wear by creating narrow flow paths that reduce molecular transmission under free molecular flow conditions (see Fig. 1). Previous research [2] shows that seal effectiveness depends mainly on corridor width and length, with the ESTL analytical model predicting lubricant mass loss in vacuum.

However, analytical models often overestimate mass loss [2,3] because they overlook factors such as surface roughness, geometric complexity, local shape variations, dynamic rotation effects, and electrostatic fields generated inside the labyrinth seal [1,2].

This study compares analytical, numerical, and experimental approaches to evaluate how labyrinth seal geometry, surface topography, electrostatic fields, and rotation influence the transmission of evaporated lubricant molecules. Understanding these effects improves labyrinth seal design to reduce lubricant loss and contamination, enhancing mission reliability and extending operational lifetime.

2 EXPERIMENTAL MEASUREMENTS

2.1 Evaporation test rig (ETR)

To quantify lubricant mass loss due to vacuum evaporation, a custom-designed evaporation test rig (ETR) was developed and employed (see Fig. 2) [2,3]. It enables continuous, high-precision measurement of mass loss under high and ultra-high vacuum conditions, providing critical experimental validation for analytical and numerical evaporation models.

The ETR is based on a modified balance-scale mechanism [3] operating within a vacuum chamber. Displacement resulting from lubricant evaporation is measured using a capacitive proximity sensor. As evaporation causes the sample pan to lose mass, the beam tilts to maintain equilibrium. This displacement is being measured and further converted into a mass loss value using a calibrated sensitivity of 10.0 µm per 1.0 mg. Under stabilized thermo-vacuum conditions, the system achieves a weighing precision of ±0.04 mg [3].

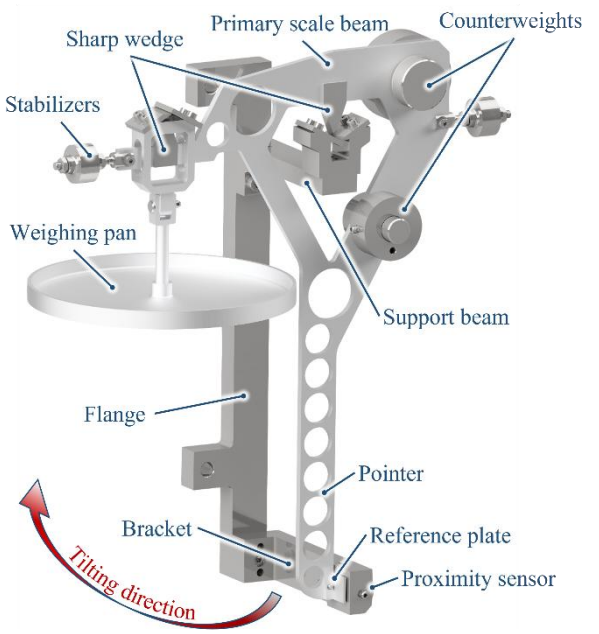

Figure 2. Evaporation test rig (ETR) description [3]

The modular design of the ETR allows for flexible adaptation to various test configurations. Components such as the weighing pan, counterweights, and test platforms are interchangeable, supporting a wide range of experimental scenarios including evaporation behaviour, outgassing phenomena or the labyrinth seal performance testing (see Fig. 3) [2].

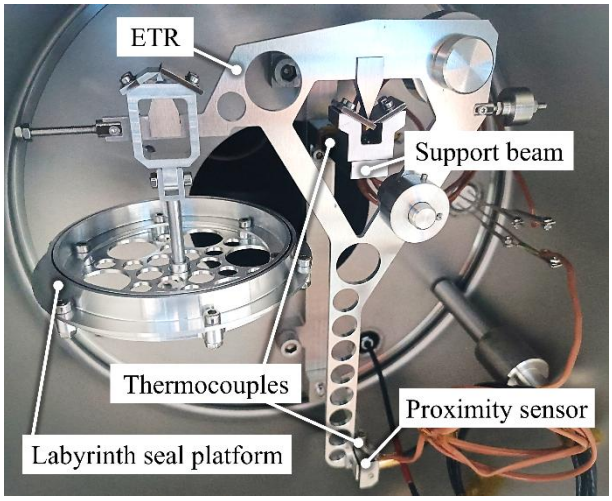

Figure 3. ETR with labyrinth seal platform [2]

For labyrinth seal testing, a dedicated modular platform is attached to the weighing pan. This platform houses an annular reservoir into which the test lubricant is applied and accommodates interchangeable seal geometries for comparative evaluation (see Fig. 4). All platform components are made of aluminium alloy 6061 to ensure thermal stability and vacuum compatibility. The low-outgassing lubricant Fomblin Y LVAC 25/6 was selected for testing due to its known vacuum performance characteristics. The amount of lubricant applied is carefully controlled to maintain a uniform liquid film across the reservoir while avoiding excess that could lead to uncontrolled creep through the seal geometry.

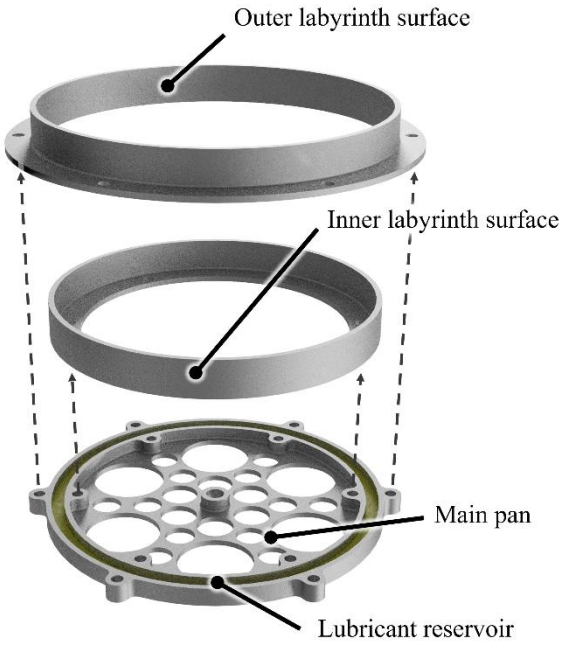

Figure 4. Labyrinth seal platform setup breakdown [2]

Three labyrinth seal configurations were experimentally tested (see Fig. 5 and Tab. 1) [2], chosen to match the analytical and simulation models in geometry and dimensions. The LONG configuration was additionally tested in two surface roughness variants to assess the influence of wall texture on molecular transmission.

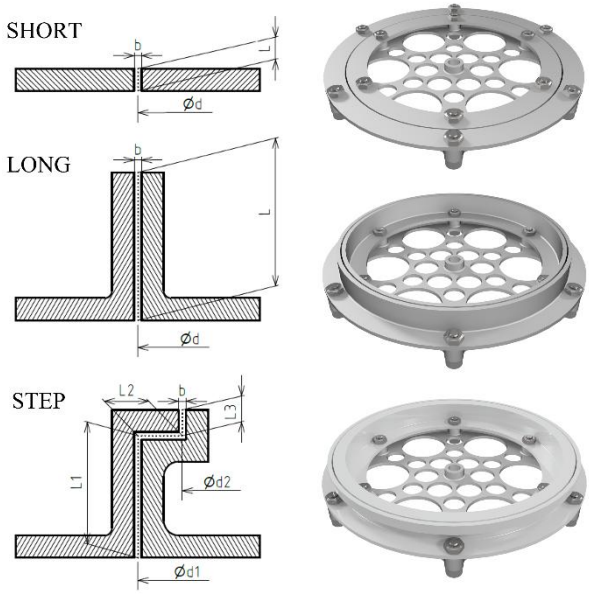

Figure 5. Labyrinth seal geometries and their experimental setup

Table 1. Labyrinth seal geometry dimensions [2]

Labyrinth	Width	Diameter	Length
	[mm]		
SHORT	b = 0.5	d = 86.5	L = 1.5
LONG	b = 0.5	d = 86.5	L = 10
STEP	b = 0.5	d_1 = 86.5	L_1 = 8.25
		d_2 = 92.5	L_2 = 3.00
			L_3 = 1.75

2.2 Electrostatic labyrinth test rig (ELTR)

To evaluate the influence of electrostatic fields on molecular transport through labyrinth seals, a dedicated electrostatic labyrinth test rig (ELTR) was developed. The system comprises a vacuum-compatible seal housing fitted with embedded electrodes, allowing the generation of a controllable electric field across the labyrinth corridor (see Fig. 6).

Figure 6. Electrostatic field configuration in a LONG-type straight labyrinth seal

Electrostatic fields are generated by applying voltages in the range of 0–50V across the cavity, simulating triboelectric charging or polarization effects. The system enables systematic investigation of field strength, polarity, and geometry on transmission probability under free molecular flow conditions. To assess the lubricant specific sensitivity to electrostatic fields, four lubricants with distinct chemical and physical properties were selected for testing, as summarized in Tab. 2.

Table 2. Tested lubricants for labyrinth electrostatic field sensitivity evaluation

Lubricant	Type
Fomblin YLVAC	Perfluoropolyether (PFPE)
Nye 2001	Multiply-alkylated cyclopentane (MAC)
EMIM-TFSI	Ionic liquid (IL1)
OMIM-TFSI	Ionic liquid (IL2)

Ionic liquids were included in the test matrix due to their expected higher sensitivity to electric fields compared to conventional lubricants. Their ionic nature and high polarizability may promote stronger interactions with electrostatic potentials within the labyrinth structure, potentially altering evaporation behaviour and transmission probability. These comparisons aim to reveal whether electrostatic field can enhance seal performance for polar or ionically active lubricants.

2.3 Dynamic labyrinth test rig (DLTR)

To study the effect of rotational motion on lubricant migration, a dynamic labyrinth seal test rig was developed (see Fig. 7). This setup includes a rotating shaft embedded within a stationary housing that contains the labyrinth seal geometry. A motorized spindle enables precise control of angular velocity, while temperature and pressure are maintained within the operating range of space-relevant environments. This configuration allows assessment of centrifugal effects and flow perturbations induced by rotation, offering insights into the dynamic modulation of seal effectiveness.

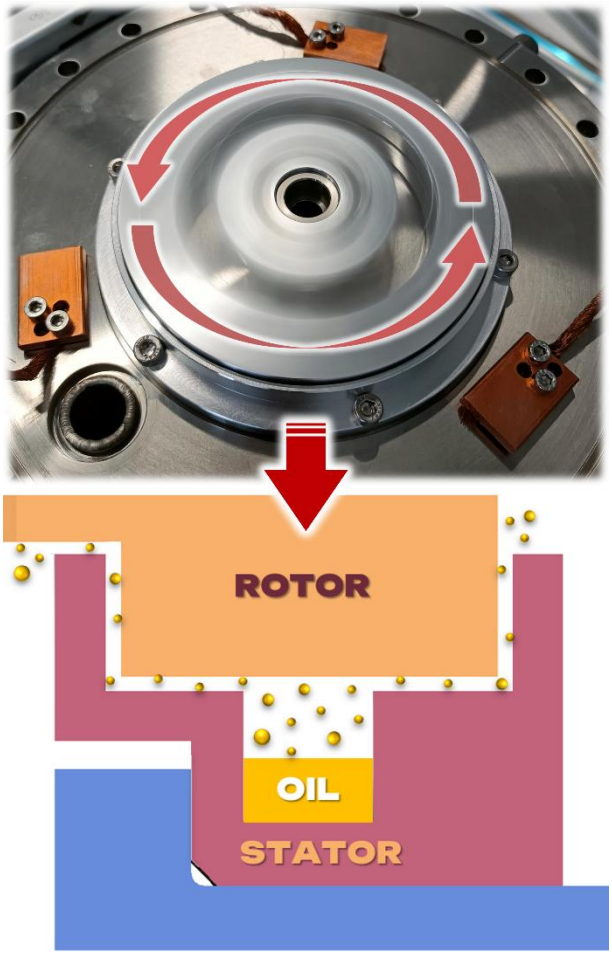

Figure 7. Dynamic test rig with integrated labyrinth seal between stator and rotor

3 ANALYTICAL MODEL

Predicting lubricant loss through labyrinth seals in space requires understanding molecular behaviour under high vacuum. This study uses an analytical model based on a modified Langmuir equation refined by the European Space Tribology Laboratory (ESTL), which assumes free molecular flow where intermolecular collisions are negligible and surface interactions dominate.

In this regime, the evaporation rate follows a zero-order Langmuir formulation, depending on vapor pressure, molecular mass, and temperature. While idealized, it omits effects like adsorption, re-condensation, or wall interactions.

To analytically evaluate molecular transport through a labyrinth seal, the complex geometry is simplified using a linearized representation, allowing for controllable calculation of mass flow rate as a function of geometry and molecular dynamics. Based on extensive experimental data, particularly from the ETSL, a more practical and empirically validated formulation was developed [4]:

$$Q_m = 0{,}0436 \cdot \frac{P_{mbar}\pi d_{cm} b_{cm} (M/T)^{0,5}}{1 + 0{,}375 \cdot L_{cm}/b_{cm}} \qquad (1)$$

This expression assumes steady-state, isothermal flow through smooth and static geometries, and does not explicitly incorporate effects such as surface roughness, electrostatic interactions, or dynamic rotation.

While the ESTL model provides an essential foundation for early-stage design evaluations and benchmarking, real-world applications may involve additional factors that influence molecular transport. In such cases, further refinements or complementary simulations can enhance predictive accuracy.

Therefore, this study compares its predictions with experimental data from the ETR and numerical simulations to identify discrepancies and support development of more comprehensive models for space-relevant conditions.

4 MODELLING AND SIMULATION

To assess molecular transport through labyrinth seals under ultra-high vacuum, numerical models were developed to complement analytical predictions and experimental data. These simulations capture effects difficult to address analytically, such as surface roughness, rotation, and local geometry variations [1,2].

Simulation boundary conditions were based on experimental measurements, including chamber pressure, temperature, and lubricant vapor properties. Since reservoir pressure could not be measured directly, it was set equal to the lubricant's vapor pressure.

Molecular transport was modelled using MolFlow+ and COMSOL Multiphysics 6.3. MolFlow+ simulated steady-state flux to assess the effect of corridor geometry on transmission. COMSOL accounted for roughness, time-dependent dynamics, and centrifugal forces via spectrally generated wall profiles and a rotating reference frame (see Fig. 8 and Fig. 9), enabling evaluation of surface and rotational effects on molecular trajectories.

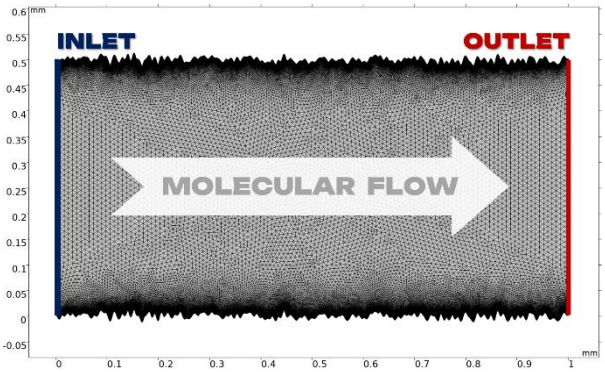

Figure 8. 2D labyrinth geometry with surface roughness profile modelled in COMSOL Multiphysics [1]

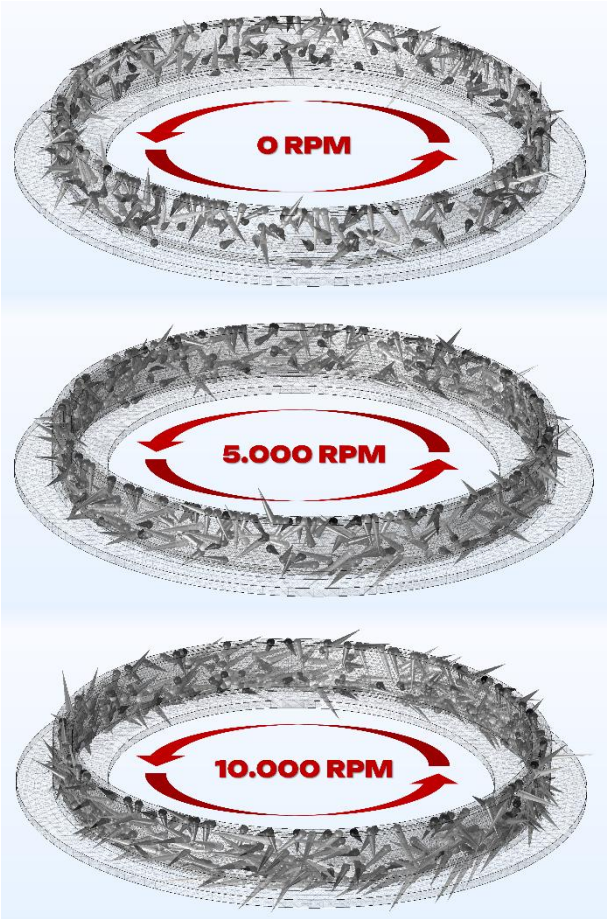

Figure 9. Molecular trajectory variations with inner wall rotation in the LONG seal configuration

All simulations were isothermal, using Fomblin Y LVAC 25/6 as the model lubricant. Inlet pressure was set to the vapor pressure of the lubricant, and the outlet to vacuum. The key output is transmission probability (TP):

$$TP = \frac{N_0}{N_1} \quad (2)$$

where N_0 denotes the number of molecules entering the channel and N_1 those exiting. TP offers a dimensionless, normalized metric for comparing seal efficiency across conditions and configurations.

These simulations validate analytical models, explain experimental deviations, and support design optimization by capturing effects beyond classical models. This integrated approach enhances understanding of molecular transport in vacuum and guides advanced seal design for space applications.

5 RESULTS AND DISCUSSION

5.1 Geometry effects on seal performance

The results presented in this section integrate analytical calculations, experimental measurements, and numerical simulations to comprehensively assess the performance of various labyrinth seal geometries. The primary focus is on three representative seal designs: SHORT, LONG, and STEP (see Fig. 5). Experimental measurements were conducted using the modified ETR setup, which records lubricant mass loss due to vacuum evaporation as a function of time.

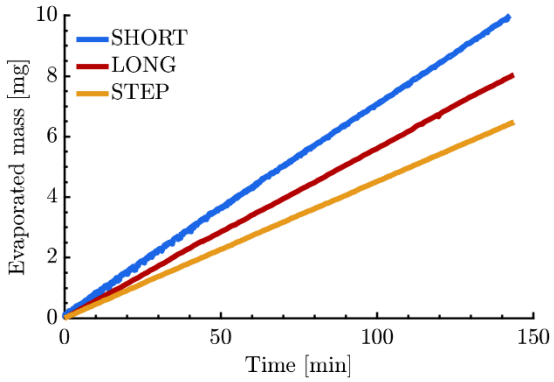

Figure 10. Experimental measurements comparison of evaporated mass loss across various seal types [2]

The resulting data, converted from displacement signals using calibration coefficients, demonstrate a clear difference in sealing performance among the geometries (see Fig. 10). Notably, the STEP geometry showed the lowest mass loss, followed by the LONG and SHORT geometries. These results were further validated through before-and-after weighing of the test setup.

To provide a comparative baseline, the analytical model and two simulation tools, were employed. The comparison (see Fig. 11 and Tab. 3) shows that both the analytical model and simulations tend to overestimate mass loss for short labyrinth geometries by more than a factor of two. For more complex labyrinth seals, the analytical model slightly underestimates mass loss, while simulation results closely match experimental data with deviations typically between 5–15%. The STEP configuration consistently yielded the lowest transmission probability and mass loss, confirming the advantage of extended and redirected flow paths [2].

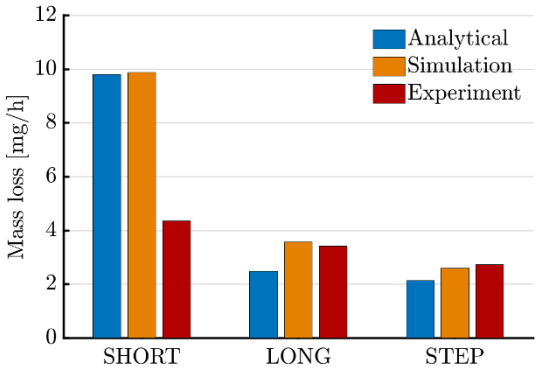

Figure 11. Comparison of analytical, experimental and simulation approaches of evaporation mass loss [2]

Table 3. Mass flow across seal types by all approaches

Mass loss [mg/h]		SHORT	LONG	STEP
Experiment		4.35	3.41	2.73
Analytical		9.80	2.48	2.14
Simulation	MolFlow+	9.46	3.24	2.33
	COMSOL	9.89	3.58	2.72

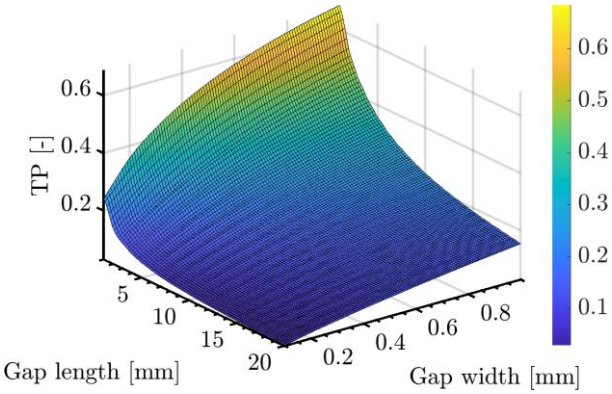

Figure 12. Identification of key labyrinth geometry parameters impacting transmission probability [2]

A deeper analysis using TP as a normalized metric (see Fig. 12) reinforces the critical role of corridor length and width. Longer and narrower seals reduce the likelihood of direct molecular transmission, thereby enhancing sealing performance [2].

The STEP geometry reveals the molecular beaming effect, where narrow, elongated channels bias molecular trajectories along the corridor, reducing sidewall interactions. Introducing abrupt direction changes helps disrupt this beaming effect. A parametric study (see Fig. 13) showed that placing the step at the corridor midpoint yields the lowest mass loss. Off-centre placements lead to increased loss, underscoring the importance of precise geometric design to counteract molecular beaming and improve sealing efficiency [2].

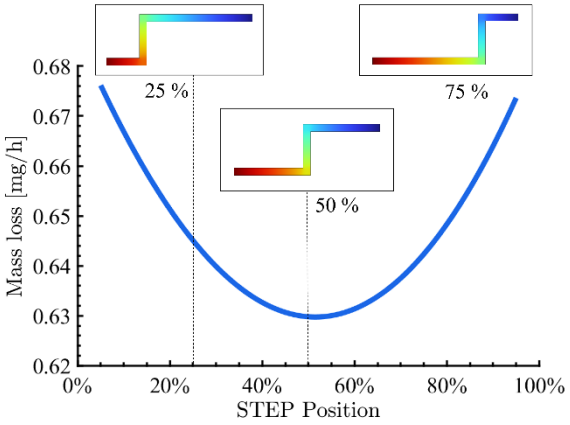

Figure 13. Evaporative mass loss vs. step position [2]

Further optimization targeted the step corner geometry. Conventional rounded corners, a by-product of manufacturing limitations, were found to facilitate molecular propagation [2]. Several modified corner designs were simulated (see Fig. 14) to assess their influence on lubricant retention. Incorporating features such as relief grooves, sharp dead-end channels, or ISO-standard grooves led to modest but meaningful reductions in mass loss (see Tab. 4). These findings suggest that even small geometric modifications, can enhance long-term sealing efficiency.

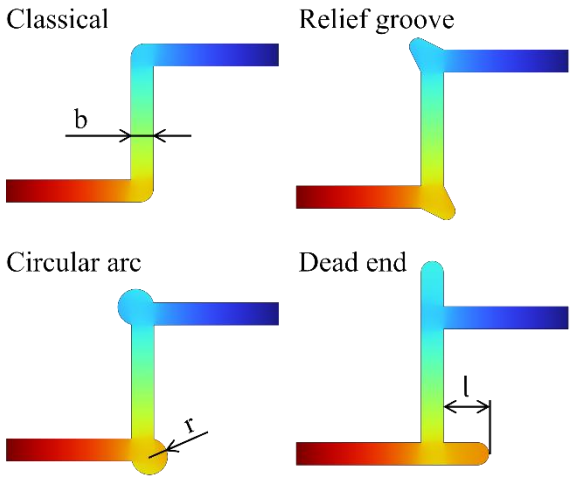

Figure 14. Corner designs in step labyrinth seals [2]

Table 4. Corner geometry vs. lubricant loss reduction

Corner geometry	Characteristic parameter	Loss reduction
Classical	–	–
Circular arc	r = b	3.8 %
Relief groove	type G *	3.9 %
Dead end	l = 2b	4.3 %

* ISO 18388:2016

Together, these results emphasize the significance of labyrinth geometry in molecular flow control. Complex, angular designs not only improve sealing performance but also mitigate adverse effects like molecular beaming. This highlights the value of incorporating detailed geometric features in the design and manufacture of vacuum seals for space applications.

5.2 Surface roughness influence

Surface roughness plays a significant role in molecular flow through labyrinth seals. To investigate its effect, both experimental tests and numerical simulations were conducted [1,2]. Two LONG type labyrinth seals with identical channel geometries but different surface finishes were fabricated: one untreated (ROUGH) and one polished (SMOOTH). A 3D optical profilometer (Bruker Contour GTX) was used to characterize surface roughness parameters (see Fig. 15 and Tab. 5).

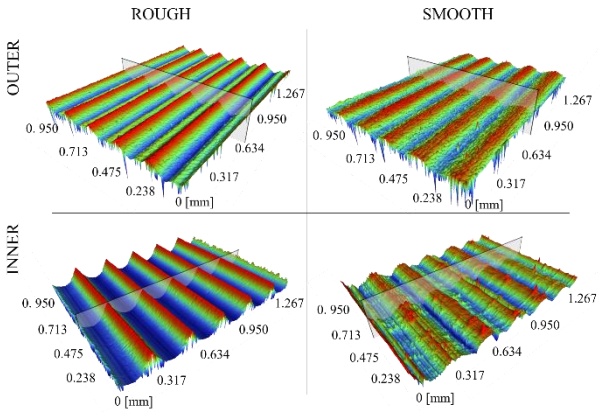

Figure 15. Surface roughness of LONG seal components measured by optical profilometer [2]

The experimental results showed a decrease in lubricant mass loss for the ROUGH seal compared to the SMOOTH seal (see Tab. 6), indicating improved sealing due to surface irregularities. This observation was further confirmed by COMSOL Multiphysics simulations incorporating the measured topographies. Simulations predicted a similar mass loss reduction, closely matching the experimental trend. The findings suggest that rougher surfaces improve sealing efficiency [1,2].

Table 5. Surface roughness of labyrinth seal walls [2]

Surface roughness	ROUGH		SMOOTH	
	Inner	Outer	Inner	Outer
Ra [µm]*	3.88	1.30	0.13	0.56
Sa [µm]	3.70	1.30	0.14	0.56
Sq [µm]	4.34	1.60	0.16	0.67
Sdr [µm]	1.99%	5.56%	0.01%	4.14%

*In the direction of highlighted mid-planes shown in Figure 15

Table 6. Surface roughness effects on labyrinth seal evaporative mass loss (experiment and simulation) [2]

	SMOOTH	ROUGH	Roughness influence
Experiment	3.8 mg/h	3.3 mg/h	– 13.2 %
Simulation	3.5 mg/h	3.1 mg/h	– 11.4 %

To generalize these observations, synthetic rough surface profiles were implemented in COMSOL and applied to a broad range of seal geometries with channel widths from 0.2 to 1 mm and lengths from 1 to 10 mm [1]. Each rough profile was benchmarked against a smooth-wall reference (Ra = 0 µm), revealing a consistent decrease in transmission probability with increasing surface roughness (see Fig. 16).

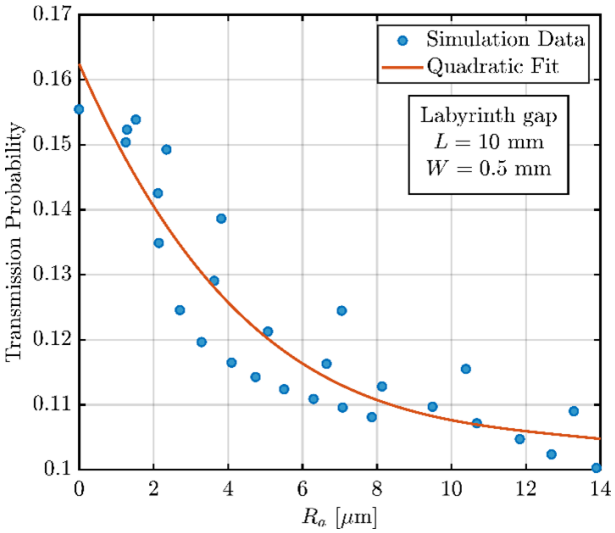

Figure 16. TP vs. surface roughness [1]

To capture these dependencies, a correction model was developed by fitting second order polynomials to TP as a function of surface roughness (Ra) for each combination of width and length:

$$TP_{corr} = A(W,L) \cdot Ra^2 + B(W,L) \cdot Ra + C(W,L) \quad (3)$$

where coefficients A, B, and C are geometry specific and derived from simulation data, provided together with our recent work [1]. This offers a rapid way to estimate transmission probability for seals with known surface roughness without the need for full simulations.

The correction model was validated using experimental data from the ROUGH and SMOOTH seals. For both cases, the predicted transmission probability ratios normalized to an ideal smooth reference showed a maximum error of only 5.1% compared to the measured mass loss. This close agreement confirms the model's reliability for early-stage design evaluations and tolerance analyses.

5.3 Electrostatic field effects

The influence of electrostatic fields on molecular transport through labyrinth seals was experimentally investigated using four configurations of the Electrostatic Labyrinth Test Rig (ELTR, see Fig. 6) and lubricants listed in Tab. 2. Each lubricant was tested under both neutral conditions and with a constant 50 V electric field applied across the labyrinth corridor. All experiments were performed under similar high-vacuum conditions, though minor variations in pressure and temperature may have occurred between test sessions.

The results in Tab. 8 show a slight reduction in mass loss for Fomblin Y LVAC 25/6 and 1-Methyl-3-octylimidazolium TFSI under an applied field, suggesting electrostatic influence on molecular flow. In contrast, Nye 2001 and 1-Ethyl-3-methylimidazolium TFSI showed minimal change, indicating low sensitivity.

Table 7. Lubricant evaporative mass loss in 0–50V field

	Mass loss [mg/h]		Electrostatic influence
	0 V	50 V	
PFPE	0.361	0.343	– 5.0 %
MAC	0.085	0.087	+ 2.0%
IL1	0.055	0.053	– 2.7 %
IL2	0.040	0.037	– 7.4 %

The results suggest that electrostatic fields may enhance sealing performance for high-molecular-weight or ionic lubricants, although the observed effects were modest. Further investigation with improved measurement accuracy, tighter control of conditions, and higher field strengths is needed to confirm these findings.

Applying electrostatic fields in seals carries inherent risks; micro-arcing may cause material damage or electronic interference. Thus, any sealing performance benefits must be carefully considered against the hazards. While the concept shows promise, further investigation is needed to determine its practical viability for space applications.

5.4 Dynamic effect of labyrinth wall rotation

The influence of inner ring rotation on labyrinth seal performance was investigated using COMSOL Multiphysics simulations for SHORT, LONG, and STEP geometries (see Fig. 5). The rotational speed was applied to the inner ring, and the transmission probability was evaluated as a function of RPM (see Fig. 17).

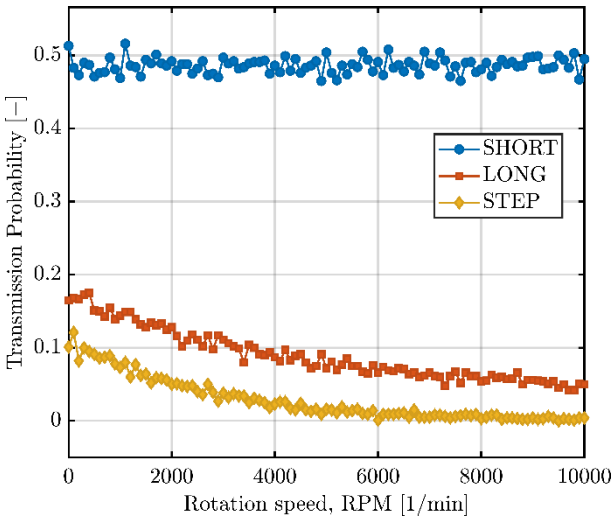

Figure 17. Transmission probability vs. rotor speed for labyrinth seal geometries

For the LONG and STEP geometries, TP decreased noticeably with increasing RPM, indicating that rotation enhances molecular scattering and reduces molecular transmission through the seal. In contrast, the SHORT geometry showed a nearly constant TP across the RPM range, consistent with static simulations. This behaviour is likely due to the short labyrinth wall length in the SHORT design, which allows molecules to pass through easily without sufficient surface interactions.

Table 8. Simulation and experimental results for static and rotating labyrinth seal (0 and 2000 rev. per minute)

	0 RPM	2000 RPM	Spin influence
Simulation	0.178 mg/h	0.161 mg/h	– 9.05 %
Experiment	0.188 mg/h	0.168 mg/h	– 10.6 %

These simulation results were corroborated by experimental measurements conducted on a rotational vacuum test device. Evaporation of Fomblin Y LVAC 25/7 lubricant was measured under static conditions and at 2000 revolutions per minute (RPM). The observed mass loss reduction at higher rotational speed closely match the simulation (see Tab. 8), confirming the impact of rotational dynamics on molecular flow and labyrinth seal effectiveness for high spinning applications. This underscores the importance of considering dynamic effects when evaluating and designing labyrinth seals for space applications, where rotational motion is common.

6 CONCLUSION

This study provides a comprehensive analysis of lubricant evaporation and molecular transport through labyrinth seals under vacuum conditions. By integrating analytical modelling, experimental data, and numerical simulations, it assesses the influence of seal geometry, surface roughness, electrostatic fields, and rotation on sealing performance. Key findings highlight critical design factors that enhance seal effectiveness:

- Stepped labyrinth seals improve sealing by increasing effective length and reducing molecular beaming effect.
- Increased surface roughness of labyrinth seal walls lowers molecular transmission probability.
- Local geometric features, such as relief grooves, can enhance sealing efficiency by up to 4%.
- Electrostatic fields have a modest impact on high molecular weight and ionic lubricants, suggesting the need for further studies at higher voltages and under controlled conditions.
- Labyrinth seal rotation reduces transmission probability, underscoring the importance of dynamic effects in seal design.

7 ACKNOWLEDGEMENT

This work was supported through the Open Space Innovation Platform under a Co-Sponsored Research Agreement funded by the European Space Agency (Contract No. 4000139889).

8 REFERENCES

[1] J. Pouzar, D. Kostal, L.-G. Westerberg, E. Nyberg, T. Polacek, K. Jurik, I. Křupka, Influence of Surface Roughness on Molecular Flow Through Labyrinth Seals for Space Applications, (2025). https://doi.org/10.2139/ssrn.5312192.

[2] J. Pouzar, D. Kostal, L.-G. Westerberg, E. Nyberg, I. Krupka, Labyrinth seal design for space applications, Vacuum 232 (2025) 113882. https://doi.org/10.1016/j.vacuum.2024.113882.

[3] J. Pouzar, D. Kostal, P. Sperka, I. Krupka, M. Hartl, Experimental study of space lubricant evaporation in a high vacuum environment, Vacuum 219 (2024) 112758. https://doi.org/10.1016/j.vacuum.2023.112758.

[4] M.J. Anderson, S. Freeman, E.W. Roberts, Evaporative losses of vacuum-compatible oils through labyrinth seals, in: R. ~A. Harris (Ed.), ESMATS, 2003: pp. 255–270. https://www.esmats.eu/esmatspapers/pastpapers/pdfs/2003/anderson.pdf (accessed June 14, 2024).